Title	Studies on Cage-Shaped Metal Complexes with Phenoxy Moieties Based on Novel Structural Design
Author(s)	Nakajima, Hideto
Citation	大阪大学, 2012, 博士論文
Version Type	VoR
URL	https://hdl.handle.net/11094/26864
rights	
Note	

Studies on Cage-Shaped Metal Complexes with Phenoxy Moieties Based on Novel Structural Design

2011

Hideto Nakajima

Department of Applied Chemistry
Graduate School of Engineering
Osaka University

Studies on Cage-Shaped Metal Complexes with Phenoxy Moieties Based on Novel Structural Design

（新規な構造設計によるフェノキシ部位を有するカゴ型金属錯体に関する研究）

2011

Hideto Nakajima

中島　秀人

Department of Applied Chemistry
Graduate School of Engineering
Osaka University

Preface and Acknowledgements

<div align="right">Hideto Nakajima</div>

Department of Applied Chemistry,

Graduate School of Engineering,

Osaka University

2-1 Yamadaoka, Suita, Osaka, 565-0871, JAPAN

January, 2012

List of Publications

1. **Synthesis and Theoretical Studies of Gallium Complexes Back-Shielded by a Cage-Shaped Framework of Tris(*m*-oxybenzyl)arene**
   Hideto Nakajima, Makoto Yasuda, Kouji Chiba, and Akio Baba
   Chem. Commun. **2010**, *46*, 4794–4796.

2. **Cage-Shaped Borate Esters with Tris(2-oxyphenyl)methane or -silane System Frameworks Bearing Multiple Tuning Factors: Geometric and Substituent Effects on Their Lewis Acid Properties**
   Makoto Yasuda, Hideto Nakajima, Ryosuke Takeda, Sachiko Yoshioka, Satoshi Yamasaki, Kouji Chiba, and Akio Baba
   Chem. Eur. J. **2011**, *17*, 3856–3867.

3. **Stabilization of Excited State Using Through-Space Interaction between Independent π-Systems Mediated by a *peri*-Substituted Hydroxy Group in 1-Arylnaphthalenes: Unexpected Blue Emission of 1,3,5-Tris(*peri*-hydroxynaphthyl)benzene**
   Hideto Nakajima, Makoto Yasuda, Kenji Shimizu, Naomi Toyoshima, Yasunori Tsukahara, Takao Kobayashi, Shinichiro Nakamura, Kouji Chiba, and Akio Baba
   Bull. Chem. Soc. Jpn. **2011**, *84*, 1118–1129.

4. **Creation of Novel Reaction Field Recognizing Aromatic Compounds by π-Pocket in a Cage-Shaped Borate Catalyst**
   Hideto Nakajima, Makoto Yasuda, Ryosuke Takeda, and Akio Baba
   Angew. Chem. Int. Ed. in press

5. **Lithium Phenolates with a Hexagonal-Prismatic Li_6O_6 Core Isolated via a Cage-Shaped Tripodal Ligands System: Crystal Structures and Their Behavior in Solution**
   Hideto Nakajima, Makoto Yasuda, and Akio Baba
   Submitted

Supplementary List of Publications

1. **Fine-Tuning of Boron Complexes with Cage-Shaped Ligand Geometry: Rational Design of Triphenolic Ligand as a Template for Structure Control**
   Makoto Yasuda, Sachiko Yoshioka, Hideto Nakajima, Kouji Chiba, and Akio Baba
   Org. Lett. **2008**, *10*, 929–932.

2. **Diastereoselective Reductive Aldol Reaction of Enones to Ketones Catalyzed by Halogenotin Hydride**
   Ikuya Shibata, Shinji Tsunoi, Kumiko Sakabe, Shinji Miyamoto, Hirofumi Kato, Hideto Nakajima, Makoto Yasuda, and Akio Baba
   Chem. Eur. J. **2010**, *16*, 13335–13338.

Award

1. **The Best Poster Award**
   M. Yasuda, H. Nakajima, A. Baba, "Synthesis of Cage-Shaped Group 13 Metal Complexes with Arene Framework", [Second International Symposium on Atomic Technologies], October 2007.

2. **CSJ Student Presentation Award**
   H. Nakajima, M. Yasuda, R. Takeda, A. Baba, "Synthesis and Property of Cage-Shaped Borate Complexes Bearing Multiple Control Unit", [90th Annual Meeting of CSJ], March 2010.

3. **The Poster Award**
   H. Nakajima, R. Takeda, M. Yasuda, and A. Baba, "Design and Evaluation of the Environment around Metal in Cage-Shaped Complexes toward Substrate-Selective Reactions", [20th Symposium on Physical Organic Chemistry], September 2010.

Contents

General Introduction

Metal complex is one of the most powerful tools for organic synthesis as catalyst. Numerous studies have been performed to alter properties of the complexes by varying the metal centers and ligands. In particular, in the case of transition metal complexes, the various types of ligands have been developed by changing the steric and/or electronic factors (Figure 1).[1] This development permits the fine-tuning of transition metal complexes. On the other hand, in the case of main group metal complexes, little attention has been focused on systematic study. In fact, there are only investigations by the simple ligand system such as alkoxide, amino, and halogen ligands. As the depletion of resources is main issue that needs to be solved for a sustainable society, it is required to expand the accessibility of the the main group metal complexes by developing the systematic ligand system.

· Transition Metal

Well-Designed Ligand System

Various Tuning Factors

- Structural Control
- Electronic Control

- phosphine   - carbene
- amine   - halogen
- pyridine   - alkoxy

· Main Group Metal

Simple Ligand System

- Electronic Control   ⟹ **Lack of Systematic Ligand Design**

MX_n (X = F, Cl, Br, I, OR, NR_2)
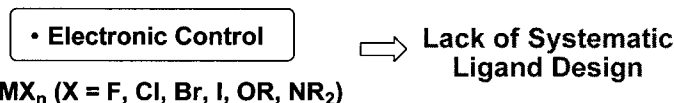
Figure 1. Control of the Properties of Metal Complexes by Using Ligands.

This thesis describes the systematic cage-shaped ligand system which binds the metal center in its organic framework as shown in Figure 2. By using this ligand system, the cage-shaped main group metal complexes were synthesized and their properties were investigated. The fine-tuning of the complexes has been achieved by introducing various factors into the cage-shaped ligand; (a) design of bottom and arm moieties (geometric tuning factor), (b) introduction of steric and/or electronic substituents (substitutent tuning factor). Furthermore, this cage-shaped structure enhanced the stability of the metal complex by chelate effect and it is expected that the new properties were induced by the cage-shaped geometry.[2,3]

Cage-Shaped Structure

M — ← Substituent   } **Substituent Tuning Factor**

← Arm

← Bottom   } **Geometric Tuning Factor**
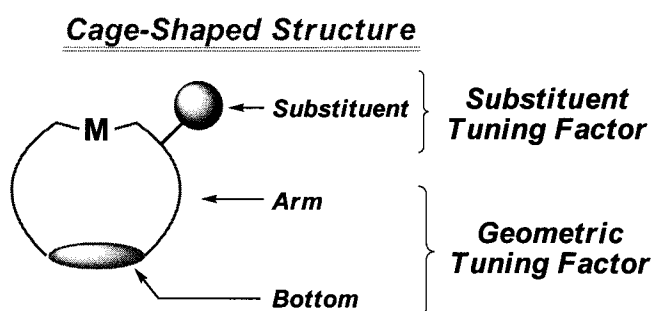
Figure 2. Concept of Cage-Shaped Ligands.

Chapter 1 deals with synthesis of the cage-shaped borate complexes by using the ligands in which three phenoxy moieties are linked by uni atom. The cage-shaped geometry enhanced catalytic activities. A fine-tuning of the cage-shaped borate complexes was achieved by changing the cage-shaped geometry and introducing various steric and/or electronic substitutents.

Chapter 2 describes the metal complexes by using the cage-shaped ligand in which three phenoxy moieties are linked by a bezene ring. In this ligand, because the space around the center metal is larger than that of the ligand linked by uni atom described in Chapter 1, introduction of gallium, which is larger than boron, was allowed into the complexes. In this gallium complex, the cage-shaped geometry also enhanced the catalytic activity. In contrast, introducing lithium as a small metal center generated a hexanuclear lithium phenolate bearing hexagonal-prismatic Li_6O_6 core which had been scarcely reported.

Chapter 3 deals with nonplanar emitting organic compound which was found in the course of the synthesis of various cage-shaped ligands. 1,3,5-Tris(*peri*-hydroxynaphthyl)benzene demonstrated unexpected blue emission. In this system, the position of the hydroxyl group is critical for their emitting properties. Theoretical calculation reveals that the hydroxyl group at *peri*-position effectively mediates independent π-framework in a through-space fashion.

References

(1) (a) Helmchen, G.; Pfaltz, A. *Acc. Chem. Res.* **2000**, *33*, 336–345. (b) Kawaguchi, H.; Matsuo, T. *J. Organomet. Chem.* **2004**, *689*, 4228–4243. (c) Surry, D. S.; Buchwald, S. L. *Angew. Chem. Int. Ed.* **2008**, *47*, 6338–6361. (d) Corberán, R.; Mas-Marzá, E.; Peris, E. *Eur. J. Inorg. Chem.* **2009**, 1700–1716. (e) Gillespie, J. A.; Dodds, D. L.; Kamer, P. C. J. *Dalton Trans.* **2010**, *39*, 2751–2764.

(2) Similar cage-shaped complexes have been reported. However, they were not applied to catalytic reaction. (a) Livant, P. D.; Northcott, J. D.; Shen, Y.; Webb, T. R. *J. Org. Chem.* **2004**, *69*, 6564–6571. (b) Kobayashi, J.; Kawaguchi, K.; Kawashima, T. *J. Am. Chem. Soc.* **2004**, *126*, 16318–16319. (c) Akagi, F.; Matsuo, T.; Kawaguchi, H. *J. Am. Chem. Soc.* **2005**, *127*, 11936–11937.

(3) The Lewis basic cage-shaped complex has been reported using P or As. Dinger, M. B.; Scott, M. J. *Inorg. Chem.* **2001**, *40*, 856–864.

Chapter 1

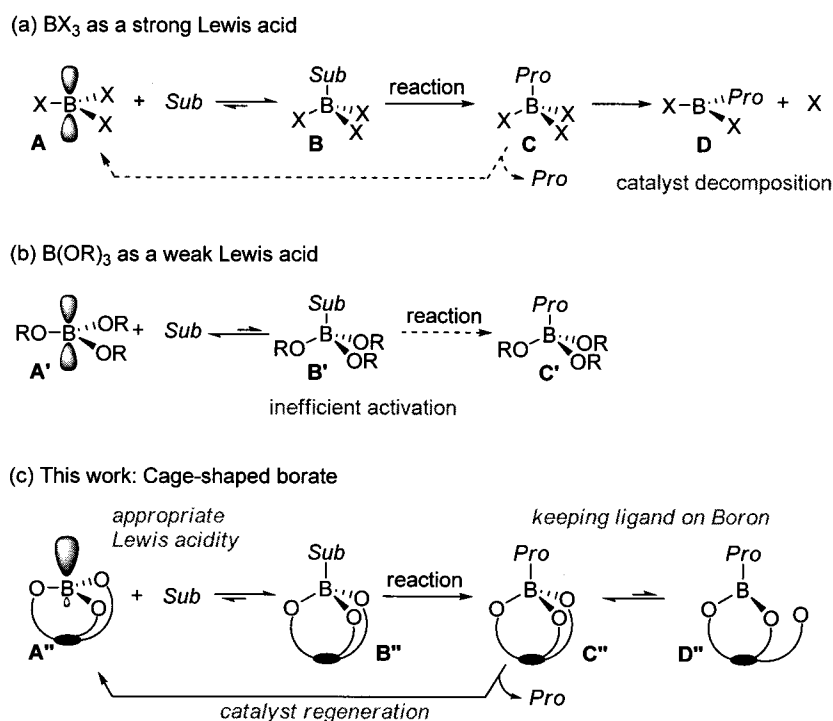## Cage-Shaped Ligands Linked by Uni Atom

1-1.Cage-Shaped Borate Esters with Tris(2-oxyphenyl)methane or -silane System Frameworks Bearing Multiple Tuning Factors: Geometric and Substituent Effects on Their Lewis Acid Properties

1-1-1. Introduction

Group 13 elements are very important to Lewis acid chemistry.[1] Among them, boron-containing compounds have been widely studied as typical Lewis acids, and have been applied to various types of organic transformations.[2] One of the most commonly available compounds is the boron trihalide BX_3 **A**, as shown in Scheme 1a. In this compound, a Lewis basic substrate (*Sub*) interacts with a strong Lewis acid **A** to form the adduct **B**. The activated substrate may react with an external reagent to give the product complex **C** that includes a B−*Pro* bond (*Pro* = product). Usually, the metal center releases the original ligand X to give **D** due to a stronger B−*Pro* bond.[3] In this pathway, an equimolar amount of the Lewis acid **A** is consumed to complete the reaction. Consequently, high Lewis acidity and high catalytic turnovers are incompatible. In contrast, the borate ester $B(OR)_3$ **A'** has low Lewis acidity due to the overlap between lone pairs on oxygen atoms with a vacant p orbital on boron (Scheme 1b).[4, 5] Unfortunately, the Lewis acidity of the borate ester $B(OR)_3$ **A'** is too low to react with the substrate. To overcome the problems associated with **A** and **A'**, we have designed a new type of Lewis acid **A"** with a cage-shaped ligand system, as shown in Scheme 1c. We used the "cage" to generate the appropriate Lewis acidity, as conformational changes in the frame of the cage could be used to activate the substrate and to keep the original oxy ligands on boron due to the chelating effect of the cage frame. Therefore, both high Lewis acidity and high catalytic turnovers would be compatible in the appropriately designed new type of Lewis acid **A"**, if it has labile boron−ligand bonds. Various types of metal complexes can be controlled by changing the geometry around the metal using special ligands,[6] but this approach often causes relatively large alterations in the metal complex properties, which interfere with its catalytic activity. The proposed cage-shaped borate **A"** could be a suitable Lewis acid catalyst and be finely tuned by many factors, such as the size of the cage or steric and electronic effects, based on the ligand design.

In this paper, we report on borate compounds with cage-shaped frameworks and their application to the catalysis of organic transformations.[7, 8] We synthesized new borate compounds **1B** with a triaryloxy ligand **1** that combined with bridgehead atom X, as shown in Scheme 2. The properties of these compounds were effectively controlled by varying R and X; that is, R provided substituent control due to electronic and steric factors,[9] while the bridgehead atom X allowed control of the geometric control.

Scheme 1. Working Hypothesis for Conceptually New Lewis Acid.

(a) BX_3 as a strong Lewis acid

(b) $B(OR)_3$ as a weak Lewis acid

inefficient activation

(c) This work: Cage-shaped borate

catalyst regeneration

Scheme 2. Cage-Shaped Borate Esters 1B with Triaryloxy Ligand 1.

R: *Substituent control*
electronic factor
steric factor

X: *Geometric control*

1B   1
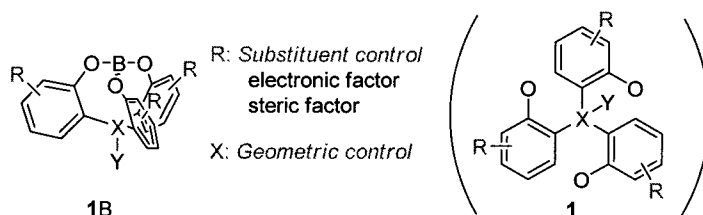
1-1-2. Results and Discussion

Synthesis of Various Ligands of Tris(*o*-oxyphenyl)methanes or -silanes 1H₃: Based on the novel concept presented in Scheme 1c, we prepared borate 1B as a structurally strained Lewis acid. Reportedly, organic components that include preorganized phenoxy moieties are effective ligand systems for metal complexes.[10,11] Scheme 3 shows the synthetic routes to ligands 1a-hH₃ that were used for the formation of the various compounds 1B.[12] Tris(2-hydroxyphenyl)methane (1aH₃) was synthesized as follows. *ortho*-Lithiation of anisole (2a) followed by treatment with ethyl chloroformate gave the triarylmethanol 3a. The treatment of 3a with *p*-toluenesulfonic acid in THF/MeCN directly gave the reduced compound 4a. The in situ-generated carbenium cation from 3a, which was stabilized by electron-donating groups,[13] was reduced by THF probably by means of either an ionic or a single-electron transfer (SET) mechanism.[14] The desired compound 1aH₃ was obtained after deprotection of 4a by BBr₃. Bromination of 1aH₃ in AcOH/CCl₄ gave the *o*- and *p*-brominated compound 1bH₃. Bromination of 4a afforded *p*-brominated 4c, which was deprotected by BBr₃ to give 1cH₃.[15] The fluorinated compound 1dH₃ was

4

prepared from 2-bromo-4-fluoroanisole (**2d**) in a manner similar to that used to prepare **1aH₃**. The phenyl- and naphthyl-substituted compounds **1eH₃** and **1fH₃** were prepared from the substituted anisole derivatives **2e** and **2f**, respectively.

For synthesis of the silane derivatives **1gH₃** and **1hH₃**, a different protecting group was required. Although we obtained (o-MeOC₆H₄)₃SiMe by the reaction of o-lithioanisole with MeSiCl₃, deprotection with BBr₃ failed and gave an undesired product due to weak Si–aryl bonds. Among the protecting groups examined, a dimethylcarbamoyl group worked very well for **1gH₃**, as shown in Scheme 3.[16] Protection of 2-bromophenol with dimethylcarbamoyl chloride and its subsequent lithiation followed by treatment with MeSiCl₃ gave the triarylmethylsilane **4g**. Deprotection of **4g** by LiAlH₄ effectively afforded **1gH₃**. In a similar manner, the isobutyl derivative **1hH₃** was obtained.

Scheme 3. Synthesis of Triphenolic Methanes and Silanes 1H₃.

2a R¹, R², R³ = H, H, H
2d R¹, R², R³ = H, F, Br
2e R¹, R², R³ = Ph, H, H
2f R¹, R², R³ = Nap, H, H

3a R¹, R² = H, H
3d R¹, R² = H, F
3e R¹, R² = Ph, H
3f R¹, R² = Nap, H

4a R¹, R² = H, H
4c R¹, R² = H, Br
4d R¹, R² = H, F
4e R¹, R² = Ph, H
4f R¹, R² = Nap, H

1aH₃ R¹, R² = H, H
1bH₃ R¹, R² = Br, Br
1cH₃ R¹, R² = H, Br
1dH₃ R¹, R² = H, F
1eH₃ R¹, R² = Ph, H
1fH₃ R¹, R² = Nap, H

R' = -CONMe₂

4g (R = Me)
4h (R = Buⁱ)

1gH₃ (R = Me)
1hH₃ (R = Buⁱ)
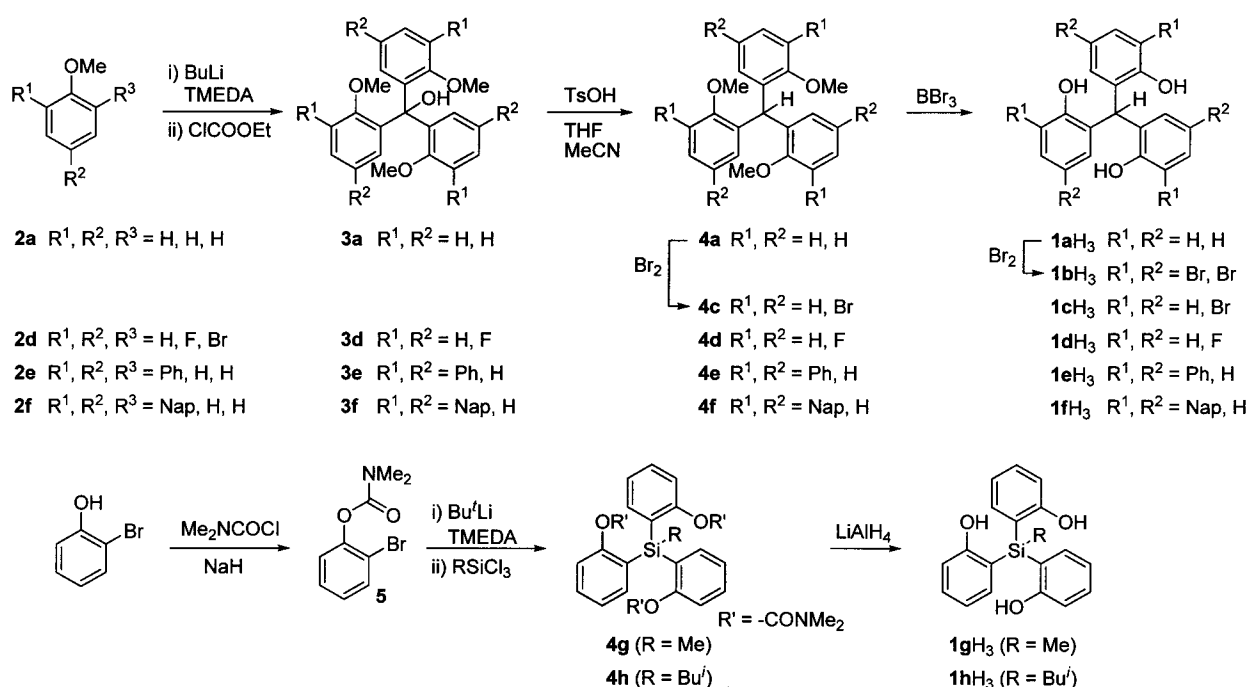
Generation of Cage-Shaped Borates: The treatment of 1H₃ with BH₃·THF readily generated the cage-shaped borates 1B·THF (Scheme 4). These compounds were thermally stable, but decomposed in air (O₂ and/or water). Thus purification and recrystallization were performed in a nitrogen-filled glove box and NMR spectroscopy measurements were performed under nitrogen. The THF-free 1B was not observed under these conditions, which suggests that cage-shaped borate had a higher Lewis acidity than that of planar borates, such as B(OPh)₃. The generated cage-shaped borates 1a-hB·L with various substituents and bridgehead atoms are shown in Scheme 4. The pyridine complexes 1B·Py were formed by addition of pyridine to the generated 1B·THF, and were thoroughly analyzed by X-ray crystallography (described later).

Scheme 4. Generation of Cage-Shaped Borates 1B·L with Various Substituents.
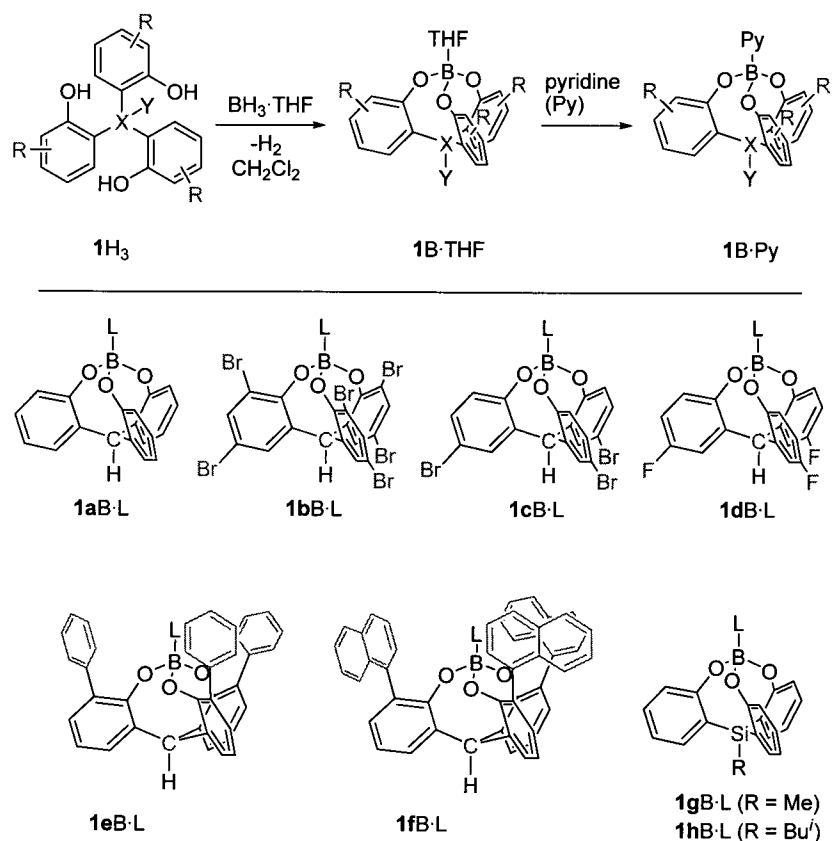
NMR Data for Cage-Shaped Borates 1B·L: Selected NMR signals for the cage-shaped borates 1B·L and their ligands 1H$_3$ are shown in Table 1. The NMR data of the generated THF-ligated cage-shaped borates (1B·THF) showed characteristic signals. For 1aB·THF, the significant upfield shift of the methine hydrogen relative to that of 1aH$_3$ (6.07→5.13 ppm) was confirmed. This shift has been observed for similar cage-shaped compounds.[17] The chemical shift $\delta(^{13}C)$ of the methine carbon of 1aB·THF was observed at 57.4 ppm (38.4 ppm for 1aH$_3$).[17] The ligated THF showed broadening and downfield-shifted signals at $\delta(^{1}H)$ = 4.46 and 2.13 ppm (free THF: $\delta(^{1}H)$ = 3.73 and 1.84 ppm). The boron NMR signals appeared at $\delta(^{11}B)$ = 5.52 ppm for 1aB·THF, while the open-shaped borate B(OPh)$_3$ appeared at 16.52 ppm.[18] Similar NMR chemical shifts were observed for the cage-shaped pyridine complex 1aB·Py. The chemical shifts for the methine moiety were $\delta(^{1}H)$ = 5.19 ppm, $\delta(^{13}C)$ = 57.9 ppm, and $\delta(^{11}B)$ = 4.45 ppm. The ligated pyridine showed downfield-shifted signals around $\delta(^{1}H)$ = 9.24, 8.20, and 7.78 ppm (free pyridine: $\delta(^{1}H)$ = 8.61, 7.61, and 7.28 ppm). Other cage-shaped complexes 1b-fB·L showed analogous chemical shifts for their ^{1}H, ^{13}C, and ^{11}B NMR spectra, as shown in Table 1. The order of the downfield shifts $\Delta\delta(^{1}H)$ of the ligated THF on 1a-dB as compared to free THF was as follows: 1bB·THF (4.85 and 2.35 ppm) > 1cB·THF (4.53 and 2.28 ppm) > 1dB·THF (4.52 and 2.26 ppm) > 1aB·THF (4.46 and 2.13 ppm). The sharper signals of the ligated THF were observed in the same order.[19] These results were probably due to the Lewis acidity of the cage-shaped borates. The number and type of halogen atoms precisely controlled the Lewis acidity; the magnitude of the effect on the enhancement of Lewis acidity was dibromo > monobromo > monofluoro > unsubstituted compounds on one phenyl

group in the cage-shaped borates.[20] For the *ortho*-phenyl substituted compound **1eB·THF**, the ligand THF showed a broadening and upfield-shifted signals around $\delta(^1\text{H})$ = 3.18 and 1.24 ppm. These results indicate that the ligated THF was surrounded by *ortho*-substituted phenyl rings and was affected by an anisotropic effect. Similar changes in the NMR chemical shifts were observed for the cage-shaped pyridine complex **1eB·Py**. The ligated pyridine showed upfield-shifted signals at $\delta(^1\text{H})$ = 7.77, 7.67 and 6.84 ppm. The *ortho*-naphthyl-substituted cage-shaped borate **1fB·L** exists as a mixture of conformational isomers owing to bulky substituents, and showed large upfield shifts for ligated THF (1.56 and 0.03 ppm) and pyridine (6.53 and 5.84 ppm; 6.20 and 5.49 ppm for 2- and 3-H, respectively).[21] For the silicon-bridging compound **1gB·THF**, the NMR data showed a characteristic shift for the Me group on Si. A downfield shift of $\delta(^1\text{H})$ of the Me group (0.95→1.06 ppm) and an upfield shift of $\delta(^{13}\text{C})$ (–3.0→–6.7 ppm) were confirmed relative to those of the ligand **1gH₃**. The ^{29}Si NMR spectrum showed an upfield chemical shift (–18.2→–21.3 ppm) relative to **1gH₃**. The ligated THF signals appeared in lower fields with a broadening ($\delta(^1\text{H})$ = 3.91 and 2.14 ppm) relative to those of free THF. The pyridine complex **1gB·Py** showed similar spectral changes with downfield-shifted pyridine signals ($\delta(^1\text{H})$ = 9.26, 8.16, and 7.75 ppm). Similar spectral data were obtained for the isobutyl derivatives **1hB·THF** and **1hB·Py**.

Table 1. NMR Chemical Shifts of the Cage-Shaped Borates.

Compounds	Ar₃CH		Ar₃SiCH			δ(^{11}B)
	δ(^{1}H)	δ(^{13}C)	δ(^{29}Si)	δ(^{1}H)	δ(^{13}C)	
1aH₃	6.07	38.4				
1bH₃	6.31	39.7				
1cH₃	6.03	37.9				
1dH₃	6.06	38.1				
1eH₃	6.46	38.3				
1fH₃	6.51	38.8				
1gH₃			–18.2	0.95	–3.0	
1hH₃			–19.8	1.50	22.2	
1aB·THF	5.13	57.4				5.52
1bB·THF	4.94	56.5				4.32
1cB·THF	4.88	55.8				5.13
1dB·THF	4.88	56.6				5.27
1eB·THF	5.37	58.2				5.04
1fB·THF	5.51	58.2				4.40
1gB·THF			–21.3	1.06	–6.7	7.11
1hB·THF			–24.4	1.73	18.8	5.87
1aB·Py	5.19	57.9				4.45
1bB·Py	5.01	57.0				4.12
1cB·Py	4.95	56.3				4.06
1dB·Py	4.95	57.1				4.19
1eB·Py	5.44	58.8				4.46
1fB·Py	5.58	58.8				3.54
1gB·Py			–21.1	1.08	–6.4	4.32
1hB·Py			–24.0	1.77	20.8	3.99
B(OPh)₃						16.52

X-ray Crystallographic Analysis of Cage-Shaped Borates: The pyridine complexes of cage-shaped borates 1a-hB·Py produced crystals of sufficient quality to be analyzed as single-crystal structures.[22] Selected crystal data and structural refinement parameters are shown in Table 2. The ORTEP drawings are shown in Figure 1. The selected bond lengths, angles, and tetrahedral character (THC)[23] of the boron atom are shown in Table 3. For 1aB·Py, boron has a distorted tetrahedral coordination sphere with average bond angles of O-B-O, 114.28° and N-B-O, 104.28°. This compound is the first example of a triphenolic methane-based mononuclear complex that acts as a Lewis acid.[24,25] The top view of 1aB·Py (Figure 2) clearly shows a nearly C_3-symmetric propeller shape. The aromatic rings deviate from a plane perpendicular to that of the three oxygen atoms (B-C_{bridge}-C-C = 19.28°), and, thus, the complex has a chirality that is caused by the cage shape.[26] A similar borate structure, with its phenolic rings connected to nitrogen, was reported, but its coordination to boron resulted in nearly perpendicular aromatic rings.[27] The bond length of B—N in 1aB·Py is 1.628(5) Å, and the sum of the angles for O-B-O and N-B-O around boron are 342.7° and 312.68°, respectively. The Br-substituted compounds 1bB·Py and 1cB·Py and F-substituted compound 1dB·Py have structures that are similar to 1aB·Py, and their THCs also are very similar, as shown in Table 3. The phenyl-substituted borate 1eB·Py has a longer B—N bond length (1.647(6) Å) with a larger Σ(O-B-O) angle (342.88°) and a smaller Σ(N-B-O) angle (312.28°) around boron, probably because of the steric hindrance of the *ortho*-phenyl groups. In the bulkier naphthyl-substituted borate 1fB·Py, the B—N bond length (1.631(8) Å) is less than that of 1eB·Py, presumably due to crystal-packing effects and/or a π-π interaction between the pyridine and naphthyl rings. A silicon-based compound with a pyridine-ligand 1gB·Py was also analyzed by X-ray crystallography. The larger size of the bridging Si atom resulted in longer Si—aryl bonds (average 1.870 Å) in 1gB·Py than the C—aryl bonds (average 1.519 Å) in 1aB·Py, and, therefore, it directly affected the geometry of the cage. The boron has a distorted tetrahedral coordination sphere and the Σ(O-B-O) and Σ(N-B-O) bond angles are 343.1° and 311.88°, respectively, while the angles of 1aB·Py are 342.7° and 312.68°, respectively. The geometries around boron in 1gB·Py and 1aB·Py were nearly identical, but that of 1gB·Py was more planar. The B—N bond length in 1gB·Py is 1.655(5) Å, which is longer than that in 1aB·Py. This geometry suggests that 1gB·Py has a lower Lewis acidity than 1aB·Py. It is worth noting that the silicon atom in 1gB·Py has an almost tetrahedral structure (Σ(Ar-Si-Ar); 330.38°), while the carbon atom at the bottom of 1aB·Py has a distorted structure with the sum of bond angles that equaled 343.78°. The *i*BuSi-bridging borate 1hB·Py was also analyzed by X-ray crystallography, and has a framework similar to that of 1gB·Py. The sum of the bond angles for 1gB·Py are as follows: Σ(O-B-O), 342.58°; Σ(N-B-O), 312.68°; Σ(Ar-Si-Ar), 328.08°. The average Si—aryl bond length for 1gB·Py is 1.879 Å.

Table 2. X-ray Data for All Crystallographically Characterized Complexes.

	1aB·Py	**1b**B·Py	**1c**B·Py	**1d**B·Py
chemical formula	$C_{24}H_{18}BNO_3$	$C_{24}H_{12}BBr_6NO_3$	$C_{24}H_{15}BBr_3NO_3$	$C_{24}H_{15}BF_3NO_3$
formula weight	379.22	852.60	615.91	433.19
space group	$Pbca$	$Pbca$	$P2_1/n$	$P\text{-}1$
μ(Mo-K) (mm^{-1})	0.087	9.290	5.436	0.116
a(Å)	14.8638(6)	9.2617(3)	10.4648(10)	8.5360(4)
b(Å)	15.4624(6)	22.1780(6)	10.6734(12)	10.5824(4)
c(Å)	16.3768(6)	25.3996(7)	20.055(2)	12.5929(5)
α(deg)	-	-	-	64.1478(12)
β(deg)	-	-	92.540(3)	71.7351(13)
γ(deg)	-	-	-	83.6755(13)
V_c (Å^3)	3763.9(2)	5217.2(3)	2237.8(4)	971.65(7)
Z	8	8	4	2
$R1$	0.0677	0.0828	0.0414	0.0402
$wR2$	0.1602	0.0859	0.0988	0.0636

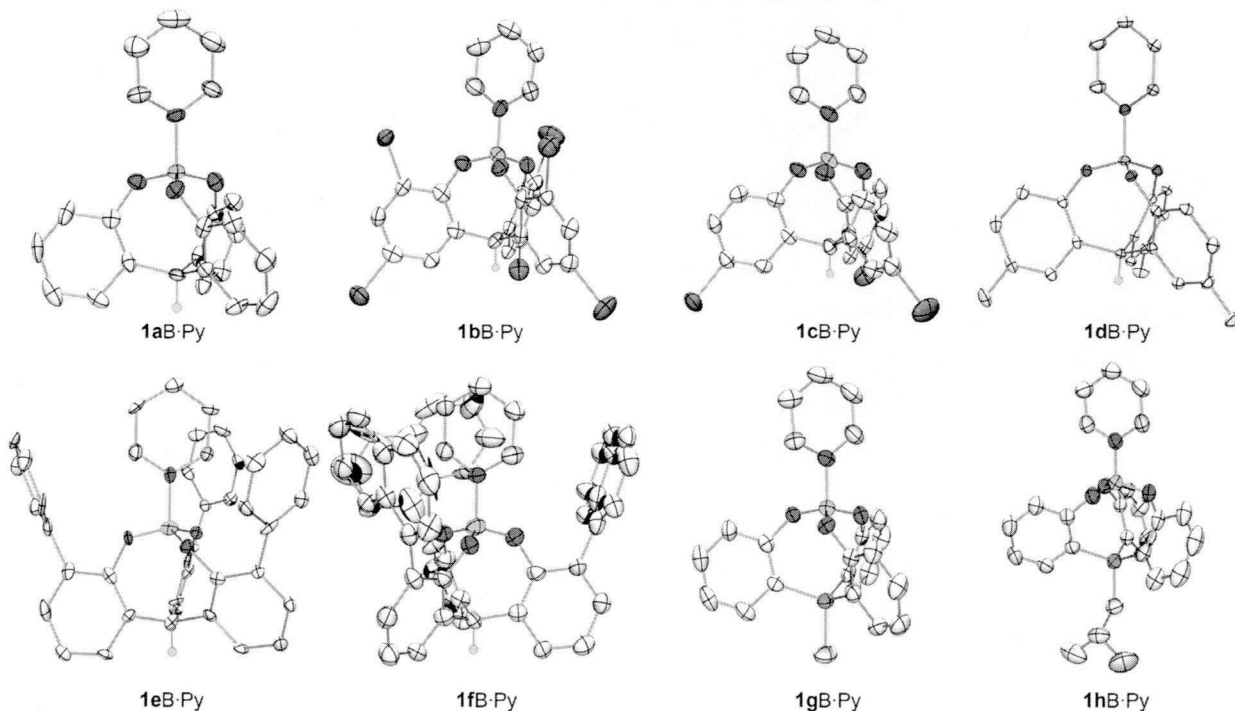|	**1e**B·Py	**1f**B·Py	**1g**B·Py	**1h**B·Py
chemical formula	$C_{42}H_{30}BNO_3$	$C_{54}H_{36}BNO_3$	$C_{24}H_{20}BNO_3Si$	$C_{27}H_{26}BNO_3Si$
formula weight	607.51	757.69	409.32	451.40
space group	$P\text{-}1$	$P2_12_12_1$	$P2_1/n$	$Pbca$
μ(Mo-K) (mm^{-1})	0.082	0.619	0.142	0.126
a(Å)	10.0002(10)	13.2269(2)	9.19210	9.1369(3)
b(Å)	10.2302(9)	13.3959(3)	15.3839(2)	20.4629(5)
c(Å)	16.9575(16)	21.9181(12)	14.4803(4)	25.7290(6)
α(deg)	100.935(3)	-	-	-
β(deg)	106.528(3)	-	98.4086(15)	-
γ(deg)	107.048(3)	-	-	-
V_c (Å^3)	1517.8(2)	3883.59(12)	2025.65(6)	4810.5(2)
Z	2	4	4	8
$R1$	0.0335	0.0732	0.0803	0.0462
$wR2$	0.0689	0.1177	0.0906	0.0553

Figure 1. ORTEP Drawings of Cage-Shaped Borates **1**B·Py (Some hydrogen atoms are omitted for clarity).

9

Table 3. Selected Bond Lengths and Angles, and THCs for the Cage-Shaped Borates.

		1aB·Py	**1b**B·Py	**1c**B·Py	**1d**B·Py	**1e**B·Py	**1f**B·Py	**1g**B·Py	**1h**B·Py
Length (Å)	B-O	1.432(4)	1.392(12)	1.439(7)	1.436(2)	1.417(5)	1.438(7)	1.426(5)	1.432(5)
	B-O	1.440(5)	1.450(11)	1.443(8)	1.452(2)	1.441(5)	1.440(8)	1.437(5)	1.437(4)
	B-O	1.457(5)	1.451(11)	1.452(8)	1.453(2)	1.462(6)	1.456(8)	1.445(6)	1.447(4)
	Average	1.443	1.431	1.445	1.447	1.440	1.445	1.436	1.439
	B-N	1.628(5)	1.619(13)	1.611(9)	1.626(2)	1.647(6)	1.631(8)	1.655(5)	1.645(5)
	B-C$_{bridge}$	2.979(5)	2.992(13)	3.025(9)	3.010(2)	2.984(7)	2.990(8)	-	-
	B-Si$_{bridge}$	-	-	-	-	-	-	3.158(5)	3.159(4)
	Ar$_3$C-H	0.95(3)	0.950(8)	0.951(5)	0.898(1)	0.950(4)	0.950(5)	-	-
	Ar$_3$Si-C	-	-	-	-	-	-	1.857(6)	1.879(3)
	Ar-C	1.515(4)	1.477(12)	1.521(8)	1.530(2)	1.528(4)	1.508(8)	-	-
	Ar-C	1.517(5)	1.503(11)	1.526(8)	1.530(3)	1.536(6)	1.535(7)	-	-
	Ar-C	1.525(4)	1.514(11)	1.529(8)	1.531(2)	1.546(5)	1.538(7)	-	-
	Average	1.519	1.498	1.525	1.530	1.537	1.527	-	-
	Ar-Si	-	-	-	-	-	-	1.864(3)	1.873(3)
	Ar-Si	-	-	-	-	-	-	1.872(4)	1.882(3)
	Ar-Si	-	-	-	-	-	-	1.874(3)	1.882(3)
	Average	-	-	-	-	-	-	1.870	1.879
Angle (degree)	O-B-O	113.4(3)	113.2(7)	112.2(5)	112.3(1)	112.1(4)	113.0(5)	114.2(3)	113.6(3)
	O-B-O	113.7(3)	114.2(7)	113.8(5)	113.1(1)	115.0(4)	113.2(5)	114.4(3)	114.4(3)
	O-B-O	115.6(3)	114.3(7)	114.0(5)	115.1(1)	115.7(4)	115.0(5)	114.5(3)	114.5(3)
	Total	342.7	341.7	340.0	340.5	342.8	341.2	343.1	342.5
	N-B-O	102.3(3)	103.4(7)	104.4(5)	104.2(1)	103.0(4)	104.2(4)	102.7(3)	102.7(3)
	N-B-O	104.4(3)	104.5(7)	105.3(5)	105.1(1)	103.9(4)	104.7(4)	104.1(3)	104.6(3)
	N-B-O	105.9(3)	105.7(7)	106.1(5)	106.0(1)	105.3(4)	105.4(4)	105.0(3)	105.3(3)
	Total	312.6	313.6	315.8	315.3	312.2	314.3	311.8	312.6
Torsion (degree)	B-C$_{bridge}$-C-C	16.7(3)	17.3(7)	19.2(5)	19.3(1)	14.8(4)	17.5(5)	-	-
	B-C$_{bridge}$-C-C	19.5(3)	17.7(8)	19.8(6)	19.8(1)	16.9(4)	17.5(5)	-	-
	B-C$_{bridge}$-C-C	21.6(3)	20.4(7)	22.6(5)	22.2(1)	17.3(4)	20.0(5)	-	-
	Average	19.3	18.5	20.5	20.4	16.3	18.3	-	-
	B-Si$_{bridge}$-C-C	-	-	-	-	-	-	16.4(3)	19.9(2)
	B-Si$_{bridge}$-C-C	-	-	-	-	-	-	17.3(3)	21.5(2)
	B-Si$_{bridge}$-C-C	-	-	-	-	-	-	17.8(3)	22.1(2)
	Average	-	-	-	-	-	-	17.2	21.2
THC (%)	boron	67	69	73	72	66	70	65	67
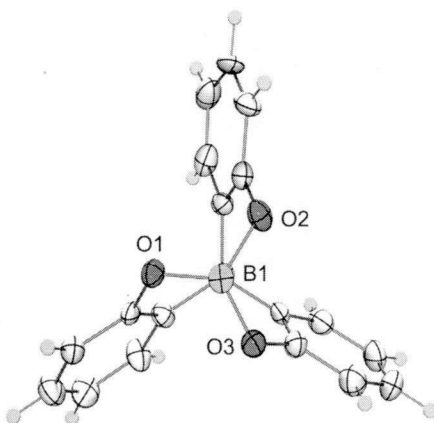
Figure 2. ORTEP Drawing of **1a**B·Py. Top View (Pyridine is omitted for clarity).

Lewis Acidity of the Cage-Shaped Borates: To investigate the ability of the cage-shaped borates 1B to activate carbonyl compounds, we synthesized their complexes with the 2,6-dimethyl-γ-pyrone **5**. A $\Delta\delta(^{13}C)$ shift of C3 in **5** clearly shows the degree of Lewis acidity. These data provide an estimate of the Lewis acidity that is more precise than the chemical shift of ligated THF coordinated to boron, as discussed above in the section on NMR data for cage-shaped borates. The $\Delta\delta(^{13}C)$ shifts of C3 in **5** are shown in Table 4 for various borates. For comparison with other Lewis acids, the planar borate $B(OPh)_3$ and the strong Lewis acid $BF_3 \cdot OEt_2$ were also employed. In fact, the complexation of **5** with $BF_3 \cdot OEt_2$ showed the largest downfield shift ($\Delta\delta(^{13}C)$ = +8.708 ppm) in C3 (entry 10), and $B(OPh)_3$ showed only a small chemical shift ($\Delta\delta(^{13}C)$ = +0.774 ppm) (entry 9). It is worth noting that all cage-shaped borates 1B showed a Lewis acidity that lay between that of $B(OPh)_3$ and $BF_3 \cdot OEt_2$. The unsubstituted borate 1aB showed a downfield shift of +6.782 ppm (entry 1). The introduction of an electron-withdrawing group onto the aryl rings in cage-shaped borates allowed for precise control of the Lewis acidity. Introduction of F onto the aryl rings of the cage-shaped borate 1dB resulted in a higher Lewis acidity than that observed for the unsubstituted borate 1aB (entry 4). The *p*-Br-substituted compound 1cB had a higher Lewis acidity (entry 3) than 1dB, and the highest Lewis acidity among the cage-shaped borates 1B was observed for the *o*- and *p*-Br-substituted compound 1bB (entry 2). This shift corresponds to the chemical shifts observed for the ligated THF discussed above. Interestingly, replacement of the bridgehead C with a bridgehead Si decreased the Lewis acidity. The silicon-bridging compounds 1gB and 1hB showed smaller downfield shifts of the pyrone, +5.844 and +4.519 ppm (entries 7 and 8), respectively, than that of the carbon-bridging compound 1aB (+6.782 ppm). The strength of the Lewis acidity based on the measurement of $\Delta\delta(^{13}C)$ was: BF_3 > 1bB > 1cB > 1dB > 1aB > 1gB > 1hB > $B(OPh)_3$. The Lewis acidities of 1eB and 1fB could not be estimated by using this $\Delta\delta(^{13}C)$ measurement method, because the *ortho*-aryl groups had a significant anisotropic effect on the chemical shifts of ligated **5**. Table 4 describes the fine-tuning of Lewis acidity using the new cage-shaped template over a range of moderate Lewis acidity that would be useful for catalysts.

Table 4. Complexation of Boron Compounds with the Carbonyl Compound **5**. [B] = Complexed Boron Compound.

entry	B compound	$\Delta\delta(^{13}C)$ of C3/ ppm
1	1aB·THF	+6.782
2	1bB·THF	+7.630
3	1cB·THF	+7.605
4	1dB·THF	+7.243
5	1eB·THF	+5.564
6	1fB·THF	+3.877
7	1gB·THF	+5.844
8	1hB·THF	+4.519
9	$B(OPh)_3$	+0.774
10	$BF_3 \cdot OEt_2$	+8.708

Theoretical Calculations: The characteristic properties of cage-shaped borates **1B** were investigated by theoretical calculations. Optimized structures and unoccupied molecular orbitals contributing to the Lewis acidity of the cage-shaped borates **1B** and the open-shaped borate $B(OPh)_3$ are shown in Figure 3. Some of the calculated data are shown in Table 5. The optimized structures of the cage-shaped borates **1B** show that the geometries around the boron centers are nearly planar, and the sums of the three O-B-O angles are nearly 360° in each case (Figure 3 and Table 5). Figure 3 also shows the molecular orbital (MO) diagram of unoccupied MOs[28] of the cage-shaped borates **1a-dB**, **1gB**, and **1hB**, and the open-shaped borate $B(OPh)_3$. The cage-shaped borates include a large and accessible lobe on boron, while the corresponding lobe in $B(OPh)_3$ (LUMO in this case) is small and buried. From the optimized borate structures, we observe that the bridgehead atom significantly affects the cage structure —for example, the dihedral angle $(C_{ipso}\text{-O-B-O})$ θ (Table 5). The bridgehead atoms, either carbon or silicon, control the dihedral angles $(C_{ipso}\text{-O-B-O})$ θ (**1aB** 48.4°; **1gB** 45.4°; **1hB** 43.6°; entries 1, 5 and 6). As the angles become smaller, the cage-shaped borates showed the lower energy levels of the unoccupied MOs[29] of Lewis acids. Their eigenvalues are on the order of **1aB** < **1gB** < **1hB**. In fact, the open-shaped borate $B(OPh)_3$ has a nearly planar structure (small dihedral angle, $\theta = 2.0°$) and a high eigenvalue (entry 7). To examine the correlation between the dihedral angle and the eigenvalue of the corresponding MO, a series of theoretical calculations were carried out. The change of the eigenvalue could be traced by changing the dihedral angle (H-O-B-O) θ under the constraints on the geometry around the boron center (planar structure in sp^2 hybridization) (Scheme 5). The angle of $\theta = 0°$ gave the highest MO energy level because of the effective conjugation between the p orbitals on O and B. Gradual changes in the MO level can be realized by varying θ, even with three B−O bonds, by keeping the structure in-plane. These results show that the dihedral angle θ controls the overlap between the p orbitals on O and B, which allows fine-tuning of the MO energy level. While the differences among the carbon-bridging borates **1a-dB** are minimal ($\theta \approx 47\text{-}48°$; entries 1-4), the energy levels of the unoccupied MOs[29] that contribute to the Lewis acids are controlled by the electronic factors of the substituents on the aryl rings. The eigenvalues are on the order of **1bB** < **1cB** < **1dB** < **1aB**. It is understandable that electron-withdrawing groups lead to favorable interactions between the borates and the Lewis basic substrates. In total, the order of the eigenvalues is **1bB** < **1cB** < **1dB** < **1aB** < **1gB** < **1hB** < $B(OPh)_3$. The pyridine complexation energies, ΔE, also showed the same order. Thus, we were able to fine-tune the Lewis acidity of the borates by structural and electronic controls. The Lewis acidity data were highly consistent with the experimental NMR data for pyrone **5**.
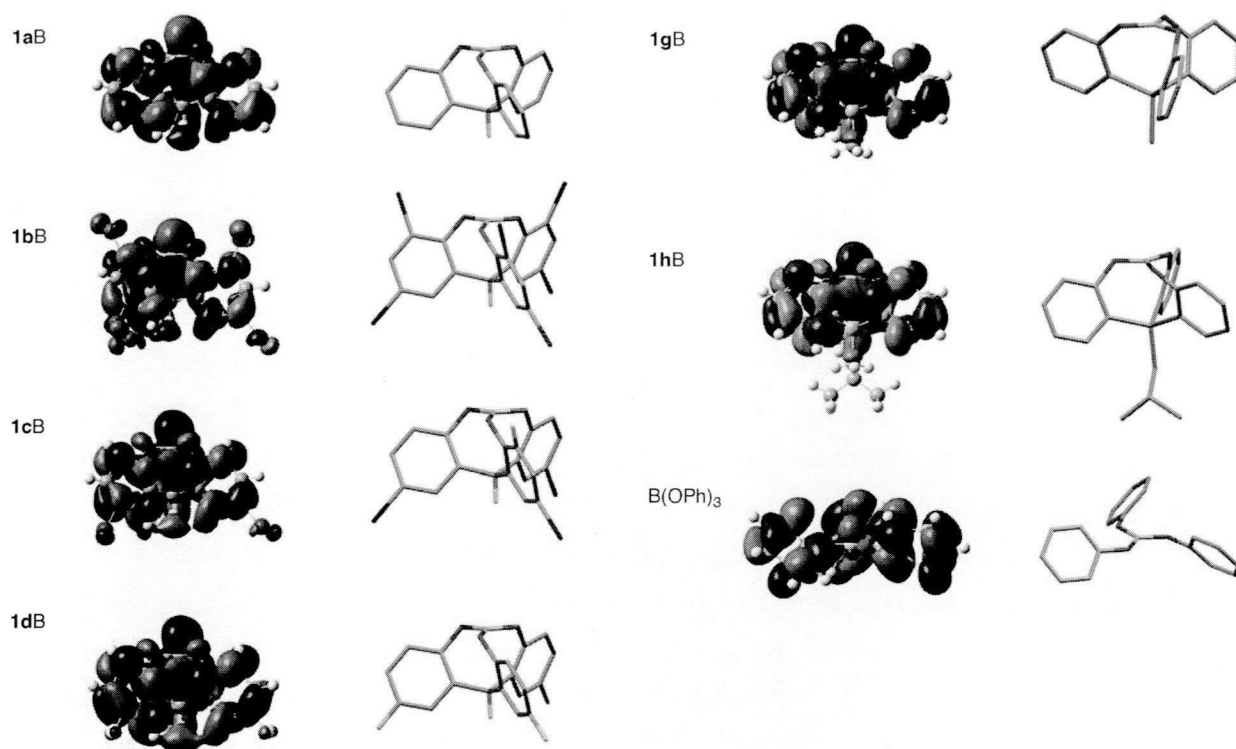
Figure 3. Optimized Structures and Unoccupied MO Diagrams of Cage-Shaped and Open-Shaped Borates.

Table 5. Theoretical Calculations for Borates.

entry	borate	Σ(O-B-O)	dihedral angle (C-O-B-O)	eigenvalue (eV)[a]	ΔE in pyridine –complexation (kcal/mol)
1	**1aB**	359.7°	48.4°	-0.79	-19.2
2	**1bB**	359.4°	46.6°	-1.67	-31.4
3	**1cB**	359.6°	48.1°	-1.31	-22.5
4	**1dB**	359.6°	47.5°	-1.12	-20.8
5	**1gB**	360.0°	45.4°	-0.73	-13.2
6	**1hB**	359.9°	43.6°	-0.71	-13.1
7	B(OPh)$_3$	360.0°	2.0°	-0.54	-5.0
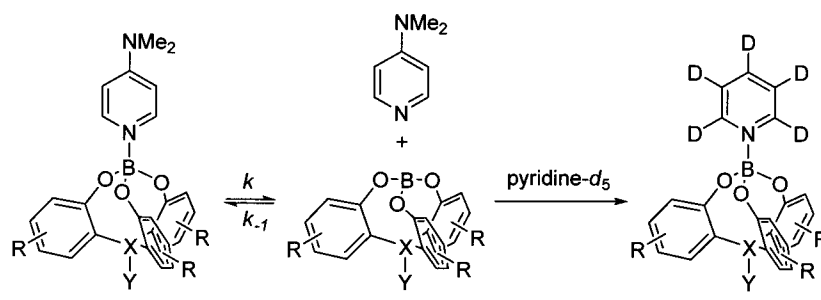
[a] Eigenvalues of MOs depicted in Figure 3.

Scheme 5. Relationship between the Dihedral Angle θ and the Energy Level of the Lowest Unoccupied MO Relative to a Lewis Acid.

13
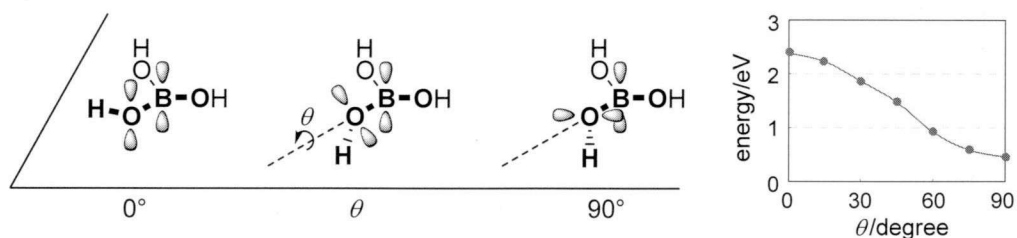
Ligand Exchange Rate of Cage-Shaped Borates: The ligand exchange rate of the cage-shaped borates 1B was investigated to obtain information on the kinetics of the ligand association-dissociation process that controls a Lewis acid catalyst reaction. Dimethylaminopyridine (DMAP) complexes of 1B were dissolved in pyridine-d_5, and the ligand dissociation rate was measured during ligand exchange from DMAP to pyridine. The results are shown in Table 6. The unsubstituted cage-shaped borate 1aB has a dissociation rate constant of $k = 2.32 \times 10^{-9}$ s^{-1}, whereas that for the fluoro-substituted compound 1dB is smaller ($k = 8.37 \times 10^{-12}$ s^{-1}; entries 1 and 2). The activation enthalpy $\Delta H^{\ddagger}$ of 1dB is much larger than that of 1aB, because the electron-withdrawing effect of fluorine increased the Lewis acidity of the boron center by stabilization of the negative charge generated during complexation. For 1eB, which has sterically demanding ortho-phenyl substituents, a decrease in the rate constant ($k = 1.16 \times 10^{-9}$ s^{-1}) is also observed (entry 3). The activation entropy $\Delta S^{\ddagger}$ of 1eB is much lower than that of 1aB, although the activation enthalpy is nearly identical. The steric repulsion caused by the bulky ortho-substituents during ligand dissociation controls the entropic effect. The electronic factor controls the ligand exchange rate by changing $\Delta H^{\ddagger}$, and the steric factor influences the rate with different $\Delta S^{\ddagger}$. It is worth noting that the silicon-bridging compound 1gB has a low $\Delta G^{\ddagger}$, mainly due to a lower $\Delta H^{\ddagger} = 26.4$ kcal mol^{-1} (entry 4). This result shows that the geometry of the cage shape is an important determinant of the character of a Lewis acid catalyst.

Table 6. Kinetic Parameters for Ligand Dissociation of the Cage-Shaped Borates 1B.

entry	borate	$\Delta H^{\ddagger}$ (kcal/mol)	$\Delta S^{\ddagger}$ (cal/K·mol)	$\Delta G^{\ddagger}$ (kcal/mol)[a]	k (s^{-1})[a]
1	1aB·L	35.1	22.3	28.6	2.32 x 10^{-9}
2	1dB·L	43.6	40.0	31.9	8.37 x 10^{-12}
3	1eB·L	31.2	7.5	29.0	1.16 x 10^{-9}
4	1gB·L	26.4	14.2	22.3	1.28 x 10^{-4}

[a] $\Delta G^{\ddagger}$ and k are calculated at $t = 20$ °C.

Catalytic Activity of Cage-Shaped Borates of Organic Transformation: The cage-shaped borates were applied as catalysts in the hetero Diels-Alder reaction of the Danishefsky's diene 6 with benzaldehyde (7a); the results are shown in Table 7.[30] For a Lewis acid catalyst, the balance between the Lewis acidity and the ability to exchange ligands is important.[31] In fact, both the weak Lewis acid B(OPh)$_3$ and the strong Lewis acid BF$_3$·OEt$_2$ gave low yields (entries 8 and 9). The cage-shaped borates

1B afforded higher yields (entries 1-7), because of their moderate Lewis acidity. The unsubstituted cage-shaped borate 1aB·THF gave the cycloaddition product 8a in 77% yield. The halogen-substituted cage-shaped borates yielded the product on the order of 1dB > 1cB > 1bB. This result suggests that a Lewis acidity that is too high leads to a strong affinity between the boron center and the product, which reduces the catalytic turnover. The silicon-bridging borate 1gB·THF was the best catalyst for the hetero Diels-Alder reaction, giving the product in 85% yield (entry 7). In this case, the Lewis acidity of the borate 1gB was slightly lowered by bridgehead-control, which promotes release of the product, contributing to an increase in catalytic activity. The phenyl-substituted borate 1eB gave the product in satisfactory yield (entry 5).

Table 7. Hetero Diels-Alder Reaction Catalyzed by Various Borates.

entry	borate	yield/ %
1	1aB·THF	77
2	1bB·THF	14
3	1cB·THF	25
4	1dB·THF	29
5	1eB·THF	77
6	1fB·THF	65
7	1gB·THF	85
8	B(OPh)$_3$	7
9	BF$_3$·OEt$_2$	<5

The Mukaiyama aldol reaction[32,33] was also examined using the ketene silyl acetal 9 substituted with methyls at the terminal olefinic moiety, as shown in Table 8. In contrast to the results of a hetero Diels-Alder reaction, the appropriate Lewis acid was the dibromo-substituted cage-shaped borate 1bB, while the unsubstituted borate 1aB was ineffective (entries 1 and 2). In this case, the activation step, rather than the catalyst-regeneration process (releasing step), was more important in the catalytic cycle. Interestingly, a relatively high yield of the product 11 was obtained by using the phenyl-substituted borate 1eB (entry 5). The open-shaped borate catalyst showed no catalytic activity (entry 8), and the strong Lewis acid afforded very low yields (entry 9). When the unsubstituted silyl nucleophile 10 was used, 1bB also afforded the product 12 in high yield (entry 11), and the cage-shaped borates also worked well. It should be noted that different reactions had different suitable catalysts, even among the cage-shaped borate catalysts.

Table 8. Mukaiyama Aldol Reaction Using Aldehyde Catalyzed by Various Borates.

9, 11: R¹, R², Si = Me, Me, Me₃Si
10, 12: R¹, R², Si = H, H, BuᵗMe₂Si
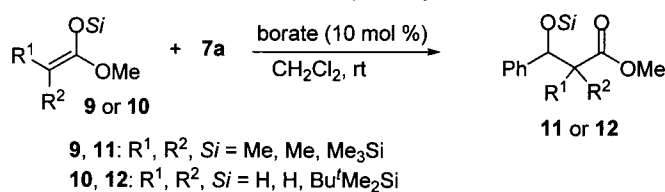
entry	nucleophile	time/h	borate	product	yield/ %
1	9	6	1aB·THF	11	<5
2	9	6	1bB·THF	11	98
3	9	6	1cB·THF	11	17
4	9	6	1dB·THF	11	<5
5	9	6	1eB·THF	11	69
6	9	6	1fB·THF	11	90
7	9	6	1gB·THF	11	20
8	9	6	B(OPh)₃	11	<5
9	9	6	BF₃·OEt₂	11	9
10	10	4	1aB·THF	12	30
11	10	4	1bB·THF	12	91
12	10	4	1cB·THF	12	50
13	10	4	1dB·THF	12	43
14	10	4	1eB·THF	12	67
15	10	4	1fB·THF	12	54
16	10	4	1gB·THF	12	31
17	10	4	B(OPh)₃	12	26
18	10	4	BF₃·OEt₂	12	8

In the case of the Mukaiyama aldol reaction that used the acetal **13** as an electrophile,[34] the dibromo- and monobromo-substituted borates **1bB** and **1cB** gave high yields among the series of cage-shaped borate catalysts (Table 9, entries 2 and 3). The phenyl- and naphthyl-substituted borates **1eB** and **1fB** did not give the product, probably because steric hindrance prevented the approach of the bulky electrophile **13** (entries 5 and 6). Based on these results, we thought that the *ortho*-aryl substituted cage-shaped borates **1eB** and **1fB** recognized the bulkiness of the substrates.

Table 9. Mukaiyama Aldol Reaction Using Acetal Catalyzed by Various Borates.

entry	borate	yield/ %
1	1aB·THF	8
2	1bB·THF	62
3	1cB·THF	61
4	1dB·THF	17
5	1eB·THF	<5
6	1fB·THF	<5
7	1gB·THF	<5
8	B(OPh)₃	<5
9	BF₃·OEt₂	31

We next investigated the generality of the aldehydes in the hetero Diels-Alder reaction using the cage-shaped borates **1aB** and **1eB** at room temperature for 4 h (Table 10). The reaction of **6** with benzaldehyde **7a** gave the product **8a** in 72% yield in the presence of a catalytic amount of **1aB** (entry 1). The substituted aldehydes **7b** and **7c** also gave the products, although a small decrease in yields was observed because of the steric effects of the *ortho*-substituents (entries 3 and 5). The aliphatic aldehydes **7d-g** were also applied to this catalytic reaction system to give the corresponding products **8d-g** (entries 7, 9, 11, and 13). Unexpectedly, the use of phenyl-substituted borate **1eB** showed almost the same results in the hetero Diels-Alder reaction as use of **1aB**, in spite of the bulky *ortho*-phenyl groups in **1eB**.

Table 10. Hetero Diels-Alder Reaction Catalyzed by Two Types of Borates: 1aB·THF and 1eB·THF.

entry	aldehyde		borate	product	yield of 8/ %
1		7a	1aB·THF	8a	72
2		7a	1eB·THF	8a	74
3		7b	1aB·THF	8b	64
4		7b	1eB·THF	8b	64
5		7c	1aB·THF	8c	53
6		7c	1eB·THF	8c	67
7		7d	1aB·THF	8d	54
8		7d	1eB·THF	8d	61
9		7e	1aB·THF	8e	56
10		7e	1eB·THF	8e	63
11		7f	1aB·THF	8f	76
12		7f	1eB·THF	8f	65
13		7g	1aB·THF	8g	38
14		7g	1eB·THF	8g	42

A careful comparison between **1aB** and **1eB** was performed by competitive reaction using a mixture of the benzaldehyde (**7a**) and *o*-phenylbenzaldehyde (**7c**) (Table 11). When the unsubstituted borate **1aB** in dichloromethane was used as the catalyst for the competitive reaction, the product ratio of **8a/8c** was 1.1 (= 52:48; entry 1). In contrast, when the phenyl-substituted borate **1eB** was used, the product ratio was 3.6 (= 78:22), and, therefore, the selectivity was increased 3.27-fold (entry 2). This result can be

explained by the steric effects of the *ortho*-phenyl substituent that prevented access of the bulky substrate to the metal center.[35,36] The use of **1eB** with acetonitrile as the solvent showed a 6.49-fold increase of the ratio compared to **1aB** (entries 3 and 4). The coordinative solvent somewhat retarded complexation with the substrate aldehyde, and, hence, the selectivity was enhanced. Notably, the naphthyl-substituted borate **1fB** gave a much higher value of 12.8 (13.2-fold greater than **1aB**) due to effective steric hindrance for substrate-selectivity (entries 3 and 5). The cage-shaped borates provide steric hindrance due to their inflexible structure; therefore, they effectively controlled the substrate-selective reaction system, as shown in Table 11.

Table 11. Competitive reaction of the Danishefsky diene with two types of aldehyde **7a** and **7c** catalyzed by the borates **1aB·THF**, **1eB·THF**, or **1fB·THF**.[a]
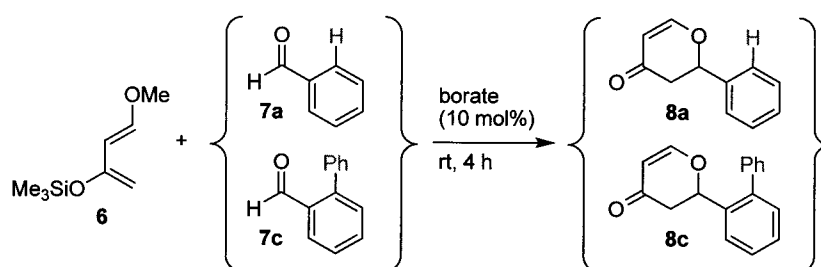
entry	borate	solvent	yield/%	ratio (8a/8c)
1	1aB·THF	CH$_2$Cl$_2$	86	1.1 ⎤ *x 3.27*
2	1eB·THF	CH$_2$Cl$_2$	87	3.6 ⎦
3	1aB·THF	acetonitrile	67	0.97 ⎤ *x 6.49* ⎤
4	1eB·THF	acetonitrile	73	6.3 ⎦ ⎮ *x 13.2*
5	1fB·THF	acetonitrile	69	12.8 ⎦

[a] The reactions were carried out using **6** (1.0 mmol), **7a** (1.0 mmol), **7c** (1.0 mmol), and borate catalyst (0.1mmol).

1-1-3. Conclusion

We have synthesized cage-shaped borates with a tris(*o*-oxyphenyl)methane or -silane moiety, with various substituents. The cage shape resulted in a novel boron center, which is a unique Lewis acid. Both the Lewis acidity and the catalytic activity of organic transformation were successfully enhanced. A moderate Lewis acidity was attained by tuning factors such as the substituents (electronic and steric control) and the bridgehead atoms (geometric control). Theoretical calculations suggested that the energy levels of the unoccupied molecular orbitals, which greatly contributed to activation of the substrate, are finely tuned by the substituent effect and the cage geometry. The *ortho*-aryl substituents on the cage-shaped borate controlled the selectivity of the competitive reaction between sterically different aldehydes. The cage-shaped template can be modified in many ways by altering either the geometry[37] or the substituents, and it is a promising template for other metal complexes to be used in catalysts, new metal complexes, or materials.

1-1-4. Experimental Section

General Procedures. IR spectra were recorded as thin films or as solids in KBr pellets on a HORIBA FT-720 spectrophotometer. ^{1}H, ^{13}C, and ^{29}Si NMR spectra were obtained with a 400, 100, and 78.7 MHz spectrometer, respectively, with TMS as internal standard. ^{11}B NMR spectra were obtained with a 127 MHz spectrometer with $BF_3 \cdot OEt_2$ as external standard. Mass spectra were recorded on a JEOL JMS-DS303. All reactions were carried out under nitrogen. Synthesis of boron complexes was performed in nitrogen-filled glove box. The crystals of **1a-hB·Py** are prepared in nitrogen-filled glove box.[38]

Materials. Dehydrated dichloromethane, THF and hexane were purchased and used as obtained. The compound **1aH₃**, **1gH₃**, **1hH₃**, **3a**, **4a**, **4g** and **4h** were prepared according to our previous report.[7] The borates **1aB·L**, **1gB·L** and **1hB·L** (L = THF or Py) were prepared according to our previous report.[7] The compound **2f**[39] were prepared by known methods. All other reagents are commercially available. The product **8a**[40], **8b**[40], **8d**[41], **8e**[30a], **8f**[40] and **8g**[42] in Table 7, 10 and 11 are known in the literature. The product **11**[43], **12**[44] in Table 8 are known in the literature. The product **14**[44] in Table 9 is known in the literature.

Tris(3,5-dibromo-2-hydoxyphenyl)methane (1bH₃)
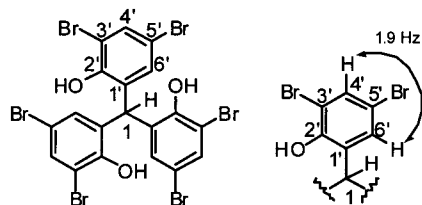
To a solution of tris(2-hydoxyphenyl)methane (1.168 g, 4 mmol) in 40 mL of CCl_4 was added 32 mL of glacial acetic acid and bromine (5 g, 32 mmol). The orange/red mixture was stirred at ambient temperature for 16 h before it was slowly poured into $Na_2S_2O_5$ aq (0.4 M, 125 mL). The aqueous layer was extracted with CH_2Cl_2 (3 x 50 mL), the combined organic extracts were washed with H_2O (3 x 100 mL), dried over $MgSO_4$ and concentrated in vacuo. The crude material was recrystallized from a acetone/hexane mixture, affording the product as a white solid (2.84 g, 93%). mp: 278-280 °C; ^{1}H NMR: (400 MHz, DMSO-d_6) 9.56 (s, 3H, OH), 7.66 (d, J = 1.9 Hz, 3H, 4'-H), 6.65 (d, J = 1.9 Hz, 3H, 6'-H), 6.29 (s, 1H, 1-H); ^{13}C NMR: (100 MHz, DMSO-d_6) 151.1 (s, C-2'), 133.6 (s, C-1'), 133.1 (d, C-4'), 130.6 (d, C-6'), 112.4 (s, C-5'), 111.1 (s, C-3'), ca.40 (obscured by DMSO but confirmed by HMQC); IR (KBr) 3410 (OH) cm^{-1}; MS: (EI, 70 eV) m/z 771 (M$^+$ + 12, 3), 769 (M$^+$ + 10, 14), 767 (M$^+$ + 8, 36), 765 (M$^+$ + 6, 49), 763 (M$^+$ + 4, 38), 761 (M$^+$ + 2, 16), 759 (M$^+$, 3), 435 (M$^+$ - C_6H_7 $Br_2O_3^+$, 99), 433 (M$^+$ - C_6H_9 $Br_2O_3^+$, 100); HRMS: (EI, 70 eV) calculated for ($C_{19}H_{10}Br_6O_3$) 759.5730 (M$^+$) found for m/z 759.5723. Analysis: calculated for $C_{19}H_{10}Br_6O_3$: C, 29.80; H, 1.32; Br, 62.61; found: C, 29.73; H, 1.47; Br, 62.65
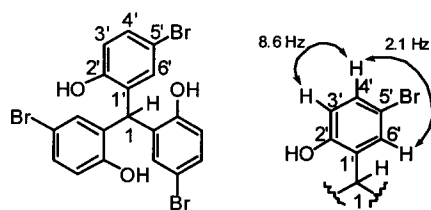
Tris(5-bromo-2-methoxyphenyl)methane (4c)
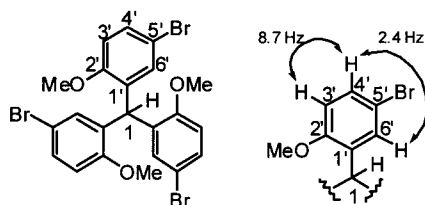
To a solution of tris(2-methoxyphenyl)methane (2.672 g, 8 mmol) in 80 mL of CCl_4 was added 64 mL of glacial acetic acid and bromine (10 g, 62.5 mmol). The orange/red mixture was stirred at ambient temperature for 16 hours before it was slowly poured into $Na_2S_2O_5$ aq (0.4 M, 250 mL). The aqueous layer was extracted with CH_2Cl_2 (3 x 100 mL), the

combined organic extracts were washed with H$_2$O (3 x 100 mL), dried over MgSO$_4$ and concentrated in vacuo. The crude material was recrystallized from a acetone/hexane mixture, affording the product as a white solid (4.25 g, 93%). mp: 233-234 °C; ^{1}H NMR: (400 MHz, CDCl$_3$) 7.32 (dd, J = 8.7, 2.4 Hz, 3H, 4'-H), 6.78 (d, J = 2.4 Hz, 3H, 6'-H), 6.74 (d, J = 8.7 Hz, 3H, 3'-H), 6.20 (s, 1H, 1-H), 3.67 (s, 9H, OMe); ^{13}C NMR: (100 MHz, CDCl$_3$) 156.2 (s, C-2'), 133.3 (s, C-1'), 131.9 (d, C-6'), 130.5 (d, C-4'), 112.7 (s, C-5'), 112.5 (d, C-3'), 55.9 (q, OMe), 37.4 (d, C-1); IR (KBr) 1246 (OMe), 1115 (OMe), 1026 (ArBr) cm^{-1}; MS: (EI, 70 eV) m/z 574 (M$^+$ + 6, 34), 572 (M$^+$ + 4, 100), 570 (M$^+$ + 2, 99.6), 570 (M$^+$, 34), 201 (M$^+$ - C$_{14}$H$_{11}$Br$_2$O$_2$ + 2, 83), 199 (M$^+$ - C$_{14}$H$_{11}$Br$_2$O$_2$, 86), 121 (M$^+$ - C$_{14}$H$_{10}$ Br$_3$O$_2$$^+$, 54); HRMS: (EI, 70 eV) calculated for (C$_{22}$H$_{19}$Br$_3$O$_3$) 567.8884 (M$^+$) found for m/z 567.8890. Analysis: calculated for C$_{22}$H$_{19}$Br$_3$O$_3$: C, 46.27; H, 3.35; Br, 41.97; found: C, 46.02; H, 3.20; Br, 42.09

Tris(5-bromo-2-hydroxyphenyl)methane (1cH$_3$)

To the solution of tris(5-bromo-2-methoxyphenyl)methane (0.57 g, 1 mmol) in dichloromethane (10 mL) was added BBr$_3$ (1M in dichloromethane, 3.3 mL, 3.3 mmol) at -78 °C. After stirring with warming up to rt for 24 h, 30 mL of water was added to the mixture at 0 °C. The mixture was extracted with Et$_2$O (3 x 30 mL). The obtained organic layer was dried (MgSO$_4$) and evaporated to give a solid. It was purified by column chromatography (hexane/ethyl acetate = 50:50, column length 10 cm, diameter 26 mm silicagel) on silicagel to give the product (0.407 g, 77%) as a white solid. mp: 215-218 °C; ^{1}H NMR: (400 MHz, DMSO-d_6) 9.71 (s, 3H, OH), 7.22 (dd, J = 8.6, 2.1 Hz, 3H, 4'-H), 6.76 (d, J = 8.6 Hz, 3H, 3'-H), 6.56 (d, J = 2.1 Hz, 3H, 6'-H), 6.02 (s, 1H, 1-H); ^{13}C NMR: (100 MHz, DMSO-d_6) 154.3 (s, C-2'), 131.7 (s, C-1'), 131.0 (d, C-6'), 130.0 (d, C-4'), 117.2 (s, C-3'), 109.7 (d, C-5'), 37.4 (d, C-1); IR (KBr) 3390 (OH) cm^{-1}; MS: (EI, 70 eV) m/z 532 (M$^+$ + 6, 12), 530 (M$^+$ + 4, 36), 528 (M$^+$ + 2, 37), 526 (M$^+$, 14), 359 (M$^+$ - C$_6$H$_4$BrO + 4, 17), 357 (M$^+$ - C$_6$H$_4$BrO + 2, 36), 355 (M$^+$ - C$_6$H$_4$BrO, 23), 341 (M$^+$ - C$_6$H$_6$BrO$_2$ + 4, 34), 339 (M$^+$ - C$_6$H$_6$BrO$_2$ + 2, 68), 337 (M$^+$ - C$_6$H$_6$BrO$_2$, 34), 277 (M$^+$ - C$_6$H$_5$Br$_2$O + 2, 99), 275 (M$^+$ - C$_6$H$_6$BrO$_2$, 100); HRMS: (EI, 70 eV) calculated for (C$_{19}$H$_{13}$Br$_3$O$_3$) 525.8415 (M$^+$) found for m/z 525.8407.
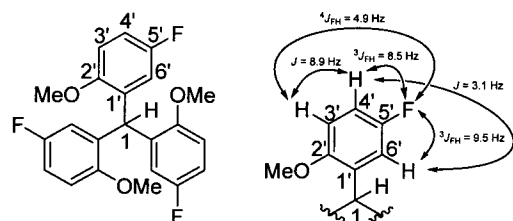
Tris(5-fluoro-2-methoxyphenyl)methanol (3d)
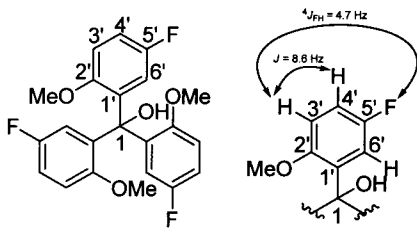
A solution of BuLi in hexane (66 mmol, 41.2 mL, 1.6 M) and N,N,N',N'-tetramethylethylenediamine (0.196 g, 1.7 mmol) was introduced in the flask. 2-Bromo-4-fluoroanisole (14.3 g, 66 mmol) was slowly added to the flask at -78 °C with stirring. After stirring for 1 h at rt, the flask was cooled to -78 °C. Ethyl chloroformate (2.16 g, 20 mmol) was slowly added to the flask. The stirring was kept for 19 h at 60 °C. H$_2$O (10 mL) was added to quench the reaction and the mixture was extracted with dichloromethane (3 x 50 mL). The organic layer was dried (MgSO$_4$) and evaporated to give the crude product, which was recrystallized to afford the pure white product (5.5 g, 68%). mp: 188-191 °C; ^{1}H NMR: (400 MHz, CDCl$_3$) 6.99-6.90 (m, 6H, 4'-H and 6'-H), 6.82 (dd, J = 8.6 Hz, $^4J_{FH}$ = 4.7 Hz, 3H, 3'-H), 5.49 (brs, 1H, OH, D$_2$O-exchangeable), 3.48 (s, 9H, OMe); ^{13}C NMR: (100 MHz, CDCl$_3$)

156.8 (s, C-5'; d by $^1J_{CF}$ = 238 Hz), 153.2 (s, C-2'; d by $^4J_{CF}$ = 3 Hz), 134.2 (s, C-1'; d by $^3J_{CF}$ = 7 Hz), 116.5 (d, C-6'; d by $^2J_{CF}$ = 26 Hz), 114.5 (d, C-4'; d by $^2J_{CF}$ = 23 Hz), 113.2 (d, C-3'; d by $^3J_{CF}$ = 8 Hz), 79.2 (s, C-1), 56.1 (q, OMe); IR (KBr) 3510 (OH), 1265 (OMe), 1211 (ArF), 1034 (OMe) cm^{-1}; MS: (EI, 70 eV) m/z 404 (M$^+$, 37), 279 (M$^+$ - C$_7$H$_6$FO, 34), 153 (M$^+$ - C$_{14}$H$_{13}$F$_2$O$_2$, 100); HRMS: (EI, 70 eV) calculated for (C$_{22}$H$_{19}$F$_3$O$_4$) 404.1235 (M$^+$) found for m/z 404.1225. Analysis: calculated for C$_{22}$H$_{19}$F$_3$O$_4$: C, 65.34; H, 4.74; found: C, 65.12; H, 4.69

Tris(5-fluoro-2-methoxyphenyl)methane (4d)

To the solution of tris(5-fluoro-2-methoxyphenyl)methanol (2.02 g, 5 mmol) in acetonitrile (15 mL) and THF (15 mL) was added TsOH·H$_2$O (1.05 g, 5.5 mmol) at 0 °C to give a black solution. After stirring at 60 °C for 12 h, to the suspension was added H$_2$O (10 mL). The suspension was extracted with Et$_2$O (3

x 50 mL). The organic layer was dried (MgSO$_4$) and evaporated to give the crude product. It was recrystallized to afford the pure product (1.48 g, 76%) as a white soild. mp: 183-185 °C; ^{1}H NMR: (400 MHz, CDCl$_3$) 6.88 (ddd, $^3J_{FH}$ = 8.5 Hz, J = 8.9, 3.1 Hz, 3H, 4'-H), 6.77 (dd, J = 8.9 Hz, $^4J_{FH}$ = 4.9 Hz, 3H, 3'-H), 6.46 (dd, $^3J_{FH}$ = 9.5 Hz, J = 3.1 Hz, 3H, 6'-H), 6.29 (s, 1H, 1-H), 3.65 (s, 9H, OMe); ^{13}C NMR: (100 MHz, CDCl$_3$) 156.9 (s, C-5'; d by $^1J_{CF}$ = 239 Hz), 153.3 (s, C-2'; d by $^4J_{CF}$ = 2 Hz), 133.1 (s, C-1'; d by $^3J_{CF}$ = 7 Hz), 116.3 (d, C-6'; d by $^2J_{CF}$ = 24 Hz), 113.3 (d, C-4'; d by $^2J_{CF}$ = 22 Hz), 111.8 (d, C-3'; d by $^3J_{CF}$ = 8 Hz), 56.2 (q, OMe), 37.6 (d, C-1); IR (KBr) 1249 (OMe), 1203 (ArF), 1034 (ArOMe) cm^{-1}; MS: (EI, 70 eV) m/z 388 (M$^+$, 100), 139 (M$^+$ - C$_{14}$H$_{11}$F$_2$O$_2$, 95), 125 (27), 109 (31); HRMS: (EI, 70 eV) calculated for (C$_{22}$H$_{19}$F$_3$O$_3$) 388.1286 (M$^+$) found for m/z 388.1278. Analysis: calculated for C$_{22}$H$_{19}$F$_3$O$_3$: C, 68.04; H, 4.93; found: C, 67.83; H, 4.88

Tris(5-fluoro-2-hydroxyphenyl)methane (1dH$_3$)
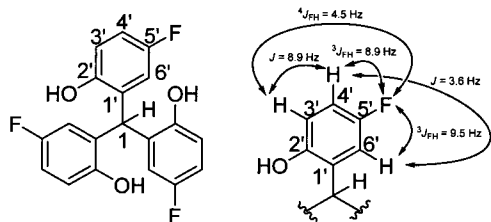
To a solution of tris(5-fluoro-2-methoxyphenyl)methane (5.82 g, 15 mmol) in dichloromethane (50 mL) was added BBr$_3$ (1 M in dichloromethane, 50 mL, 50 mmol) at -78 °C. After stirring with warming up to rt for 23 h, 50 mL of water was added to the mixture at 0 °C. The mixture was extracted with Et$_2$O (100 mL) and the

ether solution was extracted with NaOHaq (1 M, 2 x 150 mL). The aqueous layer was neutralized by HClaq (1 M, 200 mL) and extracted with Et$_2$O (2 x 200 mL). The obtained organic layer was dried (MgSO$_4$) and evaporated to give a brown solid (4.21 g, 80%), which was purified by column chromatography (hexane:EtOAc = 1:1, column length 25 cm, diameter 50 mm silicagel) on silicagel to give the product (3.12 g, 59%) as a white solid. mp: 218-222 °C; ^{1}H NMR: (400 MHz, CD$_2$Cl$_2$) 6.88 (ddd, $^3J_{FH}$ = 8.9 Hz, J = 8.9, 3.6 Hz, 3H, 4'-H), 6.78 (dd, J = 8.9 Hz, $^4J_{FH}$ = 4.5 Hz, 3H, 3'-H), 6.55 (dd, $^3J_{FH}$ = 9.5 Hz, J = 3.6 Hz, 3H, 6'-H), 6.08 (s, 1H, 1-H), 4.96 (brs, 3H, OH, D$_2$O-exchangeable); ^{13}C NMR: (100 MHz, CD$_2$Cl$_2$) 157.6 (s, C-5'; d by $^1J_{CF}$ = 239 Hz), 149.6 (s, C-2'), 129.5 (s, C-1'; d by $^3J_{CF}$ = 7 Hz), 117.1 (d, C-3'; d by $^3J_{CF}$ = 8 Hz), 116.5 (d, C-6'; d by $^2J_{CF}$ = 25 Hz), 114.9 (d, C-4'; d by $^2J_{CF}$ = 23 Hz), 38.3 (d, C-1); IR (KBr) 3371 (OH), 1180 (ArF) cm^{-1}; MS: (EI, 70 eV) m/z 346 (M$^+$, 33), 235 (M$^+$ -

C6H3FOH, 21), 233 (19), 217 (100); HRMS: (EI, 70 eV) calculated for (C19H13F3O3) 346.0817 (M+) found for m/z 346.0818. Analysis: calculated for C19H13F3O3: C, 65.90; H, 3.78; found: C, 65.95; H, 3.85.

Tris(2-methoxy-3-phenylphenyl)methanol (3e)
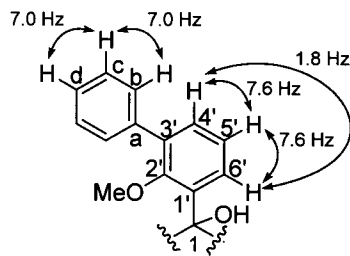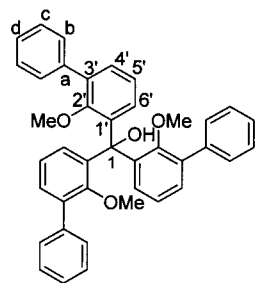
A solution of BuLi in hexane (50 mmol, 31 mL, 1.6 M) was introduced in the flask and the volatiles were removed under reduced pressure (20 torr, 30 °C). A dehydrated Et₂O (20 mL) and N,N,N′,N′-tetramethylethylenediamine (0.232 g, 2 mmol) were added to the flask. The dropping funnel was charged with 2-methoxybiphenyl (10.1 g, 50 mmol) and Et₂O (5 mL). The biphenyl solution was dropped to the flask at 0 °C. After stirring with warming up to rt for 17 h, the flask was cooled to 0 °C. The dropping funnel was charged with ethyl chloroformate (1.63 g, 15 mmol) and Et₂O (5 mL). The solution was dropped to the flask at 0 °C. The reaction mixture was stirred at rt for 2 h. H₂O (20 mL) was added to quench the reaction and the mixture was extracted with Et₂O (3 x 50 mL). The obtained organic layer was dried (MgSO₄) and evaporated to give an orange solid, which was purified by column chromatography (hexane/ethyl acetate = 89:11, column length 11 cm, diameter 21 mm silicagel) on silicagel to give a white product (4.5 g, 52%). mp: 159-161 °C; ¹H NMR: (400 MHz, CDCl₃) 7.55 (d, J = 7.0 Hz, 6H, b-H), 7.41-7.36 (m, 9H, 6'-H and c-H), 7.31 (t, J = 7.0 Hz, 3H, d-H), 7.28 (dd, J = 7.6, 1.8 Hz, 3H, 4'-H), 7.15 (dd, J = 7.6, 7.6 Hz, 3H, 5'-H), 5.90 (brs, 1H, OH, D₂O-exchangeable), 2.76 (s, 9H, OMe); ¹³C NMR: (100 MHz, CDCl₃) 156.1 (s, C-2') , 139.20 (s) , 139.17 (s), 135.0 (s, C-3'), 131.1 (d, C-4'), 129.2 (d, C-6'), 128.9 (d, C-b), 128.3 (d, C-c), 127.0 (d, C-d), 123.1 (d, C-5') , 81.3 (s, C-1), 59.9 (q, OMe); IR (KBr) 3467 (OH), 2938, 1458, 1411 cm⁻¹; MS: (EI, 70 eV) m/z 578 (M⁺, 30), 395 (M⁺ - C₁₃H₁₁O, 60), 211 (M⁺ - C₂₆H₂₃O₂, 100); HRMS: (EI, 70 eV) calculated for (C₄₀H₃₄O₄) 578.2457 (M⁺) found for m/z 578.2455. Analysis: calculated for C₄₀H₃₄O₄: C, 83.02; H, 5.92; found: C, 82.85; H, 6.00
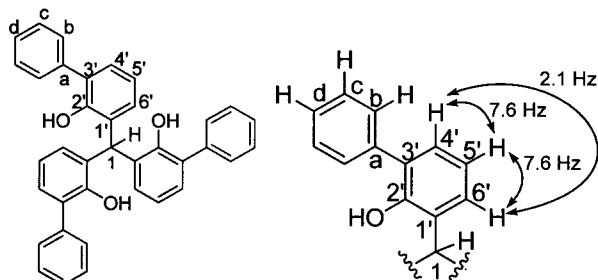
Tris(2-methoxy-3-phenylphenyl)methane (4e)
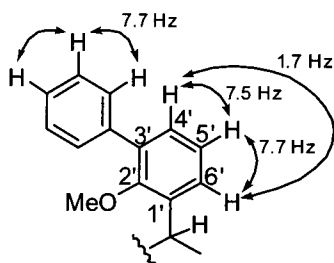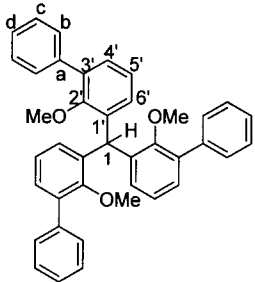
To a suspension of tris(2-methoxy-3-phenylphenyl)methanol (3.83 g, 6.6 mmol) in acetonitrile (7 mL) and THF (7 mL) was added TsOH·H₂O (1.4 g, 7.3 mmol) at 0 °C. The mixture was heated at 60 °C and stirred for 18 h. Cooling down to rt, H₂O (30 mL) was added to the resulting dark brown suspension. The mixture was extracted with Et₂O (3 x 50 mL). The organic layer was dried (MgSO₄) and evaporated to give a solid (2.6 g). It was purified by column chromatography (hexane/ethyl acetate = 97:3, column length 11 cm, diameter 21 mm silicagel) on silicagel to give the product (1.90 g, 51%) as a white solid. For further purification, it was recrystallized to give the pure product (ether/hexane = 1/1). mp: 134-135 °C; ¹H NMR: (400 MHz, CDCl₃) 7.61 (d,

J = 7.7 Hz, 6H, b-H), 7.39 (dd, J = 7.7, 7.4 Hz, 6H, c-H), 7.31 (t, J = 7.4, 3H, d-H), 7.25 (dd, J = 7.5, 1.7 Hz, 3H, 4'-H), 7.10 (dd, J = 7.7, 7.5 Hz, 3H, 5'-H), 6.97 (dd, J = 7.7, 1.7 Hz, 3H, 6'-H), 6.79 (s, 1H, 1-H,), 3.16 (s, 9H, OMe); ^{13}C NMR: (100 MHz, CDCl$_3$) 155.6 (s, C-2') , 138.9 (s, C-a) , 137.9 (s, C-1'), 134.7 (s, C-3'), 129.65 (d), 129.56 (d), 129.0 (d, C-b), 128.2 (d, C-c), 127.0 (d, C-d), 123.5 (d, C-5'), 59.9 (q, OMe), 38.3 (s, C-1); IR (KBr) 2935, 1462, 1415, 1223, 1007 cm^{-1}; MS: (EI, 70 eV) m/z 562 (M$^+$, 100), 531 (M$^+$ - CH$_3$O, 56), 333 (M$^+$ - C$_{18}$H$_{13}$, 24), 197 (M$^+$ - C$_{26}$H$_{21}$O$_2$, 60), 183 (M$^+$ - C$_{27}$H$_{23}$O$_2$, 43), 167 (M$^+$ - C$_{27}$H$_{23}$O$_3$, 28); HRMS: (EI, 70 eV) calculated for (C$_{40}$H$_{34}$O$_3$) 562.2508 (M$^+$) found for m/z 562.2495. Analysis: calculated for C$_{40}$H$_{34}$O$_3$: C, 85.38; H, 6.09; found: C, 85.09; H, 6.36

Tris(2-hydroxy-3-phenylphenyl)methane (1eH$_3$)

To a solution of tris(3-phenyl-2-methoxyphenyl)methane (4.94 g, 8.8 mmol) in dichloromethane (30 mL) was added BBr$_3$ (1 M in dichloromethane, 29.0 mL, 29.0 mmol) at -78 °C. After stirring with warming up to rt for 24 h, 30 mL of water was added to the mixture at 0 °C. The mixture was extracted with CH$_2$Cl$_2$ (3 x 30 mL). The obtained organic layer was dried (MgSO$_4$) and evaporated to give a solid (4.52 g). It was purified by column chromatography (hexane:EtOAc = 7:3, column length 25 cm, diameter 50 mm silicagel) on silicagel to give the product (2.3 g, 51%) as a white solid. For further purification, it was recrystallized to give the pure product (ether/hexane = 1/1). mp: 227-231 °C; ^{1}H NMR: (400 MHz, CDCl$_3$) 7.50-7.40 (m, 12H, b-H and c-H), 7.38-7.32 (m, 3H, d-H), 7.19 (dd, J = 7.6, 2.1 Hz, 3H, 4'-H), 7.00 (dd, J = 7.6, 2.1 Hz, 3H, 6'-H), 6.95 (dd, J = 7.6, 7.6 Hz, 3H, 5'-H), 6.46 (s, 1H, 1-H), 5.45 (brs, 3H, OH, D$_2$O-exchangeable); ^{13}C NMR: (100 MHz, CDCl$_3$) 150.2 (s, C-2'), 137.2 (s, C-a), 129.4 (d, C-6'), 129.2 (d), 129.1 (d), 128.9(s, C-1'), 128.8 (d, C-4'), 128.3 (s, C-3'), 127.7 (d, C-d), 120.3 (d, C-5'), 38.3 (d, C-1); IR (KBr) 3541 (OH), 1454, 1431 cm^{-1}; MS: (EI, 70 eV) m/z 520 (M$^+$, 29), 349 (M$^+$ - C$_{12}$H$_{11}$O, 26), 333 (100); HRMS: (EI, 70 eV) calculated for (C$_{37}$H$_{28}$O$_3$) 520.2038 (M$^+$) found for m/z 520.2032. Analysis: calculated for C$_{37}$H$_{28}$O$_3$: C, 85.36; H, 5.42; found:C, 85.22; H, 5.57

1-(2-methoxyPhenyl)Naphthalene (2f)


The flask equipped with a reflux condenser and a magnetic strring bar was charged with Pd(PPh$_3$)$_4$ (0.58 g, 0.5 mmol), 2-naphthaleneboronic acid (5.16 g, 30 mmol), Ba(OH)$_2$·8H$_2$O (7.1 g, 40 mmol), 1,2-dimethoxyethane (180 mL), H$_2$O (30 mL) and 2-iodoanisole (6.3 g, 27 mmol). The mixture was heated in an oil bath at 80 °C for 24h with stirring. After stirring, The flask was cooled to room temperature. The mixture was extracted with Et$_2$O (3 x 50 mL) and washed with brine (3 x 50 mL). The obtained organic layer was dried (MgSO$_4$) and evaporated to give a orange solid, which was purified by column chromatography (hexane:EtOAc = 7:3, column length 170 mm, diameter 48 mm silicagel) on silicagel to

give the product (4.8 g, 67%) as a white solid. The spectral data of the product was in an excellent agreement with the reported data.[39]

Tris{2-methoxy-3-(1-naphthyl)phenyl}methanol (3f)
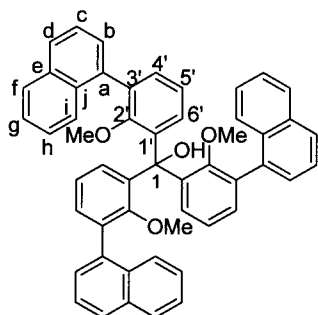
A solution of BuLi in hexane (18.86 mmol, 11.8 mL, 1.6 M) was introduced in the flask and the volatiles were removed under reduced pressure (20 torr, 30 °C). A dehydrated Et_2O (20 mL) and N,N,N',N'-tetramethylethylenediamine (0.174 g, 1.5 mmol) were added to the flask. A mixture of 1-(2-methoxyphenyl)nathphalene (4.41 g, 18.86 mmol) and Et_2O (30 mL) was added to the flask at 0 °C. After stirring with warming up to rt for 17 h, the flask was cooled to 0 °C. The dropping funnel was charged with ethyl chloroformate (0.521 g, 4.8 mmol) and Et_2O (10 mL). The solution was slowly added to the flask at 0 °C for 30 min. The reaction mixture was stirred at rt for 24 h. H_2O (20 mL) was added to quench the reaction and the mixture was extracted with ethyl acetate (3 x 50 mL). The obtained organic layer was evaporated to give a white solid, which was purified by flash column chromatography (hexane/dichloromethane = 20:80) to give a white product (2.46 g, 70%). mp: 231-233 °C; ^1H NMR: (400 MHz, $CDCl_3$) 7.87 (t, J = 8.5 Hz, 6H, Ar-H), 7.83-7.66 (brs, 3H, Ar-H), 7.66-7.31 (m, 15H, Ar-H), 7.31-7.24 (m, 3H, Ar-H), 7.24-7.17 (m, 3H, Ar-H), 5.82 (m, 1H, OH, D_2O-exchangeable), 2.65 (m, 9H, OMe) ^{13}C NMR: (100 MHz, $CDCl_3$) The signals of aryl carbons are too complicated due to broad signals to assign. See the raw NMR chart of tris{2-methoxy-3-(1-naphthyl)phenyl}methanol. 81.3 (C-1), 59.9 (OMe); IR: (KBr) 3483 (OH), 1458, 1411 (C=C), 1227 (C-O) cm^{-1}; MS: (EI, 70 eV) m/z 728 (M^+, 22), 495 (M^+ - $C_{17}H_{14}O$, 39), 261 (M^+ - $C_{34}H_{28}O_2$, 100); HRMS: (EI, 70 eV) calculated for ($C_{52}H_{40}O_4$) 728.2927 (M^+) found for m/z 728.2922.
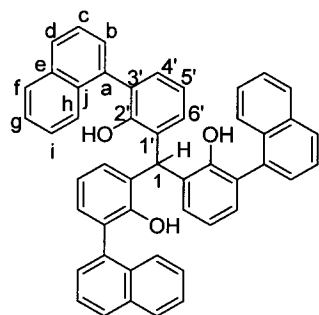
Tris{2-methoxy-3-(1-naphthyl)phenyl}methane (4f)
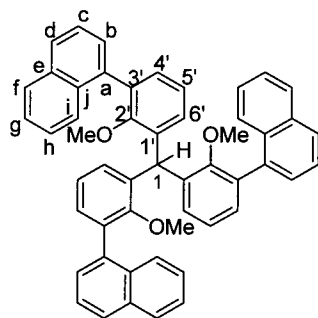
To a suspension of tris{2-methoxy-3-(1-naphthyl)phenyl}methanol (2.40 g, 3.3 mmol) in acetonitrile (7 mL) and THF (7 mL) was added TsOH·H_2O (0.69 g, 3.63 mmol) at 0 °C. The mixture was heated at 80 °C and stirred for 24 h. Cooling down to rt, H_2O (30 mL) was added to the resulting suspension. The mixture was extracted with Et_2O (3 x 25 mL). The organic layer was dried ($MgSO_4$) and evaporated to give a solid. It was purified by flash column chromatography (hexane/chloroform = 50:50) to give the product (1.64 g, 70%) as a white solid. mp: 146-148 °C; ^1H NMR: (400 MHz, $CDCl_3$) 7.87-7.81 (m, 6H, Ar-H), 7.72-7.62 (m, 3H, Ar-H), 7.54-7.46 (m, 6H, Ar-H), 7.45-7.38 (m, 3H, Ar-H), 7.37-7.14 (m, 12H, Ar-H), 6.84-6.81 (m, 1H, 1-H), 3.10-2.98 (m, 9H, OMe); ^{13}C NMR: (100 MHz, $CDCl_3$) A number of peaks were observed due to conformational isomers. 156.4 (C-2'), 156.3 (C-2'), 156.3 (C-2'), 138.2, 138.0, 137.8, 137.3, 137.2, 137.1, 137.0, 136.9, 133.6, 133.6, 133.6, 133.5, 133.5, 131.9, 131.9, 131.8, 131.8, 130.9, 130.8, 130.8, 130.7, 130.0, 129.9, 129.8, 129.7, 128.1, 128.0, 128.0, 127.7, 127.7, 127.5, 127.4, 127.4, 127.3, 126.4, 126.4, 126.4, 126.3, 125.9, 125.9, 125.9, 125.7, 125.7, 125.6, 125.3, 123.2 (C-5'), 123.1 (C-5'), 123.0 (C-5'), 60.3 (OMe), 60.2 (OMe), 60.2 (OMe), 38.3 (d, C-1); IR:

24

(KBr) 1223 (C-O) cm^{-1}; MS: (EI, 70 eV) m/z 712 (M$^+$, 100), 247 (M$^+$ - C34H$_{28}$O2, 30), 233 (C$_{17}$H$_{14}$O$^+$, 31); HRMS: (EI, 70 eV) calculated for (C$_{52}$H$_{40}$O$_3$) 712.2977(M$^+$) found for m/z 712.2984.

## Tris(2-hydroxy-3-(1-Naphthyl)phenyl)methane (1fH$_3$)

To a solution of tris(2-methoxy-3-{1-Naphthyl)phenyl}methane (1.0 g, 1.4 mmol) in dichloromethane (20 mL) was added BBr$_3$ (1 M in dichloromethane, 4.62 mL, 4.62 mmol) at -78 °C. After stirring with warming up to rt for 22 h, 20 mL of water was added to the mixture at 0 °C. The mixture was extracted with Et$_2$O (3 x 20 mL). The obtained organic layer was dried (MgSO$_4$) and evaporated to give a brown solid (1.1 g). It was purified by column chromatography (hexane:EtOAc = 7:3, column length 10 cm, diameter 26 mm silicagel) on silicagel to give the

product (0.5 g, 54%) as a white solid. For further purification, it was recrystallized to give the pure product (ether/hexane = 1/1). mp: 158-161 °C; ^{1}H NMR: (400 MHz, CDCl$_3$) 7.88 (d, J = 8.2 Hz, 6H, Ar-H), 7.63 (m, 3H, Ar-H), 7.58-7.44 (m, 9H, Ar-H), 7.42-7.32 (m, 3H, Ar-H), 7.25-7.15 (m, 6H, 3'-H and 4'-H), 7.10-7.03 (m, 3H, 5'-H), 6.51 (m, 1H, 1-H), 5.01 (m, 3H, OH, D$_2$O-exchangeable); ^{13}C NMR: (100 MHz, CDCl$_3$) A number of peaks were observed due to conformational isomers. 151.08 (s, C-2'), 151.03 (s, C-2'), 134.49, 134.42, 134.40, 134.32, 133.87 (s), 131.85 (s), 131.82 (s), 129.78, 129.66, 129.61, 129.47, 129.31, 129.22, 128.91, 128.36, 128.20, 126.66, 126.63, 126.46, 126.42 (s), 126.20, 125.83, 125.76, 125.63, 120.05 (d, C-5'), 119.99 (d, C-5'), 119.94 (d, C-5'), 38.7 (d, C-1); IR (KBr) 3525 (OH) cm^{-1}; MS: (EI, 70 eV) m/z 670 (M$^+$, 88), 451 (M$^+$ - C$_{16}$H$_{13}$O, 58), 433 (M$^+$ - C$_{16}$H$_{13}$O$_2$, 100); HRMS: (EI, 70 eV) calculated for (C$_{49}$H$_{34}$O$_3$) 670.2508 (M$^+$) found for m/z 670.2510.
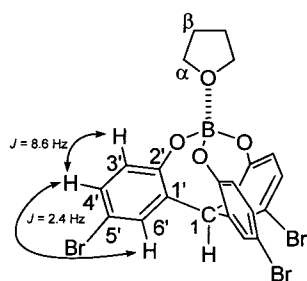
1bB·THF
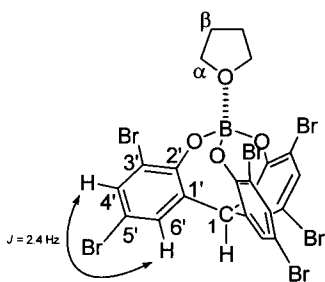
In a nitrogen-filled glove box, to a suspension of tris(3,5-dibromo-2-hydroxyphenyl)methane (0.1 mmol) in dichloromethane (3 mL) was added BH$_3$·THF in THF (0.15 mmol, 0.9 M) at rt with stirring for 2 h under release of H$_2$ gas. Evaporation of volatiles gave a viscous liquid, which was washed by hexane to give the product as a white solid almost quantitatively. ^{1}H NMR: (400 MHz, CDCl$_3$) 7.55 (d, J = 2.4 Hz, 3H, 4'-H), 7.28 (d, J = 2.4 Hz, 3H, 6'-H), 4.94 (s, 1H, 1-H) 4.86-4.83 (m, 4H, α-H$_2$), 2.37-2.33 (m, 4H, β-H$_2$); ^{13}C

NMR: (100 MHz, CDCl$_3$) 151.8 (s, C-2'), 134.4 (d, C-4'), 133.0 (d, C-6'), 131.3 (s, C-1'), 116.2 (s, C-3'), 113.5 (s, C-5'), 74.9 (t, C-α), 56.5 (d, C-1), 25.1 (t, C-β); ^{11}B NMR: (127 MHz, CDCl$_3$) (BF$_3$·Et$_2$O in CDCl$_3$ as external standard) 4.32

1bB·Py
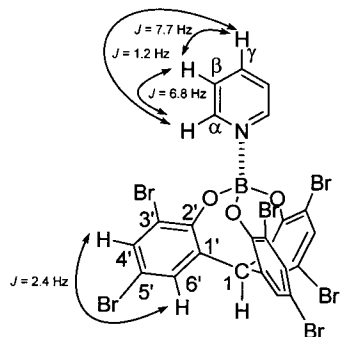
In a nitrogen-filled glove box, to a suspension of tris(3,5-dibromo-2-hydroxyphenyl)methane (0.1 mmol) in dichloromethane (3 mL) was added BH$_3$·THF in THF (0.15 mmol, 0.9 M) at rt with stirring for 2 h under release of H$_2$ gas. To the solution was added pyridine (0.2 mmol) at rt. After stirring for 1 h, volatiles were removed under reduced pressure. The obtained crude materials were washed with hexane and evaporated to give the product as a white solid almost quantitatively. The product was recrystallized from dichloromethane/hexane (1/1) for X-ray analysis. ^{1}H NMR: (400 MHz, CDCl$_3$)

9.60 (dd, J = 6.8, 1.2 Hz, 2H, α-H), 8.29 (tt, J = 7.7, 1.2 Hz, 1H, γ-H), 7.85 (dd, J = 7.7, 6.8 Hz, 2H, β-H), 7.55 (d, J = 2.4 Hz, 3H, 6'-H), 7.33 (d, J = 2.4 Hz, 3H, 4'-H), 5.01 (s, 1H, 1-H); ^{13}C NMR: (100 MHz, CDCl$_3$) 152.5 (C-2'), 144.9 (C-α), 142.8 (C-γ), 134.3 (C-4'), 132.9 (C-6'), 131.8 (C-1'), 125.5 (C-β), 116.6 (C-3'), 113.4 (C-5'), 57.0 (C-1); ^{11}B NMR: (127 MHz, CDCl$_3$) (BF$_3$·Et$_2$O in CDCl$_3$ as external standard) 4.12

1cB·THF
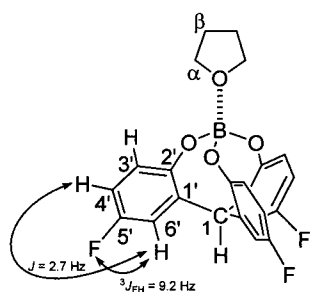

In a nitrogen-filled glove box, to a suspension of tris(5-bromo-2-hydroxyphenyl)methane (0.1 mmol) in dichloromethane (3 mL) was added BH$_3$·THF in THF (0.11 mmol, 0.9 M) at rt with stirring for 2 h under release of H$_2$ gas. Evaporation of volatiles gave a viscous liquid, which was washed by hexane to give the product as a white solid almost quantitatively. ^{1}H NMR: (400 MHz, CDCl$_3$) 7.35 (d, J = 2.4 Hz, 3H, 6'-H), 7.22 (dd, J = 8.6, 2.4 Hz, 3H, 4'-H), 6.73 (d, J = 8.6 Hz, 3H, 3'-H), 4.88 (s, 1H, 1-H), 4.52 (brs, 4H, α-H$_2$), 2.28 (brs, 4H,

β-H$_2$); ^{13}C NMR: (100 MHz, CDCl$_3$) 154.7 (s, C-2'), 133.5 (d, C-6'), 131.4 (s, C-1'), 131.2 (d, C-4'), 122.0 (d, C-3'), 113.7 (s, C-5'), 73.0 (C-α), 55.8 (C-1), 25.0 (C-β); ^{11}B NMR: (127 MHz, CDCl$_3$) (BF$_3$·Et$_2$O in CDCl$_3$ as external standard) 5.13

1cB·Py
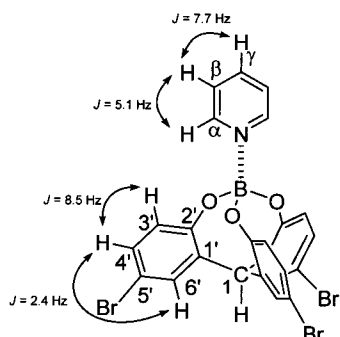
In a nitrogen-filled glove box, to a suspension of tris(5-bromo-2-hydroxyphenyl)methane (0.1 mmol) in dichloromethane (3 mL) was added BH$_3$·THF in THF (0.11 mmol, 0.9 M) at rt with stirring for 2 h under release of H$_2$ gas. To the solution was added pyridine (0.2 mmol) at rt. After stirring for 1 h, volatiles were removed under reduced pressure. The obtained crude materials were washed with hexane and evaporated to give the product as a white solid almost quantitatively. The product was recrystallized from dichloromethane/hexane (1/1) for X-ray analysis. ^{1}H NMR: (400 MHz, CDCl$_3$)

9.14 (d, J = 5.1 Hz, 2H, α-H), 8.27 (t, J = 7.7 Hz, 1H, γ-H), 7.84 (dd, J = 7.7, 5.1 Hz, 2H, β-H), 7.40 (d, J = 2.4 Hz, 3H, 6'-H), 7.21 (dd, J = 8.5, 2.4 Hz, 3H, 4'-H), 6.74 (d, J = 8.5 Hz, 3H, 3'-H), 4.95 (s, 1H, 1-H); ^{13}C NMR: (100

MHz, CDCl$_3$) 155.2 (C-2'), 143.8 (C-α), 142.6 (C-γ), 133.5 (C-6'), 131.8 (C-1'), 131.1 (C-4') 125.9 (C-β), 122.4 (C-3'), 113.5 (C-5'), 56.3 (C-1); ^{11}B NMR: (127 MHz, CDCl$_3$) (BF$_3$·Et$_2$O in CDCl$_3$ as external standard) 4.06
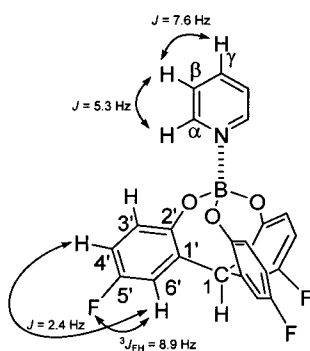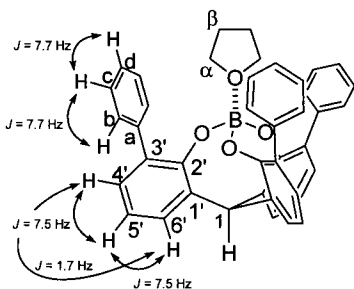
1dB·THF

In a nitrogen-filled glove box, to a suspension of tris(5-fluoro-2-hydroxyphenyl)methane (0.1 mmol) in dichloromethane (3 mL) was added BH$_3$·THF in THF (0.11 mmol, 0.9 M) at rt with stirring for 2 h under release of H$_2$ gas. Evaporation of volatiles gave a viscous liquid, which was washed by hexane to give the product as a white solid almost quantitatively. ^{1}H NMR: (400 MHz, CDCl$_3$) 6.93 (dd, $^3J_{FH}$ = 9.2 Hz, J = 2.7 Hz, 3H, 6'-H), 6.85-6.75 (m, 6H, 3'-H and 4'-H), 4.86 (s, 1H, 1-H) , 4.53 (brs, 4H, α-H$_2$), 2.26 (brs, 4H, β-H$_2$); ^{13}C NMR:

(100 MHz, CDCl$_3$) 157.5 (s, C-5'; d by $^1J_{CF}$ = 239 Hz), 151.7 (s, C-2'; d by $^4J_{CF}$ = 2.5 Hz), 130.4 (s, C-1'; d by $^3J_{CF}$ = 6.6 Hz), 120.8 (d, C-3'; d by $^3J_{CF}$ = 8.2 Hz), 117.1 (d, C-6'; d by $^2J_{CF}$ = 23 Hz), 114.7 (d, C-4'; d by $^2J_{CF}$ = 22 Hz), 72.8 (C-α), 56.6 (d, C-1), 25.0 (C-β); ^{11}B NMR: (127 MHz, CDCl$_3$) (BF$_3$·Et$_2$O in CDCl$_3$ as external standard) 5.27

1dB·Py

In a nitrogen-filled glove box, to a suspension of tris(5-fluoro-2-hydroxyphenyl)methane (0.1 mmol) in dichloromethane (3 mL) was added BH$_3$·THF in THF (0.11 mmol, 0.9 M) at rt with stirring for 2 h under release of H$_2$ gas. To the solution was added pyridine (0.2 mmol) at rt. After stirring for 1 h, volatiles were removed under reduced pressure. The obtained crude materials were washed with hexane and evaporated to give the product as a white solid almost quantitatively. The product was recrystallized from dichloromethane/hexane (1/1) for X-ray analysis. ^{1}H NMR: (400 MHz, CDCl$_3$) 9.17 (d, J = 5.3 Hz, 2H, α-H), 8.26

(t, J = 7.6 Hz, 1H, γ-H), 7.83 (dd, J = 7.6, 5.3 Hz, 2H, β-H), 6.99 (dd, $^3J_{FH}$ = 8.9 Hz, J = 2.4 Hz, 3H, 6'-H), 6.78-6.74 (m, 6H, 3'-H and 4'-H), 4.95 (s, 1H, 1-H); ^{13}C NMR: (100 MHz, CDCl$_3$) 157.4 (C-5'; d by $^1J_{CF}$ = 238 Hz), 152.1 (C-2'; d by $^4J_{CF}$ = 1.6 Hz), 143.9 (C-α), 142.4 (C-γ), 130.9 (C-1'; d by $^3J_{CF}$ = 7.4 Hz), 125.8 (C-β), 121.2 (C-3'; d by $^3J_{CF}$ = 8.2 Hz), 117.1 (C-6'; d by $^2J_{CF}$ = 23 Hz), 114.6 (C-4'; d by $^2J_{CF}$ = 22 Hz), 57.1 (C-1); ^{11}B NMR: (127 MHz, CDCl$_3$) (BF$_3$·Et$_2$O in CDCl$_3$ as external standard) 4.19
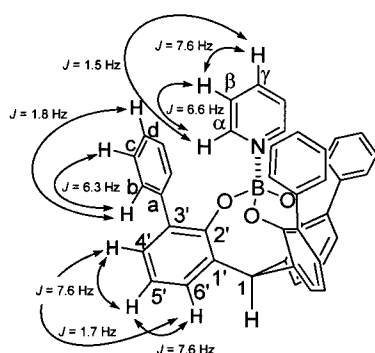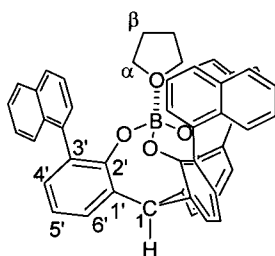
1eB·THF

In a nitrogen-filled glove box, to a solution of tris(2-hydroxy-3-phenylphenyl)methane (0.1 mmol) in dichloromethane (3 mL) was added BH$_3$·THF in THF (0.11 mmol, 0.9 M) at rt with stirring for 2 h under release of H$_2$ gas. Evaporation of volatiles gave a viscous liquid, which was washed by hexane to give the product as a white solid almost quantitatively. The product was recrystallized from dichloromethane/hexane (1/1) for X-ray analysis. ^{1}H NMR: (400 MHz, CDCl$_3$) 7.44 (d, J = 7.7 Hz, 6H, b-H), 7.33 (dd, J

27

= 7.5, 1.7 Hz, 3H, 6'-H), 7.27 (dd, J = 7.7, 7.7 Hz, 6H, c-H), 7.19 (d, J = 7.7 Hz, 3H, d-H), 7.15 (dd, J = 7.5, 1.7 Hz,

3H, 4'-H), 6.96 (dd, J = 7.5, 7.5 Hz, 3H, 5'-H), 5.37 (s, 1H, 1-H) , 3.18 (brs, 4H, α-H$_2$), 1.24 (brs, 4H, β-H$_2$); ^{13}C

NMR: (100 MHz, CDCl$_3$) 153.1 (s, C-2'), 140.2 (s, C-a), 132.8 (s, C-1'), 131.4 (s, C-3'), 130.7 (d, C-6'), 130.0 (d,

C-b), 129.0 (d, C-4'), 127.4 (d, C-c), 126.2 (d, C-d), 121.0 (d, C-5'), 71.6 (t, C-α), 58.2 (d, C-1), 23.9 (t, C-β); ^{11}B

NMR: (127 MHz, CDCl$_3$) (BF$_3$·Et$_2$O in CDCl$_3$ as external standard) 5.04

1eB·Py

In a nitrogen-filled glove box, to a solution of tris(2-hydroxy-3-phenylphenyl)methane (0.1 mmol) in dichloromethane (3 mL) was added BH$_3$·THF in THF (0.11 mmol, 0.9 M) at rt with stirring for 2 h under release of H$_2$ gas. To the solution was added pyridine (0.2 mmol) at rt. After stirring for 1 h, volatiles were removed under reduced pressure. The obtained crude materials were washed with hexane and evaporated to give the product as a white solid almost quantitatively. The product was recrystallized from dichloromethane/hexane (1/1) for X-ray analysis. ^{1}H NMR: (400 MHz,

CDCl$_3$) 7.77 (dd, J = 6.6, 1.5 Hz, 2H, α-H), 7.67 (tt, J = 7.6, 1.5 Hz, 1H, γ-H), 7.37 (dd, J = 7.6, 1.7 Hz, 3H, 6'-H),

7.24 (dd, J = 6.3, 1.8 Hz, 6H, b-H), 7.14 (dd, J = 7.6, 1.7 Hz, 3H, 4'-H), 7.10-7.00 (m, 9H, c-H and d-H), 6.95 (dd,

J = 7.6, 7.6 Hz, 3H, 5'-H), 6.84 (dd, J = 7.6, 6.6 Hz, 2H, β-H), 5.44 (s, 1H, 1-H); ^{13}C NMR: (100 MHz, CDCl$_3$)

153.7 (C-2'), 143.7 (C-α), 140.6 (C-γ), 140.3 (C-a), 133.0 (C-1'), 131.8 (C-3'), 130.8 (C-6'), 129.9 (C-b), 128.8

(C-4'), 127.2 (C-c), 125.9 (C-d), 124.0 (C-β), 120.8 (C-5'), 58.8 (C-1); ^{11}B NMR: (127 MHz, CDCl$_3$) (BF$_3$·Et$_2$O in
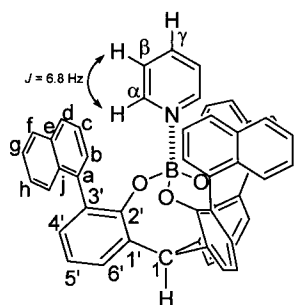
CDCl$_3$ as external standard) 4.46

1fB·THF

In a glove box, to a solution of tris{2-hydroxy-3-(1-naphthyl)phenyl}methane (0.1 mmol) in dichloromethane (3 mL) was added BH$_3$·THF in THF (0.11 mmol, 0.9 M) at rt with stirring for 3 h under release of H$_2$ gas. Evaporation of volatiles gave a viscous liquid, which was washed by hexane to give the product as a white solid almost quantitatively. The product was recrystallized from dichloromethane/hexane(1/1) for X-ray analysis. ^{1}H NMR: (400 MHz, CDCl$_3$) 7.75 (dd, J = 8.9, 8.9 Hz, 2H), 7.69-6.93

(m, 32H, Ar-H), 6.37 (dd, J = 7.5, 7.5 Hz, 1H), 5.51 (s, 1H, 1-H) , 1.56 (m, 4H, α-H$_2$), 0.03 (m, 4H, β-H$_2$); ^{13}C

NMR: (100 MHz, CDCl$_3$) 153.84 (s, C-2'), 153.75 (s, C-2'), 139.02, 138.88, 138.75, 132.94, 132.82, 132.59,

132.50, 131.99, 131.68, 131.63, 131.38, 131.29, 131.06, 131.04, 130.97, 130.92, 130.87, 129.91, 129.80, 129.76,

128.14, 128.12, 127.51, 127.44, 127.32, 127.18, 127.08, 126.97, 126.90, 126.87, 126.77, 126.69, 125.60, 125.46,

125.16, 125.01, 124.97, 124.86, 124.78, 120.88, 120.76, 120.72, 69.9 (t, C-α), 58.2 (d, C-1), 23.0 (t, C-β); ^{11}B

NMR: (127 MHz, CDCl$_3$) (BF$_3$·Et$_2$O in CDCl$_3$ as external standard) 4.40

28

1fB·Py

In a nitrogen-filled glove box, to a solution of tris{2-hydroxy-3-(1-naphthyl)phenyl}methane (0.1 mmol) in dichloromethane (3 mL) was added BH_3·THF in THF (0.11 mmol, 0.9 M) at rt with stirring for 3 h under release of H_2 gas. To the solution was added pyridine (0.2 mmol) at rt. After stirring for 2 h, volatiles were removed under reduced pressure. The obtained crude materials were washed with hexane and evaporated to give the product as a white solid almost quantitatively. The product was recrystallized from dichloromethane/hexane (1/1) for

X-ray analysis. ^{1}H NMR: (400 MHz, CDCl$_3$) 7.74-6.87 (m, 29H) 6.82 (dd, J = 7.7, 7.7 Hz, 1H), 6.53 (d, J = 6.8 Hz, 1.7H, α-H), 6.38 (dd, J = 7.7, 7.7 Hz, 1H), 6.20 (d, J = 6.8 Hz, 0.3H, α-H), 6.05 (dd, J = 7.5, 7.5 Hz, 1H), 5.84 (dd, J = 6.8, 6.8 Hz, 1.7H, β-H), 5.58 (s, 1H, 1-H), 5.49 (dd, J = 6.8, 6.8 Hz, 0.3H, β-H); ^{13}C NMR: (100 MHz, CDCl$_3$) 154.79 (s, C-2'), 154.68 (s, C-2'), 154.40 (s, C-2'), 141.74 (d, C-α), 141.53 (d, C-α), 139.34, 139.21, 138.82, 138.45, 132.76, 132.71, 132.65, 132.32, 131.19, 132.14, 131.91, 131.87, 131.77, 131.44, 131.40, 131.36, 131.14, 130.86, 129.77, 129.69, 129.61, 127.76, 127.44, 127.35, 127.28, 127.22, 127.09, 126.97, 126.95, 126.76, 126.64, 126.24, 126.04, 125.32, 125.27, 125.12, 124.98, 124.86, 124.81, 124.74, 124.50, 122.35 (d, C-β), 120.66, 120.52, 120.34, 120.25, 58.7 (d, C-1); ^{11}B NMR: (127 MHz, CDCl$_3$) (BF$_3$·Et$_2$O in CDCl$_3$ as external standard) 3.54

NMR Study of Complexes of Boranes with 2,6-Dimethyl-γ-Pyrone (Table 4)

Equimolar amount of boron compounds (BF$_3$·OEt$_2$, 1aB·THF, 1bB·THF, 1cB·THF, 1dB·THF, 1eB·THF, 1fB·THF, 1gB·THF, 1hB·THF or B(OPh)$_3$) and 2,6-dimethyl-γ-pyrone were mixed in CDCl$_3$. The chemical shifts of Δδ(^{13}C) in pyrone moieties are shown in Table S1.

Table S1

B compound +
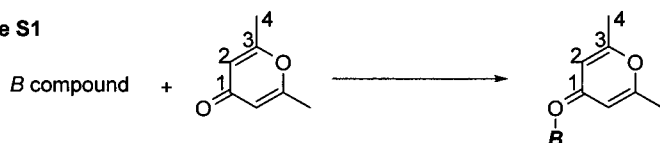
		Δδ(^{13}C)/ ppm				
carbon	δ(^{13}C)/ ppm^a	BF$_3$·OEt$_2$	1aB·THF	1bB·THF	1cB·THF	1dB·THF
C1	180.181	-0.675	-0.222	-0.881	-	-0.403
C2	113.739	-1.926	-0.658	-1.070	-0.839	-0.872
C3	165.432	8.708	6.782	7.630	7.391	7.243
C4	19.727	0.889	0.921	0.905	1.061	0.905

		Δδ(^{13}C)/ ppm				
carbon	δ(^{13}C)/ ppm^a	1eB·THF	1fB·THF	1gB·THF	1hB·THF	B(OPh)$_3$
C1	180.181	-0.856	-3.235	-0.346	-0.231	0.510
C2	113.739	-1.671	-3.399	-0.559	-0.452	-0.189
C3	165.432	5.564	3.852	5.844	4.486	0.774
C4	19.727	0.592	-0.757	0.683	0.526	0.041

^{a} δ(^{13}C) of pyron (boron-free).

General Procedure of Complexation with Pyrone

In a glove box, to a suspension of ligand (0.1 mmol) in dichloromethane (3 mL) was added BH$_3$·THF in THF (0.11 mmol, 1.0 M) at rt with stirring for 2 h under release of H$_2$ gas. Volatile was removed under reduced pressure and

the residue was washed with hexane. The evaporated residue was resolved with dichloromethane (3 mL) and 2,6-dimethyl-γ-pyrone (0.1 mmol) was added to the solution. After stirring for 1 h, volatile was removed under reduced pressure to give the crude product. NMR date of **1aB·Pyrone**, **1gB·Pyrone** and **1hB·Pyrone** have been reported by our previous paper[7b].

1bB·Pyrone

^{1}H NMR: (400 MHz, CDCl$_3$) 7.52 (d, J = 2.4 Hz, 3H), 7.29 (dd, J = 7.7, 7.7 Hz, 3H, d-H), 7.19 (s, 2H), 4.94 (s, 1H), 2.51 (s, 6H); ^{13}C NMR: (100 MHz, CDCl$_3$) 179.3, 173.1, 152.6, 134.1, 132.8, 131.8, 116.5, 113.7, 112.7, 68.0, 20.6

1cB·Pyrone

^{1}H NMR: (400 MHz, CDCl$_3$) 7.37 (d, J = 2.4 Hz, 3H), 7.19 (ddd, J = 8.6, 2.4, 1.2 Hz, 3H), 7.03 (s, 2H), 6.68 (d, J = 8.6, 1.1 Hz, 3H), 4.88 (s, 1H), 2.60 (s, 6H); ^{13}C NMR: (100 MHz, CDCl$_3$) 179.8, 172.82, 155.4, 133.4, 131.8, 130.9, 122.4, 113.0, 112.9, 56.4, 20.8

1dB·Pyrone

^{1}H NMR: (400 MHz, CDCl$_3$) 7.03 (s, 2H), 6.96 (dd, J = 9.2, 2.9 Hz, 3H), 6.79 (ddd, J = 8.2, 8.2, 3.1 Hz, 3H), 6.73 (dd, J = 8.7, 5.1 Hz, 3H), 4.88 (s, 1H), 2.52 (s, 6H); ^{13}C NMR: (100 MHz, CDCl$_3$) 179.8, 172.7, 157.2 (d, J = 237.6 Hz,), 152.3(d, J = 7.7 Hz), 130.76 (d, J = 6.6 Hz), 121.1 (d, J = 8.2 Hz), 117.0 (d, J = 22.9 Hz), 114.4 (d, J = 22.9 Hz), 112.9, 57.1, 20.6

1eB·Pyrone

^{1}H NMR: (400 MHz, CDCl$_3$) 7.53 (dd, J = 8.3, 1.4 Hz, 6H), 7.34 (dd, J = 7.7, 1.7 Hz, 3H), 7.19 (dd, J = 7.6, 1.8 Hz, 3H), 7.11 (dd, J = 7.4, 7.4 Hz, 6H), 7.03 (dd, J = 7.5, 7.5 Hz, 3H), 6.93 (dd, J = 7.6, 7.6 Hz, 3H), 6.39 (s, 2H), 5.38 (s, 1H), 2.18 (s, 6H); ^{13}C NMR: (100 MHz, CDCl$_3$) 179.3, 171.0, 153.7, 140.2, 132.2, 131.9, 130.8, 130.0, 128.8, 127.0, 125.5, 120.6, 112.1, 59.0, 20.3

1fB·Pyrone

^{1}H NMR: (400 MHz, CDCl$_3$) 7.91-6.24 (m, 42H), 5.50 (s, 1H), 5.10 (s, 1.4H), 4.83 (s, 0.54H), 2.58 (s, 4.2H), 1.49 (s, 2H); ^{13}C NMR: (100 MHz, CDCl$_3$) 176.946, 169.284, 154.816, 154.775, 139.631, 139.228, 139.162, 138.685, 132.882, 132.726, 132.586, 132.422, 132.380, 132.240, 131.845, 131.640, 131.475, 131.385, 130.965, 130.874, 130.767, 129.837, 129.689, 129.566, 128.586, 128.529, 128.405, 128.216, 127.673, 127.278, 127.195, 126.874, 126.735, 126.603, 126.298, 126.117, 125.887, 125.623, 125.220, 125.113, 125.047, 124.907, 124.735, 124.570, 124.529, 124.340, 120.019, 119.961, 119.904, 119.829, 111.023, 110.340, 58.746, 19.661, 19.397, 18.970

B(OPh)$_3$·Pyrone

^{1}H NMR: (400 MHz, CDCl$_3$) 7.32-7.22 (brm, 6H), 7.15-6.92 (brm, 9H), 6.15 (s, 2H), 2.25 (s, 6H); ^{13}C NMR: (100 MHz, CDCl$_3$) 180.7, 166.2, 153.3, 129.3, 129.1, 129.0, 123.0, 120.0, 113,6, 19.8

30

Computational Method. We applied the HF/DFT hybrid method originally proposed by Becke,[45] referenced as B3PW91 three parameter hybrid functional. All calculations were performed with Gaussian 03, Revision C.02.[46] 6-31+G(d,p) were used for basis sets. All molecular geometries were fully optimized and energies were calculated including zero point energy correction by the normal mode analysis for each structure.

All species calculated in Figure 3 and Table 5 in text are shown below (Scheme A).
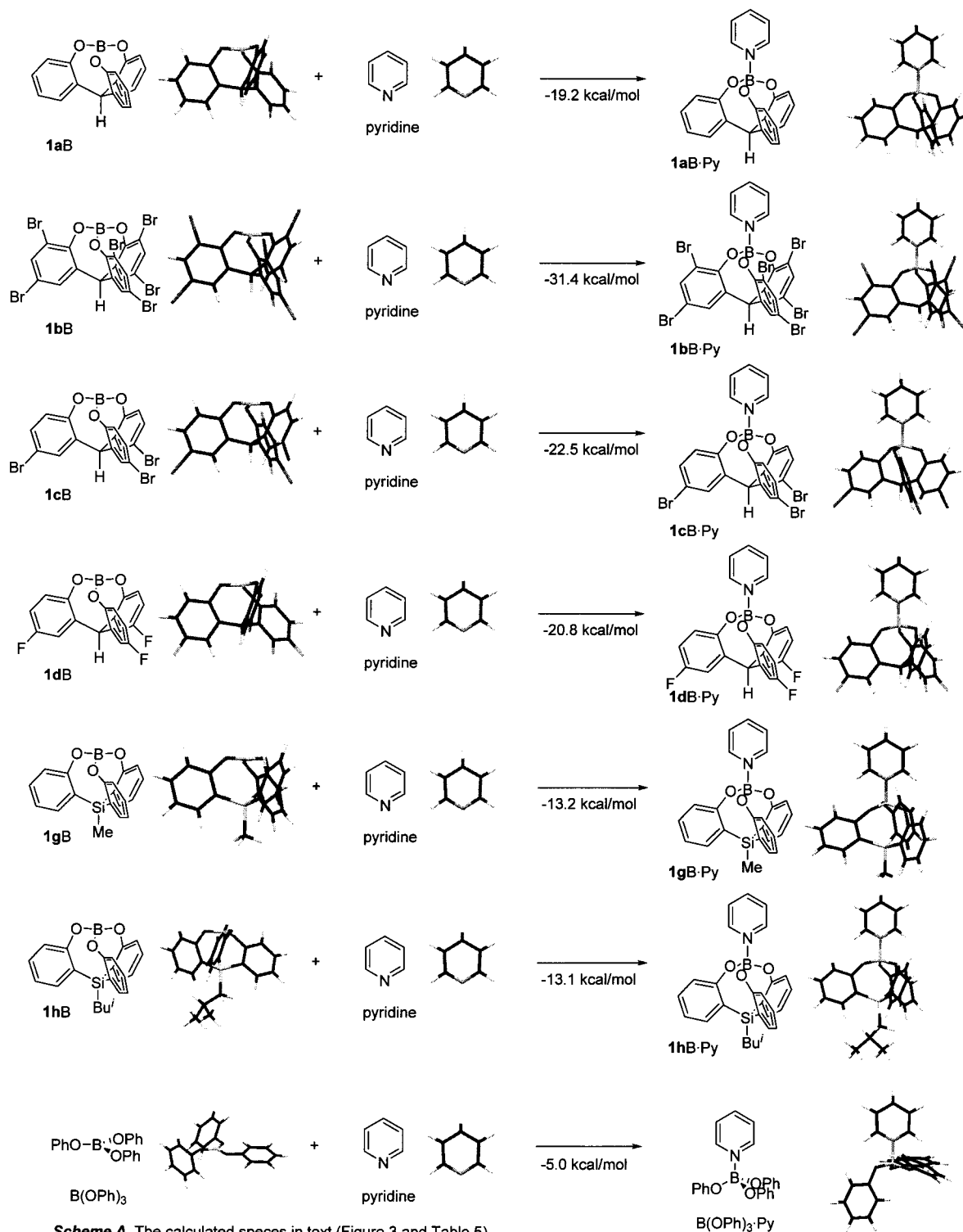
Scheme A. The calculated speces in text (Figure 3 and Table 5)

31

Total energies for all of the calculated species (in hartree). All energies includes zero point vibration energy correction.

1aB	-981.885983
1aB·Py	-1230.031378
1bB	-16408.61404
1bB·Py	-16656.77891
1cB	-8695.252484
1cB·Py	-8943.403157
1dB	-1279.516444
1dB·Py	-1527.664347
1gB	-1272.562556
1gB·Py	-1520.698427
1hB	-1390.372649
1hB·Py	-1638.508325
B(OPh)$_3$	-945.000996
B(OPh)$_3$·Py	-1193.123798
pyridine	-248.11478

All species calculated in Scheme 5 in text are shown below (Scheme B).
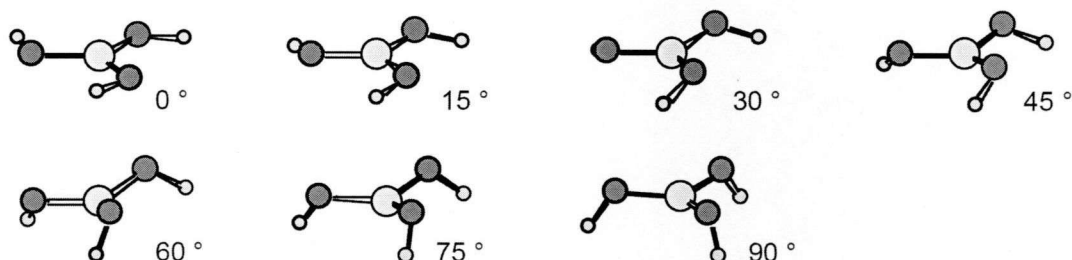
Scheme B. The calculated species B(OH)$_3$ with varied dihedral angels in Scheme 5.

Geometries (PDB)

```
B(OH)₃ (0°)
ATOM     1  B   UNK    1      0.000   0.000   0.000  1.00  0.00
ATOM     2  O   UNK    1      0.000   1.370   0.000  1.00  0.00
ATOM     3  H   UNK    1     -0.890   1.737   0.000  1.00  0.00
ATOM     4  O   UNK    1      1.187  -0.685   0.000  1.00  0.00
ATOM     5  H   UNK    1      1.949  -0.098   0.000  1.00  0.00
ATOM     6  O   UNK    1     -1.187  -0.685   0.000  1.00  0.00
ATOM     7  H   UNK    1     -1.059  -1.639   0.000  1.00  0.00
END


B(OH)₃ (15°)
ATOM     1  B   UNK    1      0.075   0.130   0.000  1.00  0.00
ATOM     2  O   UNK    1      0.008   0.125   1.369  1.00  0.00
ATOM     3  H   UNK    1      0.836  -0.148   1.777  1.00  0.00
ATOM     4  O   UNK    1     -0.947   0.676  -0.733  1.00  0.00
ATOM     5  H   UNK    1     -1.533   1.220  -0.197  1.00  0.00
ATOM     6  O   UNK    1      1.107  -0.510  -0.636  1.00  0.00
ATOM     7  H   UNK    1      1.132  -0.318  -1.580  1.00  0.00
END
```

B(OH)₃ (30°)

ATOM	1	B	UNK	1	0.057	0.099	0.000	1.00	0.00
ATOM	2	O	UNK	1	-0.005	0.044	1.370	1.00	0.00
ATOM	3	H	UNK	1	0.859	-0.059	1.780	1.00	0.00
ATOM	4	O	UNK	1	-0.998	0.617	-0.708	1.00	0.00
ATOM	5	H	UNK	1	-1.481	1.292	-0.221	1.00	0.00
ATOM	6	O	UNK	1	1.057	-0.569	-0.662	1.00	0.00
ATOM	7	H	UNK	1	1.189	-0.250	-1.560	1.00	0.00
END									

B(OH)₃ (45°)

ATOM	1	B	UNK	1	0.046	0.080	0.000	1.00	0.00
ATOM	2	O	UNK	1	0.003	-0.037	1.369	1.00	0.00
ATOM	3	H	UNK	1	0.864	0.023	1.794	1.00	0.00
ATOM	4	O	UNK	1	-1.051	0.572	-0.666	1.00	0.00
ATOM	5	H	UNK	1	-1.438	1.353	-0.259	1.00	0.00
ATOM	6	O	UNK	1	1.002	-0.614	-0.703	1.00	0.00
ATOM	7	H	UNK	1	1.252	-0.201	-1.535	1.00	0.00
END									

B(OH)₃ (60°)

ATOM	1	B	UNK	1	0.186	0.107	0.000	1.00	0.00
ATOM	2	O	UNK	1	0.025	0.072	1.368	1.00	0.00
ATOM	3	H	UNK	1	0.817	-0.106	1.881	1.00	0.00
ATOM	4	O	UNK	1	-0.530	1.033	-0.728	1.00	0.00
ATOM	5	H	UNK	1	-0.373	1.955	-0.508	1.00	0.00
ATOM	6	O	UNK	1	0.655	-1.019	-0.640	1.00	0.00
ATOM	7	H	UNK	1	1.257	-0.867	-1.374	1.00	0.00
END									

B(OH)₃ (75°)

ATOM	1	B	UNK	1	0.163	0.094	0.000	1.00	0.00
ATOM	2	O	UNK	1	0.034	-0.022	1.369	1.00	0.00
ATOM	3	H	UNK	1	0.823	-0.022	1.915	1.00	0.00
ATOM	4	O	UNK	1	-0.586	1.052	-0.654	1.00	0.00
ATOM	5	H	UNK	1	-0.329	1.974	-0.584	1.00	0.00
ATOM	6	O	UNK	1	0.600	-1.002	-0.716	1.00	0.00
ATOM	7	H	UNK	1	1.329	-0.898	-1.330	1.00	0.00
END									

B(OH)₃ (90°)

ATOM	1	B	UNK	1	0.000	0.000	0.004	1.00	0.00
ATOM	2	O	UNK	1	0.000	1.377	0.085	1.00	0.00
ATOM	3	H	UNK	1	0.000	1.945	-0.684	1.00	0.00
ATOM	4	O	UNK	1	-1.193	-0.689	0.085	1.00	0.00
ATOM	5	H	UNK	1	-1.684	-0.972	-0.684	1.00	0.00
ATOM	6	O	UNK	1	1.193	-0.689	0.085	1.00	0.00
ATOM	7	H	UNK	1	1.684	-0.972	-0.684	1.00	0.00
END									

The unoccupied MO which has appropriate lobe on boron for Lewis acid was picked in each structure with diheral angles (0, 15, 30, 45, 60, 75, 90 °).

```
Orbital     Dihedral angle/°     Hartree
21a         0                    0.09505
21a         15                   0.08879
21a         30                   0.07450
21a         45                   0.05903
20a         60                   0.03687
18a         75                   0.02352
18a         90                   0.01809
```

The MO diagrams are shown below.

0°   15°   30°   45°

60°   75°   90°
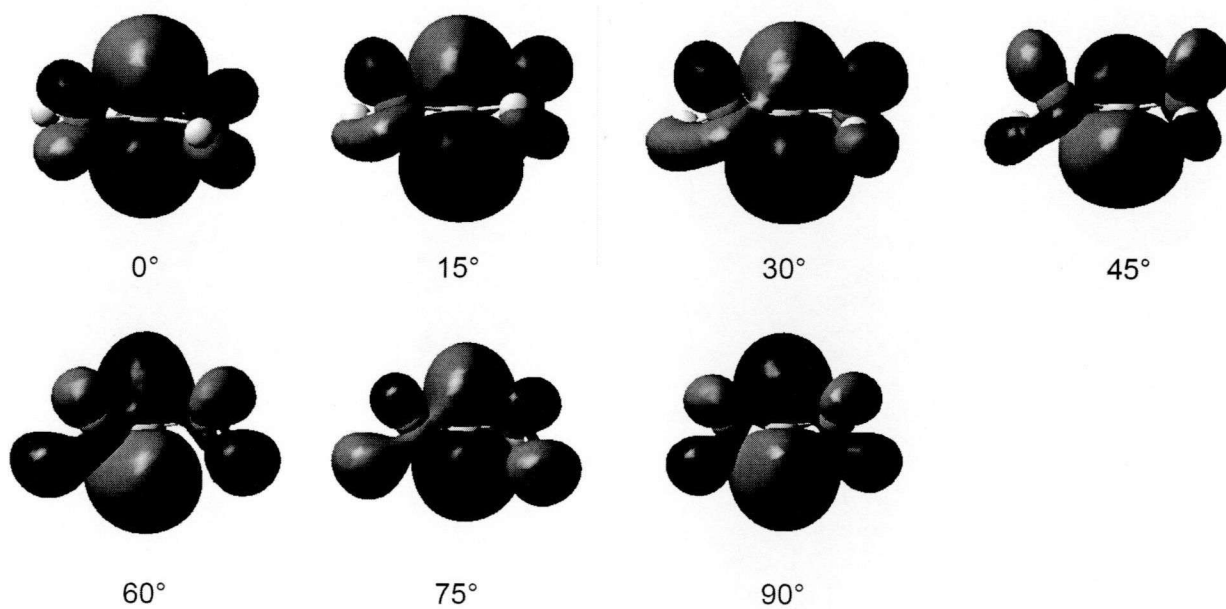
Rate of Ligand (DMAP)-Dissociation on Cage-Shaped Borates 1aB, 1dB, 1eB, and 1gB (Table 6).

A pyridine exchange can be descried below. B; cage-shaped borate, X; DMAP, Y; pyridine-d_5. Excess amount of pyridine-d_5 (Y) was used as solvent and eq 2 is considered to be irreversible. BX and X can be observed by DMAP signals by NMR.

$$BX \; \underset{k_{-1}}{\overset{k_1}{\rightleftharpoons}} \; B + X \quad (1) \qquad\qquad B + \underset{excess}{Y} \; \overset{k_2}{\longrightarrow} \; BY \quad (2)$$

No ligand-free borate B is observed.

$$[BX]_0 = [BX] + [X]$$
$$[X] = [BY]$$

$$\frac{d[B]}{dt} = k_1[BX] - k_{-1}[B][X] - k_2[B][Y] = 0$$

$$[B](k_{-1}[X] + k_2[Y]) = k_1[BX]$$

$$-\frac{d[BX]}{dt} = k_1[BX] - k_{-1}[B][X]$$

$$= k_1[BX] - \frac{k_{-1}[X]\,k_1[BX]}{k_{-1}[X] + k_2[Y]}$$

$$= k_1[BX]\left(1 - \frac{k_{-1}[X]}{k_{-1}[X] + k_2[Y]}\right)$$

$$k_{-1}[B][X] \ll k_2[B][Y]$$
$$k_{-1}[X] \ll k_2[Y]$$

$$-\frac{d[BX]}{dt} = k_1[BX]$$

$$-\int \frac{d[BX]}{[BX]} = \int k_1 dt$$

$$-\ln \frac{[BX]}{[BX]_{t_0}} = k_1(t - t_0) \qquad\qquad (A)$$

For simplification, t0 can be voluntarily set as zero (with considering stable temperature condition experimentally). Plots based on (A) furnish a linear plot (See below).

Ligand-Exchange on 1aB.
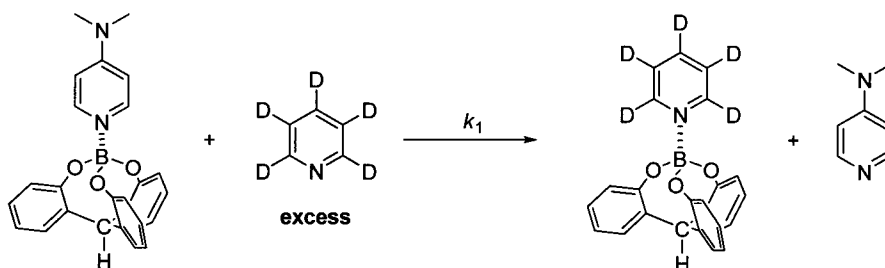
To a suspension of tris(2-hydroxyphenyl)methane (1aH₃) (0.1 mmol) in dichloromethane (2 mL) was added BH₃·THF in THF (0.12 mmol, 1.0 M) at rt with stirring for 2 h under release of H₂ gas. To the solution was added *N,N*-dimethylanimopyridine (0.2 mmol) at rt. After stirring for 1 h, volatile was removed under the reduced pressure. The obtained material was washed with dry hexane with filtration and then recrystallized from dichloromethane/hexane to give the pure complex. The complex (0.012mmol) and pyridine-*d₅* (5 mL) were added to the flask. The rate constants were determined by observing the reaction at 80, 85, 90, and 95 °C. The results are shown in Table 6.

Ligand-Exchange on 1dB.
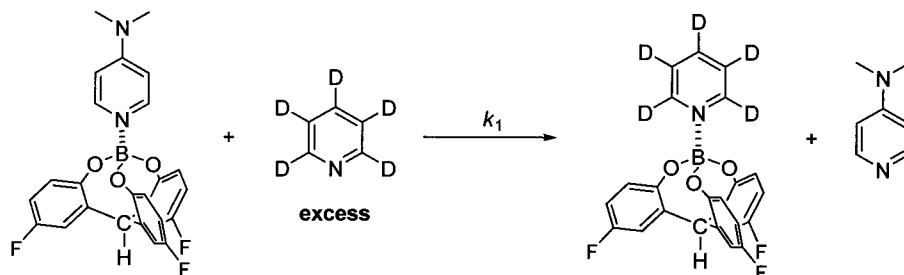
To a suspension of tris(5-fluoro-2-hydroxyphenyl)methane (1dH₃) (0.3 mmol) in dichloromethane (3 mL) was added BH₃·THF in THF (0.3 mmol, 1.0 M) at rt with stirring for 1 h under release of H₂ gas. To the solution was added *N,N*-dimethylanimopyridine (0.3 mmol) at rt. After stirring for 2 h, volatiles was removed under the reduced pressure. The obtained material was washed with dichloromethane with filtration and then recrystallized from dichloromethane/hexane to give the pure complex. The complex (0.017mmol) and pyridine-*d₅* (5 mL) were added to the flask. The rate constants were determined by observing the reaction at 95, 100, 105, and 108 °C. The results are shown in Table 6.

Ligand-Exchange on 1eB.
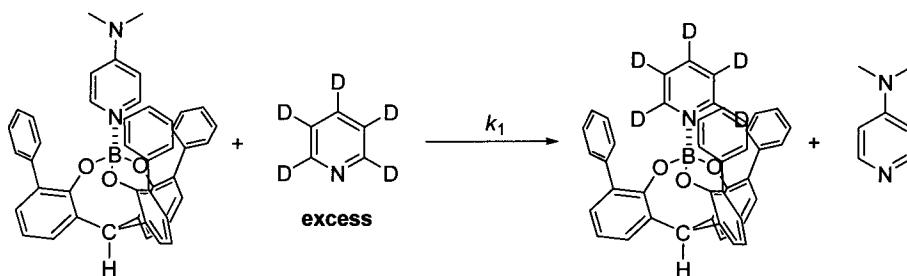
To a solution of tris(2-hydroxy-3-phenylphenyl)methane (1eH₃) (0.2 mmol) in dichloromethane (3 mL) was added BH₃·THF in THF (0.2 mmol, 1.0 M) at rt with stirring for 2 h under release of H₂ gas. To the solution was added *N,N*-dimethylanimopyridine (0.2 mmol) at rt. After stirring for 2 h, volatile was removed under the reduced pressure. The obtained material was washed with dichloromethane with filtration and then recrystallized from dichloromethane/hexane to give the pure complex. The complex (0.008mmol) and pyridine-*d₅* (5 mL) were added to the flask. The rate constants were determined by observing the reaction at 95, 100, 105, and 108 °C. The results are shown in Table 6.

Ligand-Exchange on 1gB.
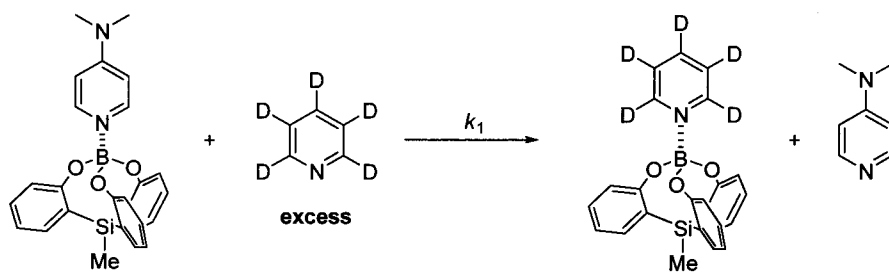
To a suspension of tris(2-hydroxyphenyl)methylsilane (**1gH₃**) (0.1 mmol) in dichloromethane (2 mL) was added BH₃·THF in THF (0.12 mmol, 1.0 M) at rt with stirring for 1 h under release of H₂ gas. To the solution was added *N,N*-dimethylanimopyridine (0.3 mmol) at rt. After stirring for 2 h, volatile was removed under the reduced pressure. The obtained material was washed with dry hexane with filtration to give the pure complex. The complex (0.011mmol) and pyridine-*d₅* (5 mL) were added to the flask. The rate constants were determined by observing the reaction at 15, 20, 25, and 30 °C. The results are shown in Table 6.

37

Figure A. Kinetics plots and Eyring plot for Dissociation of DMAP-B(OC$_6$H$_4$)$_3$CH (**1aB·DMAP**)

80 °C
$R^2 = 0.9441$
$k_{(80°)} = 7.94 \times 10^{-5}\ s^{-1}$

85 °C
$R^2 = 0.9826$
$k_{(85°)} = 1.76 \times 10^{-4}\ s^{-1}$

90 °C
$R^2 = 0.9916$
$k_{(90°)} = 3.49 \times 10^{-4}\ s^{-1}$

95 °C
$R^2 = 0.9963$
$k_{(95°)} = 6.44 \times 10^{-4}\ s^{-1}$

$y = -17754x + 35.01$

$R^2 = 0.99773$

$\Delta H^{\ddagger} = 35.1\ kcal\ mol^{-1}$
$\Delta S^{\ddagger} = 22.3\ cal\ K^{-1}\ mol^{-1}$
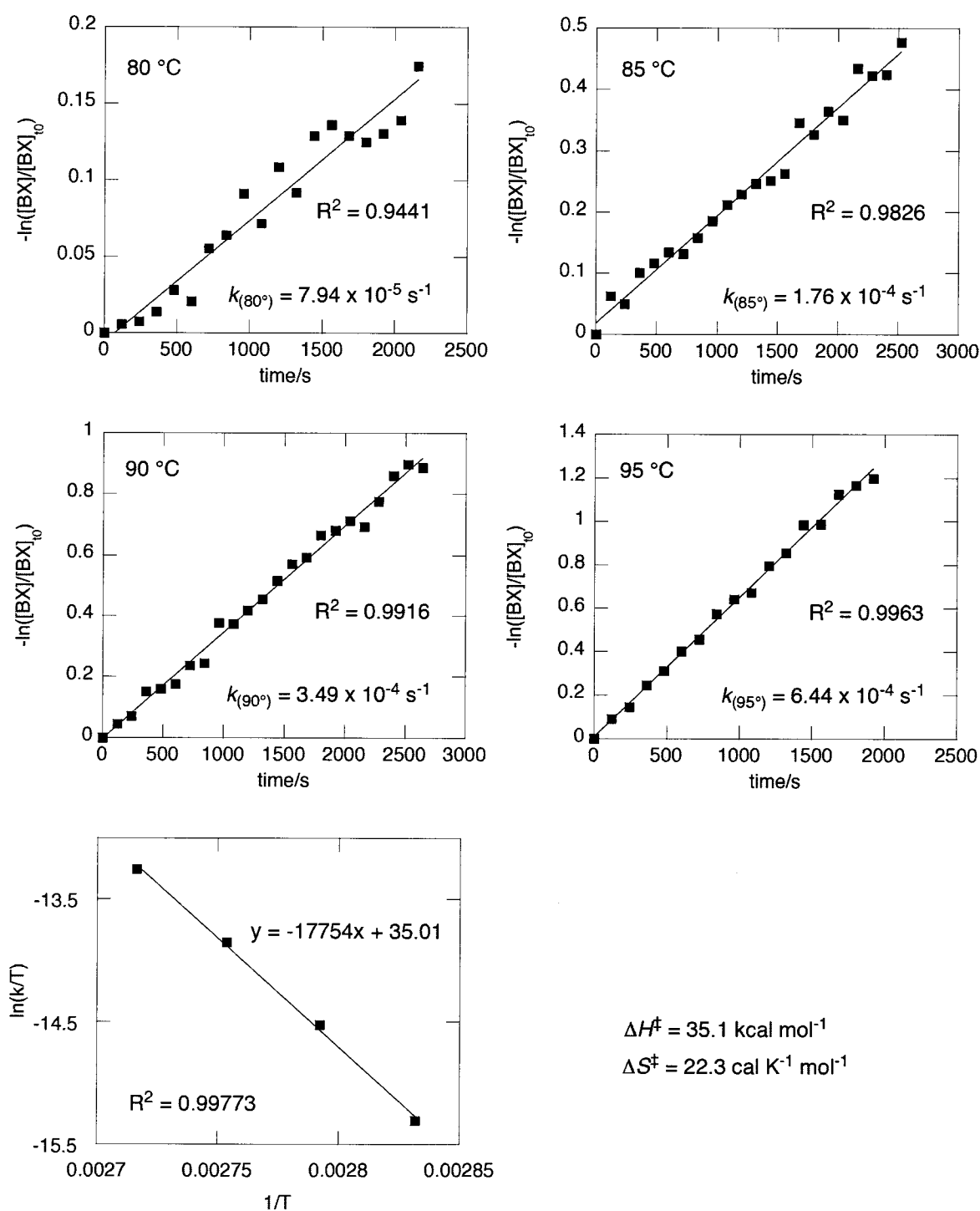
Figure B. Kinetics plots and Eyring plot for Dissociation of DMAP-B(OFC$_6$H$_3$)$_3$CH (**1dB·DMAP**)

Plot at 95 °C: $R^2 = 0.9328$, $k_{(95°)} = 4.51 \times 10^{-5}$ s^{-1}

Plot at 100 °C: $R^2 = 0.9824$, $k_{(100°)} = 1.12 \times 10^{-4}$ s^{-1}

Plot at 105 °C: $R^2 = 0.9911$, $k_{(105°)} = 2.40 \times 10^{-4}$ s^{-1}

Plot at 108 °C: $R^2 = 0.9961$, $k_{(108°)} = 3.59 \times 10^{-4}$ s^{-1}

Eyring plot: $y = -22031x + 44.0$, $R^2 = 0.99742$

$\Delta H^{\ddagger} = 43.6$ kcal mol^{-1}

$\Delta S^{\ddagger} = 40.0$ cal K^{-1} mol^{-1}
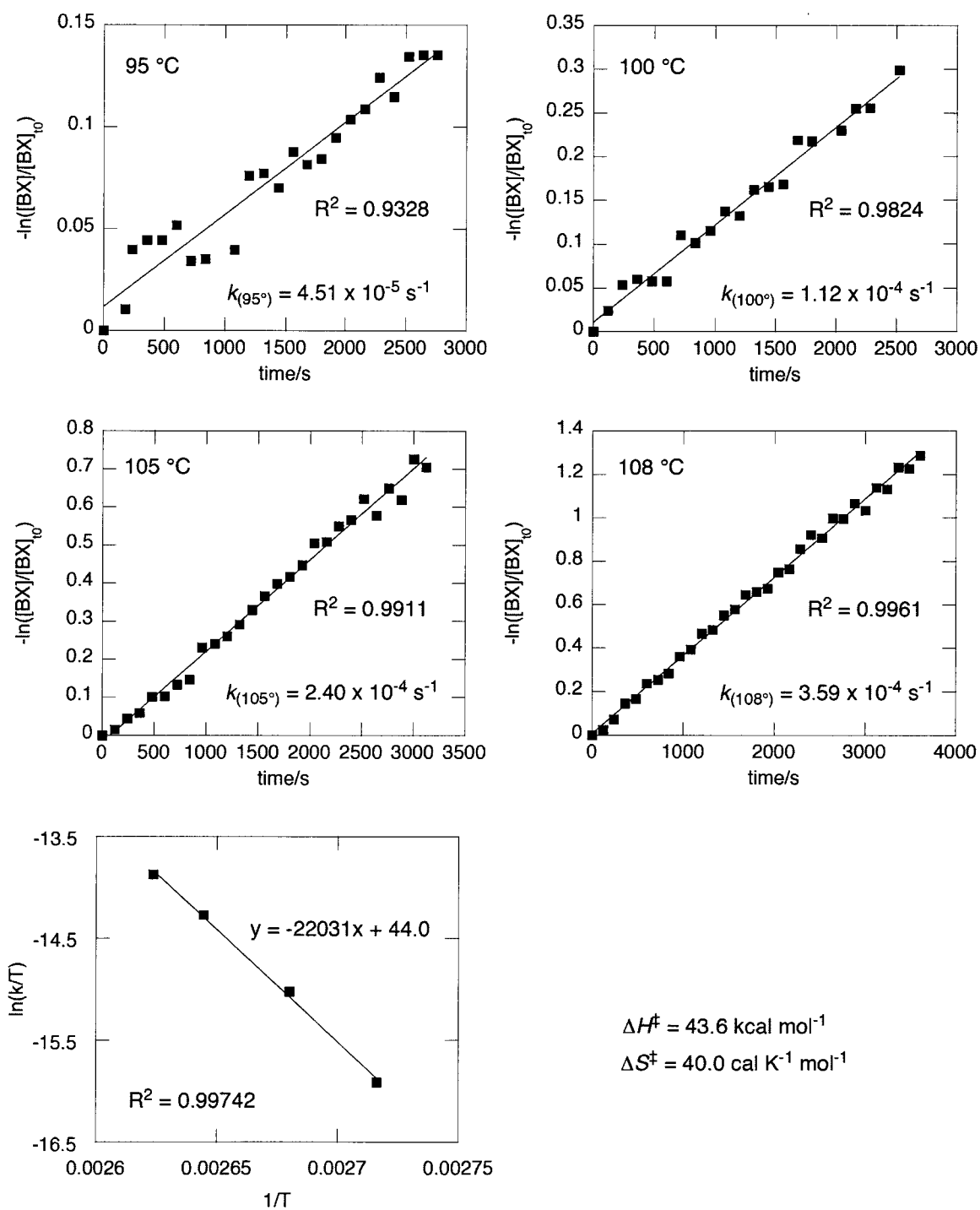
Figure C. Kinetics plots and Eyring plot for Dissociation of DMAP-B(OPhC$_6$H$_3$)$_3$CH (**1eB·DMAP**)

$\Delta H^{\ddagger}$ = 31.2 kcal mol^{-1}

$\Delta S^{\ddagger}$ = 7.52 cal K^{-1} mol^{-1}
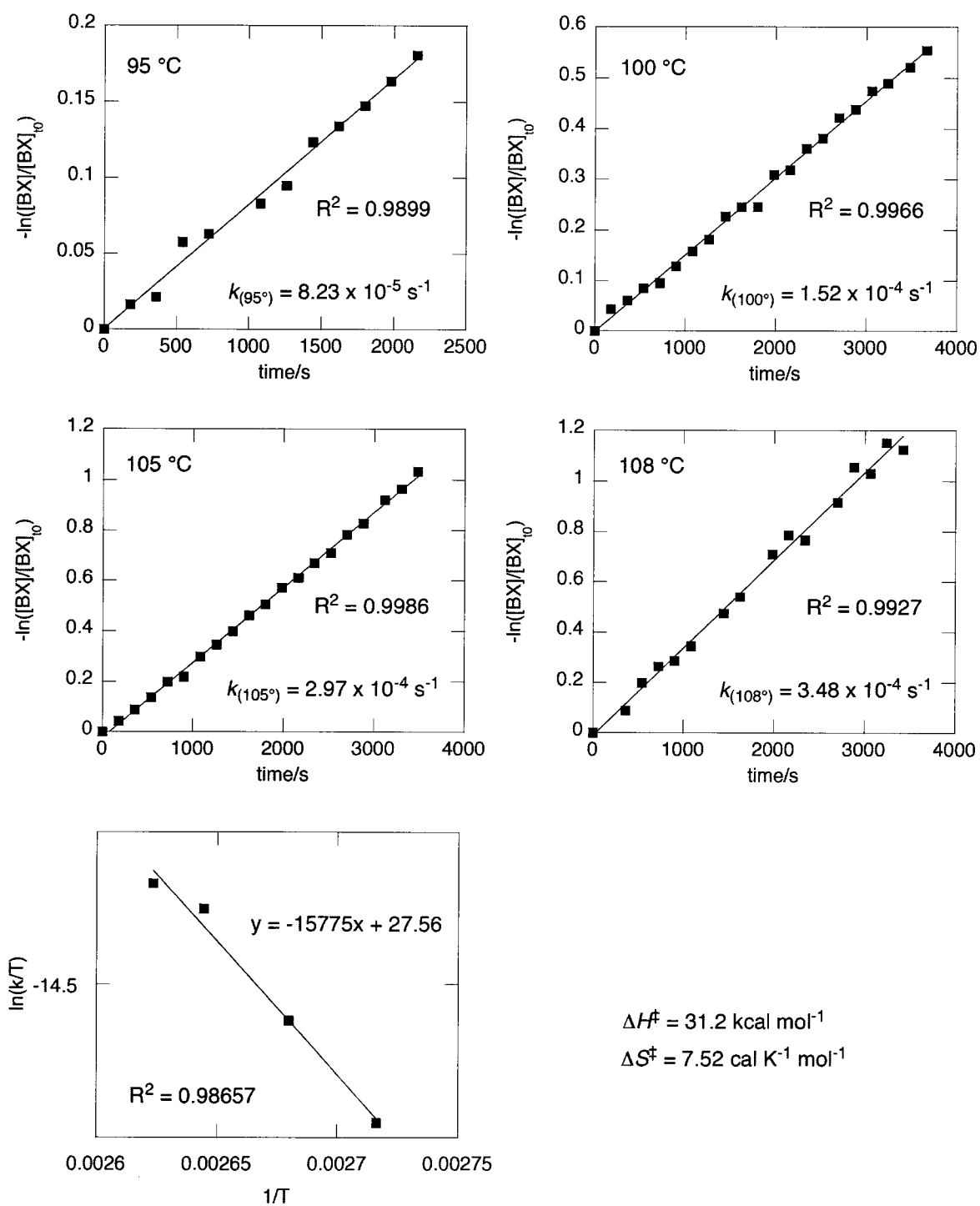
Figure D. Kinetics plots and Eyring plot for Dissociation of DMAP-B(OC$_6$H$_4$)$_3$SiMe (1gB·DMAP)

15 °C
$R^2 = 0.9864$
$k_{(15°)} = 5.47 \times 10^{-5}\ \text{s}^{-1}$
-ln([BX]/[BX]$_{t0}$)
time/s

20 °C
$R^2 = 0.9955$
$k_{(20°)} = 1.32 \times 10^{-4}\ \text{s}^{-1}$
-ln([BX]/[BX]$_{t0}$)
time/s

25 °C
$R^2 = 0.9960$
$k_{(25°)} = 2.97 \times 10^{-4}\ \text{s}^{-1}$
-ln([BX]/[BX]$_{t0}$)
time/s

30 °C
$R^2 = 0.9989$
$k_{(30°)} = 5.64 \times 10^{-4}\ \text{s}^{-1}$
-ln([BX]/[BX]$_{t0}$)
time/s

$y = -13358x + 30.92$
$R^2 = 0.99681$
ln(k/T)
1/T

$\Delta H^{\ddagger} = 26.4\ \text{kcal mol}^{-1}$
$\Delta S^{\ddagger} = 14.2\ \text{cal K}^{-1}\ \text{mol}^{-1}$
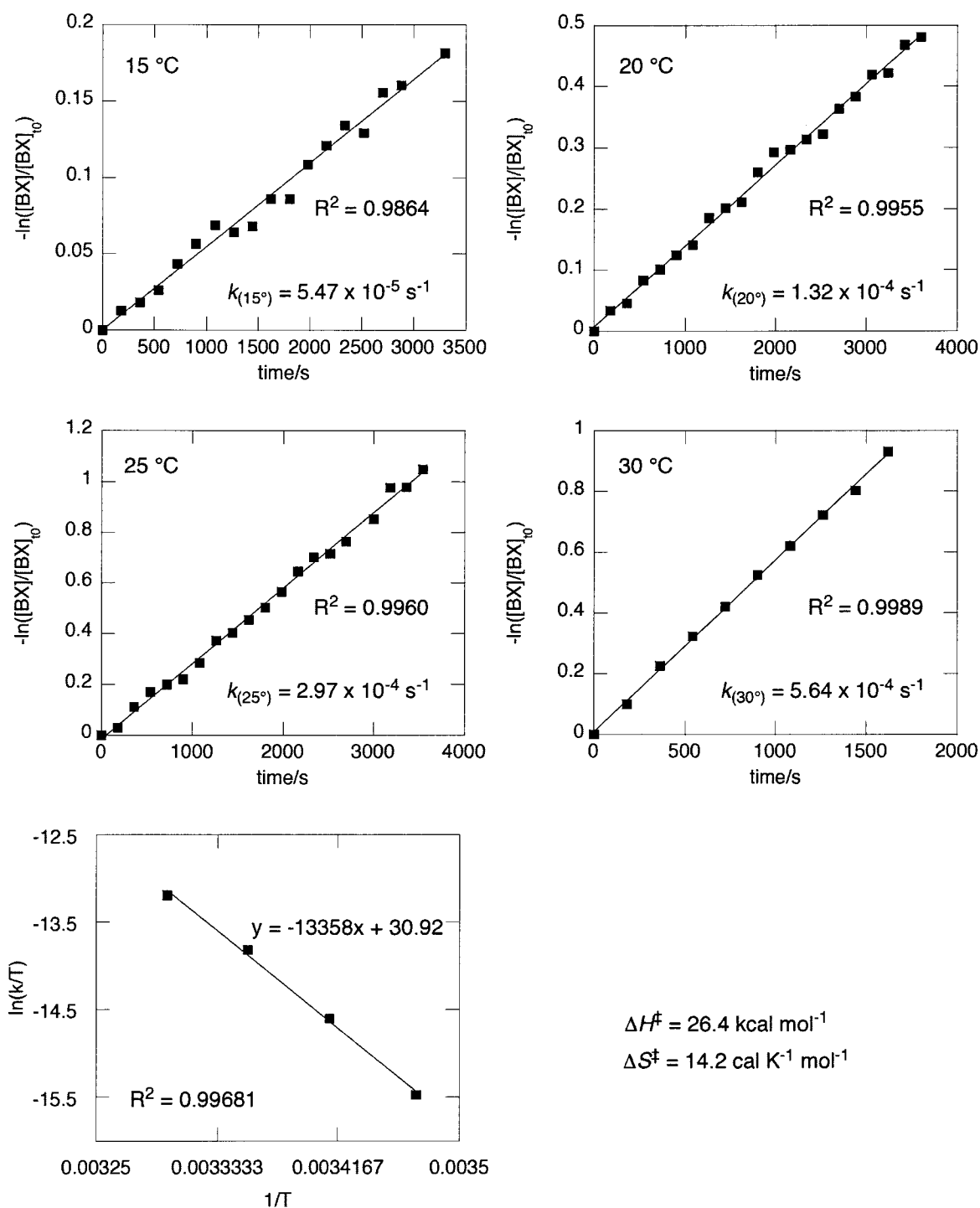
Borate-Catalyzed Hetero Diels-Alder Reaction (Table 7)

Entries 1-7: To a suspension of tris(2-hydroxyaryl)methane or -silane (0.1 mmol) in dichloromethane (3 mL) was added BH$_3$·THF in THF (0.1 mmol, 0.9 M) at rt with stirring for 2 h under release of H$_2$ gas. To the solution was added Danishefsky's diene 6 (1.0 mmol) and benzaldehyde 7a (1.1 mmol) at rt and the mixture was stirred at rt.

41

After stirring for 18 h, H$_2$O (10 mL) was added to the mixture, which was extracted with Et$_2$O (3 x 10 mL). The organic layer was dried (MgSO$_4$) and evaporated to give a crude mixture, which was analyzed by NMR.

Entries 8 and 9: To a solution of benzaldehyde **7a** (1.1 mmol) in dichloromethane (3 mL) was added Danishefsky's diene **6** (1.0 mmol) and B(OPh)$_3$ or BF$_3$ (0.1 mmol)   at rt and the mixture was stirred at rt. After stirring for 18 h, H$_2$O (10 mL) was added to the mixture, which was extracted with Et$_2$O (3 x 10 mL). The organic layer was dried (MgSO$_4$) and evaporated to give a crude mixture, which was analyzed by NMR.

Mukaiyama Aldol Reaction Using Aldehyde Catalyzed by Various Borates (Table 8)

Entries 1-7 and 10-16: To a suspension of tris(2-hydroxyaryl)methane or -silane (0.1 mmol) in dichloromethane (3 mL) was added BH$_3$·THF in THF (0.1 mmol, 0.9 M) at rt with stirring for 2 h under release of H$_2$ gas. To the solution was added silyl ketene acetal **9** or **10** (1.0 mmol) and benzaldehyde **7a** (1.0 mmol) at rt and the mixture was stirred at rt. After stirring for 4-6 h, NaHCO$_3$aq (10 mL) was added to the mixture, which was extracted with Et$_2$O (3 x 10 mL). The organic layer was dried (MgSO$_4$) and evaporated to give a crude mixture, which was analyzed by NMR.

Entries 8, 9, 17 and 18: To a solution of benzaldehyde **7a** (1.1 mmol) in dichloromethane (3 mL) was added silyl ketene acetal **9** or **10** (1.0 mmol) and B(OPh)$_3$ or BF$_3$ (0.1 mmol)   at rt and the mixture was stirred at rt. After stirring for 4-6 h, NaHCO$_3$aq (10 mL) was added to the mixture, which was extracted with Et$_2$O (3 x 10 mL). The organic layer was dried (MgSO$_4$) and evaporated to give a crude mixture, which was analyzed by NMR.

Mukaiyama Aldol Reaction Using Acetal Catalyzed by Various Borates (Table 9)

Entry 1-7: To a suspension of tris(2-hydroxyaryl)methane or -silane (0.1 mmol) in dichloromethane (3 mL) was added BH$_3$·THF in THF (0.1 mmol, 0.9 M) at rt with stirring for 2 h under release of H$_2$ gas. To the solution was added silyl ketene acetal **9** (1.0 mmol) and acetal **13** (1.0 mmol) at rt and the mixture was stirred at rt. After stirring for 6 h, NaHCO$_3$aq (10 mL) was added to the mixture, which was extracted with Et$_2$O (3 x 10 mL). The organic layer was dried (MgSO$_4$) and evaporated to give a crude mixture, which was analyzed by NMR.

Entry 8 and 9: To a solution of acetal **13** (1.1 mmol) in dichloromethane (3 mL) was added silyl ketene acetal **9** (1.0 mmol) and B(OPh)$_3$ or BF$_3$ (0.1 mmol)   at rt and the mixture was stirred at rt. After stirring for 6 h, NaHCO$_3$aq (10 mL) was added to the mixture, which was extracted with Et$_2$O (3 x 10 mL). The organic layer was dried (MgSO$_4$) and evaporated to give a crude mixture, which was analyzed by NMR.

Borate-Catalyzed Hetero Diels-Alder Reaction (Table 10)

To a suspension of tris(2-hydroxyaryl)methane (0.1 mmol) in dichloromethane (3 mL) was added BH$_3$·THF in THF (0.1 mmol, 0.9 M) at rt with stirring for 2 h under release of H$_2$ gas. To the solution was added Danishefsky's diene **6** (1.0 mmol) and aldehyde **7** (1.1 mmol) and at rt and the mixture was stirred at rt. After stirring for 4 h, H$_2$O (10 mL) was added to the mixture, which was extracted with Et$_2$O (3 x 10 mL). The organic layer was dried (MgSO$_4$) and evaporated to give a crude mixture, which was analyzed by NMR.

2,3-dihydro-2-(_o_-phenylphenyl)-4H-pyran-4-one (8c)

mp: 101-103 °C; ^{1}H NMR: (400 MHz, CDCl$_3$) 7.66 (d, J = 7.7 Hz, 1H, 6'-H), 7.53-7.20 (m, 9H, 6-H and Ar-H), 5.48 (ddd, J = 15.2, 2.0, 1.5 Hz, 1H, 2-H), 5.43 (ddd, J = 6.2, 2.0, 1.5 Hz, 1H, 5-H), 2.92 (ddd, J = 17.5, 15.2, 2.0 Hz, 1H, 3-H^a), 2.47 (dddd, J = 17.5, 3.0, 1.5, 1.5 Hz, 1H, 3-H^b); ^{13}C NMR: (100 MHz, CDCl$_3$) 192.0 (s, C-4), 163.3 (d, C-6), 141.3 (s), 139.8 (s), 135.3 (s), 130.4 (d), 129.0 (d), 128.7 (s), 128.5 (d), 128.0 (d), 127.7 (d), 126.4 (d, C-6'), 107.1 (d, C-5), 78.3 (d, C-2), 43.3 (t, C-3); IR (KBr) 1674 (C=O), 1589 (C=C), 1265 (C=C-O-C), 1038 (C=C-O-C) cm^{-1}; MS: (EI, 70 eV) m/z 250 (M$^+$, 26), 179 (94), 165 (100); HRMS: (EI, 70 eV) calculated for (C$_{17}$H$_{14}$O$_2$) 250.0994 (M$^+$) found for m/z 250.0997. Analysis: calculated for C$_{17}$H$_{14}$O$_2$: C, 81.58; H, 5.64, found: C, 81.29; H, 5.56

Borate-Catalyzed Competitive Hetero Diels-Alder Reaction (Table 11)

To a suspension of tris(2-hydroxyaryl)methane (0.1 mmol) in dichloromethane (3 mL) or acetonitrile (3 mL) was added BH$_3$·THF in THF (0.1 mmol, 0.9 M) at rt with stirring for 2 h under release of H$_2$ gas. To the solution was added Danishefsky's diene **6** (1.0 mmol), benzaldehyde **7a** (1.0 mmol) and _o_-phenylbenzaldehyde **7c** (1.0 mmol) at rt and the mixture was stirred at rt. After stirring for 4 h, H$_2$O (10 mL) was added to the mixture, which was extracted with Et$_2$O (3 x 10 mL). The organic layer was dried (MgSO$_4$) and evaporated to give a crude mixture, which was analyzed by NMR.

1-1-5. References

(1) (a) *Lewis Acids in Organic Synthesis*; Yamamoto, H., Ed.; Wiley-VCH: Weinheim, Germany, 2000; Vols 1. (b) *Lewis Acids in Organic Synthesis*; Yamamoto, H., Ed.; Wiley-VCH: Weinheim, Germany, 2000; Vols 2. (c) Reetz, M. T. *Acc. Chem. Res.* **1993**, *26*, 462–468. (d) Snider, B. B. *Acc. Chem. Res.* **1980**, *13*, 426–432.

(2) (a) Ishihara, K.; Yamamoto, H. *Eur. J. Org. Chem.* **1999**, 527–538. (b) Piers, W. E. *Adv. Organomet. Chem.* **2004**, *52*, 1–76.

(3) We use the term "metal" for boron in this manuscript although boron is generally classified as a metalloid.

(4) Carbocations, which are isoelectronic and isostructural with trivalent boron compounds, can be stabilized by the hetero atoms bearing lone pairs that can overlap with the empty p orbital on a carbon atom as well as trivalent boron compounds can. The relationship between the structure and stability of carbocations was extensively investigated; (a) Olah, G. A. *J. Org. Chem.* **2001**, *66*, 5943–5957. (b) Olah, G. A. *J. Org. Chem.* **2005**, *70*, 2413–2429.

(5) Soderquist first explicitly demonstrated that Lewis acidity is attenuated by the introduction of heteroatomic ligands bearing lone pairs that can overlap with the empty p orbital on boron: Matos, K.; Soderquist, J. A. *J. Org. Chem.* **1998**, *63*, 461–470.

(6) For selected examples see: (a) Denmark, S. E.; Griedel, B. D.; Coe, D. M.; Schnute, M. E. *J. Am. Chem. Soc.* **1994**, *116*, 7026–7043. (b) Nelson, S. G.; Kim, B.-K.; Peelen, T. J. *J. Am. Chem. Soc.* **2000**, *122*, 9318–9319. (c) Kobayashi, J.; Kawaguchi, K.; Kawashima, T. *J. Am. Chem. Soc.* **2004**, *126*, 16318–16319. (d) Wagner, C. E.; Kim, J.-S.; Shea, K. J. *J. Am. Chem. Soc.* **2003**, *125*, 12179–12195.

(7) (a) Yasuda, M.; Yoshioka, S.; Yamasaki, S.; Somyo, T.; Chiba, K.; Baba, A. *Org. Lett.* **2006**, *8*, 761–764. (b) Yasuda, M.; Yoshioka, S.; Nakajima, H.; Chiba, K.; Baba, A. *Org. Lett.* **2008**, *10*, 929–932.

(8) A triphenolic methane-based complex with aluminum does not give a mononuclear cage-shaped complex but a multinuclear one with the methane hydrogen inside: Cottone III, A.; Morales, D.; Lecuivre, J. L.; Scott, M. J. *Organometallics* **2002**, *21*, 418–428.

(9) For elegant examples of stereo-controlled aryloxy aluminum Lewis acids, see: (a) Yamamoto, H.; Saito, S. *Pure Appl. Chem.* **1999**, *71*, 239–245. (b) Maruoka, K.; Araki, Y.; Yamamoto, H. *J. Am. Chem. Soc.* **1988**, *110*, 2650–2652. (c) Yamamoto, H.; *Tetrahedron* **2007**, *63*, 8377–8412.

(10) Matsuo, T.; Kawaguchi, H. *Chem. Lett.* **2004**, *33*, 640–645.

(11) (a) Fujita, M.; Lightbody, O. C.; Ferguson, M. J.; McDonald, R.; Stryker, J. M. *J. Am. Chem. Soc.* **2009**, *131*, 4568–4569. (b) Fujita, M.; Qi, G.; Verkerk, U. H.; Dzwiniel, T. L.; McDonald, R.; Stryker, J. M. *Org. Lett.* **2004**, *6*, 2653–2656. (c) Verkerk, U.; Fujita, M.; Dzwiniel, T. L.; McDonald, R.; Stryker, J. M. *J. Am. Chem. Soc.* **2002**, *124*, 9988–9989.

(12) Some substituted triphenoxymethane compounds were reported, although unsubstituted species were not synthesized: Dinger, M. B.; Scott, M. J. *Eur. J. Org. Chem.* **2000**, 2467–2478.

(13) Wada, M.; Kirishima, K.; Oki, Y.; Miyamoto, M.; Asahara, M.; Erabi, T. *Bull. Chem. Soc. Jpn.* **1999**, *72*, 779–785.

(14) Wada, M.; Mishima, H.; Watanabe, T.; Natsume, S.; Konishi, H.; Hayase, S.; Erabi, T. *J. Chem. Soc. Chem. Commun.* **1993**, 1462–1463.

(15) (a) de La Mare, P. B. D.; Vernon, C. A. *J. Chem. Soc.* **1951**, 1764–1767. (b) Majetich, G.; Hicks, R.; Reister, S. *J. Org. Chem.* **1997**, *62*, 4321–4326. (c) Chung, M.-K.; Lightbody, O. C.; Stryker, J. M. *Org. Lett.* **2008**, *10*, 3825–3828.

(16) Godard, A.; Robin, Y.; Queguiner, G. *J. Organomet. Chem.* **1987**, *336*, 1–12.

(17) Dinger, M. B.; Scott, M. J. *Inorg. Chem.* **2001**, *40*, 856–864.

(18) A similar upfield shift in ^{11}B NMR was reported in the boron compound with other trivalent ligands: (a) Müller, E.; Bürgi, H. B. *Helv. Chim. Acta* **1987**, *70*, 499–510. (b) Gillis, E. P.; Burke, M. D. *J. Am. Chem. Soc.* **2007**, *129*, 6716–6717.

(19) See NMR spectra in the Experimental Section.

(20) The difference of the chemical shifts between **1cB·THF** and **1dB·THF** was quite small and difficult to compare their Lewis acidities accurately owing to broadening signals. Therefore we investigated Lewis acidity by using other ligand and describe later (Lewis acidity of the cage-shaped borates).

(21) Two sets of pyridine signals were observed by ^{1}H NMR spectroscopy, but their 4-H signals were obscured by other aryl signals.

(22) The CIF data for **1aB·Py**, **1gB·Py**, and **1hB·Py** were reported previously (reference 7).

(23) Hcpfl, H. *J. Organomet. Chem.* **1999**, *581*, 129–149.

(24) The Lewis basic similar cage-shaped complex has been reported by using P or As (reference 17).

(25) A titanium complex with a similar cage-shape ligand has been reported: Akagi, F.; Matsuo, T.; Kawaguchi, H. *J. Am. Chem. Soc.* **2005**, *127*, 11936–11937.

(26) Linear triphenolic compounds shows chirality when complexed with Al: Appiah, W. O.; DeGreeff, A. D.; Razidlo, G. L.; Spessard, S. J.; Pink, M.; Young, V. G., Jr.; Hofmeister, G. E. *Inorg. Chem.* **2002**, *41*, 3656–3667.

(27) Livant, P. D.; Northcott, J. D.; Shen, Y.; Webb, T. R. *J. Org. Chem.* **2004**, *69*, 6564–6571.

(28) The shown MOs are the lowest unoccupied orbitals to which boron p_z orbitals contribute to acting as Lewis acid.

(29) The described MOs are the lowest unoccupied orbitals with suitable lobes on boron as a Lewis acid.

(30) (a) Danishefsky, S.; Kerwin, J. F.; Kobayashi, S. *J. Am. Chem. Soc.* **1982**, *104*, 358–360. (b) Hattori, K.; Yamamoto, H. *Synlett* **1993**, 129–130.

(31) (a) Yasuda, M.; Yamasaki, S.; Onishi, Y.; Baba, A. *J. Am. Chem. Soc.* **2004**, *126*, 7186–7187. (b) Yasuda, M.; Saito, T.; Ueba, M.; Baba, A. *Angew. Chem.* **2004**, *116*, 1438–1440; *Angew. Chem. Int. Ed.* **2004**, *43*, 1414–1416. (c) Onishi, Y.; Ogawa, D.; Yasuda, M.; Baba, A. *J. Am. Chem. Soc.* **2002**, *124*, 13690–13691. (d) Yasuda, M.; Onishi, Y.; Ueba, M.; Miyai, T.; Baba, A. *J. Org. Chem.* **2001**, *66*, 7741–7744.

(32) Mukaiyama, T.; Narasaka, K.; Banno, K. *Chem. Lett.* **1973**, 1011–1014.

(33) Mukaiyama aldol reaction was used for estimating of Lewis acid property: Raders, S. M.; Verkade, J. G. *J. Org. Chem.* **2009**, *74*, 5417–5428.

(34) Mukaiyama, T.; Hayashi, M. *Chem. Lett.* **1974**, 15–16.

(35) Hirsch, J. A. *Top. Stereochem.* **1967**, *1*, 199–222.

(36) (a) Maruoka, K.; Saito, S.; Concepcion, A. B.; Yamamoto, H. *J. Am. Chem. Soc.* **1993**, *115*, 1183–1184. (b) Maruoka, K.; Saito, S.; Yamamoto, H. *Synlett* **1994**, 439–440.

(37) Nakajima, H.; Yasuda, M.; Chiba, K.; Baba, A. *Chem. Commun.* **2010**, *46*, 4794–4796.

(38) CCDC-794455 (**1bB·Py**), 794456 (**1cB·Py**), 794457 (**1dB·Py**), 794458 (**1eB·Py**), and 794459 (**1fB·Py**) contain the supplementary crystallographic data for this paper. These data can be obtained free of charge from The Cambridge Crystallographic Data Centre via www.ccdc.cam.ac.uk/data_request/cif.

(39) Terao, Y.; Wakui, H.; Nomoto, M.; Satoh, T.; Miura, M.; Nomura, M. *J. Org. Chem.* **2003**, *68*, 5236.

(40) Aikawa, K.; Irie, R.; Katsuki, T. *Tetrahedron* **2001**, *57*, 845–851.

(41) Furuno, H.; Hayano, T.; Kambara, T.; Sugimoto, Y.; Hanamoto, T.; Tanaka, Y.; Jin, Y. Z.; Kagawa, T.; Inanaga, J. *Tetrahedron* **2003**, *59*, 10509–10523.

(42) Huang, Y.; Rawal, V. H. *Org. Lett.* **2000**, *2*, 3321–3323.

(43) Nakagawa, T.; Fujisawa, H.; Nagata, Y.; Mukaiyama, T. *Bull. Chem. Soc. Jpn.* **2004**, *77*, 1555–1567.

(44) Soga, T.; Takenoshita, H.; Yamada, M.; Mukaiyama, T. *Bull. Chem. Soc. Jpn.* **1990**, *63*, 3122–3131.

(45) Becke, A. D. *J. Chem. Phys.* **1993**, *98*, 5648–5652.

(46) Gaussian 03, Revision C.02, Frisch, M. J.; Trucks, G. W.; Schlegel, H. B.; Scuseria, G. E.; Robb, M. A.; Cheeseman, J. R.; Montgomery, Jr., J. A.; Vreven, T.; Kudin, K. N.; Burant, J. C.; Millam, J. M.; Iyengar, S. S.; Tomasi, J.; Barone, V.; Mennucci, B.; Cossi, M.; Scalmani, G.; Rega, N.; Petersson, G. A.; Nakatsuji, H.; Hada, M.; Ehara, M.; Toyota, K.; Fukuda, R.; Hasegawa, J.; Ishida, M.; Nakajima, T.; Honda, Y.; Kitao, O.; Nakai, H.; Klene, M.; Li, X.; Knox, J. E.; Hratchian, H. P.; Cross, J. B.; Adamo, C.; Jaramillo, J.; Gomperts, R.; Stratmann, R. E.; Yazyev, O.; Austin, A. J.; Cammi, R.; Pomelli, C.; Ochterski, J. W.; Ayala, P. Y.; Morokuma, K.; Voth, G. A.; Salvador, P.; Dannenberg, J. J.; Zakrzewski, V. G.; Dapprich, S.; Daniels, A. D.; Strain, M. C.; Farkas, O.; Malick, D. K.; Rabuck, A. D.; Raghavachari, K.; Foresman, J. B.; Ortiz, J. V.; Cui, Q.; Baboul, A. G.; Clifford, S.; Cioslowski, J.; Stefanov, B. B.; Liu, G.; Liashenko, A. ; Piskorz, P.; Komaromi, I.; Martin, R. L.; Fox, D. J.; Keith, T.; Al-Laham, M. A.; Peng, C. Y.; Nanayakkara, A.; Challacombe, M.; Gill, P. M. W.; Johnson, B.; Chen, W.; Wong, M. W.; Gonzalez, C.; Pople, J. A. Gaussian, Inc., Wallingford CT, 2004.

1-2. Creation of Novel Reaction Field Recognizing Aromatic Compounds by π-Pocket in a Cage-Shaped Borate Catalyst

1-2-1. Introduction

Molecular recognition greatly contributes to various fields in nature and in artificial synthesis. Enzymes utilize an affinity for chemical bonding and steric demand to distinguish an appropriate target.[1] In addition, metal complexes have been often applied to the selective recognition of targeted molecules.[2] In almost cases, the useful protocols deal with the metal-heteroatom affinity[3,4] and steric interaction between the ligands and the targeted molecules.[5] Namely, the recognition has been done in terms of electronic and/or steric factors. Therefore, usual metal complexes have never been applied to fine discrimination between similar size of aromatic aldehydes and aliphatic ones that have no functional anchors. To overcome this problem, we focused on clathrate compounds such as molecular clips,[6] molecular tweezers,[7] and cyclophane,[8] which are known to accept aromatic compounds into the cavity of a π-space via an aromatic-aromatic interaction. The combination of a Lewis acid and clathrate compound, giving compound **X**, could lead to a new strategy for a selective reaction of aromatic over aliphatic compounds (Scheme 1). The metal center of the Lewis acid in **X** is expected to capture certain aldehydes via the usual carbonyl-acid interaction, and a "π-pocket" surrounded by aromatic moieties precisely distinguishes aromatic over aliphatic aldehydes. However, to use compound **X** as a practical catalyst, the carful adjustment of both the strength of Lewis acidity and π-affinity is required.

Scheme 1. Concept of Catalyst Bearing a π-Pocket Recognition Site.

Lewis acid bearing π-pocket as recognition site

cage-shaped metal complexes
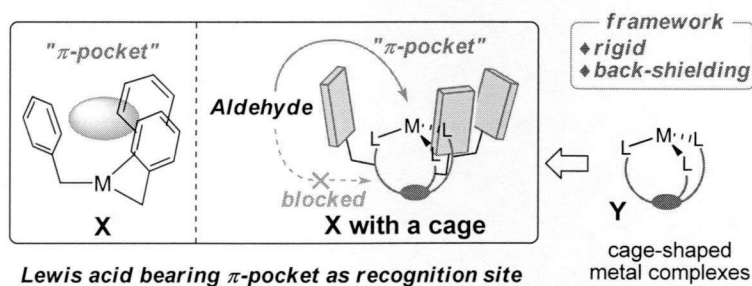
Recently, we designed a tripodal cage-shaped metal complex, **Y**, which precisely tunes Lewis acidity by changing the structure and/or substituents.[9] The cage-shaped complexes of **Y** have rigid structures; thus, we expected a high potential for the creation of a "π-pocket" by introducing various types of aromatic substituents at appropriate positions as shown in **X with a cage** (Scheme 1). Furthermore, the back-shielding framework of the cage effectively blocks the attack of aldehydes to the opposite side of the 'π-pocket'. Herein, we report the synthesis of Lewis acid catalysts that selectively recognize aromatic aldehydes and their application to an unprecedented substrate-selective reaction. The properties of the recognition site can be tuned by introducing various aryl groups into the cage-shaped complexes.

1-2-2. Results and Discussion

We chose a hetero Diels-Alder addition as a model reaction to distinguish an aromatic aldehyde from an aliphatic one. The competitive reaction between butanal (**1**) and benzaldehyde (**2a**), which has similar steric demands,[10] was performed with Danishefsky's diene **3**[11] to produce cycloadducts **4** and **5a**, respectively (Table 1).[12] The cage-shaped borate catalyst **6B·THF** (10 mol%) bearing no π-pocket, which was previously reported,[9a-b, 9d, 13] gave the products in a 73% total yield with a **5a/4** ratio of 0.92/1 in a dichloromethane solvent (entry 1). This result seemed reasonable as the two aldehydes, **1** and **2a**, had similar affinities to the boron center. Next, the phenyl-substituted cage-shaped borate **7B·THF** was used as a catalyst (10 mol%) in dichloromethane to afford the products **5a** and **4** in a ratio of 2.37/1 (entry 5).[14] The increase of **5a** apparently indicated the π-pocket effect of the three phenyl rings. Gratifyingly, this selectivity is the first example of recognizing an aromatic aldehyde over an aliphatic one in a catalytic manner. An interesting difference between the catalysts **6B·THF** and **7B·THF** was observed in the effect of solvents employed. In the case of **6B·THF**, the use of coordinating solvents like diethyl ether, THF and dioxane decreased the addition from 73% to around 20% (entries 2-4), in particular the adduct **5a** produced from benzaldehyde was completely depressed from 35% to around 0%. In contrast, no change of the yield by solvents was observed in the reactions using **7B·THF** (entries 5-8). These results suggested that the phenyl-substituents in **7B·THF** blocked the external solvent from coordination to the boron center and accelerated the addition of benzaldehyde more effectively than butanal. The π-pocket supported by the rigid structure of the cage selectively recognized the aromatic aldehyde.

Table 1. Competitive Reaction of Danishefsky's Diene with an Aliphatic Aldehyde **1** and an Aromatic one **2a** Catalyzed by the Borates **6B·THF** or **7B·THF** in Various Solvents.

entry	catalyst	solvent	total yield (5a/4)	ratio (5a/4)
1		CH_2Cl_2	73(35/38)%	0.92/1
2		Et_2O	24(5/19)%	0.26/1
3		THF	18(nd/18)%	≈0/1
4	6B·THF	dioxane	19(nd/19)%	≈0/1
5		CH_2Cl_2	71(50/21)%	2.37/1
6		Et_2O	69(50/19)%	2.63/1
7		THF	66(37/29)%	1.30/1
8	7B·THF	dioxane	64(45/19)%	2.37/1

The catalyst 7B·THF was applied to a Mukaiyama Aldol reaction using 1-methoxy-1-(trimethylsilyloxy)-2-methyl-1-propene (8) with a mixture of aldehydes 1 and 2a (Scheme 2). The phenyl-substituted borate catalyst 7B·THF showed a high π-pocket effect to give the predominant formation of the adduct 10 from benzaldehyde with a very high selectivity (10/9 = 15.3/1).[15]

Scheme 2. Competitive Reaction of Mukaiyama Aldol Reaction with Butanal (1) and Benzaldehyde (2a) Catalyzed by the Borate 7B·THF.
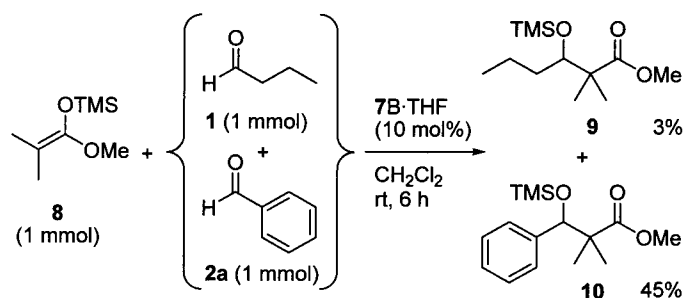
Next, we performed the competitive reaction (Scheme 3) using pentafluorobenzaldehyde (2b) instead of benzaldehydes (2a). Perfluorophenyl ring having similar size to benzene ring is known to well-associate with other arenes owing to the electrostatic attraction induced by their reversed quadrupoles.[16] The phenyl-substituted borate catalyst 7B·THF showed significantly raised the ratio (5b/4 = 6.33/1) as compared with that in benzaldehyde system (5a/4= 2.37/1) in entry 5 of Table 1. In contrast, the unsubstituted borate catalyst 6B·THF showed no selectivity (5b/4 = 0.94/1). These results suggest that the recognition was ascribed to the difference in the aromatic-aromatic interaction between the substituted-phenyl rings of catalysts and aromatic ring of aldehydes.[17]

Scheme 3. Competitive Reaction of Danishefsky's Diene with Butanal (1) and Pentafluorobenzaldehyde (2b) Catalyzed by the Borates 6B·THF or 7B·THF.
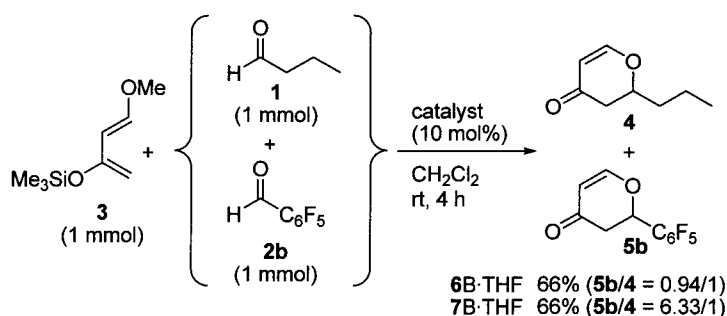
The reaction rates were estimated by the yields at 30 sec, because the hetero Diels-Alder reaction proceeds too fast (Table 2).[18] By using 6B·THF as a catalyst, butanal gave the cycloadduct in higher yield than benzaldehyde (entries 1 and 2). On the contrary, 7B·THF gave a higher yield of the adduct from benzaldehyde (entries 3 and 4). The increase of the yield of 5a in switching from catalyst 6B·THF to

7B·THF strongly indicated the enhancement of the catalytic activity of 7B·THF. These results clearly show acceleration of the reaction by π-π interaction between 7B·THF and benzaldehyde.

Table 2. Experiment for Rate of Hetero Diels-Alder Reaction of Danishefsky's Diene with an Aldehyde (**1** or **2a**) Catalyzed by the Borates **6B·THF** or **7B·THF**.

entry	catalyst	R	product	yield
1	6B·THF	^nPr	**4**	75%
2	6B·THF	Ph	**5a**	56%
3	7B·THF	^nPr	**4**	53%
4	7B·THF	Ph	**5a**	64%

To create a more effective π-pocket, we modified 7B·THF by introducing 1-naphthyl- or 2-naphthyl groups instead of a phenyl one as shown in Figure 1.[19] Compared with the phenyl groups, the naphthyl groups were expected to interact with the aromatic moiety more effectively due to their large π-framework. Crystals of pyridine-ligated borates 7B·Py,[9d] 11B·Py[9d] and 12B·Py (Py = pyridine), suitable for X-ray analysis, were grown from a mixture of dichloromethane and hexane.[20] The results of the structural determination are shown in Figure 1. The top view of 11B·Py shows that the boron center was well covered by the three 1-naphthyl rings as compared with the phenyl rings in 7B·Py. The distances between the rings in 11B·Py were shorter (3.06 Å, 3.28 Å and 5.92 Å) than those in 7B·Py (4.84 Å, 5.25 Å and 6.08 Å). A side view of 12B·Py revealed that a deep pocket was generated around boron by the three 2-naphthyl rings. The average distance of the top of substituted aromatic rings from boron in 12B·Py was longer (8.58 Å) than that in 7B·Py (6.52 Å). The fine-tuned environments around boron were successfully created by introducing various aromatic rings into the cage framework.
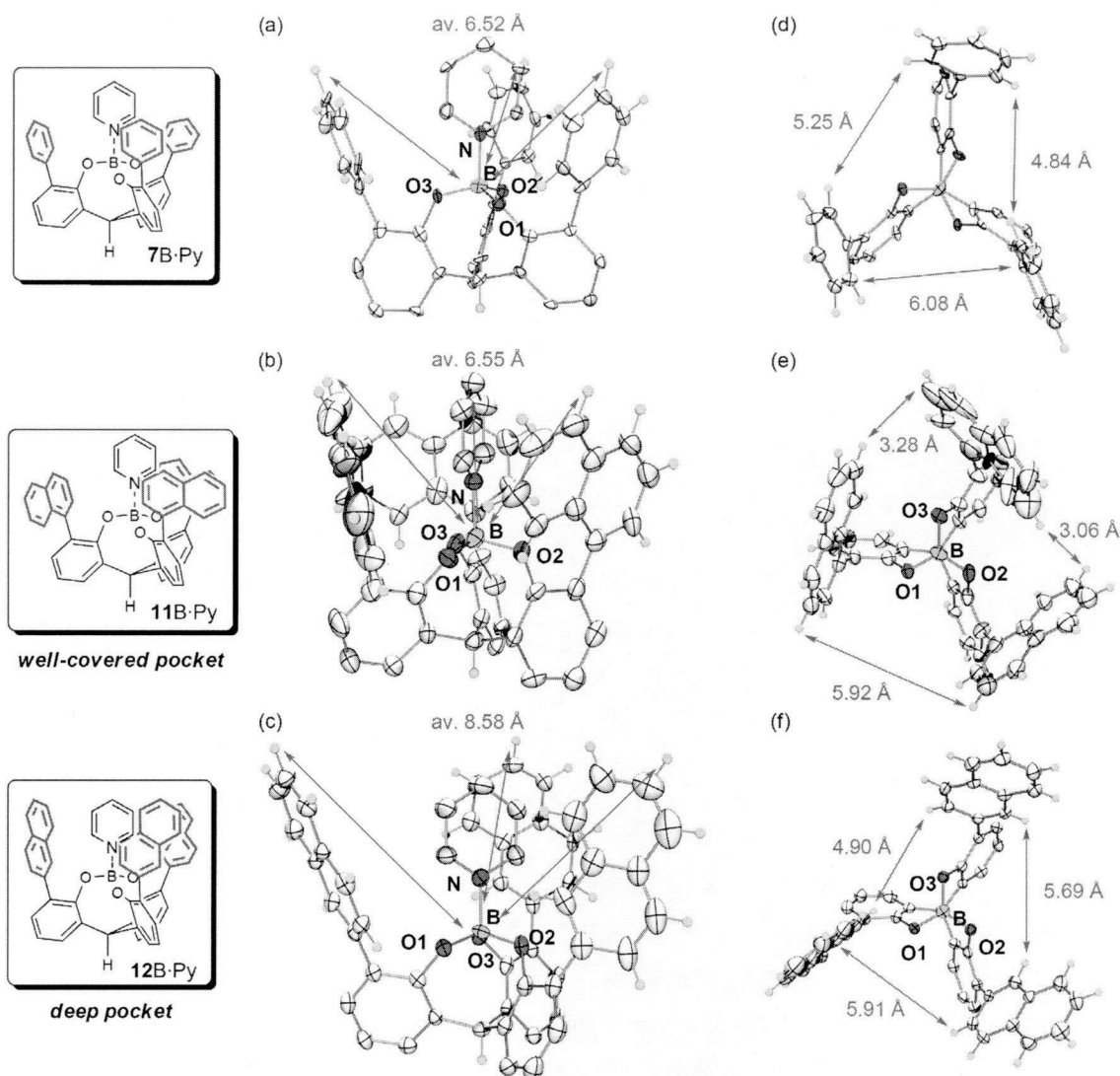
Figure 1. ORTEP Drawing of **7**B·Py, **11**B·Py and **12**B·Py (Thermal ellipsoids are at 50% probability level. Some hydrogens are omitted for clarity. (a) Side view of **7**B·Py (b) Side view of **11**B·Py. (c) Side view of **12**B·Py (d) Top view of **7**B·Py (pyridine is omitted for clarity) (e) Top view of **11**B·Py (pyridine is omitted for clarity) (f) Top view of **12**B·Py (pyridine is omitted for clarity).

We examined the ability of the aryl-substituted borates (**7** B·THF, **11**B·THF and **12**B·THF) to recognize aromatic aldehydes in a competitive reaction of butanal **1** with various aromatic aldehydes **2a-c** (Table 3). In the case of benzaldehyde (**2a**), the naphthyl-substituted borates **11**B·THF and **12**B·THF more selectively catalyzed the aromatic aldehyde (**5a/4** = 2.71/1, and 3.62/1, respectively) than **7**B·THF (**5a/4** = 2.37/1) (entries 2-4). When pentafluorobenzaldehyde (**2b**) was used as an aromatic aldehyde, the ratios of **5b/4** in the cases of aryl-substituted borates (entries 6-8) were significantly raised relative to those of **5a/4** (entries 2-4). A very high selectivity was observed by using **11**B·THF (**5b/4** = 15.9/1) (entry 7). In the case of the other electron-deficient aldehyde (**2c**), the selectivities for **5c/4** were also high (entries 10-12). Interestingly, the **5c/4** product ratio was raised to a high level (27.5/1) by using **12**B·THF. These results suggest that the naphthyl rings in **11-12**B·THF are more effective for the recognition of

aromatic compounds than the phenyl rings in 7B·THF. The substituents at the ortho-positions on the cage significantly influenced the shape of the "π-pocket," and the reaction field can be controlled to give a different selectivity. Each substrate has its own appropriate Lewis acid catalyst with a suitable π-pocket for high selectivity. This method precisely controlled the selectivity via a change in the substituents.

Table 3. Competitive Hetero Diels-Alder Reaction by Using **1** and Various Aldehydes **2a-c** Catalyzed by the Cage-Shaped Borates.

entry	catalyst	Ar	total yield (4 + 5)	ratio (5/4)
1	6B·THF		73%	0.92/1
2	7B·THF		71%	2.37/1
3	11B·THF		63%	2.71/1
4	12B·THF	**2a**	60%	3.62/1
5	6B·THF		66%	0.94/1
6	7B·THF		66%	6.33/1
7	11B·THF		74%	15.9/1
8	12B·THF	**2b**	63%	6.00/1
9	6B·THF		72%	2.00/1
10	7B·THF		79%	8.88/1
11	11B·THF		27%	12.5/1
12	12B·THF	**2c**	57%	27.5/1

1-2-3. Conclusion

We synthesized cage-shaped boron complexes bearing a recognition site for aromatic aldehydes. Application of a competitive reaction revealed that the aryl-substituted borates were able to selectively activate aromatic aldehydes by using an aromatic-aromatic interaction. This is the first example of a Lewis acid effectively distinguishing between aromatic and aliphatic aldehydes in a catalytic manner.

1-2-4. Experimental Section

General. IR spectra were recorded as thin films or as solids in KBr pellets on a HORIBA FT-720 spectrophotometer. ^{1}H and ^{13}C spectra were obtained with a 400 and 100 MHz spectrometer, respectively, with TMS as internal standard. ^{11}B NMR spectra were obtained with a 127 MHz spectrometer with BF$_3$·OEt$_2$ as external standard. Mass spectra were recorded on a JEOL JMS-DS303. All reactions were carried out under nitrogen. Synthesis of boron complexes was performed in nitrogen-filled glove box.

52

Materials. Dehydrated dichloromethane, THF, acetonitrile, diethylether and hexane were purchased and used as obtained. The borates 6B·L, 7B·L and 11B·L (L = THF or Py) were prepared according to our previous report.[9a,9b,9d] 2-(2-methoxyphenyl)naphthalene **12a**[21] were prepared by known methods. All other reagents are commercially available. The product **4**[22], **4b**[23],**4c**[24], **5a**[23], **5c**[25] are known in the literature.

Compound 12 was prepared as shown below.
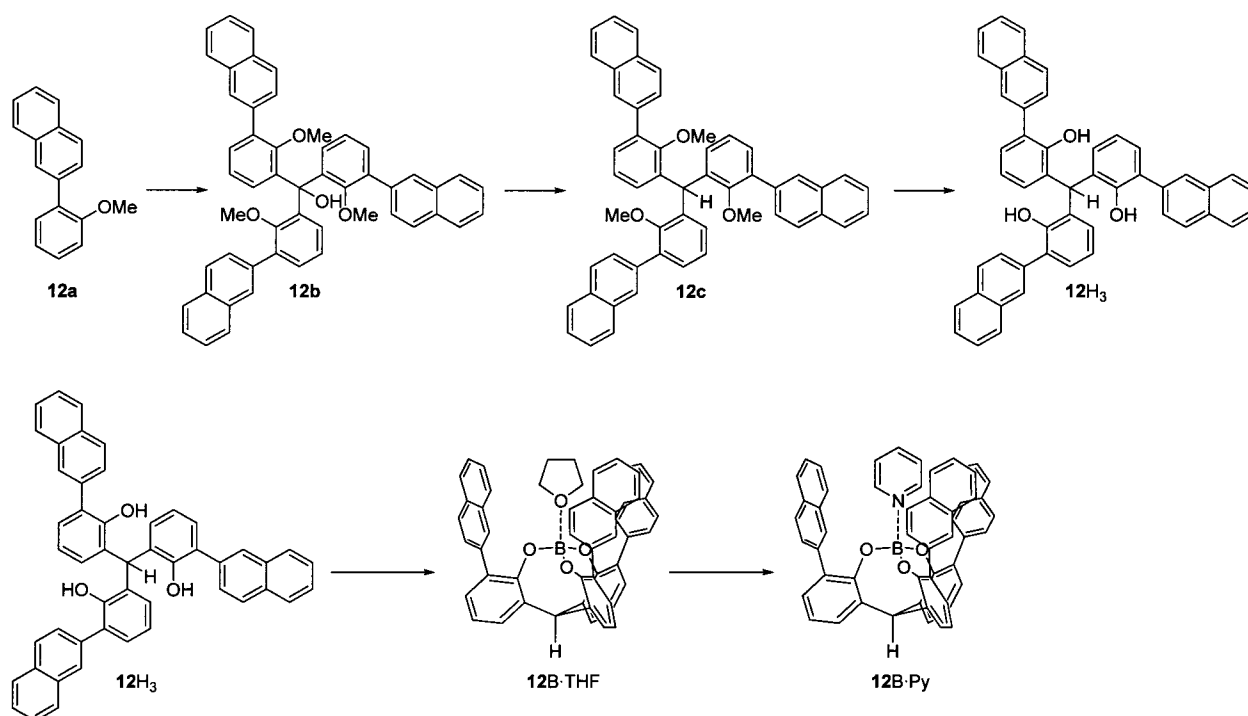
2-(2-methoxyPhenyl)Naphthalene (12a)

The flask equipped with a reflux condenser and a magnetic strring bar was charged with Pd(PPh₃)₄ (0.58 g, 0.5 mmol), 2-naphthaleneboronic acid (5.16 g, 30 mmol), Ba(OH)₂·8H₂O (7.1 g, 40 mmol), 1,2-dimethoxyethane (180 mL), H₂O (30 mL) and 2-iodoanisole (6.3 g, 27 mmol). The mixture was heated in an oil bath at 80 °C for 24h with stirring. After stirring, The flask was cooled to room temperature. The mixture was extracted with Et₂O (3 x 50 mL) and washed with brine (3 x 50 mL). The obtained organic layer was dried (MgSO₄) and evaporated to give a orange solid, which was purified by column chromatography (hexane:EtOAc = 7:3, column length 170 mm, diameter 48 mm silicagel) on silicagel to give the product (5.2 g, 73%) as a white solid. The spectral data of the product was in an excellent agreement with the reported data.

Tris{2-methoxy-3-(2-naphthyl)phenyl}methanol (12b)
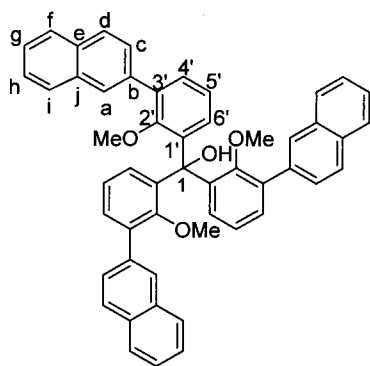
A solution of ^{n}BuLi in hexane (50 mmol, 31 mL, 1.6 M) was introduced in the flask and the volatiles were removed under reduced pressure (20 torr, 30 °C). A dehydrated Et_2O (30 mL) and N,N,N',N'-tetramethylethylenediamine (0.232 g, 2 mmol) were added to the flask. The dropping funnel was charged with 2-(2-methoxyphenyl)nathphalene (11.7 g, 50 mmol) and Et_2O (40 mL). The solution was dropped to the flask at 0 °C. After stirring with warming up to rt for 17 h, the flask was cooled to 0 °C. The dropping funnel was charged with ethyl chloroformate (1.63 g, 15 mmol) and Et_2O (20 mL). The solution was dropped to the flask at 0 °C. The reaction mixture was stirred at rt for 2 h. H_2O (30 mL) was added to quench the reaction and the mixture was extracted with Et_2O (3 x 50 mL). The obtained organic layer was dried ($MgSO_4$) and evaporated to give an orange solid, which was purified by column chromatography (hexane/ethyl acetate = 89:11, column length 11 cm, diameter 21 mm silicagel) on silicagel to give a white product (7.4 g, 68%). mp: 158-160 °C; ^{1}H NMR: (400 MHz, $CDCl_3$) 8.00 (s, 3H, a-H), 7.85 (m, 9H, Ar-H), 7.74 (dd, J = 8.6, 1.2 Hz, 3H, c-H), 7.48 (m, 9H, 6'-H, Ar-H), 7.41 (dd, J = 8.0, 1.6 Hz, 3H, 4'-H), 7.22 (dd, J = 8.0, 8.0 Hz, 3H, 5'-H), 6.01 (s, 1H, OH, D_2O-exchangeable), 2.80 (s, 9H, OMe); ^{13}C NMR: (100 MHz, $CDCl_3$) 156.4 (s, C-2'), 139.3 (s, C-1'), 136.9 (s, C-b), 135.0 (s, C-3'), 133.5 (s, C-e or C-j), 132.4 (s, C-e or C-j), 131.5 (d, C-4'), 129.4 (d, C-6'), 128.0 (d), 127.8 (d), 127.6 (d, C-c), 127.4 (d, C-a), 126.1 (d), 125.9 (d), 123.3 (d, C-5'), 81.4 (s, C-1), 60.1 (q, OMe); IR: (KBr) 3749 (OH), 1223 (C-O) cm^{-1}; MS: (EI, 70 eV) m/z 728 (M$^+$, 15), 495 (M$^+$ - $C_{17}H_{13}O$, 495), 211 (M$^+$ - $C_{34}H_{26}O_2$ - H, 100); HRMS: (EI, 70 eV) calculated for ($C_{52}H_{40}O_4$) 728.2927 (M$^+$) found for m/z 728.2930; Analysis: calculated for $C_{52}H_{40}O_4$: C, 85.69; H, 5.53; found: C, 85.40; H, 5.62.

Tris{2-methoxy-3-(2-naphthyl)phenyl}methane (12c)
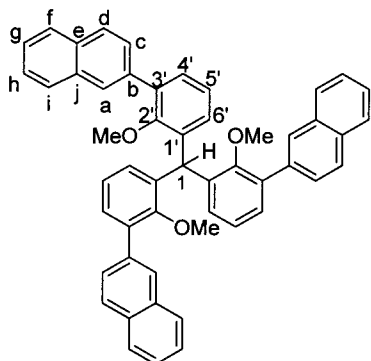
To a suspension of tris{2-methoxy-3-(2-naphthyl)phenyl}methanol (2.4 g, 3.3 mmol) in acetonitrile (7 mL) and THF (7 mL) was added TsOH·H_2O (0.69 g, 3.63 mmol) at 0 °C. The mixture was heated at 80 °C and stirred for 18 h. Cooling down to rt, H_2O (20 mL) was added to the resulting dark brown suspension. The mixture was extracted with Et_2O (3 x 30 mL). The organic layer was dried ($MgSO_4$) and evaporated to give a solid. It was purified by column chromatography (hexane/ethyl acetate = 97:3, column length 11 cm, diameter 21 mm silicagel) on silicagel to give the product (1.7 g, 72%) as a white solid. mp: 128-132 °C; ^{1}H NMR: (400 MHz, $CDCl_3$) 8.08 (s, 3H, a-H), 7.87-7.78 (m, 13H, Ar-H), 7.47 (m, 7H, Ar-H), 7.38 (m, 2H, Ar-H), 7.17 (m, 2H, Ar-H), 7.12-7.00 (m, 3H, Ar-H), 6.90 (s, 0.58, 1-H), 6.82 (s, 0.37H, 1-H), 5.57 (s, 0.28H, 1-H), 3.19 (m, 9H, OMe); ^{13}C NMR: (100 MHz, $CDCl_3$) A number of peaks were observed due to conformational isomers. 155.9, 155.8, 150.2, 138.0, 137.3, 136.6, 134.7, 134.6, 133.5, 132.4, 130.8, 129.9, 129.8, 129.7, 129.0, 128.7, 128.1, 127.9, 127.6, 127.6, 126.5, 126.3, 126.0, 125.9, 123.8, 123.7, 120.2, 60.2 (OMe), 60.1 (OMe), 38.4 (C-1); IR: (KBr) 1223 (C-O) cm^{-1}; MS: (EI, 70 eV) m/z 712 (M$^+$, 100), 681 (M$^+$ - CH_3O, 44), 635

(30), 433 (84), 247 (M⁺ - C₃₄H₂₆O₂, 57), 233 (C₁₇H₁₃O⁺, 47), 217 (32); HRMS: (EI, 70 eV) calculated for (C₅₂H₄₀O₃) 712.2977 (M⁺) found for m/z 712.2980.

Tris{2-hydroxy-3-(2-naphthyl)phenyl}methane (12H₃)
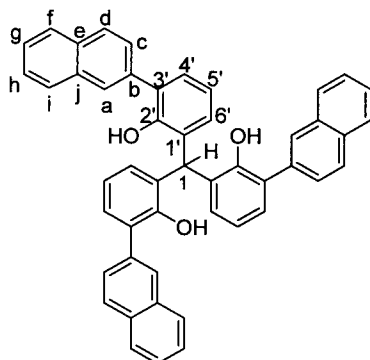
To a solution of tris{2-methoxy-3-(2-naphthyl)phenyl}methane (1.0 g, 1.4 mmol) in dichloromethane (20 mL) was added BBr₃ (1 M in dichloromethane, 4.62 mL, 4.62 mmol) at -78 °C. After stirring with warming up to rt for 22 h, 20 mL of water was added to the mixture at 0 °C. The mixture was extracted with Et₂O (3 x 20 mL). The obtained organic layer was dried (MgSO₄) and evaporated to give a brown solid. It was purified by column chromatography (hexane:EtOAc = 7:3, column length 10 cm, diameter 26 mm silicagel) on silicagel to give the product (282 mg, 30%) as a white solid. For further purification, it was recrystallized to give the pure product (ether/hexane = 1/1). mp: 157-159 °C; ¹H NMR: (400 MHz, CDCl₃) 7.95 (s, 3H, a-H), 7.90 (d, J = 8.4 Hz, 3H, Ar-H), 7.83 (m, 6H, Ar-H), 7.58 (dd, J = 8.4, 1.2 Hz, 3H, Ar-H), 7.48 (m, 6H, Ar-H), 7.30 (dd, J = 7.6, 1.4 Hz, 3H, 4'-H), 7.10 (dd, J = 7.6, 1.4 Hz, 3H, 6'-H), 7.02 (dd, J = 7.6, 7.6 Hz, 3H, 5'-H), 6.60 (s, 1H, 1-H), 5.62 (brs, 3H, OH, D₂O-exchangeable); ¹³C NMR: (100 MHz, CDCl₃) 150.4 (s, C-2'), 134.7 (s, C-b), 133.5 (s, C-e or C-j), 132.6 (s, C-e or C-j), 129.5 (d), 129.2 (s, C-3'), 129.0 (d, C-4' or C-6'), 128.9 (d, C-4' or C-6'), 128.3 (s, C-1'), 127.9 (d), 127.9 (d), 127.7 (d), 127.4 (d), 126.5 (d), 126.3 (d), 120.5 (d, C-5'), 38.3 (d, C-1); IR: (KBr) 3749 (OH) cm⁻¹; MS: (EI, 70 eV) m/z 670 (M⁺, 20), 451 (M⁺ - C₁₆H₁₁O, 24), 434 (M⁺ - C₁₆H₁₁O - OH, 45), 433 (M⁺ - C₁₆H₁₁O - OH - H, 100); HRMS: (EI, 70 eV) calculated for (C₄₉H₃₄O₃) 670.2508 (M⁺) found for m/z 670.2505.

12B·THF
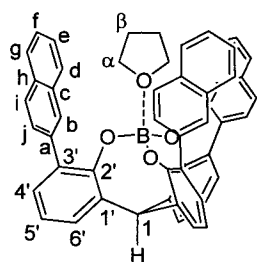
In a glove box, to a solution of tris{2-hydroxy-3-(2-naphthyl)phenyl}methane (0.1 mmol) in dichloromethane (3 mL) was added BH₃·THF in THF (0.11 mmol, 0.9 M) at rt with stirring for 3 h under release of H₂ gas. Evaporation of volatiles gave a viscous liquid, which was washed by hexane to give the product as a white solid. ¹H NMR: (400 MHz, CDCl₃) 7.97-7.02 (m, ca. 30H, Ar-H), 5.61 (m, 0.45H, 1-H), 5.47 (s, 0.55H, 1-H), 3.01 (brs, 2.4H, α-H), 0.64 (brs, 3H, β-H) A borate complex without coordinating THF was partly observed. ¹³C NMR: (100 MHz, CDCl₃) A number of peaks were observed due to conformational isomers. 153.3, 150.4, 150.4, 137.8, 134.7, 133.5, 133.1, 132.7, 132.6, 132.0, 131.5, 130.9, 129.6, 129.3, 129.2, 129.1, 129.0, 128.9, 128.8, 128.3, 128.0, 127.9, 127.7, 127.6, 127.4, 126.5, 126.5, 126.3, 125.8, 125.5, 121.3, 120.5, 71.6, 58.3, 23.3; ¹¹B NMR: (127 MHz, CDCl₃) 5.11 ppm.

12B·Py
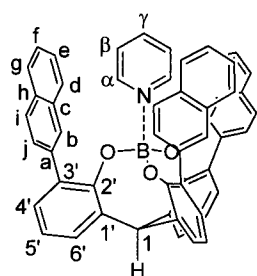
In a nitrogen-filled glove box, to a solution of tris{2-hydroxy-3-(2-naphthyl)phenyl}methane (0.1 mmol) in dichloromethane (3 mL) was added BH_3·THF in THF (0.11 mmol, 0.9 M) at rt with stirring for 3 h under release of H_2 gas. To the solution was added pyridine (0.2 mmol) at rt. After stirring for 2 h, volatiles were removed under reduced pressure. The obtained crude materials were washed with hexane and evaporated to give the product as a white solid. The product was recrystallized from dichloromethane/hexane (2/1) for X-ray analysis. ^{1}H NMR: (400 MHz, CDCl₃) A number of peaks were observed due to conformational isomers. ca. 8.2- 7.16 (m, 32H, Ar-H), 7.04 (dd, J = 7.5, 7.5 Hz, 3H, 5'-H), 6.02 (t, J = 6.9 Hz, 1.5H), 5.52 (s, 1H, 1-H); ^{13}C NMR: (100 MHz, CDCl₃) 154.0 (s, C-2'), 143.3 (d), 140.2 (d), 137.9 (s), 133.0 (s), 132.9 (s), 131.8 (s), 131.0 (d), 128.9 (s), 128.8 (d), 128.3 (d), 127.7 (d), 127.2 (d), 126.2 (d), 125.5 (d), 125.3 (d), 123.5 (d), 121.0 (d, C-5'), 58.8 (d, C-1); ^{11}B NMR (127 MHz, CDCl₃) 4.47 ppm.

Competitive Reaction of Danishefsky's Diene with Two Types of Aldehydes 1 and 2a Catalyzed by the Borates 6B·THF or 7B·THF in Various Solvents. (Table 1)

To a suspension of tris(2-hydroxyaryl)methane (0.1 mmol) in solvent (3 mL) was added BH_3·THF in THF (0.1 mmol, 0.9 M) at rt with stirring for 2 h under release of H_2 gas. To the solution was added butanal 1 (1.0 mmol), benzaldehyde 2a (1.0 mmol) and Danishefsky's diene 3 (1.0 mmol) and the mixture was stirred at rt. After stirring for 4 h, H_2O (10 mL) was added to the mixture, which was extracted with Et_2O (3 x 10 mL). The organic layer was dried ($MgSO_4$) and evaporated to give a crude mixture, which was analyzed by NMR.

The methyne and/or methylene hydrogens of the cyclic products were integrated using 1,1,2,2-tetrachloroethane as an internal standard. All data in this communication were obtained based on two or three experiments in each run. The reproducibility was confirmed. The material balance in these experiments was good, and there were no side products.

The competitive hetero Diels-Alder reactions by using cyclohexanecarbaldehyde 1b or isobutyraldehyde 1c as an aliphatic aldehyde were performed under the same condition with that of Table 1 by using dichloromethane as a solvent.

entry	cat.	aldehyde (R)	total yield (4 + 5a)	ratio (5a/4)
1	6B·THF		69	1.6/1
2	7B·THF	1b	74	5.8/1
3	6B·THF		77	2.1/1
4	7B·THF	1c	77	7.3/1

Competitive Mukaiyama-aldol Reaction of 1-methoxy-1-(trimethylsilyloxy)-2-methyl-1-propene (8) with Butanal (1) and Benzaldehyde (2a) Catalyzed by the Borates 7B·THF. (Scheme 2)

To a suspension of Tris(2-hydroxy-3-phenylphenyl)methane (0.1 mmol) in dichloromethane (3 mL) was added BH₃·THF in THF (0.1 mmol, 0.9 M) at rt with stirring for 2 h under release of H₂ gas. To the solution was added butanal 1 (1.0 mmol), aromatic aldehyde 2 (1.0 mmol) and 1-methoxy-1-(trimethylsilyloxy)-2-methyl-1-propene (1.0 mmol) at rt and the mixture was stirred at rt. After stirring for 6 h, H₂O (10 mL) was added to the mixture, which was extracted with Et₂O (3 x 10 mL). The organic layer was dried (MgSO₄) and evaporated to give a crude mixture, which was analyzed by NMR.

Competitive Reaction of Danishefsky's Diene with Butanal 1 and Pentafluorobenzaldehyde 2b Catalyzed by the Borates 6B·THF or 7B·THF. (Scheme 3)

To a suspension of tris(2-hydroxyaryl)methane (0.1 mmol) in dichloromethane (3 mL) was added BH₃·THF in THF (0.1 mmol, 0.9 M) at rt with stirring for 2 h under release of H₂ gas. To the solution was added butanal 1 (1.0 mmol), pentafluorobenzaldehyde 2b (1.0 mmol) and Danishefsky's diene 3 (1.0 mmol) and the mixture was stirred at rt. After stirring for 4 h, H₂O (10 mL) was added to the mixture, which was extracted with Et₂O (3 x 10 mL). The organic layer was dried (MgSO₄) and evaporated to give a crude mixture, which was analyzed by NMR.

2-(Pentafluorophenyl)-2,3-dihydro-4H-pyran-4-one (5b)
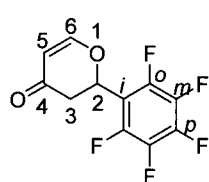
^{1}H NMR: (400 MHz, CDCl₃) 7.48 (d, J = 6.0 Hz, 1H, 6-H), 5.79 (dd, J = 15.6, 3.6 Hz, 1H, 2-H), 5.58 (dd, J = 6.0, 0.8 Hz, 1H, 5-H), 3.26 (dd, J = 16.4, 15.6 Hz, 1H, 3-H^a), 2.58 (ddd, J =16.4, 3.6, 0.8 Hz, 1H, 3-H^b); ^{13}C NMR: (100 MHz, CDCl₃) 190.1 (s, C-4), 162.7 (d, C-6), 145.2 ($^1J_{CF}$ = 233.4 Hz, C-o), 141.8 ($^1J_{CF}$ = 256.4 Hz, C-p), 137.7 ($^1J_{CF}$ = 256.4 Hz,

C-*m*), 110.9 (m, C-*i*), 107.6 (d, C-5), 71.4 (d, C-2), 40.3 (dd, C-3); IR: (neat) 1689 (C=O), 1601 (C=C) cm^{-1}; MS: (EI, 70 eV) *m/z* 264 (M$^+$, 10), 194 (100); HRMS: (EI, 70 eV) calculated for (C$_{11}$H$_5$F$_5$O$_2$) 264.0210 (M$^+$) found for *m/z* 264.0205; Analysis: calculated for C$_{11}$H$_5$ F$_5$O$_2$: C, 50.02; H, 1.91; found: C, 49.76; H, 2.00.

Experiment for Rate of Hetero Diels-Alder Reaction. (Table 2)

To a suspension of tris(2-hydroxyaryl)methane (0.05 mmol) in CD$_2$Cl$_2$ (3.5 mL) was added BH$_3$·THF in THF (0.055 mmol, 0.9 M) at rt with stirring for 2 h under release of H$_2$ gas. To the solution was added aldehyde **1** or **2a** (1.0 mmol)) and Danishefsky's diene **3** (1.0 mmol) and the mixture was stirred at rt. After stirring for 30 s, the portion of the mixture was quenched by D$_2$O and the yield of **4** or **5a** was analyzed by NMR.

Competitive Hetero Diels-Alder Reaction by Using 1 and Electrically Different Aromatic Aldehyde 2 Catalyzed by the Cage-Shaped Borates. (Table 3)

To a suspension of tris(2-hydroxyaryl)methane (0.1 mmol) in dichloromethane (3 mL) was added BH$_3$·THF in THF (0.1 mmol, 0.9 M) at rt with stirring for 2 h under release of H$_2$ gas. To the solution was added butanal **1** (1.0 mmol), aromatic aldehyde **2** (1.0 mmol) and Danishefsky's diene **3** (1.0 mmol) and the mixture was stirred at rt. After stirring for 4 h, H$_2$O (10 mL) was added to the mixture, which was extracted with Et$_2$O (3 x 10 mL). The organic layer was dried (MgSO$_4$) and evaporated to give a crude mixture, which was analyzed by NMR.

X-ray Crystallographical Analysis of THF-ligated Complexes 7B·THF and 11B·THF

CCDC-837103 (**7B**·THF), and CCDC-837104 (**11B**·THF)
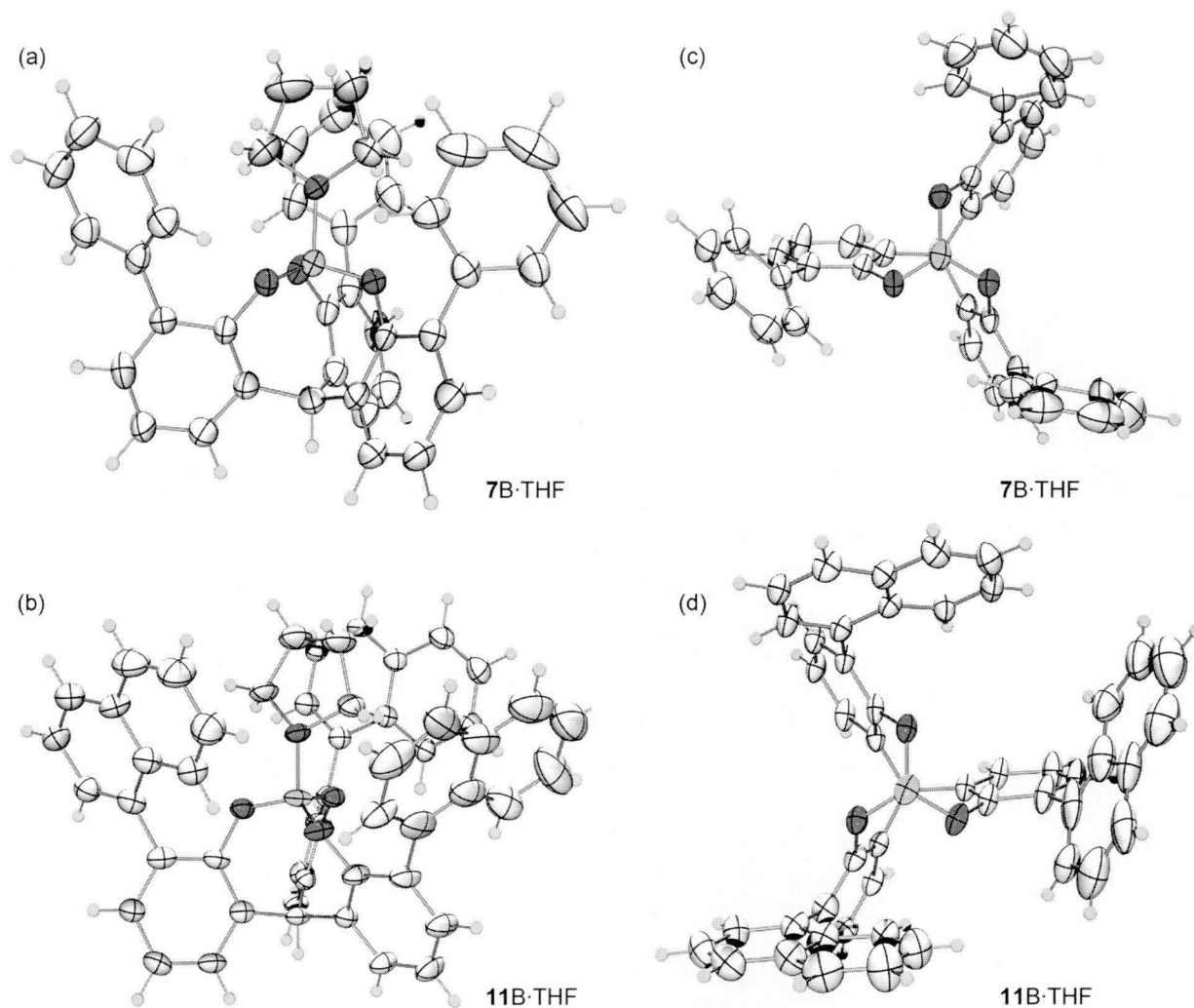
Figure S1. ORTEP Drawing of **7B**·THF and **11B**·THF (Thermal ellipsoids are at 50% probability level.(a) Side View of **7B**·THF (b) Side View of **11B**·THF. (c) Top View of **7B**·THF (THF is omitted for clarity) (d) Top View of **11B**·THF (Pyridine is omitted for clarity)

1-2-5. References

(1) (a) Jencks, W. P. Catalysis in Chemistry and Enzymology, McGraw-Hill, New York, 1969. (b) Ma, B.; Russinov, R. *Curr. Opin. Chem. Biol.* **2010**, *14*, 652-659. (c) Koshland, D. E., Jr. *Proc. Natl. Acad. Sci. USA*, **1958**, *44*, 98-104.

(2) (a) Pearson, R. G. *J. Am. Chem. Soc.* **1963**, *85*, 3533-3539. (b) Woodward, S. *Tetrahedron* **2002**, *58*, 1017-1050.

(3) (a) Kobayashi, S.; Nagayama, S. *J. Org. Chem.* **1997**, *62*, 232-233. (b) Kobayashi, S.; Nagayama, S. *J. Am. Chem. Soc.* **1997**, *119*, 10049-10053. (b) Kobayashi, S.; Busujima, T.; Nagayama, S. *Chem. Eur. J.* **2000**, *6*, 3491-3494. (c) Angelini, E.; Balsamini, C.; Bartoccini, F.; Lucarini, S.; Piersanti, G. *J. Org. Chem.* **2008**, *73*, 5654-5657.

(4) (a) Yamamoto, Y. *J. Org. Chem.* **2007**, *72*, 7817-7831. (b) Zhou, G.; Zhang, J. *Chem. Commun,* **2010**, *46*, 6593-6595.

(5) (a) Maruoka, K.; Saito, S.; Concepcion, A. B.; Yamamoto, H. *J. Am. Chem. Soc.* **1993**, *115*, 1183-1184. (b) Maruoka, K.; Saito, S.; Yamamoto, H. *Synlett* **1994**, 439-440. (c) Yamamoto, H.; Saito, S. *Pure. Appl. Chem.* **1999**, *71*, 239-245.

(6) (a) Zimmerman, S. C.; VanZyl, C. M.; Hamilton, G. S. *J. Am. Chem. Soc.* **1989**, *111*, 1373-1381. (b) Klärner, F.-G.; Burkert, U.; Kamieth, M.; Boese, R.; Benet-Buchholz, J. *Chem. Eur. J.* **1999**, *5*, 1700-1707. (c) Klärner, F. G.; Kahlert, B. *Acc. Chem. Res.* **2003**, *36*, 919-932. (d) Klärner, F. G.; Kahlert, B.; Nellesen, A.; Zienau, J.; Ochsenfeld, C.; Schrader, T. *J. Am. Chem. Soc.* **2006**, *128*, 4831-4841. (e) Schaller, T.; Büchele, U. P.; Klärner, F.-G.; Bläser, D.; Boese, R.; Brown, S. P.; Spiess, H. W.; Felix, K.; Kussmann, J.; Ochsenfeld, C. *J. Am. Chem. Soc.* **2007**, *129*, 1293-1303.

(7) (a) Sijbesma, R. P.; Nolte, R. J. M. *J. Am. Chem. Soc.* **1991**, *113*, 6695-6696. (b) Reek, J. N. H.; Priem, A. H.; Engelkamp, H.; Rowan, A. E.; Elemans, J. A. A. W.; Nolte, R. J. M. *J. Am. Chem. Soc.* **1997**, *119*, 9956-9964. (c) Elemans, J. A. A. W.; Claase, M. B.; Aarts, P. P. M.; Rowan, A. E.; Schenning, A. P. H. J.; Nolte, R. J. M. *J. Org. Chem.* **1999**, *64*, 7009-7016. (d) Klärner, F.-G.; Panitzky, J.; Bläser, D.; Boese, R. *Tetrahedron* **2001**, *57*, 3673-3687.

(8) (a) Tabushi, I.; Sasaki, H.; Kuroda, Y. *J. Am. Chem. Soc.* **1976**, *98*, 5727-5728. (b) Odashima, K.; Itai, A.; Iitaka, Y.; Koga, K. *J. Am. Chem. Soc.* **1980**, *102*, 2504-2505. (c) Diederich, F.; Griebcl, D. *J. Am. Chem. Soc.* **1984**, *106*, 8037-8046. (d) Diederich, F. *Angew. Chem. Int. Ed.* **1988**, *27*, 362-386. (e) Ferguson, S. B.; Sanford, E. M.; Seward, E. M.; Diederich, F. *J. Am. Chem. Soc.* **1991**, *113*, 5410-5419. (f) West, A. P., Jr.; Mecozzi, S.; Dougherty, D. A. *J. Phys. Org. Chem.* **1997**, *10*, 347-350. (g) Meyer, E. A.; Castellano, R. K.; Diederich, F. *Angew. Chem. Int. Ed.* **2003**, *42*, 1210-1250.

(9) (a) Yasuda, M.; Yoshioka, S.; Yamasaki, S.; Somyo, T.; Chiba, K.; Baba, A. *Org. Lett.* **2006**, *8*, 761-764. (b) Yasuda, M.; Yoshioka, S.; Nakajima, H.; Chiba, K.; Baba, A. *Org. Lett.* **2008**, *10*, 929-932. (c) Nakajima, H.; Yasuda, M.; Chiba, K.; Baba, A. *Chem. Commun.* **2010**, *46*, 4794-4796. (d) Yasuda, M.; Nakajima, H.; Takeda, R.; Yoshioka, S.; Yamasaki, S.; Chiba, K.; Baba, A. *Chem. Eur. J.* **2011**, *17*, 3856-3867.

(10) Hirsch, J. A. *Topics in Stereochemistry* **1967**, *1*, 199-222.

(11) Danishefsky, S.; Kitahara, T. *J. Am. Chem. Soc.* **1974**, *96*, 7807-7808.

(12) The hetero Diels-Alder reaction of Danishefsky's diene with aldehyde (butanal or benzaldehyde) did not proceed under uncatalyzed conditions at room temperature.

(13) The external THF ligand was always at the boron center after our preparation procedure for the cage-shaped borates because the borate has a Lewis acidity that is higher than the normal planar structural borate.[9a-b,9d]

(14) We used other aliphatic aldehydes such as cyclohexanecarbaldehyde (**1b**) or isobutyraldehyde (**1c**) instead of butanal (**1**) in the competitive hetero Diels-Alder reaction by using dichloromethane as a solvent under the same conditions as shown in Table 1. The cage-shaped borates 7B·THF gave the products with a **5a/4b** ratio = 5.8/1 (74% yield) and **5a/4c** = 7.3/1 (77% yield), respectively. These ratios were higher than that of **5a/4** (= 2.37/1). These results show that the bulkiness of the substrate controlled the selectivity as well as the π-π interaction. To focus on the only π-π interaction, the less bulky butanal **1** was chosen as an aliphatic aldehyde for the estimation of catalyst properties.

(15) The unsubstituted borate 6B·THF did not give the products and we are not able to precisely compare the catalytic activity between 6B·THF and 7B·THF. Therefore, the selectivity was discussed by performing the hetero Diels-Alder reaction.

(16) (a) Patrick, C. R.; Prosser, G. S. *Nature* **1960**, *187*, 1021. (b) Williams, J. H.; Cockcroft, J. K.; Fitch, A. N. *Angew. Chem. Int. Ed.* **1992**, *31*, 1655-1657.

(17) (a) Hunter, C. A. *Angew. Chem. Int. Ed.* **1993**, *32*, 1584-1586. (b) Hunter, C. A.; Lawson, K. R.; Perkins, J.; Urch, C. J. *J. Chem. Soc., Perkin Trans.* **2001**, *2*, 651-669. (c) Waters, M. L. *Curr. Opin. Chem. Biol.* **2002**, *6*, 736-741.

(18) See Experimenta Section for further details.

(19) The materials and methods are given in Experimenta Section.

(20) Crystals of THF-ligated borates 7B·THF and 11B·THF suitable for X-ray diffraction were successfully obtained. Unfortunately, in the case of 12B·THF, a crystal suitable for X-ray diffraction was not obtained. However, the structural features of 7B·THF and 11B·THF were similar to those of pyridine-ligated borates 7B·Py and 11B·Py. Therefore, we discussed the structure of the cage-shaped borates 7B, 11B and 12B by using pyridine-ligated complexes. The results of the structural determination of 7B·THF and 11B·THF are provided in the Experimental Section. X-ray crystallographic coordinates for 12B·Py, 7B·THF and 11B·THF have been deposited at the Cambridge Crystallographic Database, numbers 837105, 837103, and 837104, respectively.

(21) Li, B.-J.; Li, Y.-Z.; Lu, X.-Y.; Liu, J.; Guan, B.-T.; Shi, Z.-J. *Angew. Chem. Int. Ed.* **2008**, *47*, 10124-10127.

(22) Furuno, H.; Hayano, T.; Kambara, T.; Sugimoto, Y.; Hanamoto, T.; Tanaka, Y.; Jin, Y. Z.; Kagawa, T.; Inanaga, J. *Tetrahedron*, **2003**, *59*, 10509-10523.

(23) Aikawa, K.; Irie, R.; Katsuki, T. *Tetrahedron*, **2001**, *57*, 845-851.

(24) Danishefsky, S.; Kerwin, J. F., Jr.; Kobayashi, S. *J. Am. Chem. Soc.* **1982**, *104*, 358-360.

(25) Long, J.; Hu, J.; Shen, X.; Ji, B.; Ding, K. *J. Am. Chem. Soc.* **2002**, *124*, 10-11.

Chapter 2

Cage-Shaped Ligands Linked by Benzene Ring

2-1. Synthesis and Theoretical Studies of Gallium Complexes Back-Shielded by a Cage-Shaped Framework of Tris(*m*-oxybenzyl)arene

2-1-1. Introduction

The chemistry of Lewis acids has been developed quite extensively because of their effective activation of reactant reagents.[1] A representative class of Lewis acids contains group 13 elements because they have a vacant p-orbital to contribute to an accepting basic substrate.[2] In Chapter 1, we designed tris(*o*-hydroxyphenyl)methane $1H_3$ and tris(*o*-hydroxyphenyl)silane $2H_3$ as ligands to synthesize cage-shaped borates 1B and 2B (Scheme 1a).[3,4] The cage-shaped geometry created a highly accessible vacant molecular orbital (MO) on boron in 1B and 2B and enhanced catalytic activity. We expected this cage-shape concept to lend a greater advantage for larger group 13 metal compounds. In contrast to boron complexes, the open shape of ML_3, having either a Ga or an In center, has four, or more, coordinated spheres[5] and easily accepts an external ligand (L_{ex}) to lower the Lewis acidity (Scheme 2a). That is a disadvantage for activation of the substrate as a Lewis acid. It was suggested that the cage-shaped framework could overcome this problem by inhibiting the external ligand (L_{ex}) coordination (Scheme 2b). Herein, we report a new type of cage-shaped gallium complex, 3aGa, with a back-shielding framework (Scheme 1b) and interesting properties.

Scheme 1. Cage-Shaped Metal Complexes and Their Ligands.

(a) *Previous Work (Chapter 1)* (b) *This Work*

Z-R = C-H   1H₃
    = Si-Me   2H₃
1B
2B
3aH₃
3aGa
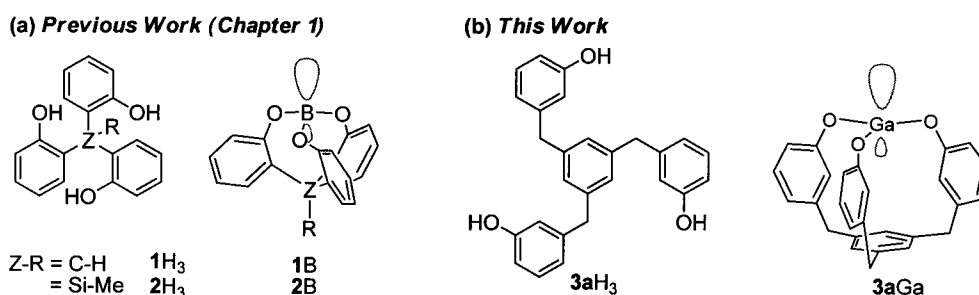
Scheme 2. Concept of the Back-Shielding Effect.

(a) *Open-Shape*

Coordination of
External Ligand

⇩

Low
Lewis Acidity

(b) *Cage-Shape*

Back-Shielded
by Ligand Framework

⇩

Enhanced
Lewis Acidity
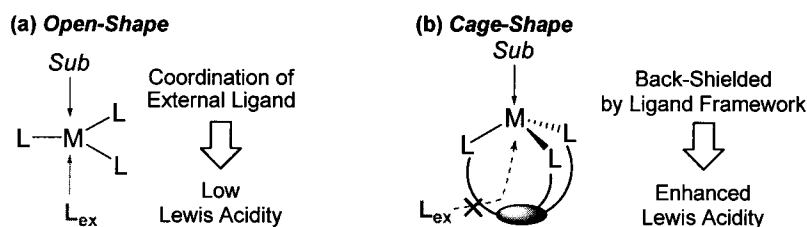
2-1-2. Results and Discussion

First, we attempted to synthesize cage-shaped gallium complexes with the previously reported ligands $1H_3$ and $2H_3$, but no desired complexes were obtained due to their narrow space. Therefore, we designed new ligands $3H_3$, as shown in Scheme 3, in which three oxybenzyl moieties were linked to a benzene ring.[6] The Cu(I)-catalyzed coupling between the Grignard reagent **4a** and 1,3,5-tris(bromomethyl)benzene (**5a**) gave the compound **6a** bearing three m-methoxybenzyl moieties. Treatment of **6a** with BBr_3 afforded the compound $3aH_3$. Three more types of $3b$-dH_3 derivatives bearing substituents on benzene rings were similarly synthesized. The reaction of $3aH_3$ with $GaCl_3$ in the presence of pyridine gave the cage-shaped gallium complex $3aGa \cdot Py$.[7] In the ^1H NMR of $3aGa \cdot Py$, the upfield-shift of the proton at the m- and p-positions of the oxygen moiety relative to that of $3aH_3$ was confirmed (m-position, 7.15→7.07 ppm; p-position, 6.78→6.68 ppm). Analogous results for spectral analysis were obtained for $3b$-$3dGa \cdot Py$.

Scheme 3. Preparation of Ligands $3H_3$ and Their Gallium Complexes $3Ga \cdot Py$.
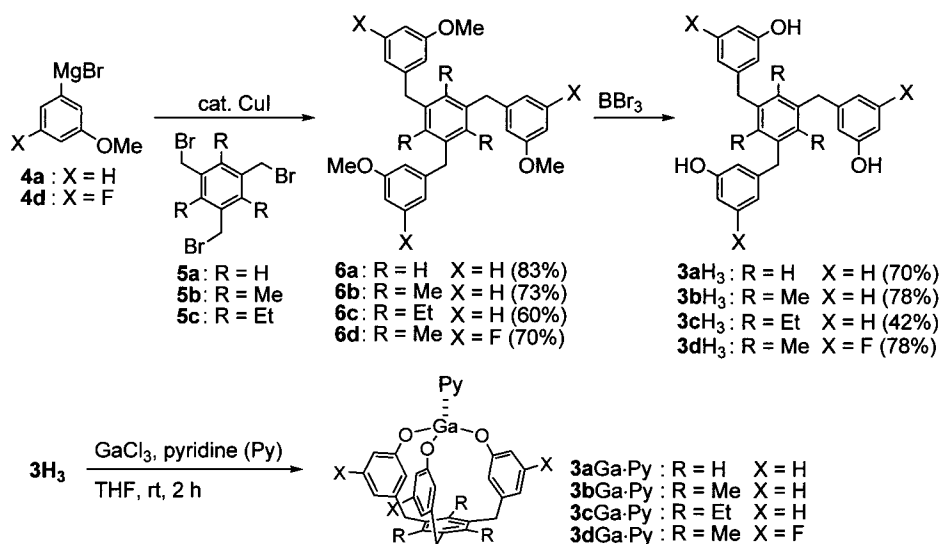
The structure of gallium complex $3bGa \cdot Py$ was analyzed by X-ray crystallography.[8] Considering the occupancy factor of the gallium atom was 0.44, the refinement of the crystal structure was carried out successfully by using disorder modeling. We think that a part of the complex was decomposed by pyridine hydrochloride during recrystallization because it took several months to obtain a crystal which was suitable for X-ray analysis. The structure shown in Figure 1 supports the generation of $3bGa \cdot Py$. The top view shows that the Ga atom lies above the center of the benzene ring (Figure 1b). The average lengths of the Ga−O bond, 3.06 Å, and of the Ga−N1 bond, 3.28 Å, were considerably longer than usual (1.94 Å and 2.02 Å, respectively),[9] because of a deficiency of ca. half the gallium atoms in the crystal.
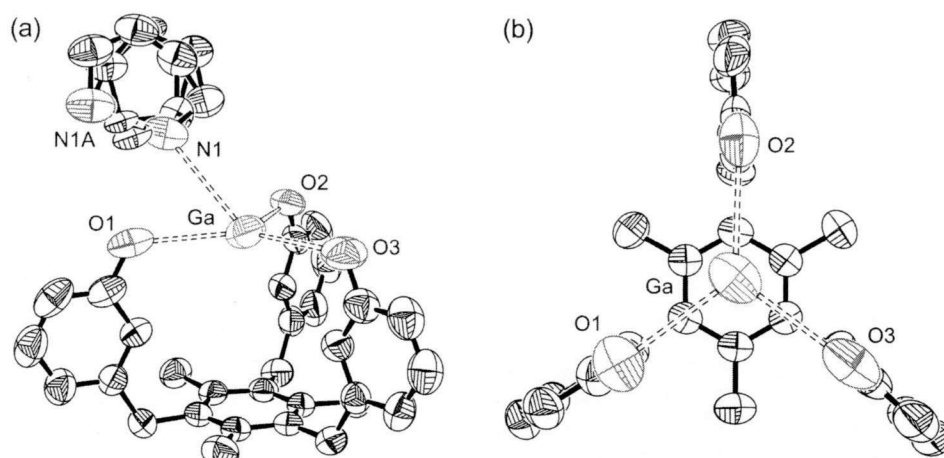
Figure 1. ORTEP Drawing of **3bGa·Py** with Disorder Modelled in (Thermal ellipsoids are at 50% probability level. Hydrogens are omitted for clarity. The occupancy factor of the gallium atom is 0.44): (a) Side View (b) Top View (Pyridine is omitted for clarity).

Theoretical calculations were performed to investigate the properties of the cage-shaped gallium complex, **3bGa**, in comparison with the open-shaped one, Ga(OPh)$_3$ **7**, using the hybrid density functional theory B3PW91/6-31+G(d,p) method with the Gaussian 03 program.[10] The stabilization energies in pyridine complexation reveal that the back-shielding effect of the cage-shaped structure should be effective for keeping Lewis acidity high (Scheme 4). The open-shaped gallium complex **7·Py** coordinated by pyridine has a stabilization energy of 39.2 kcal mol^{-1} (path a), and coordination of the second pyridine leads to additional stabilization of 14.2 kcal mol^{-1} (path b), as shown in Scheme 4a. These results show that the second ligand coordination-dissociation step (path b) mainly contributes to Lewis acidity. However, the cage-shaped gallium complex, **3bGa**, disturbs the second coordination to get one stabilization energy of 39.3 kcal mol^{-1} that contributes to Lewis acid-mediated reactions (path c), as shown in Scheme 4b. This is the reason the cage-shaped complex has high potential as a Lewis acid.

Scheme 4. Stabilization Energy of **7** and **3bGa** in a Pyridine Complexation (Gaussian03 D.01, B3PW91/6-31+G(d,p), gas phase).
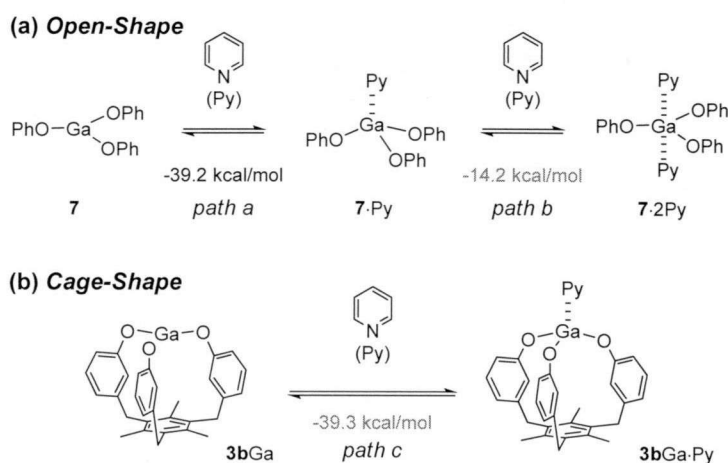
The optimized structures and the MO diagrams of **3bGa**, **7** and **7·Py** are shown in Scheme 5.[11] The complex **3bGa** has a small concave geometry around gallium while **7** has a planar geometry (sum of ∠OGaO: **3bGa**, 352.01; **7**, 360.01). The diagram of the unoccupied orbital of **3bGa**, which contributes to Lewis acidity (corresponding to LUMO+n),[12] shows a large and accessible lobe on gallium, while the corresponding lobes in **7** and **7·Py** are small and buried. These results indicate that the MO of **3bGa** is more suited to accepting a reagent than that of either **7** or **7·Py**.

Scheme 5. Comparison of Open- and Cage-Shaped Gallium Complexes (**3bGa**, **7** and **7·Py**) by First Principles Calculations (B3PW91/6-31+G(d,p)).

	3bGa	7	7·Py
Optimized structure (Aryl Hs omitted)	Ga	Ga	Ga
sum of ∠O-Ga-O	352.0°	360.0°	348.7°
MO diagram of LUMO+n	LUMO+5	LUMO+10	LUMO+7
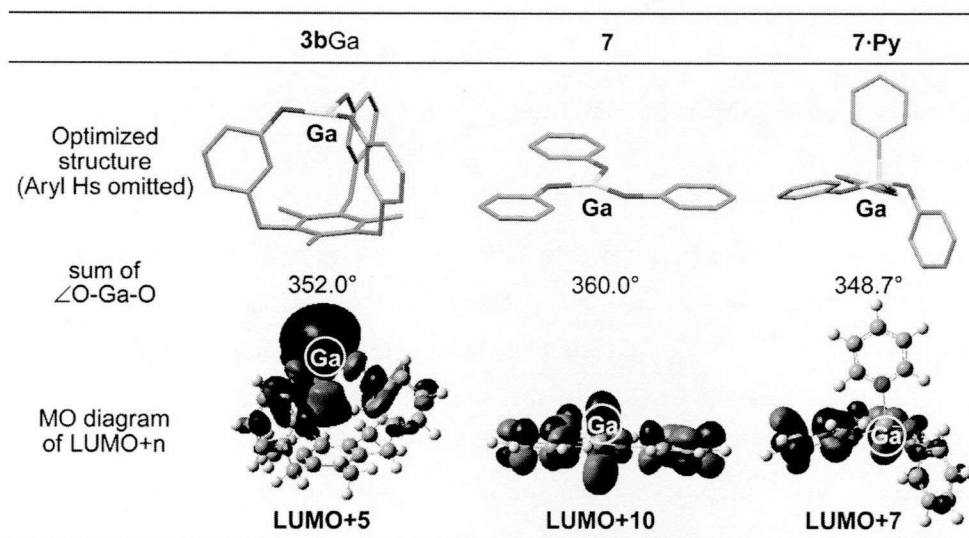
We examined the catalytic activity of the gallium complexes during the hetero Diels-Alder reaction of Danishefsky's diene **8** with benzaldehyde (**9**) to give pyran **10** (Eq 1).[13,14] The open-shaped gallium complex **7·nPy** (n = 1 or 2) afforded **10** in only 34% yield. In contrast, the cage-shaped gallium complex **3bGa·Py** gave **10** in a higher yield of 61%. The cage-shaped structure apparently enhanced catalytic activity of the complex.
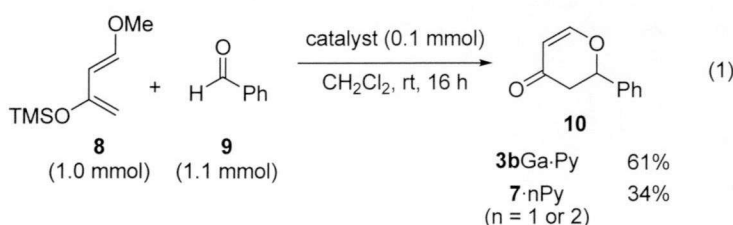
Next, we examined the effect of the substituents on the cage-shaped gallium complexes **3a-dGa** by theoretical calculation (Scheme 6 and 7). The substituents, R, on the bottom benzene ring changed the geometry around the gallium as shown in Scheme 6. In the complex with bulky substituents, both the benzene rings of the arm and the bottom benzene ring approach a perpendicular state because of the

steric hindrance between the substituents (dihedral angle (C1-C2-C3-C4): **3a**Ga, 68.61°; **3b**Ga, 78.01°; **3c**Ga, 85.71°). The large dihedral angle of **3c**Ga creates a more concave geometry around gallium than those of **3a**Ga and **3b**Ga (sum of ∠OGaO: **3a**Ga, 353.21°; **3b**Ga, 352.01°; **3c**Ga, 351.51°). These geometric changes produce differences in the energy levels of the LUMOs and LUMOs+n[12] of **3a-c**Ga, as shown in Scheme 7.[15] These orbitals are the unoccupied orbitals to which gallium p_z orbitals contribute. LUMOs+n have upward lobes on gallium, which contribute to Lewis acidity, while LUMOs have downward lobes that are not suitable for accepting a nucleophile. The order of energy levels for LUMOs+n, **3a**Ga < **3b**Ga < **3c**Ga, is reverse to that of LUMOs, **3a**Ga > **3b**Ga > **3c**Ga. Although the reason for this relationship is not yet clear, the bulkiness of the substituents on the bottom benzene ring would finely tune the eigenvalue of the orbital to which the gallium p_z orbitals contribute. The pyridine-complexation energy also showed the same order for the eigenvalue of LUMO+n. On the other hand, the electron withdrawing character of the fluoro groups on the benzene rings of the arm led to larger pyridine-complexation energy and lower energy levels for LUMO and LUMO+n than for **3b**Ga. These results reveal that the steric substituents on the bottom benzene ring and the strongly electronegative substituents on the benzene arm affect the Lewis acidity of the gallium complexes.

Scheme 6. Structural Change Caused by the Substituents on the Bottom Benzene Ring.
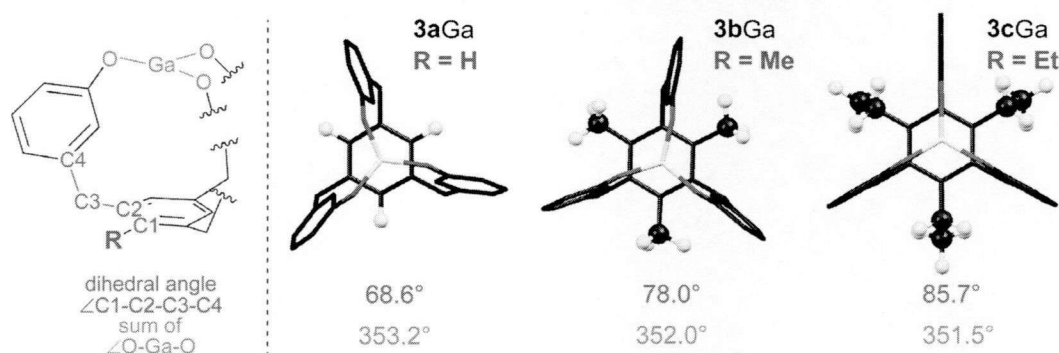
Scheme 7. Theoretical Calculation of **3a-d**Ga.

complex	**3aGa** [R = H] [X = H]	**3bGa** [R = Me] [X = H]	**3cGa** [R = Et] [X = H]	**3dGa** [R = Me] [X = F]
LUMO+n (eV)	-0.59	-0.43	-0.37	-0.76
LUMO (eV)	-1.99	-2.08	-2.12	-2.69
sum of ∠O-Ga-O	353.2°	352.0°	351.5°	352.3°
E in pyridine complexation (kcal/mol)	-39.8	-39.3	-38.9	-41.3

66
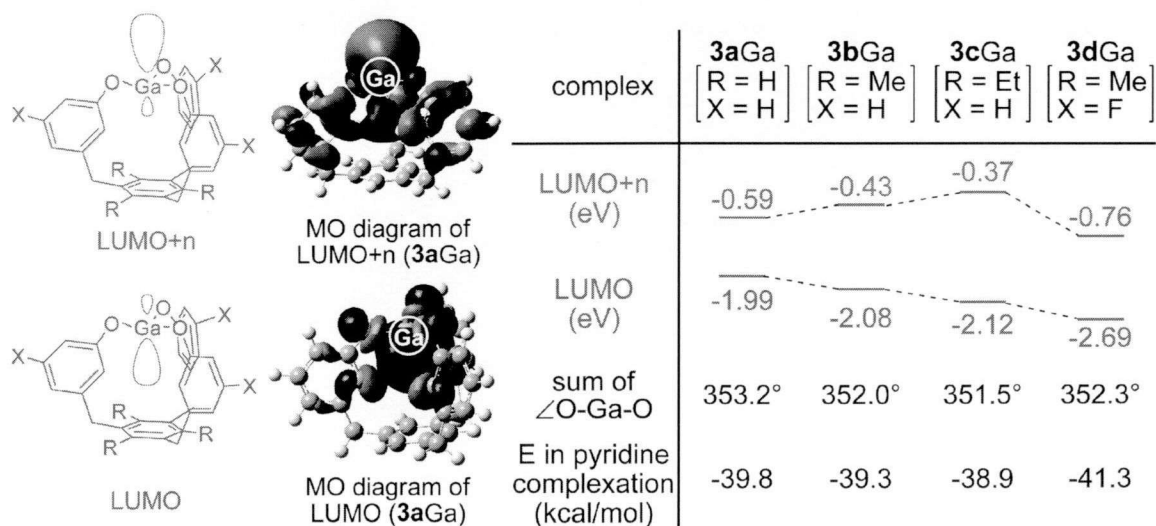
The results of the hetero Diels-Alder reaction using the cage-shaped derivatives **3b-dGa·Py** are summarized in Table 1. The unsubstituted **3aGa·Py** gave a lower yield than the methyl-substituted **3bGa·Py** despite having almost the same pyridine complexation energy. This result suggests that methyl groups on the bottom benzene ring disturbed the inversion of the benzene rings on the arm to keep them on the same side as the gallium metal even when the Ga–O bond was cleaved, consequently preventing the decomposition of the complex. The bulkier ethyl group provided no improvement, likely due to the high energy level of its LUMO+n. The fluoro derivative **3dGa·Py** showed lower catalytic activity than **3bGa·Py**. The larger stabilization energy in the pyridine complexation of **3dGa** probably inhibits the release of an original pyridine and a product from the gallium metal at the start and at the end of the reaction. The generation and regeneration of an active catalyst are important in this case, and **3bGa·Py** was the best catalyst among **3a-dGa·Py**.

Table 1. Hetero Diels-Alder Reaction Using Cage-Shaped Derivatives.

entry	catalyst	yield/ %
1	**3aGa·Py**	42
2	**3bGa·Py**	61
3	**3cGa·Py**	57
4	**3dGa·Py**	46

2-1-3. Conclusion

We synthesized gallium complexes with Lewis acidity enhanced by a cage-shaped structure. Theoretical calculations and application to a hetero Diels-Alder reaction suggest that the back-shielding framework shows promise for the high activation of carbonyl compounds. The substituents on the bottom benzene ring finely tuned the energy level and controlled the stability of the complexes.

2-1-4. Experimental Section

General Procedures. IR spectra were recorded as thin films or as solids in KBr pellets on a HORIBA FT-720 spectrophotometer. ^1H and ^{13}C NMR spectra were obtained with a 400 and 100 MHz spectrometer, respectively, with TMS as internal standard. Mass spectra were recorded on a JEOL JMS-DS303. All reactions were carried out under nitrogen. Synthesis of gallium complexes was performed in nitrogen filled glove box. Column chromatography was performed on silica gel.

Materials. Dehydrated dichloromethane THF, and hexane were purchased and used as obtained. The compound 1H₃ and 2H₃ were prepared according to our previous report.[4] The compound **5b**[16] and **5c**[17] were prepared by known methods. All other reagents are commercially available.
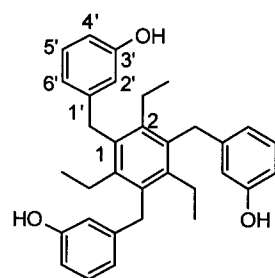
1,3,5-Tris(3-methoxybenzyl)benzene (6a)
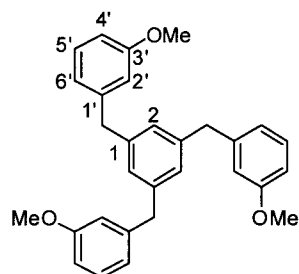
To a stirred suspension of magnesium powder (366 mg, 15 mmol) in THF (10 mL) were slowly added *m*-bromoanisole (1.87 g, 10 mmol) and iodine (one portion) at 25 °C under nitrogen, and the resulting mixture was stirred for an additional 1 h. This Grignard solution was transferred dropwise to a mixture of 1,3,5-tris(bromomethyl)benzene (793 mg, 2 mmol) and CuI (38 mg, 0.2 mmol) in THF (10 mL) at 60 °C, and the resulting mixture was further stirred for 12 h at the same temperature. The mixture was allowed to cool to 25 °C and quenched with a saturated aqueous NaHCO₃ solution (20 mL). The mixture was extracted with ethyl acetate (3 x 10 mL). The combined organic layer was dried over MgSO₄ and evaporated. The residue was purified by flash column chromatography (hexane/EtOAc, 85/15) to give the product as colorless liquid (728 mg, 83%). ¹H NMR: (400 MHz, CDCl₃) 7.17 (dd, J = 8.0, 7.9 Hz, 3H, 5'-H), 6.87 (s, 3H, 2-H), 6.73 (m, 6H, 4'-H and 6'-H), 6.67 (s, 3H, 2'-H), 3.86 (s, 6H, 1-CH₂), 3.72 (s, 9H, OMe); ¹³C NMR: (100 MHz, CDCl₃) 159.6 (s, C-3'), 142.8 (s, C-1'), 141.1 (s, C-1), 129.3 (d, C-5'), 127.5 (d, C-2), 121.2 (d, C-6'), 114.4 (d, C-2'), 111.4 (d, C-6'), 55.0 (q, OMe), 41.8 (t, 1-CH₂); IR : 1597 (C=C) cm⁻¹, 1261 (C-O) cm⁻¹; MS: (EI, 70eV) *m/z* 438 (M⁺, 100), 317 (M⁺ – CH₂C₆H₄OMe, 30), 121 (31); HRMS: (EI, 70 eV) calculated for (C₃₀H₃₀O₃) 438.2195 (M⁺) found for *m/z* 438.2193. Analysis: calculated for C₃₀H₃₀O₃: C, 82.16; H, 6.89; found: C, 82.19; H, 6.92.

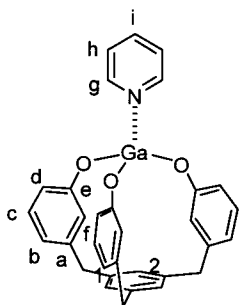### 1,3,5-Tris(3-hydroxybenzyl)benzene (3aH₃)
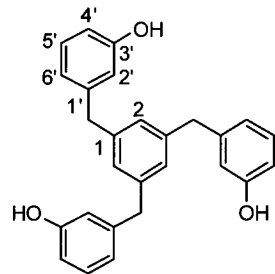
To the solution of 1,3,5-Tris(3-methoxybenzyl)benzene (876 mg, 2.0 mmol) in CH₂Cl₂ (10 mL) was slowly added BBr₃ (1M in CH₂Cl₂, 6.6 mL, 6.6 mmol) at -78 °C. The mixture was stirred for 1 h at -78 °C and overnight at rt. The mixture was cooled to 0 °C and water was added carefully (HBr gas was generated.). The mixture was extracted with Et₂O (3 x 10 mL). The combined organic layer was dried over MgSO₄ and evaporated. The residue was purified by flash column chromatography (hexane/EtOAc, 50/50) to give the product as a white solid (555 mg, 70%). mp: 137-138 °C; ¹H NMR: (400 MHz, DMSO-d_6) 9.19 (s, 3H, OH, D₂O exchangeable), 6.95 (dd, J = 8.1, 7.7 Hz, 3H, 5'-H), 6.80 (s, 3H, 2-H), 6.51 (d, J = 7.7 Hz, 3H, 6'-H), 6.48 (m, 6H, 2'-H and 4'-H), 3.66 (s, 6H, 1-CH₂); ¹H NMR: (400 MHz, CDCl₃) 7.15 (dd, J = 8.0, 7.8 Hz, 3H, 5'-H), 6.88 (s, 3H, 2-H), 6.78 (d, J = 7.8 Hz, 3H, 6'-H), 6.66 (d, J = 8.0 Hz, 3H, 4'-H), 6.55 (s, 3H, 2'-H), 4.93 (s, 3H, OH, D₂O exchangeable), 3.86 (s, 6H, 1-CH₂); ¹³C NMR: (100 MHz, DMSO-d_6) 157.3 (s, C-3'), 142.6 (s, C-1'), 141.3 (s, C-1), 129.3 (d, C-5'), 127.0 (d, C-2), 119.3 (d, C-6'), 115.6 (d, C-2'), 112.9 (d, C-4'), 41.1 (t, 1-CH₂); IR (KBr): 3405 (OH) cm⁻¹, 1589 (C=C) cm⁻¹, 1261 (C-O) cm⁻¹; MS: (EI, 70eV) *m/z* 396 (M⁺, 100), 289 (M⁺– CH₂C₆H₄OH, 69), 195 (36), 107 (92); HRMS: (EI, 70 eV) calculated for (C₂₇H₂₄O₃) 396.1725 (M⁺) found for *m/z* 396.1723. Analysis: calculated for C₂₇H₂₄O₃: C, 81.79; H, 6.10; found: C, 81.52; H, 6.10.

1,3,5-Tris(3-methoxybenzyl)-2,4,6-trimethylbenzene (6b)
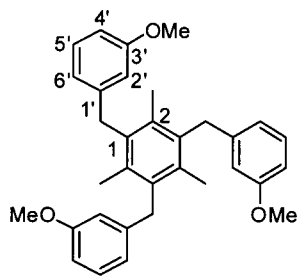
To a stirred suspension of magnesium powder (1.83 g, 75 mmol) in THF (50 mL) were slowly added *m*-bromoanisole (9.35 g, 50 mmol) and iodine (one portion) at 25 °C under nitrogen, and the resulting mixture was stirred for an additional 1 h. This Grignard solution was transferred dropwise to a mixture of 1,3,5-tris(bromomethyl)mesitylene (3.99 g, 10 mmol) and CuI (190 mg, 1 mmol) in THF (50 mL) at 60 °C, and the resulting mixture was further stirred for 12 h at the same temperature. The mixture was allowed to cool to 25 °C and quenched with a saturated aqueous NaHCO$_3$ solution (100 mL). The mixture was extracted with ethyl acetate (3 x 50 mL). The combined organic layer was dried over MgSO$_4$ and evaporated. The residue was purified by flash column chromatography (hexane/EtOAc, 85/15) to give the product as a white solid (3.51 g, 73%). mp: 78-82 °C; ^{1}H NMR: (400 MHz, CDCl$_3$) 7.15 (dd, J = 8.3, 8.0 Hz, 3H, 5'-H), 6.68 (m, 6H, 6'-H and 4'-H), 6.54 (s, 3H, 2'-H), 4.12 (s, 6H, 1-CH$_2$), 3.71 (s, 9H, OMe), 2.14 (s, 9H, 2-CH$_3$); ^{13}C NMR: (100 MHz, CDCl$_3$) 159.7 (s, C-3'), 142.1 (s, C-1'), 134.8 (s, C-1 or C-2), 134.6 (s, C-1 or C-2), 129.2 (d, C-5'), 120.3 (d, C-6'), 113.4 (d, C-2'), 110.9 (d, C-4'), 55.0 (q, OMe), 36.0 (t, 1-CH$_2$), 16.7 (q, 2-CH$_3$); IR (KBr): 1601 (C=C) cm^{-1}, 1250 (C-O) cm^{-1}; MS: (EI, 70eV) *m/z* 480 (M$^+$, 100), 359 (M$^+$ – CH$_2$C$_6$H$_4$OMe, 37), 121 (45); HRMS: (EI, 70 eV) calculated for (C$_{33}$H$_{36}$O$_3$) 480.2664 (M$^+$) found for *m/z* 480.2670. Analysis: calculated for C$_{33}$H$_{36}$O$_3$: C, 82.46; H, 7.55; found: C, 82.45; H, 7.43.

1,3,5-Tris(3-hydroxybenzyl)-2,4,6-trimethylbenzene (3bH$_3$)
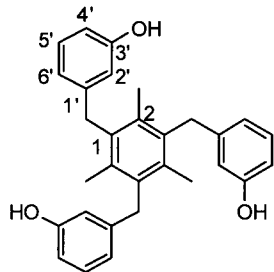
To the solution of 1,3,5-Tris(3-methoxybenzyl)-2,4,6-trimethylbenzene (961.27 mg, 2.0 mmol) in CH$_2$Cl$_2$ (10 mL) was slowly added BBr$_3$ (1M in CH$_2$Cl$_2$, 6.6 mL, 6.6 mmol) at -78 °C. The mixture was stirred for 1 h at -78 °C and overnight at rt. The mixture was cooled to 0 °C and water was added carefully (HBr gas was generated.). The mixture was extracted with Et$_2$O (3 x 10 mL). The combined organic layer was dried over MgSO$_4$ and evaporated. The residue was purified by flash column chromatography (hexane/EtOAc, 50/50) to give the product as a white solid (683 mg, 78%). mp: 245-247 °C; ^{1}H NMR: (400 MHz, CDCl$_3$) 7.15 (m, 3H, 5'-H), 6.82 (m, 3H, 6'-H), 6.63 (m, 3H, 4'-H), 6.29 (s, 3H, 2'-H), 5.43 (s, 3H, OH, D$_2$O exchangeable), 4.13 (s, 6H, 1-CH$_2$), 2.12 (s, 9H, 2-CH$_3$)

1,3,5-Tris(3-methoxybenzyl)-2,4,6-triethylbenzene (6c)
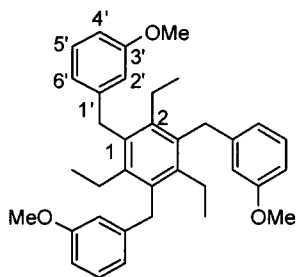
To a stirred suspension of magnesium powder (912 mg, 37.5 mmol) in THF (25 mL) were slowly added *m*-bromoanisole (4.675 g, 25 mmol) and iodine (one portion) at 25 °C under nitrogen, and the resulting mixture was stirred for an additional 1 h. This Grignard solution was transferred dropwise to a mixture of 1,3,5-tris(bromomethyl)-2,4,6-triethylbenzene (2.205 g, 5 mmol) and CuI (95 mg, 0.5 mmol) in THF (25 mL) at 60 °C, and the resulting mixture was further stirred for 16 h at the same temperature. The mixture was allowed to cool to 25 °C and quenched with a saturated aqueous NaHCO$_3$ solution (50 mL). The mixture was extracted with ethyl acetate (3 x 25 mL). The combined organic layer was dried over MgSO$_4$ and evaporated. The residue was purified by flash column chromatography (hexane/EtOAc, 85/15) to give the product as a white solid (1.568 g, 60%). mp: 143-145 °C; ^{1}H

NMR: (400 MHz, CDCl₃) 7.13 (dd, J = 8.0, 8.0 Hz, 3H, 5'-H), 6.68 (m, 6H, 6'-H and 4'-H), 6.47 (s, 3H, 2'-H), 4.12 (s, 6H, 1-CH₂), 3.68 (s, 9H, OMe), 2.43 (q, J = 7.5 Hz, 6H, 2-CH₂), 1.13 (t, J = 7.5 Hz, 9H, 2-CH₂CH_3); ¹³C NMR: (100 MHz, CDCl₃) 159.7 (s, C-3'), 143.0 (s, C-1'), 141.4 (s, C-2), 133.8 (s, C-1), 129.1 (d, C-5'), 120.3 (d, C-6'), 113.0 (d, C-2'), 111.2 (d, C-4'), 54.9 (q, OMe), 34.4 (t,1-CH₂), 23.6 (t, 2-CH₂), 15.2 (q, 2-CH₂CH₃); IR (KBr): 1593 (C=C) cm⁻¹, 1277 (C-O) cm⁻¹; MS: (EI, 70eV) m/z 522 (M⁺, 100), 401 (M⁺ – CH₂C₆H₄OMe, 43), 121 (87); HRMS: (EI, 70 eV) calculated for (C₃₆H₄₂O₃) 522.3134 (M⁺) found for m/z 522.3125. Analysis: calculated for C₃₆H₄₂O₃: C, 82.72; H, 8.10; found: C, 82.62; H, 8.09.

1,3,5-Tris(3-hydroxybenzyl)-2,4,6-triethylbenzene (3cH₃)

To the solution of 1,3,5-Tris(3-methoxybenzyl)-2,4,6-triethylbenzene (648.2 mg, 1.24 mmol) in CH₂Cl₂ (5 mL) was slowly added BBr₃ (1M in CH₂Cl₂, 4.1 mL, 4.1 mmol) at -78 °C. The mixture was stirred for 1 h at -78 °C and overnight at rt. The mixture was cooled to 0 °C and water was added carefully (HBr gas was generated.). The mixture was extracted with Et₂O (3 x 5 mL). The combined organic layer was dried over MgSO₄ and evaporated. The residue was purified by flash column chromatography (hexane/EtOAc, 40/60) to give the product as a white solid (251 mg, 42%). mp: 184 °C; ¹H NMR: (400 MHz, CDCl₃) 7.15 (dd, J = 7.9, 7.8 Hz, 3H, 5'-H), 6.87 (d, J = 7.8 Hz, 3H, 6'-H), 6.62 (d, J = 7.9 Hz, 3H, 4'-H), 6.21 (s, 3H, 2'-H), 5.78 (s, 3H, OH, D₂O exchangeable), 4.11 (s, 6H, 1-CH₂), 2.38 (q, J = 7.4 Hz, 6H, 2-CH₂), 1.12 (t, J = 7.4 Hz, 9H, 2-CH₂CH₃)

1,3,5-Tris(3-fluoro-5-methoxybenzyl)-2,4,6-trimethylbenzene (6d)
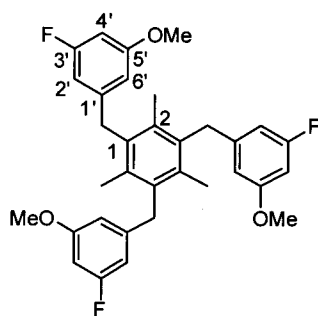
To a stirred suspension of magnesium powder (366 mg, 15 mmol) in THF (10 mL) were slowly added 3-bromo-5-fluoroanisole (2.05 g, 10 mmol) and iodine (one portion) at 25 °C under nitrogen, and the resulting mixture was stirred for an additional 1 h. This Grignard solution was transferred dropwise to a mixture of 1,3,5-tris(bromomethyl)mesitylene (798 mg, 2 mmol) and CuI (38 mg, 0.2 mmol) in THF (10 mL) at 60 °C, and the resulting mixture was further stirred for 12 h at the same temperature. The mixture was allowed to cool to 25 °C and quenched with a saturated aqueous NaHCO₃ solution (20 mL). The mixture was extracted with ethyl acetate (3 x 10 mL). The combined organic layer was dried over MgSO₄ and evaporated. The residue was purified by flash column chromatography (hexane/EtOAc, 85/15) to give the product as a white solid (748 mg, 70%). mp: 142-143 °C; ¹H NMR: (400 MHz, CDCl₃) 6.42 (d, ³J_{FH} = 10.4 Hz, 3H, 4'-H), 6.32 (m, 6H, 2'-H and 6'-H), 4.09 (s, 6H, 1-CH₂), 3.71 (s, 9H, OMe), 2.12 (s, 9H, 2-CH₃); ¹³C NMR: (100 MHz, CDCl₃) 163.7 (s, d by ¹J_{CF} = 244.1 Hz, C-3'), 160.9 (s, d by ³J_{CF} = 11.5 Hz, C-5'), 143.6 (s, d by ³J_{CF} = 9.0 Hz, C-1'), 135.0 (s, C-1 or C-2), 134.2 (s, C-1 or C-2), 109.1 (d, C-6'), 106.9 (d, d by ²J_{CF} = 22.1 Hz, C-2'), 99.0 (d, d by ²J_{CF} = 25.4 Hz, C-4'), 55.3 (q, OMe), 35.9 (t,1-CH₂), 16.7 (q, 2-CH₃); IR (KBr): 1624 (C=C) cm⁻¹, 1304 (C-O) cm⁻¹; MS: (EI, 70eV) m/z 534 (M⁺, 100), 395 (M⁺ – CH₂C₆H₃FOMe, 52), 269 (23), 255 (21), 139 (64); HRMS: (EI, 70 eV) calculated for (C₃₃H₃₃F₃O₃) 534.2382 (M⁺) found for m/z 534.2385. Analysis: calculated for C₃₃H₃₃F₃O₃: C, 74.14; H, 6.22; found: C, 74.15; H, 6.23.

1,3,5-Tris(3-fluoro-5-hydroxybenzyl)-2,4,6-trimethylbenzene (3dH₃)
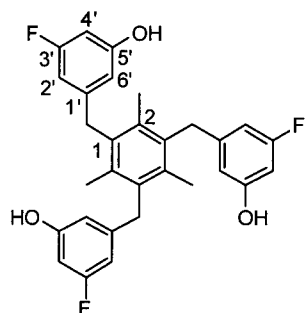
To the solution of 1,3,5-Tris(3-fluoro-5-methoxybenzyl)-2,4,6-trimethylbenzene (1.97 g = 3.7 mmol) in CH_2Cl_2 (20 mL) was added BBr_3 (1M in CH_2Cl_2, 12.2 mL, 12.2 mmol) at -78 °C. The mixture was stirred for 1 h at -78 °C and overnight at rt. The mixture was cooled to 0 °C and water was added carefully (HBr gas was generated.). The mixture was extracted with Et_2O (3 x 20 mL). The combined organic layer was dried over $MgSO_4$ and evaporated. The residue was purified by flash column chromatography (hexane/EtOAc, 50/50) to give the product as a white solid (1.42 g, 78%). mp: 233-237 °C; ^1H NMR: (400 MHz, DMSO-d_6) 9.78 (s, 3H, OH, D_2O exchangeable), 6.36 (d, $^3J_{FH}$ = 10.6 Hz, 3H, 4'-H), 6.28 (s, 3H, 2'-H), 6.21 (d, $^3J_{FH}$ = 9.7 Hz, 3H, 6'-H), 4.02 (s, 6H, 1-CH_2), 2.08 (s, 9H, 2-CH_3); ^1H NMR: (400 MHz, $CDCl_3$) 6.49 (d, $^3J_{FH}$ = 9.6 Hz, 3H, 4'-H or 6'-H), 6.36 (d, $^3J_{FH}$ = 10.0 Hz, 3H, 4'-H or 6'-H), 6.08 (s, 3H, 2'-H), 5.98 (s, 3H, OH, D_2O exchangeable), 4.08 (s, 9H, 1-CH_2), 2.09 (s, 9H, 2-CH_3); ^{13}C NMR: (100 MHz, DMSO-d_6) 163.1 (s, d by $^1J_{CF}$ = 241.7 Hz, C-3'), 158.9 (s, d by $^3J_{CF}$ = 12.3 Hz, C-5'), 143.8 (s, d by $^3J_{CF}$ = 9.8 Hz, C-1'), 134.4 (s, C-1 or C-2), 134.2 (s, C-1 or C-2), 110.8 (d, C-6'), 104.7 (d, d by $^2J_{CF}$ = 21.3 Hz, C-2'), 100.1 (d, d by $^2J_{CF}$ = 23.8 Hz, C-4'), 35.4 (t,1-CH_2), 16.5 (q, 2-CH_3); IR (KBr): 3455 cm^{-1} (OH), 1620 cm^{-1} (C=C), 1300 cm^{-1} (C-O); MS: (EI, 70eV) m/z 492 (M⁺, 100), 367 (M⁺ − $CH_2C_6H_3FOH$, 49), 255 (21), 241 (30), 125 (82); HRMS: (EI, 70 eV) calculated for ($C_{30}H_{27}F_3O_3$) 492.1912 (M⁺) found for m/z 492.1909. Analysis: calculated for $C_{30}H_{27}F_3O_3$: C, 73.16; H, 5.53; found: C, 73.07; H, 5.52.

Pyridine complex of 3aGa (with pyridine hydrochloride)

In a nitrogen filled glove box, to a mixture of 1,3,5-tris(3-hydroxybenzyl)benzene 3aH₃ (0.1 mmol, 39.6 mg) and pyridine (1.0 mmol, 79 mg) in THF (3 mL) was added $GaCl_3$ (0.11 mmol, 19.1 mg) with stirring for 2 h at room temperature. Evaporation of volatiles gave a viscous liquid. The obtained crude materials were washed with hexane and evaporated to give the gallium complex 3aGa·Py accompanied by pyridine hydrochloride. ^1H NMR: (400 MHz, $CDCl_3$) 9.49 (s, 3H, Py·HCl), 8.63 (m, 8H, g-H and g'-H), 7.84 (m, 4H, i-H, i'-H), 7.43 (m, 8H, h-H, h'-H), 7.07 (dd, J = 7.6, 7.6 Hz, 3H, c-H), 6.89 (s, 3H, 2-H), 6.68 (m, 6H, b-H and d-H), 6.62 (s, 3H, f-H), 3.80 (s, 6H, 1-CH_2); ^{13}C NMR: (100 MHz, $CDCl_3$) 156.9 (s, C-e), 147.9 (d, C-g and C-g'), 142.9 (s, C-a), 141.1 (s, C-1), 138.9 (d, C-i and C-i'), 129.4 (d, C-c), 127.7 (d, C-2), 124.9 (d, C-h and C-h'), 120.4 (d, C-b), 116.3 (d, C-f), 113.5 (d, C-d), 41.5 (t, 1-CH_2)

Pyridine complex of 3bGa (with pyridine hydrochloride)
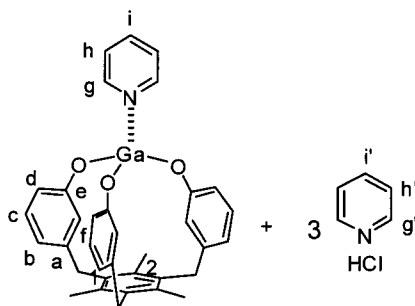
In a nitrogen filled glove box, to a mixture of 1,3,5-tris(3-hydroxybenzyl)-2,4,6-trimethylbenzene **3bH₃** (0.1 mmol, 43.8 mg) and pyridine (1.0 mmol, 79 mg) in THF (3 mL) was added GaCl₃ (0.11 mmol, 19.1 mg) with stirring for 2 h at room temperature. Evaporation of volatiles gave a viscous liquid. The obtained crude materials were washed with hexane and evaporated to give the gallium complex **3bGa·Py** accompanied by pyridine hydrochloride. The product

was recrystallized from dichloromethane/hexane (2/1) for X-ray analysis. ^{1}H NMR: (400 MHz, CDCl₃) 10.03 (s, 3H, Py·HCl), 8.65 (m, 8H, g-H and g'-H), 7.90 (m, 4H, i-H and i'-H), 7.47 (m, 8H, h-H and h'-H), 7.06 (dd, J = 7.8, 7.8 Hz, 3H, c-H), 6.68 (d, J = 7.8 Hz, 3H, b-H), 6.62 (d, J = 7.8 Hz, 3H, d-H), 6.46 (s, 3H, f-H), 4.03 (s, 6H, 1-CH₂), 2.08 (s, 9H, 2-CH₃); ^{13}C NMR: (100 MHz, CDCl₃) 157.2 (s, C-e), 147.5 (d, C-g or C-g'), 147.4 (d, C-g or C-g'), 142.1 (s, C-a), 139.6 (d, C-i and C-i'), 134.6 (s, C-1 or C-2), 134.5 (s, C-1 or C-2), 129.3 (d, C-c), 125.1 (d, C-h and C-h'), 119.9 (d, C-b), 115.2 (d, C-f), 113.2 (d, C-d), 35.7 (t, 1-CH₂), 16.6 (q, 2-CH₃)

Pyridine complex of 3cGa (with pyridine hydrochloride)
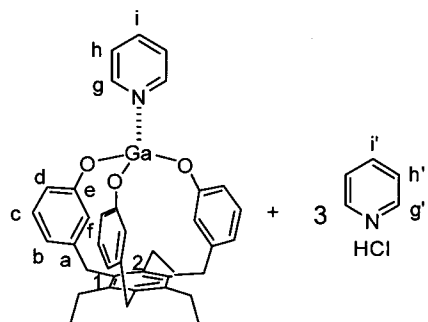
In a nitrogen filled glove box, to a mixture of 1,3,5-tris(3-hydroxybenzyl)-2,4,6-triethylbenzene **3cH₃** (0.1 mmol, 48.1 mg) and pyridine (1.0 mmol, 79 mg) in THF (3 mL) was added GaCl₃ (0.11 mmol, 19.1 mg) with stirring for 2 h at room temperature. Evaporation of volatiles gave a viscous liquid. The obtained crude materials were washed with hexane and evaporated to give the gallium complex **3cGa·Py** accompanied by pyridine hydrochloride. ^{1}H NMR:

(400 MHz, CDCl₃) 9.94 (s, 3H, Py·HCl), 8.66 (m, 8H, g-H and g'-H), 7.90 (m, 4H, i-H and i'-H), 7.48 (m, 8H, h-H and h'-H), 7.06 (dd, J = 7.6, 7.4 Hz, 3H, c-H), 6.76 (d, J = 7.6 Hz, 3H, b-H), 6.59 (d, J = 7.4 Hz, 3H, d-H), 6.43 (s, 3H, f-H), 4.07 (s, 6H, 1-CH₂), 2.39 (d, J = 7.3 Hz, 6H, 2-CH₂), 1.09 (t, J = 7.3 Hz, 9H, 2-CH₂CH₃); ^{13}C NMR: (100 MHz, CDCl₃) 157.1 (s, C-e), 147.2 (d, C-g or C-g'), 147.1 (d, C-g or C-g'), 143.1 (s, C-a), 141.3 (d, C-i and C-i'), 140.0 (s, C-2), 133.7 (s, C-1), 129.2 (d, C-c), 125.3 (d, C-h or C-h'), 125.2 (d, C-h or C-h'), 120.1 (d, C-b), 115.3 (d, C-f), 113.2 (d, C-d), 34.1 (t, 1-CH₂), 23.5 (t, 2-CH₂), 15.2 (q, 2-CH₂CH₃)

Pyridine complex of 3dGa (with pyridine hydrochloride)
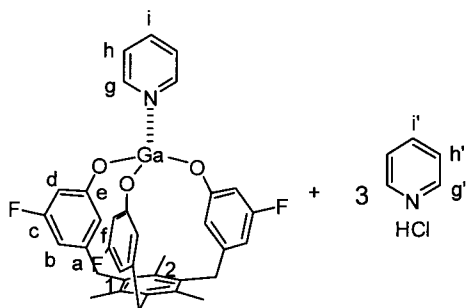
In a nitrogen filled glove box, to a mixture of 1,3,5-tris(3-hydroxybenzyl)-2,4,6-trimethylbenzene **3dH₃** (0.1 mmol, 49.3 mg) and pyridine (1.0 mmol, 79 mg) in THF (3 mL) was added GaCl₃ (0.11 mmol, 19.1 mg) with stirring for 2 h at room temperature. Evaporation of volatiles gave a viscous liquid. The obtained crude materials were washed with hexane and evaporated to give the gallium complex **3dGa·Py** accompanied by pyridine hydrochloride.

^{1}H NMR: (400 MHz, CDCl$_3$) 10.92 (s, 3H, Py·*H*Cl), 8.66 (m, 8H, g-H and g'-H), 7.95 (m, 4H, i-H and i'-H), 7.52 (m, 8H, h-H and h'-H), 6.34 (m, 6H, b-H and d-H), 6.28 (s, 3H, f-H), 4.00 (s, 6H, 1-CH$_2$), 2.06 (s, 9H, 2-CH$_3$); ^{13}C NMR: (100 MHz, CDCl$_3$) 163.6 (s, d by $^1J_{CF}$ = 244.1 Hz, C-c), 158.6 (s, d by $^3J_{CF}$ = 12.3 Hz, C-e), 147.1 (d, C-g or C-g'), 147.0 (d, C-g or C-g'), 143.6 (s, d by $^3J_{CF}$ = 9.0 Hz, C-1'), 140.1 (d, C-i and C-i'), 134.8 (s, C-1 or C-2), 134.2 (s, C-1 or C-2), 125.4 (d, C-h or C-h'), 111.0 (d, C-f), 106.3 (d, d by $^2J_{CF}$ = 22.1 Hz, C-b), 101.1 (d, d by $^2J_{CF}$ = 24.6 Hz, C-d), 35.7 (t,1-CH$_2$), 16.6 (q, 2-CH$_3$)

Pyridine complex of 7 (with pyridine hydrochloride)

(n = 1 or 2)
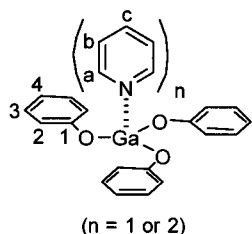
In a nitrogen filled glove box, to a mixture of phenol (0.3 mmol, 28.2 mg) and pyridine (1.0 mmol, 79 mg) in THF (3 mL) was added GaCl$_3$ (0.11 mmol, 19.1 mg) with stirring for 2 h at room temperature. Evaporation of volatiles gave a viscous liquid. The obtained crude materials were washed with hexane and evaporated to give the gallium complex 7·nPy (n = 1 or 2) accompanied by pyridine hydrochloride.

The amount of pyridine coordinated to gallium was varied by workup conditions (hexane washing). In this case, the amount was 1.5 eq. ^{1}H NMR: (400 MHz, CDCl$_3$) 11.1 (s, 3H, Py·*H*Cl), 8.69 (m, 10H, a-H and a'-H), 7.91 (m, 5H, c-H and c'-H), 7.50 (m, 10H, b-H and b'-H), 7.19 (m, 6H, 3-H), 6.90 (m, 6H, 2-H), 6.84 (m, 3H, 4-H); ^{13}C NMR: (100 MHz, CDCl$_3$) 157.4 (C-1), 147.6 (C-a), 139.2 (C-c), 129.4 (C-3), 125.0 (C-h), 119.5 (C-4), 116.1 (C-2)

General experimental procedure for the cage-shaped gallium complexes-catalyzed hetero Diels-Alder reaction (Eq 1).

To a solution of the cage-shaped ligand (3a-3dH$_3$, 0.1 mmol) and pyridine (1.0 mmol) in THF (3 mL) was added GaCl$_3$ (0.11 mmol) with stirring for 2 h at rt. Volatiles were removed under reduced pressure and the residue was washed with hexane. The remained residue was dissolved in dichloromethane (10 mL). To the solution was added Danishefsky's diene 9 (1.0 mmol) and benzaldehyde 10 (1.1 mmol) at rt and the mixture was stirred at rt. After stirring for 16 h, H$_2$O (10 mL) was added to the mixture, which was extracted with Et$_2$O (3 x 10 mL). The organic layer was dried (MgSO$_4$) and evaporated to give a crude mixture, which was analyzed by NMR.

7·nPy (n = 1 or 2) catalyzed-hetero Diels-Alder reaction (Eq 1).

To a solution of phenol (0.3 mmol) and pyridine (1.0 mmol) in THF (3 mL) was added GaCl$_3$ (0.11 mmol) with stirring for 2 h at rt. Volatiles were removed under reduced pressure and the residue was washed with hexane. The remained residue was dissolved in dichloromethane (10 mL). To the solution was added Danishefsky's diene 9 (1.0 mmol) and benzaldehyde 10 (1.1 mmol) at rt and the mixture was stirred at rt. After stirring for 16 h, H$_2$O (10 mL) was added to the mixture, which was extracted with Et$_2$O (3 x 10 mL). The organic layer was dried (MgSO$_4$) and evaporated to give a crude mixture, which was analyzed by NMR.

Pyridine hydrochloride catalyzed-hetero Diels-Alder reaction (reference 14).

To a solution of pyridine hydrochloride (0.3 mmol, 36.7 mg) in dichloromethane (10 mL) was added Danishefsky's diene **9** (1.0 mmol) and benzaldehyde **10** (1.1 mmol) at rt and the mixture was stirred at rt. After stirring for 16 h, H_2O (10 mL) was added to the mixture, which was extracted with Et_2O (3 x 10 mL). The organic layer was dried ($MgSO_4$) and evaporated to give a crude mixture, which was analyzed by NMR.

Computational Method. We applied the HF/DFT hybrid method originally proposed by Becke,[18] referenced as B3PW91 three parameter hybrid functional. All calculations were performed with Gaussian 03, Revision C.02.[10] 6-31+G(d,p) were used for basis sets. All molecular geometries were fully optimized and energies were calculated including zero point energy correction by the normal mode analysis for each structure.

All species calculated in this communication are shown in Scheme A.

Scheme A. The calculated species in this communication.
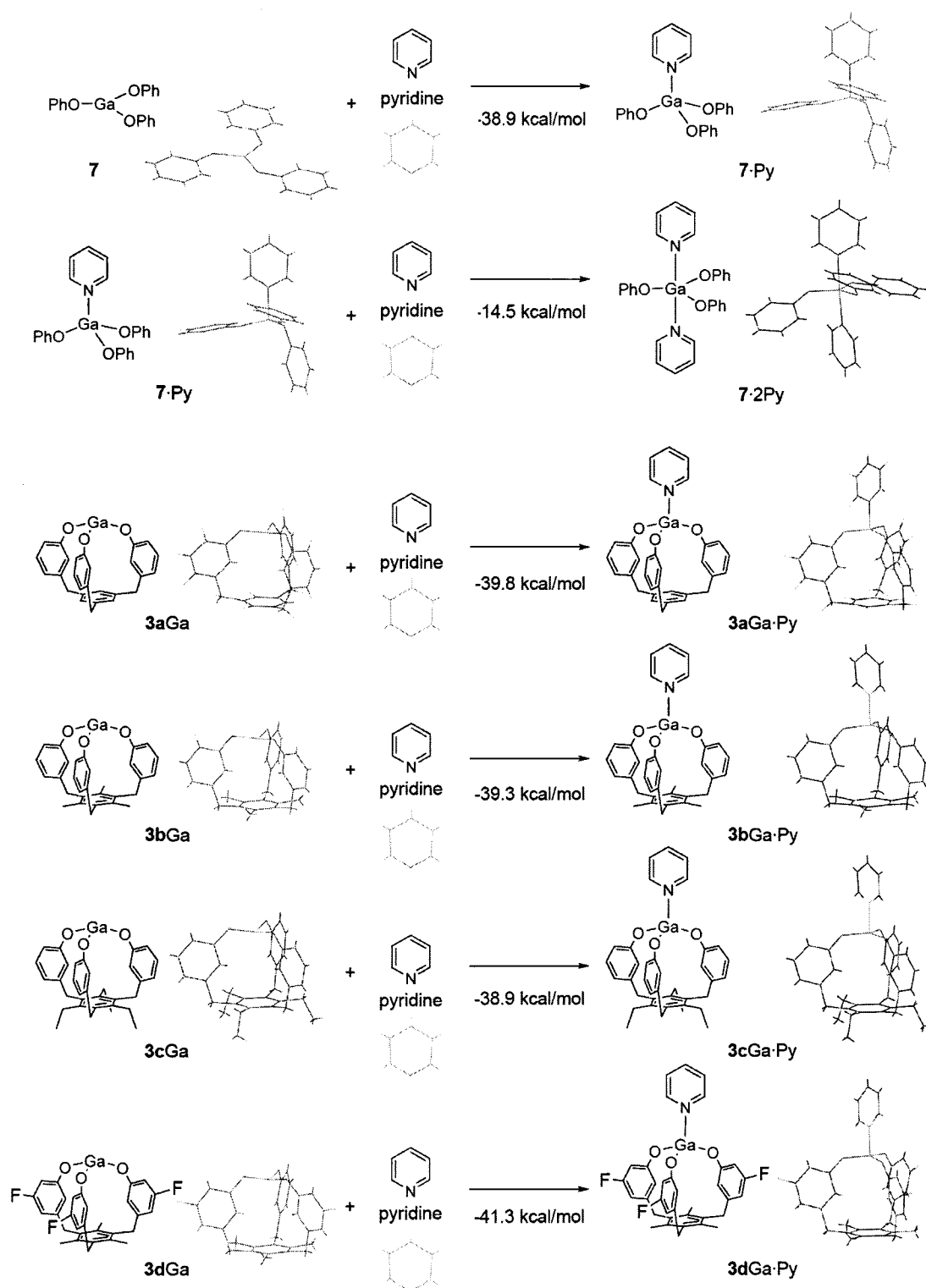
7 + pyridine → 7·Py (-38.9 kcal/mol)

7·Py + pyridine → 7·2Py (-14.5 kcal/mol)

3aGa + pyridine → 3aGa·Py (-39.8 kcal/mol)

3bGa + pyridine → 3bGa·Py (-39.3 kcal/mol)

3cGa + pyridine → 3cGa·Py (-38.9 kcal/mol)

3dGa + pyridine → 3dGa·Py (-41.3 kcal/mol)

75

Total energies for all of the calculated species (in hartree). All energies includes zero point vibration energy correction.

7	-2843.035121
7·Py	-3091.212409
7·2Py	-3339.349811
3aGa	-3189.382051
3aGa·Py	-3437.560188
3bGa	-3307.1995
3bGa B·Py	-3555.376976
3cGa	-3425.020456
3cGa·Py	-3673.197241
3dGa	-3604.836783
3dGa·Py	-3853.017408
pyridine	-248.11478

The top view of the calculated structure of **3a-d**Ga and their bond lengths of Ga-O.

	3aGa	**3b**Ga	**3c**Ga	**3d**Ga
Ga-O bond length	1.804 Å	1.804 Å	1.804 Å	1.803 Å
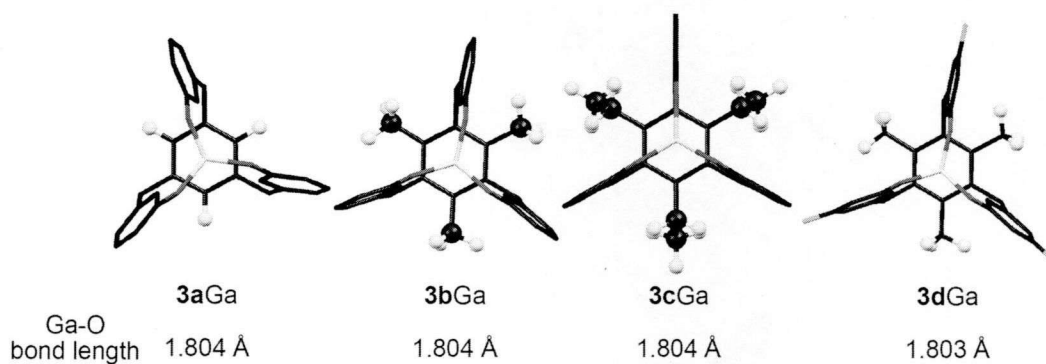
There is no change of the position of the Ga to the plane OOO in the calculated structure of **3a-d**Ga·Py. Ga lies in the center of the plane OOO in all case.

76

The MO diagrams of LUMO are shown below.

3aGa

3bGa

3cGa

3dGa

7
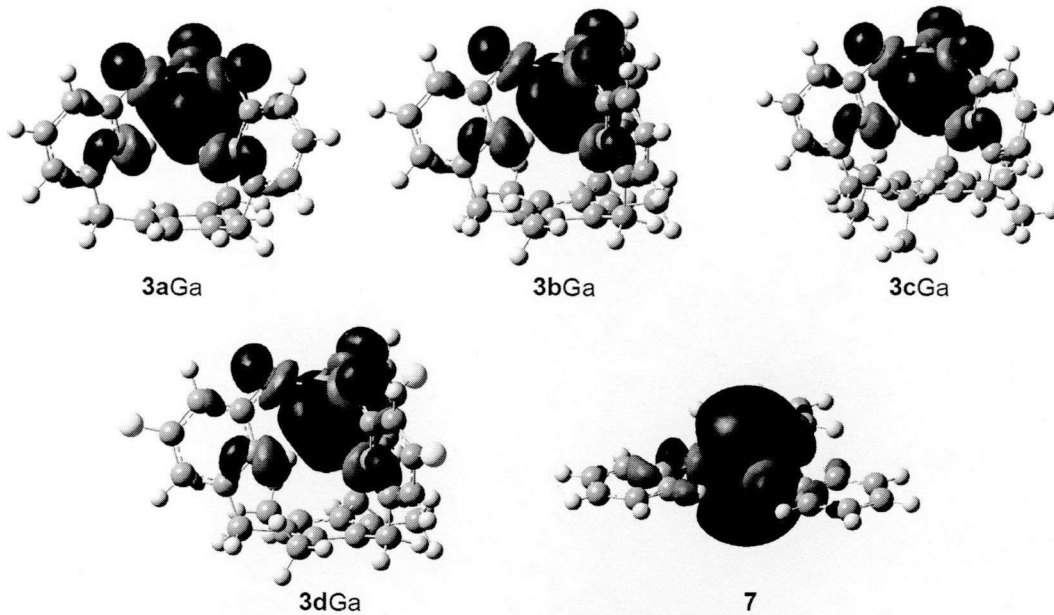
The MO diagrams of LUMO+n are shown below.

3aGa
(LUMO+3)

3bGa
(LUMO+5)

3cGa
(LUMO+5)

3dGa
(LUMO+5)

7
(LUMO+10)
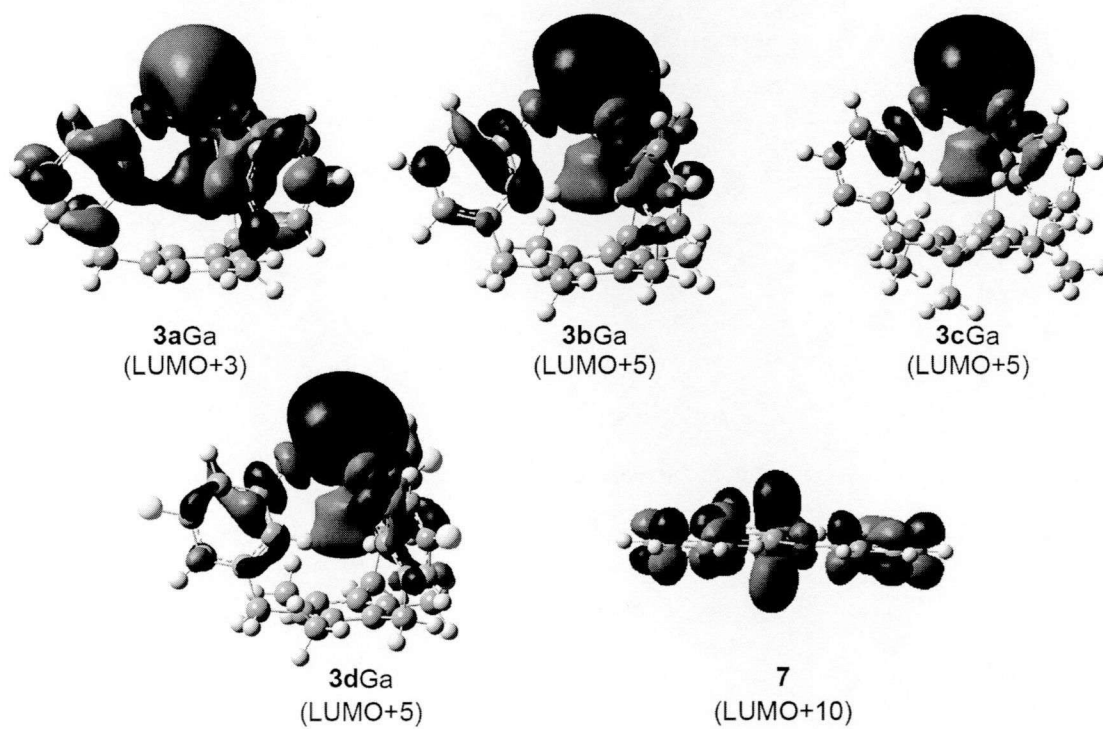
2-1-5. References

(1) *Lewis Acids in Organic Synthesis*; Yamamoto, H., Ed.; Wiley-VCH: Weinheim, Germany, 2000; Vols 1 and 2.

(2) *Acid Catalysis in Modern Organic Synthesis*; Yamamoto, H. and Ishihara, K.; Wiley-VCH: Weinheim, Germany, 2006, Vol. 1, pp. 187–467.

(3) Similar Lewis base cage-shaped complexes have been reported. (a) Dinger M. B.; Scott, M. J. *Inorg. Chem.* **2001**, *40*, 856–864. A titanium complex with a similar cage-shaped ligand was reported. (b) Akagi, F.; Matsuo T.; Kawaguchi, H. *J. Am. Chem. Soc.* **2005**, *127*, 11936–11937.

(4) (a) Yasuda, M.; Yoshioka, S.; Yamasaki, S.; Somyo, T.; Chiba K.; Baba, A. *Org. Lett.* **2006**, *8*, 761–764. (b) Yasuda, M.; Yoshioka, S.; Nakajima, H.; Chiba K.; Baba, A. *Org. Lett.* **2008**, *10*, 929–932.

(5) Five coordinate monomeric gallium(III) complexes: (a) Zanias, S.; Raptopoulou, C. P.; Terzis A.; Zafiropoulos, T. F. *Inorg. Chem. Commun.* **1999**, *2*, 48–51 and references cited therein. (b) Crispini, A.; Aiello, I.; Deda, M. L.; Franco, I. D.; Amati, M.; Lelj F.; Ghedini, M. *Dalton Trans.* **2006**, 5124–5134. (c) Rajeswaran, M.; Place, D. W.; Deaton, J. C.; Brown C. T.; Lenhart, W. C. *Acta Crystallogr., Sect. E: Struct. Rep. Online,* **2007**, *63*, m550–m552. (d) Deaton, J. C.; Place, D. W.; Brown, C. T.; Rajeswaran, M.; Kondakova, M. E. *Inorg. Chim. Acta* **2008**, *361*, 1020–1035.

(6) The ligands 3bH₃ and 3cH₃ were synthesized but were not applied to metal complexes. Kim, J.; Kim, Y. K.; Park, N.; Hahn J. H.; Ahn, K. H. *J. Org. Chem.* **2005**, *70*, 7087–7092.

(7) We were not able to remove pyridine hydrochloride from the gallium complexes (see Experimental Section for further details).

(8) CCDC-764736 (3bGa·Py) contains the supplementary crystallographic data for this paper. These data can be obtained free of charge from The Cambridge Crystallographic Data Centre via www.ccdc.cam.ac.uk/data_request/cif.

(9) The average value of 1.94 Å and 2.02 Å is based on a statistical analysis of all of the Ga−O and Ga−N covalent bonds described for compounds in the Cambridge Structural Database, respectively.

(10) Gaussian 03, Revision D.01; Gaussian, Inc.: Wallingford CT, 2004. Frisch, M. J.; Trucks, G. W.; Schlegel, H. B.; Scuseria, G. E.; Robb, M. A.; Cheeseman, J. R.; Montgomery, J. A., Jr.; Vreven, T.; Kudin, K. N.; Burant, J. C.; Millam, J. M.; Iyengar, S. S.; Tomasi, J.; Barone, V.; Mennucci, B.; Cossi, M.; Scalmani, G.; Rega, N.; Petersson, G. A.; Nakatsuji, H.; Hada, M.; Ehara, M.; Toyota, K.; Fukuda, R.; Hasegawa, J.; Ishida, M.; Nakajima, T.; Honda, Y.; Kitao, O.; Nakai, H.; Klene, M.; Li, X.; Knox, J. E.; Hratchian, H. P.; Cross, J. B.; Bakken, V.; Adamo, C.; Jaramillo, J.; Gomperts, R.; Stratmann, R. E.; Yazyev, O.; Austin, A. J.; Cammi, R.; Pomelli, C.; Ochterski, J. W.; Ayala, P. Y.; Morokuma, K.; Voth, G. A.; Salvador, P.; Dannenberg, J. J.; Zakrzewski, V. G.: Dapprich, S.; Daniels, A. D.; Strain, M. C.; Farkas, O.; Malick, D. K.; Rabuck, A. D.; Raghavachari, K.; Foresman, J. B.; Ortiz, J. V.; Cui, Q.; Baboul, A. G.; Clifford, S.; Cioslowski, J.; Stefanov, B. B.; Liu, G.; Liashenko, A.; Piskorz, P.; Komaromi, I.; Martin, R. L.; Fox, D. J.; Keith, T.; Al-Laham, M. A.; Peng, C. Y.; Nanayakkara, A.; Challacombe, M.; Gill, P. M. W.; Johnson, B.; Chen, W.; Wong, M. W.; Gonzalez, C.; Pople, J. A. Gaussian, Inc., Wallingford CT, 2004.

(11) In **3bGa**, there is no interaction between Ga and the bottom benzene (the Ga–C distances are 4.9 Å). This length is much longer than that of a usual gallium–arene interaction. Review of arene complexes of gallium; Gorlov M.; Kloo, L. *Coord. Chem. Rev.* **2008**, *252*, 1564–1576.

(12) The LUMOs+n are most important for Lewis acid because the LUMOs+n have upward lobes and are suitable for accepting a reagent: **3aGa**, LUMO+3; **3bGa**, **3cGa** and **3dGa**, LUMO+5; **7**, LUMO+10; **7·Py**, LUMO+7.

(13) (a) Danishefsky, S.; Kerwin J. F.; Kobayashi, S. *J. Am. Chem. Soc.* **1982**, *104*, 358–360. (b) Hattori K.; Yamamoto, H. *Synlett* **1993**, 129–130.

(14) Although the catalyst contains pyridine hydrochloride (reference 7), pyridine hydrochloride did not act as a catalyst; hetero Diels–Alder reaction of **8** with **9** resulted in no reaction (see Experimental Section).

(15) (a) Denmark, S. E.; Griedel, B. D.; Coe D. M.; Schnute, M. E. *J. Am. Chem. Soc.* **1994**, *116*, 7026–7043. (b) Nelson, S. G.; Kim B.-K.; Peelen, T. J. *J. Am. Chem. Soc.* **2000**, *122*, 9318–9319. (c) Kobayashi, J.; Kawaguchi K.; Kawashima, T. *J. Am. Chem. Soc.* **2004**, *126*, 16318–16319. (d) Wagner, C. E.; Kim J.-S.; Shea, K. J. *J. Am. Chem. Soc.* **2003**, *125*, 12179–12195.

(16) van der Made, A. W.; van der Made, R. H. *J. Org. Chem.* **1993**, **58**, 1262–1263.

(17) Vacca, A.; Nativi, C.; Cacciarini, M.; Pergoli, R.; Roelens, A. *J. Am. Chem. Soc.* **2004**, **126**, 16456–16465.

(18) Becke, A. D. *J. Chem. Phys.* **1993**, *98*, 5648–5652.

2-2. Lithium Phenolates with a Hexagonal-Prismatic Li_6O_6 Core Isolated via a Cage-Shaped Tripodal Ligands System: Crystal Structures and Their Behavior in Solution

2-2-1. Introduction

Alkali metal phenolates has been extensively investigated[1] to prove a close relation between their aggregated structures and reactivity.[2] Therefore, the construction of new types of aggregated structure should attract much attention. Because lithium phenolates have the highest stability among alkali metal ones, various aggregated contact ion pairs have been reported as shown in Figure 1A.[3-7] Hexameric species, however, has been little explored, and Jackman has only characterized the hexameric lithium phenolate $(LiOC_6H_3-3,5-OMe_2)_6 \cdot (dioxolane)_6$ as a mixture with the tetrameric one in dioxolane solvent below -50 °C.[4e] Only one example of X-ray crystallographic analysis of hexamer $(LiOPh)_6 \cdot (THF)_6$ has been reported.[8,9]

General structures of lithium phenolates are based on a 4-membered Li_2O_2 ring to stably form both of dimers and tetramers probably because of the less steric hindrance between their aryl moieties and the ligand (L) coordinating to lithium than a 6-membered Li_3O_3 ring (Figure 1B). In contrast, structure based on a 6-membered Li_3O_3 ring (trimer) is generated only by introducing bulky substituents at *ortho*-position of phenols which prevents the ligand coordination to lithium center to reduce the problematic steric hindrance.[6] However, this method is inapplicable to the creation of hexamer because the environment around Li_3O_3 ring is too congested for two Li_3O_3 rings to stack upon another. No method to create hexameric lithium phenolate bearing hexagonal-prismatic Li_6O_6 core has been established as yet.

Recently, we designed some cage-shaped ligands bearing 3 phenoxy moieties to control the Lewis acidity of group 13 metal complexes.[10] In those studies we designed 1,3,5-tris(*m*-hydroxybenzyl)benzene $1H_3$, in which 3 tether phenyl moieties were linked by the bottom benzene ring (Figure 1C). In gallium complexes bearing **1** as a ligand, 3 tether phenyl rings were fixed almost perpendicularly to a plane consisting of phenoxy oxygens.[10c] From these results, we expected that the tripodal ligand would reduce the steric hindrance in the 6-membered Li_3O_3 ring by fixing the phenoxy moieties and enable the 6-membered Li_3O_3 ring to exist stably (Figure 1C, top view). Furthermore, these ligands organized 3 tether aromatic rings on one side of the Li_3O_3 plane, and the opposite side of the Li_3O_3 plane was less sterically hindered. This geometry would enable 2 Li_3O_3 rings to stack upon each other, leading to a hexagonal-prismatic Li_6O_6 core structure (Figure 1C, side view). Herein, we report the full-characterization of the lithium phenolates with a hexagonal prismatic Li_6O_6 core in both solution and solid state.

(A)

Li—O—Ar
monomer

Ar–O–Li / Li–O–Ar
dimer

Ar–O–Li / Li–O–Li / O–Ar
trimer
(*rare*)

Ar–O–Li / Li–O / Li–O–Ar / Ar–O–Li
tetramer

Ar–O–Li / Ar–O–Li–O–Ar / Ar–O–Li–O–Li–O–Ar
hexamer (*very rare*)

(B)

$(L)_n$ Li–O / O–Li $(L)_n$
stable
four-member
Li_2O_2 ring

congested

$(L)_n$ Li–O–Li $(L)_n$ / O–Li–O / $(L)_n$
unstable
six-member
Li_3O_3 ring

stable **>** unstable

(C)

tether aryl ring

OH OH HO

1H₃

bottom aryl ring

Cage-Shaped Ligand

⟹

Top View

fixing aryl rings   *less sterically hindered*

$(L)_n$ Li–O–Li $(L)_n$ / O–Li–O / $(L)_n$

Reduce Steric Hindrance → Six-Member Ring

Side View

O–Li–O / Li–O–Li–O / O–Li–O / O–Li

Stack upon One Another → Hexagonal-Prismatic Li₆O₆ core

Figure 1. (A) Various types of lithium phenolates (ligands coordinating to Li are omitted for clarify). (B) Steric hindrance in lithium phenolates bearing a 4-membered Li_2O_2 ring and 6-membered Li_3O_3 ring. (C) Working hypothesis for creating lithium phenolates with hexagonal-prismatic Li_6O_6 core.

2-2-2. Results and Discussion

On the basis of our strategy, we succeeded in isolating lithium phenolates $(1Li_3)_2 \cdot (THF)_6$ with a hexagonal-prismatic Li_6O_6 structure by using cage-shaped triphenolic ligands $1H_3$. The phenolates $(1Li_3)_2 \cdot (THF)_6$ were quantitatively generated by the reaction of $1H_3$ with *n*-BuLi in THF as shown in Scheme 1 and were thoroughly analyzed by X-ray crystallography (described later). These compounds $(1Li_3)_2 \cdot (THF)_6$ were highly stable at room temperature and even at an elevated temperature (110 °C).[11] Selected NMR signals for $(1Li_3)_2 \cdot (THF)_6$ and their parent ligands $1H_3$ are shown in Table 1. In ^1H NMR of $(1aLi_3)_2 \cdot (THF)_6$, a set of the signals corresponding to the ligand clearly demonstrated a C_3 symmetrical structure. This observation indicated that a 6-membered Li_3O_3 ring was created in an intramolecular fashion within the cage-shaped ligand **1a**, leading to a trinuclear $1aLi_3$ unit. The upfield-shift for the hydrogens of the tether aryl rings in $(1aLi_3)_2 \cdot (THF)_6$, in comparison to those of $1aH_3$, showed increased electron density on the tether aromatic rings. The ligated THF showed significant up-field shifted signals at $\delta(^1H)$ 3.19 and 1.47 ppm (free THF; 3.73 ppm and 1.84 ppm, respectively), in contrast to a small down-field shift in the coordination to an alkali metal.[12] This upfield shift was induced by the anisotropic effect of neighboring phenyl groups.[13] The integration of protons revealed that a THF molecule coordinated to a lithium center. In ^7Li NMR, the peak of $(1aLi_3)_2 \cdot (THF)_6$ appeared at 0.08 ppm, which is similar to that of lithium phenolate derived from simple phenol.[3b,7a] Analogous spectral data were

obtained for (**1b-dLi₃**)₂·(THF)₆, as shown in Table 1. These NMR observations suggested that the generated lithium complexes had a C_3 symmetry and possessed a THF molecule on each lithium.

Scheme 1. Synthesis of the Lithium Phenolates with Cage-Shaped Ligands **1**.

1aH₃ : R = H X = H
1bH₃ : R = Me X = H
1cH₃ : R = Et X = H
1dH₃ : R = Me X = F

(**1aLi₃**)₃·THF
(**1bLi₃**)₃·THF
(**1cLi₃**)₃·THF
(**1dLi₃**)₃·THF
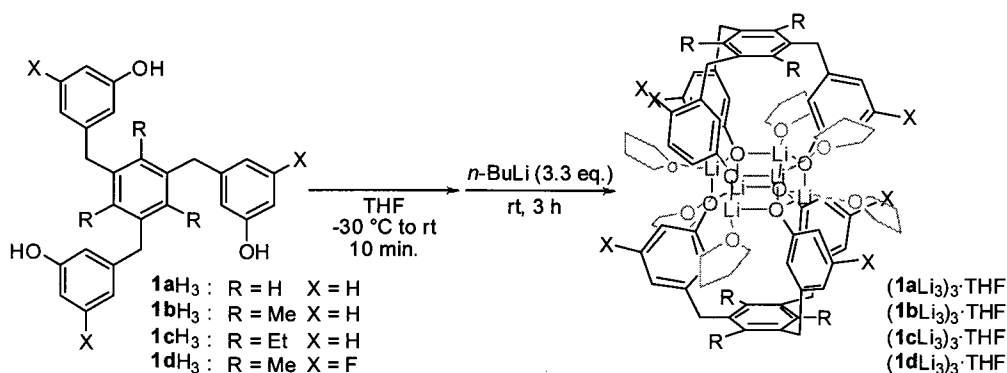
Table 1. NMR Chemical Shifts of (**1Li₃**)₂·(THF)₆ and **1H₃**.

compound	δ(^{1}H)							δ(^{7}Li)
	b-H	c-H	d-H	f-H	1-CH₂	g-H	h-H	
(**1aLi₃**)₂·(THF)₆	6.49	6.88	6.23	5.86	3.91	3.19	1.47	0.08
(**1bLi₃**)₂·(THF)₆	6.58	6.90	6.20	5.91	4.13	3.13	1.51	0.06
(**1cLi₃**)₂·(THF)₆	6.57	6.88	6.20	5.92	4.04	3.07	1.47	-0.01
(**1dLi₃**)₂·(THF)₆	6.31	-	5.90	5.62	4.07	3.14	1.56	-0.18
1aH₃	6.78	7.15	6.66	6.55	3.86	-	-	-
1bH₃	6.82	7.15	6.63	6.29	4.13	-	-	-
1cH₃	6.87	7.15	6.62	6.21	4.11	-	-	-
1dH₃	6.31	-	5.90	6.08	4.08	-	-	-

(5THFs are omitted)
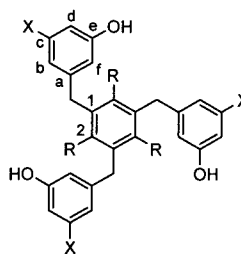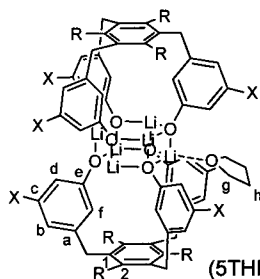
To investigate the aggregation state of lithium phenolates with a cage-shaped ligand **1** in solution state, the following NMR studies in CDCl₃ were carried out. Lithium phenolates are generally expected to exist as trinuclear **1Li₃**, hexanuclear (**1Li₃**)₂, or more complicated aggregated species (**1Li₃**)ₙ. Jackman determined qualitatively the aggregation state of ArOLi complexes in solution based on ^{13}C NMR chemical shifts δ(^{13}C).[4g] Specifically, the difference-value (Δ) between the ^{13}C chemical shift (δ(^{13}C)$_{ArOLi}$) found for the *para*-carbon of an oxygen moiety in lithium complexes ArOLi and that of (δ(^{13}C)$_{ArOMe}$) in the corresponding anisole ArOMe accurately reflects the number of lithium atoms that surround an oxygen atom of phenolate.[14] Following this established precedent, a series of NMR experiments[15] gave Δ values ranging from 4.29 to 6.05 ppm (**1a**: Δ = 6.05; **1b**: Δ = 4.29; **1c**: Δ = 4.67; **1d**: Δ = 4.41), which

82

revealed that in solution each oxygen is bound to 3 lithium centers. Therefore, the possibility of the trinuclear species $1Li_3$ was ruled out.

Next, we used the method of continuous variation developed by Collum to determine the detailed aggregation state, and formed species were observed by NMR in various mixing ratios of homoaggregated lithium phenolates $(1bLi_3)_2 \cdot (THF)_6$ and $(1dLi_3)_2 \cdot (THF)_6$.[4a] In any mixing ratio, only a single heteroaggregated lithium phenolate was observed along with the starting homoaggregated species. This observation clearly showed that the ligand exchange took place in our lithium phenolates with tridentate ligands **1** as well as lithium phenolates derived from simple phenol studied by Collum.[4a] Plots of molar ratios of formed species versus the loaded molar ratio χ of $(1dLi_3)_2 \cdot (THF)_6$ are illustrated in Figure 2. This statistical distribution is the typical pattern of a dimer. Therefore, $1bLi_3$ and $1dLi_3$ exist as dimeric forms in solution at room temperature as shown in Eq 1. Judging from ^{13}C NMR chemical shifts and the method of continuous variation, the lithium phenolates with the cage-shaped ligand **1** exist solely as a hexanuclear species in solution. This is the first example of lithium phenolates that maintain a hexagonal-prismatic Li_6O_6 structure in solution at room temperature.
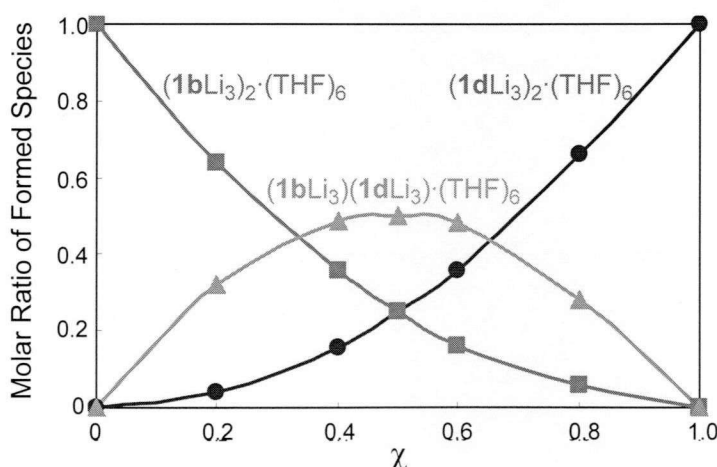
Figure 2. Job plot showing molar ratio of formed species versus χ (χ : loaded molar ratio of $(1dLi_3)_2 \cdot (THF)_6$) to sum of $(1bLi_3)_2 \cdot (THF)_6$ and $(1dLi_3)_2 \cdot (THF)_6$ in $CDCl_3$.

$$(1bLi_3)_2 \cdot (THF)_6 \ + \ (1dLi_3)_2 \cdot (THF)_6 \ \rightleftharpoons \ 2 \ (1dLi_3)(1dLi_3) \cdot (THF)_6 \quad (1)$$
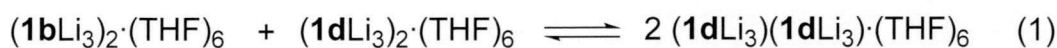
The structures of solid-state lithium phenolates $(1a-dLi_3)_2 \cdot (THF)_6$ were analyzed by X-ray crystallography.[16] Their ORTEP drawings are shown in Figure 3.[17] All the lithium complexes $(1a-dLi_3)_2 \cdot (THF)_6$ were hexanuclear lithium compounds. A 6-membered Li_3O_3 ring was constructed with 3 phenolate oxygen atoms from 1 cage-shaped ligand and 3 lithium atoms creating a $(1Li_3) \cdot (THF)_3$ unit. These $(1Li_3) \cdot (THF)_3$ units stacked upon each other, which led to a hexagonal-prismatic Li_6O_6 core structure. The top view of $(1bLi_3)_2 \cdot (THF)_6$ (Figure 3e) clearly shows that the tether phenyl rings were almost perpendicular to the 6-membered Li_3O_3 ring of the Li_6O_6 core. In fact, the angle between the

phenoxy ring and a least-squares plane drawn through O(1A)-O(1B)-O(1C) in (**1bLi₃**)₂·(THF)₆ was 88.77°. This result suggested that the tripodal ligand system **1** had a minimized steric hindrance between the tether phenyl moieties and the THF coordinating to the lithium atom. The THF molecule coordinated to the lithium center and laid between 2 tether benzene rings. These results were consistent with the isotropic effect of THF observed in ^{1}H NMR. The closest contact between the THF molecules and the tether phenyl rings ranged from 2.561 Å to 2.590 Å, suggesting the presence of the CH-π interaction, which may play a role in stabilizing the structure of the THF adduct.[18] The 6-membered Li₃O₃ rings were nearly regular hexagons, and their conformation was somewhat similar to the chair conformation of cyclohexane, as shown in Figure 3f. Li(1A) or O(1C) were located out of the plane drawn through O(1A)-O(1B)-Li(1B)-Li(1C) (distance from the plane to Li(1A) or O(1C) is 0.239 Å or 0.244 Å, respectively). For (**1bLi₃**)₂·(THF)₆, the Li-(μ₃-O) bond lengths in the hexagonal-prismatic Li₆O₆ core ranged from 1.985(5) Å to 1.953(5) Å (mean of 1.969 Å), while the Li-O_THF bond length was 2.041(5) Å. The bond angles of Li-(μ₃-O)-Li and (μ₃-O)-Li-(μ₃-O) in the 4-membered rings in the Li₆O₆ core ranged from 84.3(2)° to 85.2(2)° (mean of 84.8°) and 94.7(2)° to 95.8(2)° (mean of 95.3°), respectively. The bond angles of Li-(μ₃-O)-Li and (μ₃-O)-Li-(μ₃-O) in the 6-membered rings in the Li₆O₆ core were 117.4(2)° and 121.3(2)°. The O_THF-Li-(μ₃-O) bond angles ranged from 111.4(2)° to 117.1(2)° (mean of 114.2°).

These values suggested that (**1bLi₃**)₂·(THF)₆ had structural features similar to the hexamer previously reported for simple lithium phenolate.[8] Therefore, it was expected that the behavior of (**1bLi₃**)₂·(THF)₆ would show similar properties to those of the lithium phenolates derived from simple phenols. The structures of (**1a-dLi₃**)₂·(THF)₆ are very analogous, except for small differences in the conformations of the phenyl and THF groups relative to the Li₆O₆ core. In the case of (**1dLi₃**)₂·(THF)₆,[19] the Li-O_THF bond lengths are shorter than those of (**1bLi₃**)₂·(THF)₆ because the electronegativity of fluorine increases the positive charge of lithium to create a stronger Li-O_THF bond.
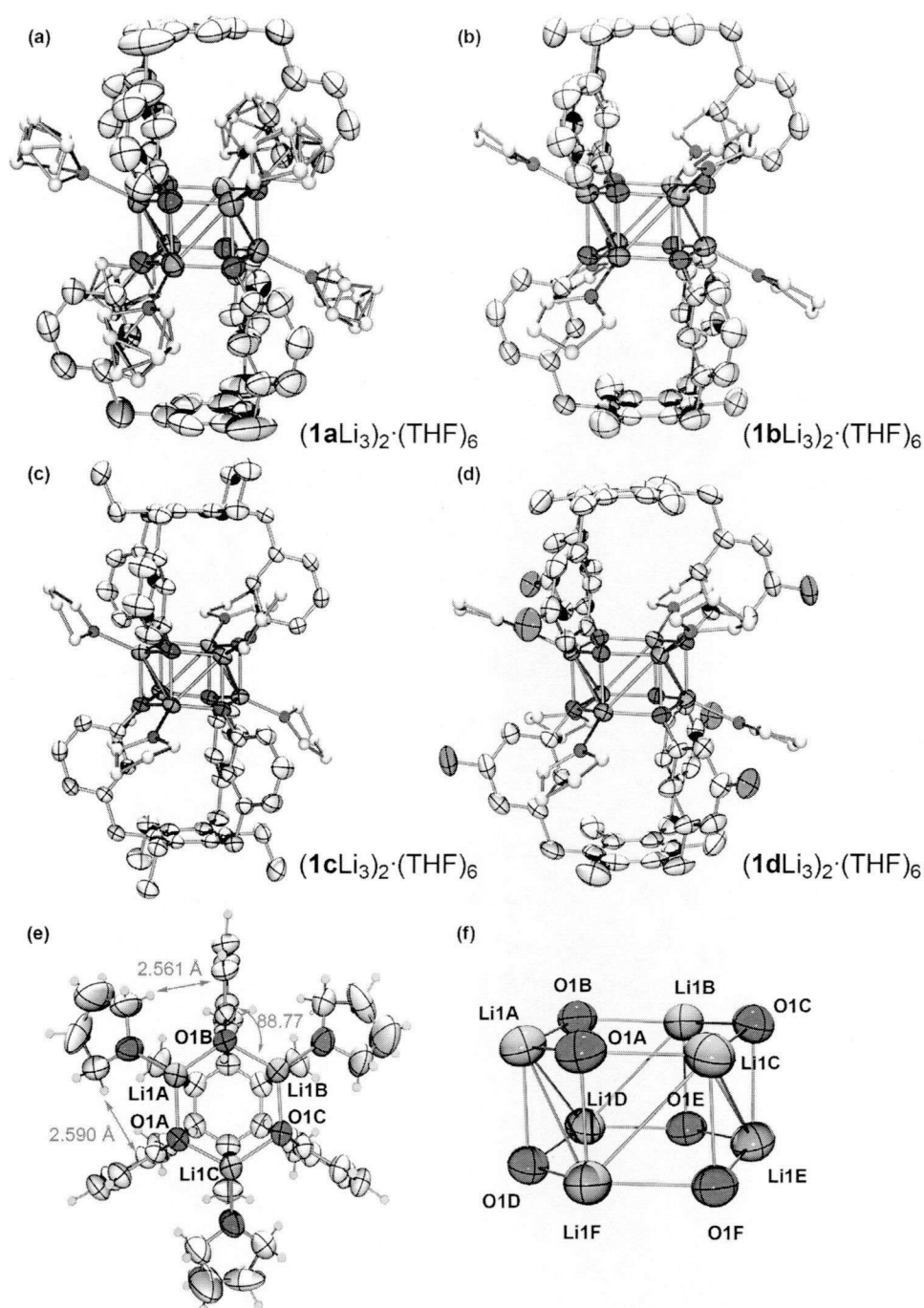
Figure 3. ORTEP drawings of lithium phenolates $(1Li_3)_2 \cdot (THF)_6$ (some hydrogens are omitted for clarity) (a) $(1aLi_3)_2 \cdot (THF)_6$ (coordinating THFs are disordered.) (b) $(1bLi_3)_2 \cdot (THF)_6$ (c) $(1cLi_3)_2 \cdot (THF)_6$ (d) $(1dLi_3)_2 \cdot (THF)_6$ (e) Top view (one unit of $(1bLi_3) \cdot (THF)_3$ is omitted for clarity). (f) Hexagonal-prismatic Li_6O_6 core of $(1bLi_3)_2 \cdot (THF)_6$.

For the mechanistic study of the lithium phenolate with hexagonal-prismatic Li_6O_6 core, we investigated the rate of their ligand-exchange. It is very difficult to measure the rate of the ligand-exchange in hexameric lithium phenolate derived from simple phenols because of their instability and complicated equilibrium. However, the cage-shaped triphenolic ligand system is able to stabilize the Li_6O_6 structure and simplify the equilibrium analysis of the lithium phenolate. Therefore, we examined

85

the ligand exchange between $(\mathbf{1b}Li_3)_2 \cdot (THF)_6$ and $(\mathbf{1d}Li_3)_2 \cdot (THF)_6$. The rate of ligand exchange was estimated by the time $t_{1/2}$ in which the equilibrium was half completed (Table 2). The rate of ligand exchange decreased as the amount of THF increased. This means that the release of THF from the complex is a trigger of this ligand exchange. It is interesting that we unexpectedly obtained the crystal of the lithium phenolate $(\mathbf{1b}Li_3)_2 \cdot (THF)_4$ in which 2 of 6 lithium atoms have no coordinative solvent.[20] The ORTEP drawings are shown in Figure 4. Although the hexagonal-prismatic Li_6O_6 core was maintained even without THF, Li(1C) and O(1B) got closer (3.478 Å) than $(\mathbf{1b}Li_3)_2 \cdot (THF)_6$ (3.928 Å), and the 6-membered Li_3O_3 ring was distorted, as shown in Figure 4b. The distances for Li(1A)-Li(1C) and Li(1B)-Li(1C) were 3.147 Å and 3.217 Å, respectively, which were shorter than those of $(\mathbf{1b}Li_3)_2 \cdot (THF)_6$ (3.365 Å). This structural change might have compensated for the electron deficiency of the THF-free lithium by clustering. The isolation of $(\mathbf{1b}Li_3)_2 \cdot (THF)_4$ indicated that a lithium phenolate, which lost some coordinating THF, $(\mathbf{1}Li_3)_2 \cdot (THF)_{6-m}$, was generated, and it triggered the ligand exchange process. The excess amount of THF may have prevented the generation of $(\mathbf{1b}Li_3)_2 \cdot (THF)_{6-m}$, leading to a slow exchange rate (Table 2, Entry 5).

Table 2. Rate of Ligand-Exchange.

$$(\mathbf{1b}Li_3)_2 \cdot (THF)_6$$
(1 eq.)

+

$$(\mathbf{1d}Li_3)_2 \cdot (THF)_6$$
(1 eq.)

$\xrightarrow{\text{solvent, rt}}$ 2 $(\mathbf{1b}Li_3)(\mathbf{1d}Li_3) \cdot (THF)_6$

entry	solvent	$t_{1/2}$
1	$CDCl_3$	4 h
2	$CDCl_3$/THF (59/1)	8 h
3	$CDCl_3$/THF (29/1)	19 h
4	$CDCl_3$/THF (11/1)	120 h
5	excess THF	> 1 week
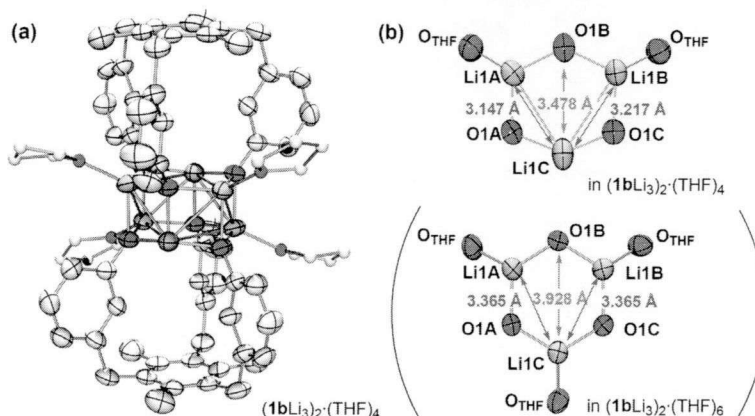
Figure 4. ORTEP drawing of $(\mathbf{1b}Li_3)_2 \cdot (THF)_4$. (a) Side view (some hydrogens are omitted for clarity) (b) Li_3O_3 ring with oxygen atoms of THF in $(\mathbf{1b}Li_3)_2 \cdot (THF)_4$ and $(\mathbf{1b}Li_3)_2 \cdot (THF)_6$.

2-2-3. Conclusion

We synthesized hexanuclear lithium phenolates with a hexagonal-prismatic Li_6O_6 core stabilized by cage-shaped triphenolic ligands. This is the first example of hexameric lithium phenolates that are stable either in solid state or in solution. Their properties were examined by X-ray crystallography and NMR measurements. This study succeeded in obtaining a novel type of lithium phenolate and opening new aspects of lithium phenolate chemistry.

2-2-4. Experimental Section

General. IR spectra were recorded as thin films or as solids in KBr pellets on a HORIBA FT-720 spectrophotometer. ^1H and ^{13}C spectra were obtained with a 400 and 100 MHz spectrometer, respectively, with TMS as internal standard. ^{19}F NMR spectra were obtained with a 372 MHz spectrometer with $BF_3 \cdot OEt_2$ in $CDCl_3$ as external standard. ^7Li NMR spectra were obtained with a 154 MHz spectrometer with LiCl in D_2O as external standard. ^{19}F NMR spectra were obtained with a 372 MHz spectrometer with $BF_3 \cdot OEt_2$ in $CDCl_3$ as external standard. Mass spectra were recorded on a JEOL JMS-DS303. All reactions were carried out under nitrogen. Synthesis of lithium complexes was performed in nitrogen-filled glove box.

Crystallographic Date. CCDC-861321 $\{1aLi_3)_2 \cdot (THF)_6\}$ CCDC-861322 $\{1bLi_3)_2 \cdot (THF)_6\}$, CCDC-861323 $\{1cLi_3)_2 \cdot (THF)_6\}$, CCDC-861324 $\{1dLi_3)_2 \cdot (THF)_6\}$, and CDC-861325 $\{1bLi_3)_2 \cdot (THF)_4\}$ contain the supplementary crystallographic data for this paper. These data can be obtained free of charge from The Cambridge Crystallographic Data Centre via www.ccdc.cam.ac.uk/data_request/cif

Materials. Dehydrated dichloromethane, THF, and hexane were purchased and used as obtained. The compounds $1a$-dH_3 were prepared according to our previous report.[10c] All other reagents are commercially available.

$(1aLi_3)_2 \cdot (THF)_6$
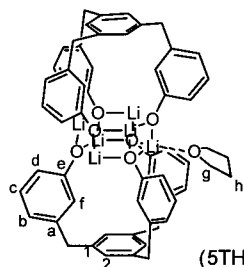
(5THFs is omitted)

In a glove box, to a mixture of 1,3,5-tris(3-hydroxybenzyl)benzene (0.1 mmol = 39.8 mg) in THF (5 mL) was added n-BuLi in hexane (0.318 mmol, 0.2 mL, 1.59 M) at -30 °C with stirring. The stirring was kept for 2 h with warming up to rt. Evaporation of volatiles gave a white solid. The obtained crude materials were washed with hexane and evaporated to give the product quantitatively. The product was recrystallized from dichloromethane/hexane(2/1) for X-ray analysis. ^1H NMR: (400 MHz, $CDCl_3$) 6.88 (m, 12H, c-H and 2-H), 6.49 (d, J = 7.6 Hz, 6H, b-H), 6.23 (dd, J = 7.6, 1.8 Hz, 6H, d-H), 5.86 (s, 6H, f-H), 3.91 (s, 12H, 1-CH_2), 3.19 (br, 24H, g-H_2), 1.47 (br, 24H, h-H_2); ^{13}C NMR: (100 MHz, $CDCl_3$) 166.0 (s, C-e), 143.7 (s, C-a), 141.7 (s, C-1), 130.0 (d, C-2), 128.6 (d, C-c), 121.2 (d, C-f), 116.7 (d, C-d), 115.2 (d, C-b), 67.6 (t, C-g), 40.6 (t, 1-CH_2), 25.1 (t, C-h); ^7Li NMR: (153.7 MHz, $CDCl_3$) 0.08.

(1bLi₃)₂·(THF)₆

(5THFs is omitted)
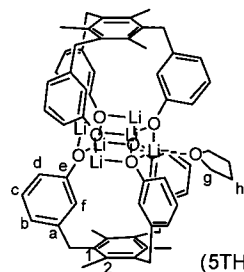
In a glove box, to a mixture of 1,3,5-tris(3-hydroxybenzyl)-2,4,6-trimethylbenzene (0.1 mmol = 43.8 mg) in THF (5 mL) was added n-BuLi in hexane (0.318 mmol, 0.2 mL, 1.59 M) at -30 °C with stirring. The stirring was kept for 2 h with warming up to rt. Evaporation of volatiles gave a white solid. The obtained crude materials were washed with hexane and evaporated to give the product quantitatively. The product was recrystallized from dichloromethane/hexane(2/1) for X-ray analysis. ^{1}H NMR: (400 MHz, CDCl₃) 6.90 (dd, J =8.0, 7.8 Hz, 6H, c-H), 6.58 (d, J = 7.8 Hz, 6H, b-H), 6.20 (dd, J = 8.0, 1.8 Hz, 6H, d-H), 5.91 (s, 6H, f-H), 4.13 (s, 12H, 1-CH₂), 3.13 (br, 24H, g-H₂), 2.08 (s, 18H, 2-CH₃), 1.51 (br, 24H, h-H₂); ^{13}C NMR: (100 MHz, CDCl₃) 165.9 (s, C-e), 141.8 (s, C-a), 135.5 (s, C-2), 134.5 (s, C-1), 128.7 (d, C-c), 119.4 (d, C-f), 116.5 (d, C-d), 116.1 (d, C-b), 67.6 (t, C-g), 34.8 (t, 1-CH₂), 25.3 (t, C-h), 16.3 (q, 2-CH₃); ^{7}Li NMR: (153.7 MHz, CDCl₃) 0.06.

(1cLi₃)₂·(THF)₆

(5THFs is omitted)
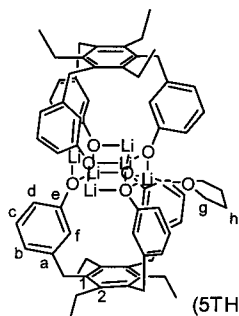
In a glove box, to a mixture of 1,3,5-tris(3-hydroxybenzyl)-2,4,6-triethylbenzene (0.1 mmol = 48.3 mg) in THF (5 mL) was added n-BuLi in hexane (0.318 mmol, 0.2 mL, 1.59 M) at -30 °C with stirring. The stirring was kept for 2 h with warming up to rt. Evaporation of volatiles gave a white solid. The obtained crude materials were washed with hexane and evaporated to give the product quantitatively. The product was recrystallized from dichloromethane/hexane(2/1) for X-ray analysis. ^{1}H NMR: (400 MHz, CDCl₃) 6.88 (dd, J = 7.8, 7.8 Hz, 6H, c-H), 6.57 (d, J = 7.8 Hz, 6H, b-H), 6.20 (d, J = 7.8, 1.6 Hz, 6H, d-H), 5.92 (s, 6H, f-H), 4.04 (s, 12H, 1-CH₂), 3.07 (t, J = 6.5 Hz, 24H, g-H₂), 2.30 (q, J = 7.4 Hz, 12H, 2-CH₂), 1.47 (t, J = 6.5 Hz, 24H, h-H₂), 1.22 (t, J = 7.4 Hz, 18H, 2-CH₂CH_3); ^{13}C NMR: (100 MHz, CDCl₃) 166.3 (s, C-e), 142.3 (s, C-a), 141.5 (s, C-2), 134.4 (s, C-1), 128.5 (d, C-c), 120.0 (d, C-f), 116.6 (d, C-d), 115.6 (d, C-b), 67.5 (t, C-g), 33.6 (t, 1-CH₂), 25.3 (t, C-h), 23.5 (t, 2-CH₂), 16.0 (q, 2-CH₂CH_3); ^{7}Li NMR: (153.7 MHz, CDCl₃) -0.01.

(1dLi₃)₂·(THF)₆

(5THFs is omitted)
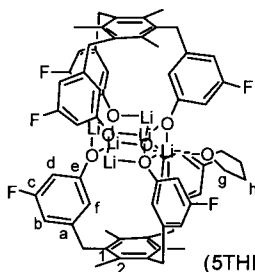
In a glove box, to a mixture of 1,3,5-tris(3-fluoro-5-hydroxybenzyl)-2,4,6-trimethylbenzene (0.1 mmol = 49.2 mg) in THF (5 mL) was added n-BuLi in hexane (0.318 mmol, 0.2 mL, 1.59 M) at -30 °C with stirring. The stirring was kept for 2 h with warming up to rt. Evaporation of volatiles gave a white solid. The obtained crude materials were washed with hexane and evaporated to give the product quantitatively. The product was recrystallized from dichloromethane/hexane(2/1) for X-ray analysis. ^{1}H NMR: (400 MHz, CDCl₃) 6.31 (d, $^3J_{FH}$ = 9.4 Hz, 6H, b-H), 5.90 (dd, $^3J_{FH}$ = 12.0, 1.6 Hz, 6H, d-H), 5.62 (s, 6H, f-H), 4.07 (s, 12H, 1-CH₂), 3.14 (br, 24H, g-H₂), 2.04 (s, 18H, 2-CH₃), 1.56 (br, 24H, h-H₂); ^{13}C NMR: (100 MHz, CDCl₃) 167.6

88

(s, d by $^3J_{CF}$ = 11.5 Hz, C-e), 164.3 (s, d by $^1J_{CF}$ = 243.6 Hz, C-c), 142.7 (s, d by $^3J_{CF}$ = 10.3 Hz, C-a), 135.1 (s, C-1 or C-2), 134.7 (s, C-1 or C-2), 115.1 (d, C-f), 103.5 (d, d by $^2J_{CF}$ = 19.7 Hz, C-d), 102.5 (d, d by $^2J_{CF}$ = 21.4 Hz, C-b), 67.8 (t, C-g), 34.9 (t, 1-CH$_2$), 25.3 (t, C-h), 16.3 (q, 2-CH$_3$); ^{7}Li NMR: (153.7 MHz, CDCl$_3$) -0.18; ^{19}F NMR: (372.35 MHz, CDCl$_3$) 37.38 (dd, $^3J_{FH}$ = 10.7, 10.7 Hz)

(1bLi$_3$)(1dLi$_3$)·(THF)$_6$
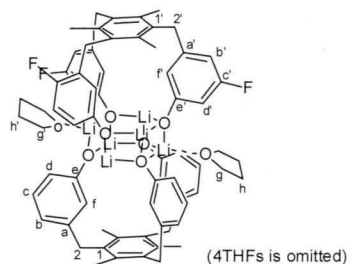
(4THFs is omitted)

Each compound (1bLi$_3$)$_2$·(THF)$_6$ and (1dLi$_3$)$_2$·(THF)$_6$ was dissolved in CDCl$_3$ to prepare 0.01 M solutions. They were mixed with ratios of 1/1 at room temperature. In the resulting mixture, (1bLi$_3$)(1dLi$_3$)·(THF)$_6$ was observed accompanied with the starting homoaggregated species (1bLi$_3$)$_2$·(THF)$_6$ and (1dLi$_3$)$_2$·(THF)$_6$. Selected signals for (1dLi$_3$)(1dLi$_3$)·(THF)$_6$ are shown. ^{1}H NMR: (400 MHz, CDCl$_3$) 6.90 (m, 3H, c-H), 6.58 (m, 3H, b-H), 6.31 (m, 3H, b'-H), 6.18 (m, 3H, d-H), 5.90 (m, 6H, f-H and d'-H), 5.62 (s, 3H, f'-H), 4.13 (s, 6H, 1-CH$_2$), 4.07 (s, 6H, 1'-CH$_2$), 3.13 (br, 24H, g-H$_2$ and g'-H$_2$), 2.07 (s, 9H, 2-CH$_3$), 2.05 (s, 9H, 2'-CH$_3$), 1.57 (br, 24H, h-H$_2$ and h'-H$_2$); ^{7}Li NMR: (153.7 MHz, CDCl$_3$) -0.05; ^{19}F NMR: (372.35 MHz, CDCl$_3$) 37.22 (dd, $^3J_{FH}$ = 10.7, 10.7 Hz)

^{1}H NMR

^{19}F NMR

^{7}Li NMR

89
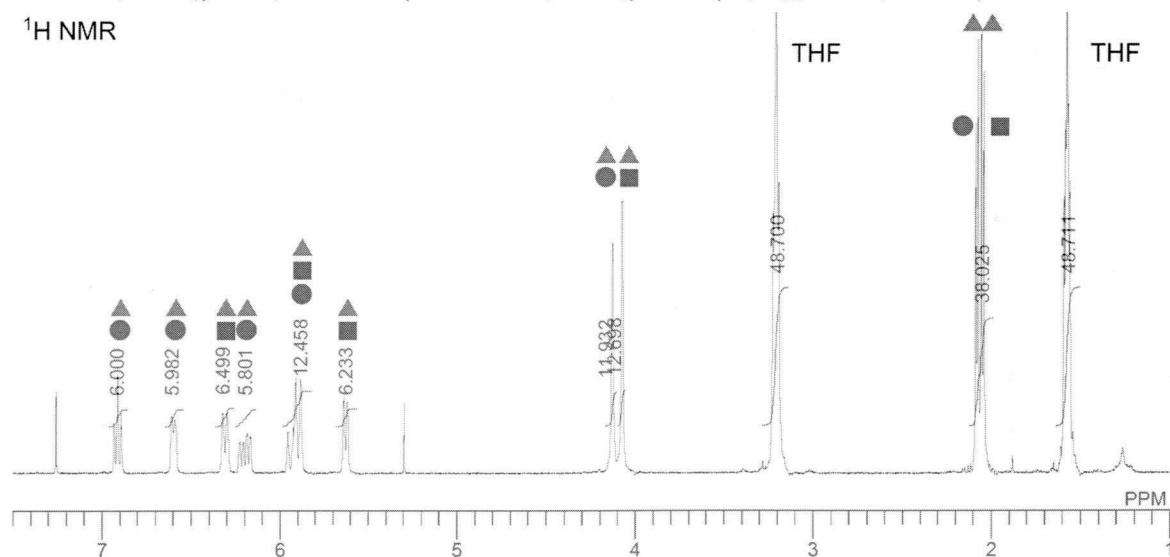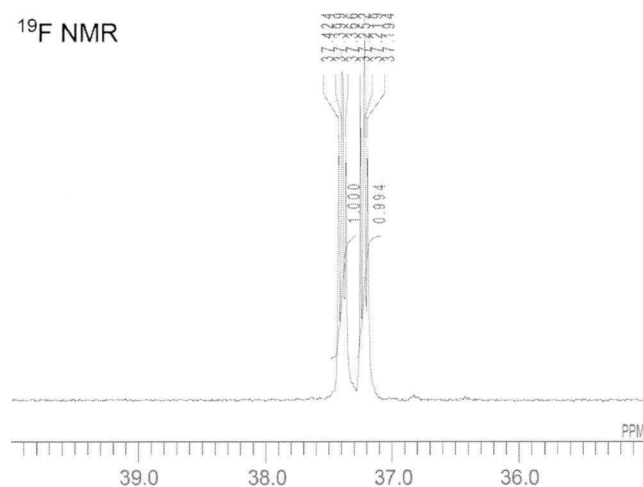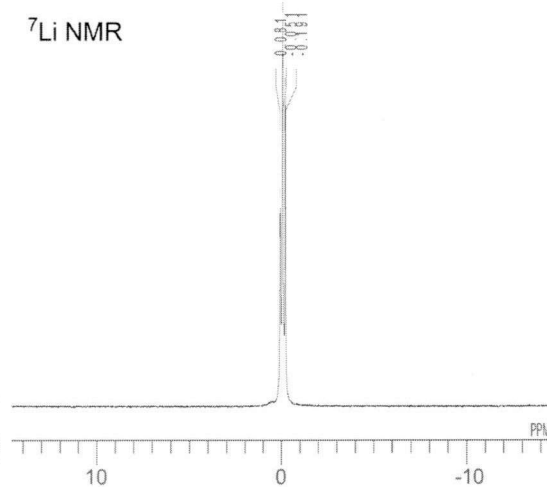
Method of Continuous Variation (Figure 2)

A ligand exchange between lithium phenolates ($1bLi_3)_2 \cdot (THF)_6$ and ($1dLi_3)_2 \cdot (THF)_6$ is described below.

| ($1bLi_3)_2 \cdot (THF)_6$ | ($1dLi_3)_2 \cdot (THF)_6$ | ($1bLi_3)(1dLi_3) \cdot (THF)_6$ |
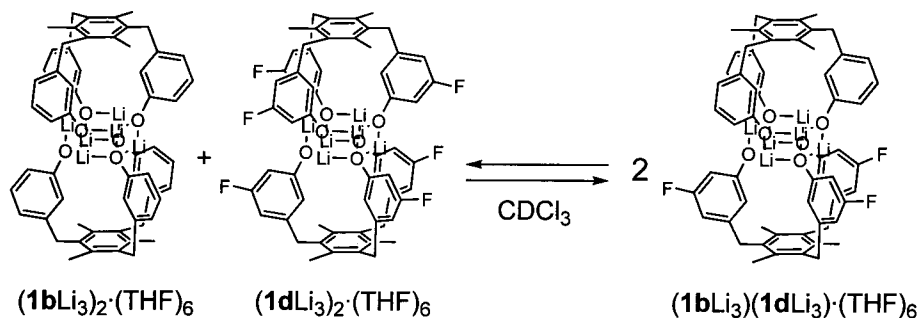
	($1bLi_3)_2 \cdot (THF)_6$	($1dLi_3)_2 \cdot (THF)_6$	($1bLi_3)(1dLi_3) \cdot (THF)_6$
molar ratios at an initial state	1	r	0
molar ratios at an equilibrium state	$1-\alpha$	$r-\alpha$	2α

Molar ratio s of ($1dLi_3)_2 \cdot (THF)_6$ to ($1bLi_3)(1dLi_3) \cdot (THF)_6$ was measured by ^{19}F NMR integration.

$$s = \frac{[(1dLi_3)_2 \cdot (THF)_6]}{[(1bLi_3)(1dLi_3) \cdot (THF)_6]}$$

Molar ratios of formed lithium phenolates under an equibrium state were expressed by following equation.

$$s = \frac{r-\alpha}{2\alpha}$$

$$\alpha = \frac{r}{2s+1}$$

molar ratio of ($1bLi_3)_2 \cdot (THF)_6$ $= \dfrac{1-\alpha}{1+r}$ (1)

molar ratio of ($1dLi_3)_2 \cdot (THF)_6$ $= \dfrac{r-\alpha}{1+r}$ (2)

molar ratio of ($1bLi_3)(1dLi_3) \cdot (THF)_6$ $= \dfrac{2\alpha}{1+r}$ (3)

Each compound ($1bLi_3)_2 \cdot (THF)_6$ and ($1dLi_3)_2 \cdot (THF)_6$ was dissolved in $CDCl_3$ to prepare 0.01 M solutions. They were mixed with ratios of 1/4, 2/3, 1/1, 3/2, and 4/1 (χ = 0.2, 0.4, 0.5, 0.6, and 0.8) at room temperature. Molar ratios of formed species were estimated by equations 1-3 described above.

Rate of Lignad-Exchange (Table 2)

Each compound (**1bLi₃**)₂·(THF)₆ and (**1dLi₃**)₂·(THF)₆ was dissolved in $CDCl_3$ to prepare 0.01 M solutions. The pre-mixed solvents were prepared from $CDCl_3$ and THF at various ratios ($CDCl_3$:THF = 50/50, 80/20, 90/10, 100/0). To the pre-mixed solvents (0.1 mL), the solutions of (**1bLi₃**)₂·THF (0.25 mL) and (**1dLi₃**)₂·THF (0.25 mL) were added at room temperature. Molar ratios of (**1bLi₃**)(**1dLi₃**)·(THF)₆ were estimated by equation 3 described above.
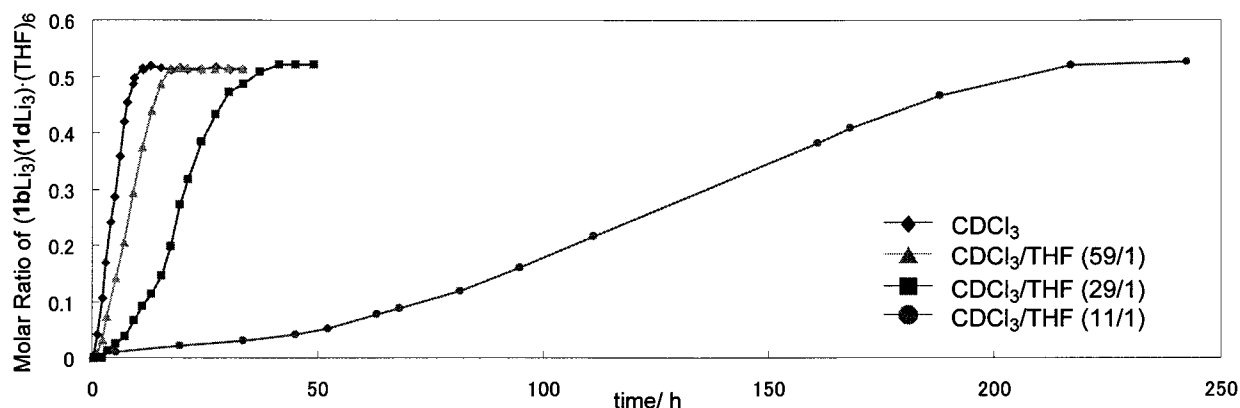
Figure S1. Effect of solvent systems on relationship between formed amount of (**1bLi₃**)(**1dLi₃**)·(THF)₆ and reaction time.

Table S1. X-ray data for all crystallographically characterized complexes.

	(1aLi₃)₂·6THF	(1bLi₃)₂·6THF	(1cLi₃)₂·6THF	(1dLi₃)₂·6THF	(3bLi₃)₂·4THF
chemical formula	$C_{78}H_{90}Li_6O_{12}$	$C_{84}H_{102}Li_6O_{12}$	$C_{93}H_{113}Li_6O_{12}$	$C_{171}H_{195}F_{12}Li_{12}O_{24}$	$C_{94}H_{104}Li_6O_{10}$
formula weight	1261.21	1345.37	1468.51	2945.68	1435.50
space group	Pa-3	Pa-3	$P2_1/n$	$Pcca$	P-1
μ(Mo-K) (mm⁻¹)	0.076	0.077	0.072	0.086	0.073
a(Å)	19.2239(12)	19.5449(6)	12.3152(5)	31.5198(6)	12.9238(13)
b(Å)	-	-	15.6985(7)	16.6893(3)	13.6966(15)
c(Å)	-	-	22.3318(8)	31.2344(6)	14.6695(15)
α(deg)	-	-	-	-	67.099(2)
β(deg)	-	-	94.310(1)	-	64.141(2)
γ(deg)	-	-	-	-	64.306(2)
V_c (Å³)	7104.4(8)	7466.2(4)	4305.2(3)	16430.6(5)	2040.5(4)
Z	4	4	2	4	1
$R1$	0.1035	0.0845	0.0737	0.0784	0.0946
$wR2$	0.2582	0.2687	0.2325	0.2628	0.2804

Table S2. Selected bond lengths [Å] and angles [degree] for (1a-cLi₃)₂·(THF)₆.

		$(1aLi_3)_2 \cdot (THF)_6$		$(1bLi_3)_2 \cdot (THF)_6$		$(1cLi_3)_2 \cdot (THF)_6$	
Length (Å)	Li-O$_{Ar}$ (six-member ring)	1.965(8)	1.968(8)	1.985(5)	1.953(5)	1.983(4) 1.990(4) 1.975(4)	1.959(4) 1.974(4) 1.984(5)
	Li-O$_{Ar}$ (vertical)	1.955(8)		1.969(5)		1.944(5) 1.958(5)	1.996(4)
	Li-O(THF)	2.031(8)		2.041(5)		2.004(4) 2.053(5)	1.976(4)
	Li-Li (six-member ring)	3.39(1)		3.364(6)		3.347(5) 3.393(6)	3.459(6)
	Li-Li (four-member ring)	2.64(1)		2.653(6)		2.627(6) 2.639(6)	2.644(5)
	O-O (six-member ring)	3.400(4)		3.432(2)		3.422(2) 3.451(2)	3.359(2)
	O-O (four-member ring)	2.898(4)		2.910(2)		2.948(2) 2.912(2)	2.937(2)
angle (degree)	Li-O$_{Ar}$-Li (six-member ring)	118.8(3)		117.4(2)		115.5(2) 119.2(2)	121.0(2) 1.990(4)
	Li-O$_{Ar}$-Li (four-member ring)	84.7(3)	84.8(3)	84.3(2)	85.2(2)	84.9(2) 84.3(2) 84.2(2)	82.6(2) 83.1(2) 84.4(2)
	O$_{Ar}$-Li-O$_{Ar}$ (six-member ring)	119.6(4)		121.3(2)		119.2(2) 122.7(2)	115.9(2)
	O$_{Ar}$-Li-O$_{Ar}$ (four-member ring)	95.3(4)	95.2(4)	95.8(2)	94.7(2)	96.4(2) 95.3(2) 96.6(2)	96.8(2) 96.0(2) 95.4(2)
	C-C$_{methylene}$-C	113.8(7)		114.2(3)		113.5(2) 113.2(2)	113.2(2)

Table S3. Selected bond lengths [Å] and angles [degree] for $(1dLi_3)_2{\cdot}(THF)_6$ and $(1dLi_3)_2{\cdot}(THF)_4$.

		$(1dLi_3)_2{\cdot}(THF)_6(1)$		$(1dLi_3)_2{\cdot}(THF)_6(2)$		$(1bLi_3)_2{\cdot}(THF)_4$	
Length (Å)	Li-O$_{Ar}$ (six-member ring)	1.969(5)	1.979(4)	1.978(5)	1.975(5)	1.904(8)	1.919(9)
		1.986(5)	1.990(4)	1.963(5)	1.986(5)	1.976(8)	1.971(9)
		1.952(5)	1.974(5)	1.976(5)	1.968(5)	1.94(1)	1.95(1)
	Li-O$_{Ar}$ (vertical)	1.963(5)	1.984(5)	1.941(5)	1.969(4)	1.887(8)	1.967(7)
		1.941(4)		1.946(5)		1.950(8)	
	Li-O(THF)	1.990(5)	2.004(5)	2.014(5)	2.016(5)	1.945(8)	2.001(9)
		1.987(5)		1.989(4)			
	Li-Li (six-member ring)	3.435(6)	3.356(6)	3.402(6)	3.373(6)	3.561(9)	3.22(2)
		3.434(6)		3.410(6)		3.15(2)	
	Li-Li (four-member ring)	2.664(6)	2.668(6)	2.664(6)	2.648(6)	2.58(1)	2.56(1)
		2.685(6)		2.655(6)		2.62(1)	
	O-O (six-member ring)	3.342(2)	3.418(2)	3.429(2)	3.407(2)	3.523(3)	3.252(6)
		3.452(2)		3.426(2)		3.312(6)	
	O-O (four-member ring)	2.890(2)	2.855(2)	2.891(2)	2.907(2)	2.889(5)	2.881(4)
		2.922(2)		2.878(2)		2.885(4)	
angle (degree)	Li-O$_{Ar}$-Li (six-member ring)	118.8(2)	119.2(2)	117.2(2)	120.6(2)	128.9(4)	109.3(4)
		117.8(2)		120.1(2)		113.2(4)	
	Li-O$_{Ar}$-Li (four-member ring)	84.1(2)	85.3(2)	86.5(2)	84.3(2)	83.9(4)	83.3(4)
		85.7(2)	85.5(2)	84.6(2)	84.8(2)	83.2(4)	83.0(4)
		85.2(2)	85.0(2)	83.3(2)	83.3(2)	84.6(4)	84.4(4)
	O$_{Ar}$-Li-O$_{Ar}$ (six-member ring)	120.5(3)	119.0(3)	120.4(3)	115.9(3)	134.3(5)	115.8(5)
		120.8(3)		120.8(2)		111.8(4)	
	O$_{Ar}$-Li-O$_{Ar}$ (four-member ring)	95.3(2)	95.3(2)	94.6(2)	94.5(2)	94.6(4)	98.9(5)
		94.7(2)	94.6(2)	94.8(2)	95.8(2)	98.6(5)	94.0(4)
		95.1(2)	94.2(2)	96.6(2)	96.6(2)	95.0(4)	95.9(4)
	C-C$_{methylene}$-C	113.6(3)	113.1(3)	113.6(3)	112.9(3)	113.3(4)	113.2(5)
		113.7(3)		113.4(3)		112.7(4)	

2-2-5. References

(1) (a) MacDougall, D. J.; Morris, J. J.; Noll, B. C.; Henderson, K. W. *Chem. Commun.* **2005**, 456-458. (b) Stanciu, C.; Olmstead, M. M.; Phillips, A. D.; Stender, M.; Power, P. P. *Eur. J. Inorg. Chem.* **2003**, 3495-3500. (c) Kosugi, Y.; Rahim, Md. A.; Takahashi, K.; Imaoka, Y.; Kitayama, M.; *Appl. Organomet. Chem.* **2000**, *14*, 841-843. (d) Cole, M. L.; Junk, P. C.; Proctor, K. M.; Scott, J. L.; Strauss, C. R. *Dalton Trans.* **2006**, 3338-3349.

(2) (a) Jackman, L. M.; Chen, X. *J. Am. Chem. Soc.* **1997**, *119*, 8681-8684. (b) Jackman, L. M.; Petrei, M. M.; Smith, B. D. *J. Am. Chem. Soc.* **1991**, *113*, 3451-3458.

(3) For selected study in solid state, see: (a) MacDougall, D. J.; Noll, B. C.; Kennedy, A. R.; Henderson, K. W. *Dalton, Trans.* **2006**, 1875-1884 and references cited therein. (b) Boyle, T. J.; Pedrotty, D. M.; Alam, T. M.; Vick, S. C.; Rodriguez, M. A. *Inorg. Chem.* **2000**, *39*, 5133-5146.

(4) For selected study in solution state, see: (a) Vries, T. S. D.; Goswami, A.; Liou, L. R.; Gruver, J. M.; Jayne, E.; Collum, D. B. *J. Am. Chem. Soc.* **2009**, *131*, 13142–13154. (b) Jackman, L. M.; Chen, X. *J. Am. Chem. Soc.* **1992**, *114*, 403-411. (c) Jackman, L. M.; Rackiewicz, E. F.; Bensei, A. J. *J. Am. Chem. Soc.* **1991**, *113*, 4101-4109. (d) Jackman, L. M.; Rackiewicz, E. F. *J. Am. Chem. Soc.* **1991**, *113*, 1202-1210. (e) Jackman, L. M.; Smith, B. D. *J. Am. Chem. Soc.* **1988**, *110*, 3829-3835. (f) Jackman, L. M.; Scarmoutzos, L. M.; DeBrosse, C. W. *J. Am. Chem. Soc.* **1987**, *109*, 5355-5361. (g) Jackman, L. M.; DeBrosse, C. W. *J. Am. Chem. Soc.* **1983**, *105*, 4177-4184.

(5) X-ray analysis of dimer: (a) Fernandez, I.; Price, R. D.; Bolton, P. D.; Mahon, M. F.; Davidson, M. G.; López-Ortiz, F. *J. Organomet. Chem.* **2004**, *689*, 1890. (b) Clegg, W.; Lamb, E.; Liddle, S. T.; Snaith, R.; Wheatley, A. E. H. *J. Organomet. Chem.* **1999**, *573*, 305. (c) Matilainen, L.; Klinga, M.; Leskelä, M.; *Polyhedron*, **1995**, *14*, 635. (d) Kociok-Köhn, G.; Pickardt, J.; Schumann, H. *Acta Crystallogr., Sect C: Cryst. Struct. Commun.*, **1991**, *47*, 2649.

(6) X-ray analysis of trimer: (a) Vilardo, J. S.; Fanwick, P. E.; Rothwell, I. P. *Polyhedron* **1998**, *17*, 769-771. (b) van der Schaaf, P. A.; Hogerheide, M. P.; Grove, D. M.; Spek, A. L.; van Koten, G. *J. Chem. Soc., Chem. Comm.* **1992**, 1703-1705.

(7) X-ray analysis of tetramer: (a) Rosen, T. C.; Kirschbaum, K.; Giolando, D. M. *Inorg. Chim. Acta,* **2005**, *358*, 3680. (b) Tombul, M.; Errington, R. J.; Coxall, R. A.; Clegg, W. *Acta Crystallogr., Sect. E: Struct. Reports Online,* **2003**, *59*, m137-m139. (c) Thiele, K.; Gorls, H.; Seidel, W. *Z. Anorg. Allg. Chem.,* **1998**, *624*, 1391-1392. (d) Walther, D.; Ritter, U.; Gessler, S.; Seiler, J. *Z. Anorg. Allg. Chem.,* **1994**, *620*, 101-106.

(8) Crystallographic data of hexameric lithium phenolate was reported. However, in the solution state, the overwhelming predominant aggregate of lithium phenolate was the tetramer. Jackman, L. M.; Çizmeciyan, D.; Williard, P. G.; Nichols, M. A. *J. Am. Chem. Soc.* **1993**, *115*, 6262-6267.

(9) In the use of specific phenolic ligand, isolation of stable hexameric lithium phenolates is reported with intramolecular coordination of pyridinic nitrogen to lithium center. (a) Begley, W. J.; Rajeswaran, M. *Acta Cryst.* **2006**, *E62*, m1200-m1202. (b) Rajeswaran, M.; Begley, W. J.; Olson, L. P.; Huo, S. *Polyhedron* **2007**, *26*, 3653-3660.

(10) (a) Yasuda, M.; Yoshioka, S.; Yamasaki, S.; Somyo, T.; Chiba, K.; Baba, A. *Org. Lett.* **2006**, *8*, 761-764. (b) Yasuda, M.; Yoshioka, S.; Nakajima, H.; Chiba, K.; Baba, A. *Org. Lett.* **2008**, *10*, 929-932. (c) Nakajima, H.; Yasuda, M.; Chiba, K.; Baba, A. *Chem. Commun.* **2010**, *46*, 4794-4796. (d) Yasuda, M.; Nakajima, H.; Takeda, R.; Yoshioka, S.; Yamasaki, S.; Chiba, K.; Baba, A. *Chem. Eur. J.* **2011**, *17*, 3856-3867.

(11) The phenolates $(1Li_3)_2 \cdot (THF)_6$ were not decomposed even at 110 °C in toluene.

(12) Schaschchel, E.; Day, M. C. *J. Am. Chem. Soc.* **1968**, *90*, 503-504.

(13) Shobotake, K.; Nakamoto, K. *Inorg. Chim. Acta,* **1970**, *4*, 485-487.

(14) $\Delta = |\, \delta(^{13}C)_{ArOMe} - \delta(^{13}C)_{ArOLi}\, |$: three lithium cations (hexamer and tetramer), 6 ppm; two lithium cations (dimer and trimer), 12 ppm; one lithium cation (monomer), >15 ppm.

(15) **1a**: $\delta(^{13}C)_{ArOMe} = 121.24$, $\delta(^{13}C)_{ArOLi} = 115.19$; **1b**: $\delta(^{13}C)_{ArOMe} = 120.35$, $\delta(^{13}C)_{ArOLi} = 116.06$; **1c**: $\delta(^{13}C)_{ArOMe} = 120.29$, $\delta(^{13}C)_{ArOLi} = 115.62$; **1d**: $\delta(^{13}C)_{ArOMe} = 106.94$, $\delta(^{13}C)_{ArOLi} = 102.53$.

(16) Selected crystal date and structure refinement parameters are given in Experimental Section.

(17) The selected bond lengths and angles of the lithium phenolate $(1Li_3)_n \cdot (THF)_6$ are given in Experimental Section.

(18) Nishio, M.; Umezawa, Y.; Honda, K.; Tsuboyamad, S.; Suezawa, H. *CrystEngComm*, **2009**, *11*, 1757-1788.

(19) In the asymmetric unit of $(1dLi_3)_2 \cdot (THF)_6$, two crystallographycally-independent lithium phenolate·THF were observed. The structures of two lithium phenolates are almost same.

(20) Changing the solvent system for recrystallization gave $(1bLi_3)_2 \cdot (THF)_4$. Crystals of $(1bLi_3)_2 \cdot (THF)_4$ suitable for X-ray diffraction were grown from a mixture of benzene and hexane while the crystals of $(1a-dLi_3)_2 \cdot (THF)_6$ were grown from a mixture of dichloromethane and hexane. In the unit cell of $(1Li_3)_2 \cdot (THF)_4$, two benzene molecules were included along with $(1Li_3)_2 \cdot (THF)_4$.

Chapter 3

Stabilization of Excited State Using Through-Space Interaction between Independent π-Systems Mediated by a *peri*-Substituted Hydroxy Group in 1-Arylnaphthalenes: Unexpected Blue Emission of 1,3,5-Tris(*peri*-hydroxynaphthyl)benzene

3-1. Introduction

Control of photoluminescence wavelength is undoubtedly important for emitting materials. For this purpose, organic compounds are prepared based on π-conjugation systems with numerous types of structures and substituents. Conjugation in organic molecules can be designed employing synthetic chemistry, and various types of extended conjugation systems have been developed to bind independent conjugation systems through covalent bonds.[1] One of the most effective protocols is aryl–aryl coupling to expand π-systems.[2] Although a planar structure of π-systems could accomplish efficient conjugation, geometry around the aryl–aryl covalent bond usually does not show a planar structure, owing to the steric factor.[3] Deviation from the planar structure decreases the effectiveness of the extension of conjugation systems. It often causes limitations in designing conjugated molecules. In this context, a methodology to link different π-systems that cannot be placed in a planar sphere would supply new strategies to design emitting materials. We herein report a novel "through-space" protocol for stabilization of the excited state using a hydroxy group that mediates independent π-systems (Scheme 1). This "through-space" effect is more effective in the excited state than in the ground state, so a large Stokes shift is observed. Based on the proposed concept, an unexpected blue emission was realized by a tris(*peri*-hydroxynaphthyl)benzene system.

Scheme 1. Through-Space Interaction of a Biaryl Compound in the S_1 State.
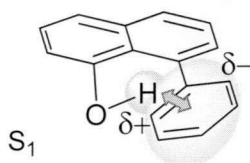
Stabilization by Electrostatic Attractive Force

3-2. Results and Discussion

Synthesis and Characterization of Tris(hydroxynaphthyl)benzenes and Their Derivatives: 1,3,5-Tris(8-hydroxy-1-naphthyl)benzene (**1**) was prepared from its methoxyprotected form **2**, which was formed by Suzuki-Miyaura coupling[4,5] between 1,3,5-tribromobenzene and the boric acid **A**,[6] as shown in Scheme 2. Regioisomers of **4** and **5**, bearing OH and OMe groups, respectively, on the *para*-positions, were also prepared in a similar manner using boric acid derivative **B**. NMR study was employed using tris(hydroxynaphthyl)benzenes in DMSO-d_6.[7] The ^{1}H NMR spectrum of **1** at room temperature (22 °C)

showed one conformer that had a conformationally rigid structure bearing two of three OH groups in naphthyl groups on above the plane of a central benzene ring, and another OH group placed below the plane (OH direction; up-up-down); two types of signals, corresponding to hydroxyl protons, were observed with a 2:1 integration ratio.[8] At a higher temperature (70 °C), OH moieties of compound **1** showed a single broad signal caused by fast equilibrium of the conformers. Compound **2**, with methoxy groups, showed a spectrum of mixtures of the two conformers (OMe direction; up-up-up and up-up-down) in a range from 160 °C to rt.[9] A broad signal caused by fast equilibrium was observed at 60 °C. On the other hand, *para*-isomers **4** and **5** showed only one set of signals in ¹H NMR because of fast equilibrium based on a facile aryl–aryl bond rotation, even at room temperature. These observations suggest that, compared with the *para*-form, the *peri*-substituent led to a higher energy barrier for aryl–aryl bond rotation, and the *peri*-OH-substituted compound **1** exists mainly as one conformer with an up-up-down form at room temperature.
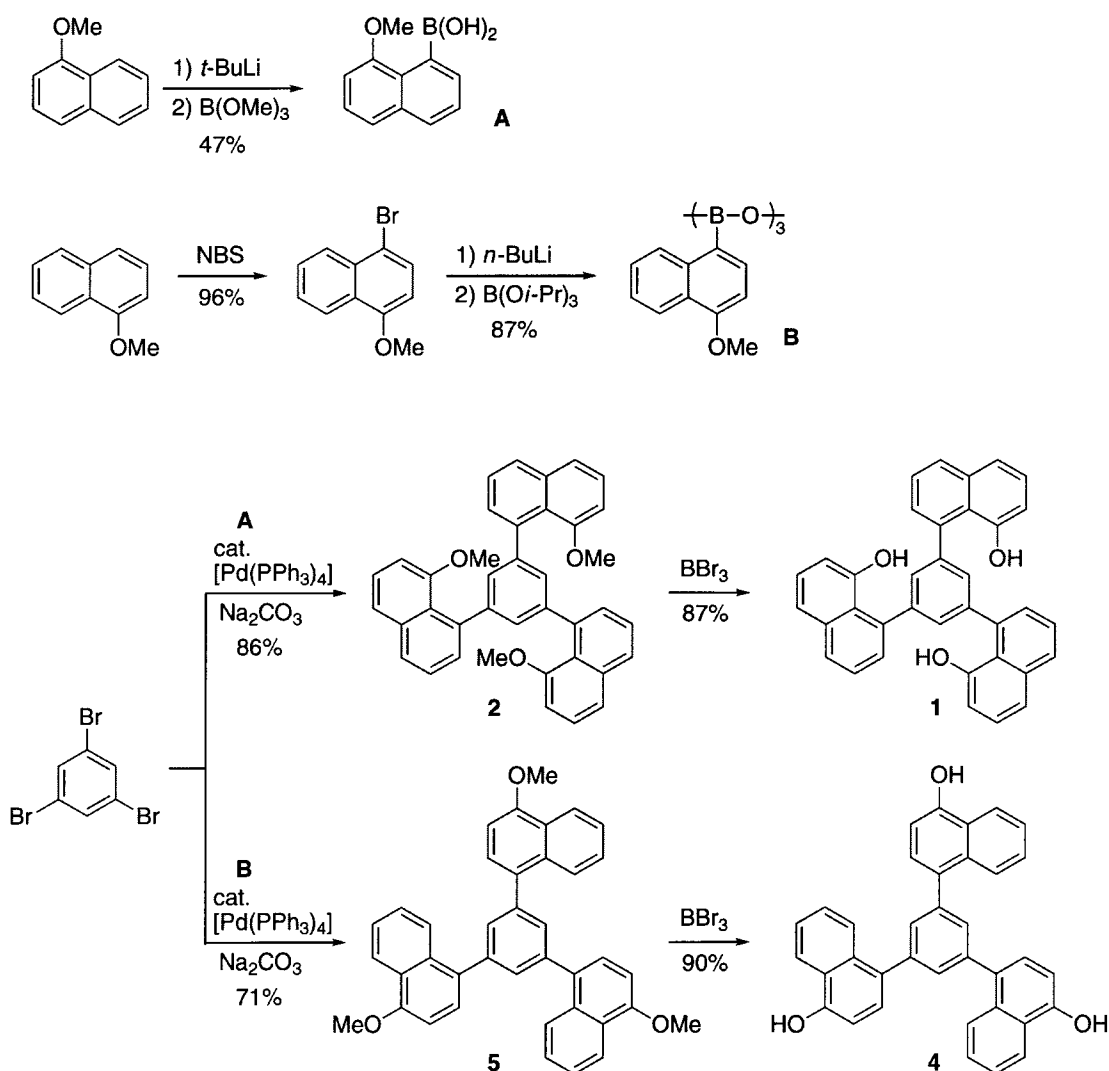
Scheme 2. Synthesis of Tris(hydroxynaphthyl)benzenes.

97

The solid-state structure of **1** was analyzed by X-ray crystallography, and the ORTEP drawing is shown in Figure 1. The structure showed an up-up-down conformation. Its geometry was the same in the solution state at room temperature, as observed by ^{1}H NMR measurement. The torsion angles between the central benzene ring and naphthyl groups on the same side were almost perpendicular (89.10° and 89.53°). The other naphthyl ring was at 69.21° to the central phenyl ring. No hydrogen bonding between two hydroxy groups was observed, either intra- or intermolecularly.[10] One of the OH groups was directed toward the bottom benzene ring, probably because of the interaction between protic hydrogen and the π-orbital of the central benzene.[11]
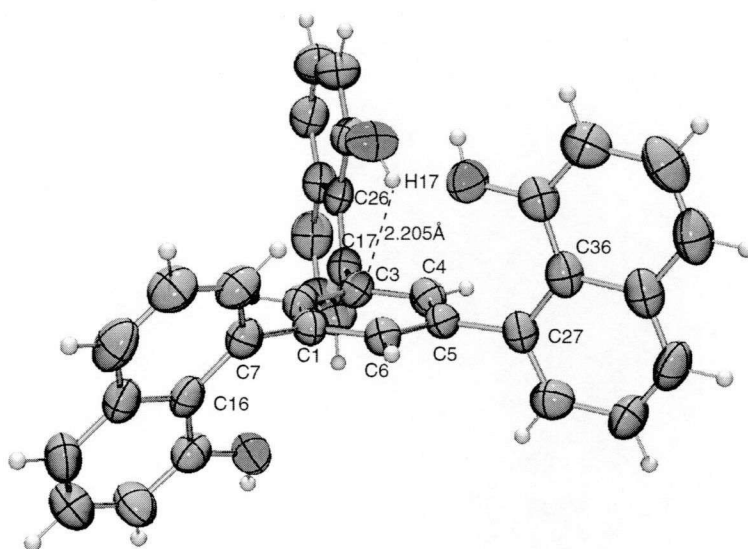
Figure 1. ORTEP Drawing of **1**. Selected Torsion Angles and Distance: C(6)-C(5)-C(27)-C(36) 89.10°, C(4)-C(3)-C(17)-C(26) 89.53°, C(6)-C(1)-C(7)-C(16) 69.21°, H(17)−C(3) 2.205 Å.

Photophysical Properties of Tris(hydroxynaphthyl)benzenes and Their Related Compounds: 1,3,5-Tri-1-naphthylbenzene (**3**), with an unsubstituted structural form, might have efficient conjugation relative to naphthalene between the three naphthyl groups and the central benzene moiety. However, the absorption maximum of **3** was observed at ca. 296 nm, which was only a small shift from simple naphthalene **8** (278 nm), because the structure could not be planar due to a steric hindrance.[3] Photophysical data of various types of trinaphthylbenzenes **1-5** and naphthalene derivatives **6-8** (Chart 1) are shown in Table 1, and electronic absorption spectra are shown in Figure 2. Since the shapes of spectra of examined molecules were similar, we discussed the photophysical properties by using absorption and emission maxima.[12] The OH-substituted compound **1** at the *peri*-positions had an absorption maximum of ca. 320 nm, which was bathochromically shifted compared with that of the unsubstituted **3** (Δ(**3**→**1**) = 24 nm). The *para*-OH-substituted compound **4**, which is an isomer of the *peri*-compound **1**, showed almost the same absorption maximum (ca. 316 nm) with that of **1**. In simple naphthalene framework, substitution by an OH group lead to a red shift (Δ(**8**→**6**) = 21 nm) with a value approximately equal to those of **1** and **4**. These results indicate that the OH group of **1** has no special effect on absorption.

Table 1. Photophysical Data of Trinaphthylbenzene Derivatives.

Compound	Absorption		Emission	
	λ_{max} [nm]	$\varepsilon/10^4$ [$M^{-1}cm^{-1}$]	λ_{max} (λ_{ex}) [nm]	Φ
1	320	2.69	446 (334)	0.01
2	307	2.70	382 (306)	0.04
3	296	3.91	360 (298)	0.22
4	316	2.77	392 (320)	0.01
5	309	3.93	376 (316)	0.18
6	299	0.579	366 (300)	0.07
7	295	0.717	340 (296)	0.38
8	278	0.608	336 (278)	0.31

Chart 1
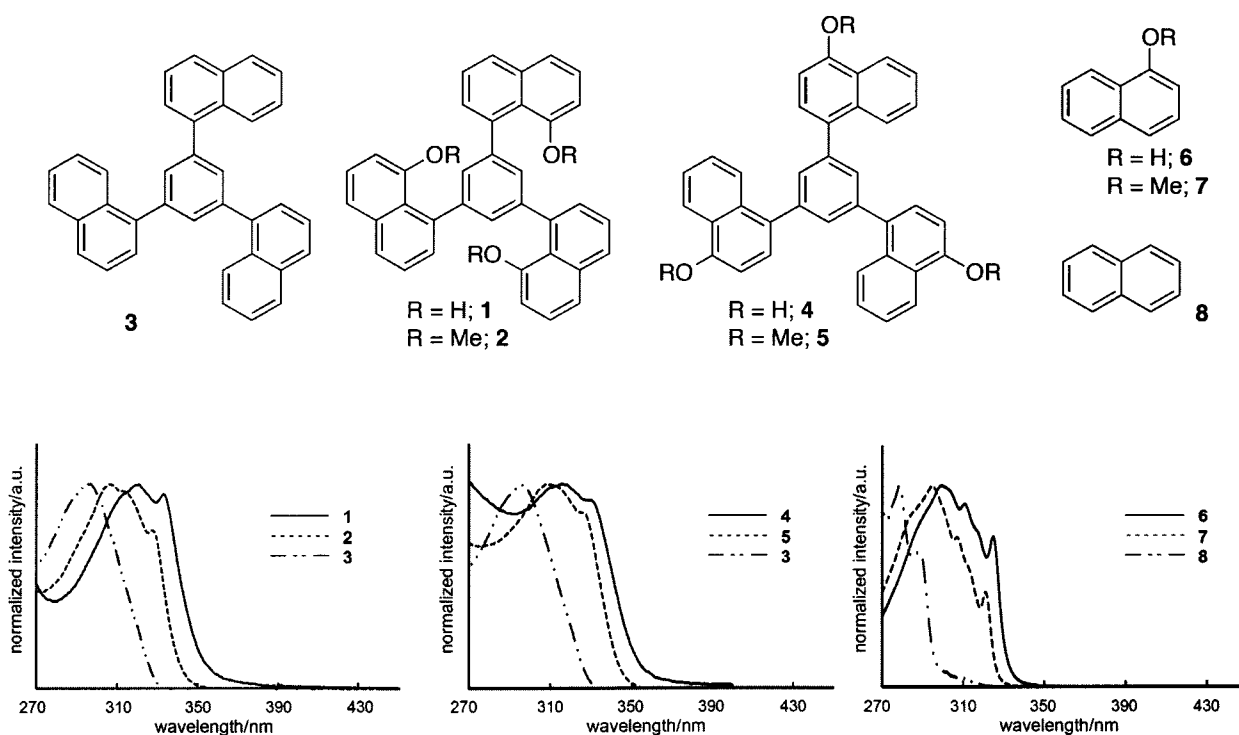
Figure 2. Absorption Spectra of **1-8** in DMSO.

The emission spectra and data for compounds **1-8** are shown in Figure 3 and Table 1. Surprisingly, compound **1** had a characteristic feature for emission, which was observed at around 446 nm, bathochromically shifted by 86 nm from that of unsubstituted compound **3**. As substitution by an OH group in a simple naphthalene system showed less shift (Δ(**8**→**6**) = 30 nm), the bathochromic shift in **1** was found to be derived from the extra factor based on its characteristic structure. The *para*-OH-substituted compound **4** showed less shift (Δ(**3**→**4**) = 32 nm), suggesting the position of the OH group is critical for the emitting properties of a trinaphthylbenzene system.[13] The observed effect of the OH group was larger on emission than absorption. The methoxy-substituted compound **2** also had a

relatively larger shift than the corresponding **5** and **7**, although the degree of the shift was not huge as compared to the hydroxy-substituted compound **1**. Therefore, the protic hydrogen appears to be critical in effectively extending the conjugation of the biaryl system.[14]
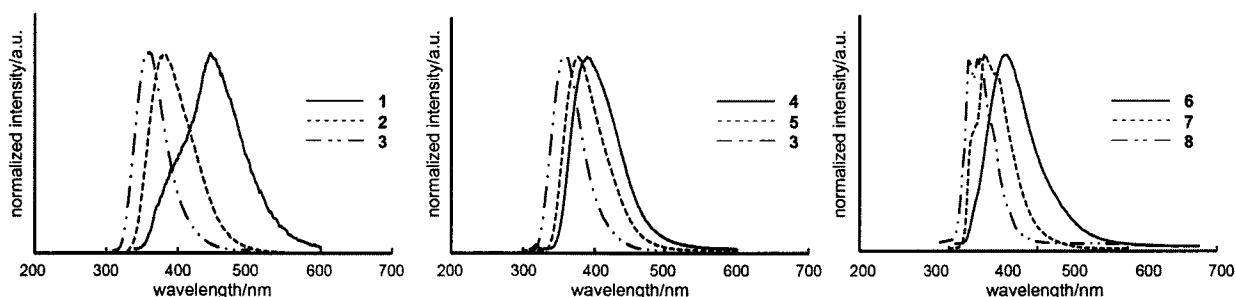
Figure 3. Emission Spectra of **1-8** in DMSO Excited at 334nm for **1**, 306 nm for **2**, 298 nm for **3**, 320 nm for **4**, 316 nm for **5**, 300 nm for **6**, 296 nm for **7**, and 278 nm for **8**.

Mono(hydroxynaphthyl)benzene: To simplify the discussion of photophysical properties of the trisubstituted benzene **1**, single naphthyl-substituted benzenes **9-13** were examined. The *peri*-OH, or OMe-substituted compounds **9** and **10**, and the *para*-substituted compounds **12** and **13** were prepared by arylation of 1-naphthol[15] or by the Suzuki-Miyaura coupling reaction.[4,5] Compounds **9-13** were investigated by UV-vis absorption and emission spectroscopy (Table 2 and Figure 4).[16] The *peri*-OH-substituted naphthylbenzene **9** showed emission maximum at a much longer wavelength (422 nm) than the parent unsubstituted compound **11** (352 nm), and significant bathochromic shift of emission from **11** (Δ(**11**→**9**) = 70 nm). However, the *para*-OH-substituted compound **12** showed a normal emission wavelength (386 nm) because the shift (Δ(**11**→**12**) = 34 nm) was almost the same value as that of **6** from **8** (Δ(**8**→**6**) = 30 nm). These results mean that the singly-substituted compound can be used to clarify the mechanism of the "abnormal" photophysical properties of the *peri*-OH-substituted biaryl system.

Table 2. Photophysical Data of Mononaphthylbenzene Derivatives.

Compound	Absorption		Emission	
	λ_{max} [nm]	$\varepsilon/10^4$ [M^{-1}cm^{-1}]	λ_{max} (λ_{ex}) [nm]	Φ
9	331	1.79	422 (312)	0.01
10	303	0.83	382 (304)	0.05
11	291	1.09	352 (294)	0.23
12	317	1.29	386 (316)	0.09
13	301	1.37	374 (308)	0.16
6	299	0.579	366 (300)	0.07
7	295	0.717	340 (296)	0.38
8	278	0.608	336 (278)	0.31

Compound	R^1	R^2
9	OH	H
10	OMe	H
11	H	H
12	H	OH
13	H	OMe

Compound	R^3
6	OH
7	OMe
8	H
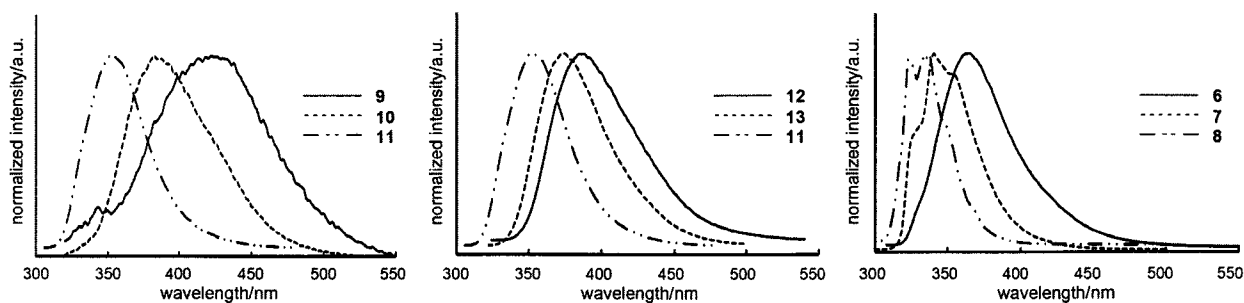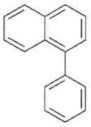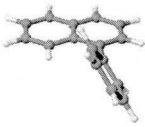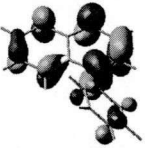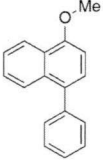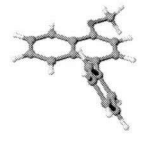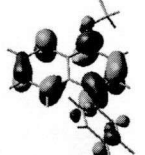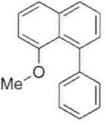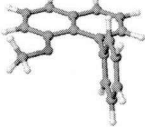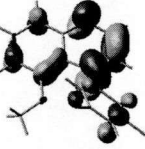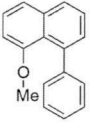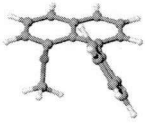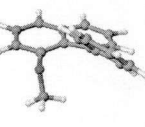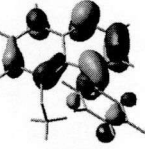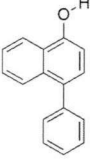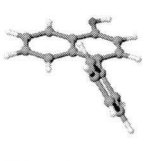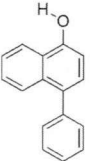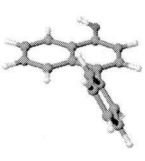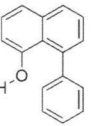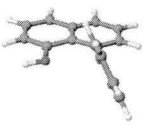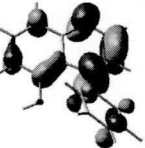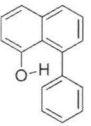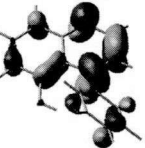
Figure 4. Emission Spectra of **6-13** in DMSO Excited at 312 nm for **9**, 304 nm for **10**, 294 nm for **11**, 316 nm for **12**, 308 nm for **13**, 300 nm for **6**, 296 nm for **7**, and 278 nm for **8**.

Theoretical Calculations: Compounds **9-13** were theoretically investigated to understand the origin of the unexpected bathochromic shift of the *peri*-OH- or *peri*-OMe-substituted compounds **9** and **10**. The calculated optimized structures of the ground states (S_0) and the excited states (S_1) are shown in Table 3. MO diagrams of the higher singly occupied MOs (SOMOs) in the S_1 states, which correspond to LUMOs in the S_0 state, are included. We will focus on the substituent dependencies of emission wavelengths from the S_1 state. The calculation for *para*-OH-substituted compound **12** gave two stable conformers, **12-R** and **12-L**, in which the OH bonds point in different directions, as shown in Table 3.[17] The **12-R** form was more stable than the **12-L** form (E(L) − E(R) = 1.75 kcal mol^{-1}) at the S_0 state, probably because there was less steric hindrance between *ana*-hydrogen and the OH group in **12-R**. The more stable species in the *peri*-OMe-substituted compound **10** was also the R-type (E(L) − E(R) = 2.20 kcal mol^{-1}), due to a lower steric hindrance between OMe and the phenyl group. On the other hand, in the case of the *peri*-OH-substituted compound **9**, the L-type was more stable than the R-type (E(L) − E(R) = 12.94 kcal mol^{-1}) despite its larger steric hindrance.[18] The electric interaction of OH with the phenyl group would prefer the structure of **9-L**, and the details are discussed later. Also in the S_1 state, **9-L** was much more stable than **9-R** (E(L) − E(R) = 18.28 kcal mol^{-1}). These results suggest that the *peri*-OH group controls the excited state more efficiently than the ground state.[20]

In all S_0 states, the dihedral angles between the naphthyl and phenyl rings were close to perpendicular (56.4−92.4°), while in the S_1 states, the angles became smaller, and the biaryl framework approached a planar shape (25.7−35.9°).[21] This is because the double-bond character of the C−C bond between naphthyl and phenyl is strengthened by the HOMO→LUMO excitation. In fact, an in-phase orbital interaction can be seen in the C−C bonds at higher SOMOs in S_1 states, but not in HOMOs at S_0 states (Table 3 and Experimental Section). The distances between *peri*-carbon in the naphthyl group and *ortho*-carbon in the phenyl group ($C_{Naph-peri}$-$C_{Ph-ortho}$) in S_1 states were shorter than the corresponding distances in S_0 states.[22] The structural change to planar in the S_1 state led to a large Stokes shift. The unsubstituted compound **11** and the *para*-OMe-substituted compound **13** had almost the same structures in S_0 and S_1 states, and the calculated Stokes shifts showed almost the same values (60 and 61 nm, respectively).[23] On the other hand, a larger Stokes shift for *peri*-OMe-substituted compound **10** was theoretically estimated (86 nm)[24] than those for **11** and **13**. It was noted that *peri*-OMe-substituted

101

Table 3. Calculated Results of the S_0min and S_1min Structures and Higher SOMOs of the S_1 State for **9-13**.

Compound	S_0		S_1		MO diagram of higher SOMO at S_1	Higher SOMO energies of the S_1 state/eV
	Optimized structure	Dihedral angle of biaryl/°	Optimized structure	Dihedral angle of biaryl/°		
11		57.2		32.5		1.84
13		56.4		32.8		2.13
10-R		92.4		25.7		1.85
	$\Delta E(\text{L} - \text{R})$ $= 2.20\,\text{kcal mol}^{-1}$		$\Delta E(\text{L} - \text{R})$ $= 2.97\,\text{kcal mol}^{-1}$			
10-L		61.9		25.8		1.71
12-R		56.6		33.4		2.07
	$\Delta E(\text{L} - \text{R})$ $= 1.75\,\text{kcal mol}^{-1}$		$\Delta E(\text{L} - \text{R})$ $= 1.19\,\text{kcal mol}^{-1}$			
12-L		57.1		35.9		1.91
9-R		66.7		27.8		1.82
	$\Delta E(\text{L} - \text{R})$ $= -2.94\,\text{kcal mol}^{-1}$		$\Delta E(\text{L} - \text{R})$ $= -8.28\,\text{kcal mol}^{-1}$			
9-L		91.7		31.9		1.67

compounds **10-R** and **10-L** in S_1 states showed a more planar structure (dihedral angles between naphthyl and phenyl groups of 25.7° and 25.8°, respectively) than that of *para*-OMe-substituted compound **13** (32.8°). To avoid the steric repulsion between the *peri*-substituent and the phenyl group, the aryl−aryl

102

bond rises from the naphthyl plane. That structural change can decrease the dihedral angle and bring the two aryl planes close to planar. In the case of *peri*-OH-substituted **9**, the R-type compound had a small dihedral angle (27.8°), while **9-L** showed a larger angle (31.9°) because OH was directed to the phenyl ring. Even in this case, the dihedral angle was less than that of either unsubstituted compound **11** (32.5°) or **12** (R; 33.4°, L; 35.9°). The higher SOMOs in the S_1 states were interesting, showing that *peri*-OH- or *peri*-OMe-substituted compounds **9** and **10** had efficient populations on the phenyl rings as compared to those on the phenyl moiety in unsubstituted compound **11** and *para*-substituted species **12** and **13** (Table 3). Compounds **9** and **10** thus had significant conjugation extended through the biaryl system in S_1 states. The lower orbital energies of the higher SOMO in **10** (**10-R**; 1.85 eV, **10-L**; 1.71 eV) in S_1 states were also confirmed, as compared to the *para*-OMe species **13** (2.13 eV). As a result of changes in the positions or directions of OH or OMe substituents, the variations of lower SOMO energies in the S_1 state, which correspond to HOMO energies in the S_0 state, are smaller than those of higher SOMO energies (see Experimental Section). Thus the stabilization of higher SOMOs is ascribed to a bathochromic shift of the emissions. Efficient conjugation is promoted by the planarity of the structure in **10** as compared to **13**. In addition, in OH-substituted compounds **9** and **12**, the higher SOMO energies of *peri*-OH-form **9** were lower than those of *para*-OH-form **12**. Interestingly, conformer **9-L** had much lower orbital energy (1.67 eV) than **9-R** (1.82 eV), despite the large dihedral angle of **9-L**. This effect is not fully explained by planarity, and thus the through-space interaction between naphthyl and phenyl moieties mediated by the OH group would be important. In the *peri*-OH compound **9**, the L-type, which has a lower orbital energy, was a dominant conformer, hence, the origin of the stability of **9-L** was next investigated by using the relationship between structure and atomic charge.

The charges of the H of OH, phenyl-ring, and naphthyl-ring calculated from the natural atomic orbital (NAO) charges in the S_0 and S_1 states of naphthol **6-R**, *peri*-substituted **9-L**, and *para*-substituted **12-R**, which are more stable conformers, are shown in Table 4.[25] The unsubstituted phenylnaphthalene and the conformation isomer of the main compound **9-L** (**11** and **9-R**) are also included in Table 4. In **9-L**, the positive charge was localized at the naphthyl ring and the hydroxy proton, and the negative charge was localized at the phenyl ring. The charge-separated state in **9-L** was more highly polarized in the S_1 state than in the S_0 state, so the focus was on the charges in the S_1 states to compare the compounds.

Next, the NAO charges of **6-R**, **9-L**, and **11** in the S_1 states were compared to investigate how the phenyl group and hydroxy group affect the charge-separated state. One of the large differences among them was the charge at the naphthyl ring {**6-R**; neutral (S_1; −0.003), **9-L**; positive (S_1; 0.283), and **11**; negative (S_1; −0.231)}. In **6-R**, the positive charge of the hydroxy proton was smaller than that in **9-L**. In **11**, the charge of the phenyl ring was almost neutral, while **9-L** had a negative charge at the phenyl ring. The presence of both the phenyl group and the hydroxy group played an important role in creating a more highly polarized charge-separated state in **9-L**.

We examined the importance of the substituting position of the hydroxy group by comparing the compounds *peri*-form **9-L** and *para*-form **12-R**. In the S_1 state, although the charges at the naphthyl ring were equally positive in both **9-L** and **12-R**, the negative charge at the phenyl ring in **9-L** was about three

Table 4. Charges of the H for OH, Phenyl-Ring, and Naphthyl-Ring Calculated from the NAO Atomic Charges.[a]

Compound	State	R/L	H of OH	Ph	Naph
9	S_0	R	0.499	0.008	0.238
		L	0.523	-0.005	0.246
9	S_1	R	0.496	0.011	0.230
		L	0.520	-0.060	0.283
6	S_0	R	0.501	-	0.008
6	S_1	R	0.498	-	-0.003
11	S_0		-	0.001	-0.242
11	S_1		-	-0.005	-0.231
12	S_0	R	0.501	-0.003	0.259
12	S_1	R	0.498	-0.018	0.256

[a] The charge of Ph was defined as a sum of atomic charges on atoms of phenyl (C_6H_5) and that of Naph was done as a sum of atomic charges on atoms of $C_{10}H_6$ in naphthyl moiety.

9-R   9-L   6-R   11   12-R
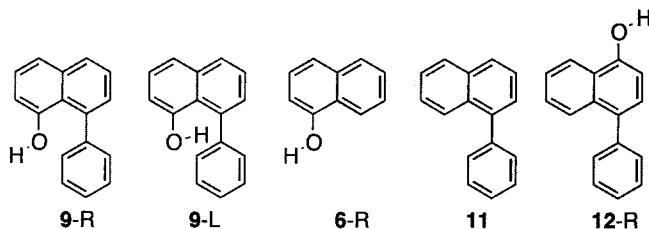
times higher than that in **12-R**. These results show that the hydroxyl group in the *peri*-position is an important factor in inducement of the negative charge at the phenyl ring.

To determine how the hydroxy group interacts with the phenyl group, we compared the NAO charges of **9-L** and **9-R**, with hydroxy protons that orient toward and away from the phenyl ring, respectively. The charge of the phenyl ring in **9-L** was negative while that in **9-R** was positive. This means that the hydroxy group electrostatically interacts with the phenyl group through the hydroxy proton directed to the phenyl ring. In fact, the positive charge of the hydroxy proton in **9-L** was larger than that in **9-R**. This electrostatic interaction contributes to lowering the higher SOMO energy (1.67 eV) in **9-L**, despite the steric hindrance between the hydroxy proton and the phenyl group.

The calculation data in Tables 3 and 4 reveal that the relationship between the phenyl group and the hydroxy group in the *peri*-position in the naphthyl ring generates electrostatic interaction, which is mediated by the hydroxy proton. This interaction leads to a highly polarized charge-separated state and increases planarity between phenyl and naphthyl rings, and could contribute to a large bathochromic shift for emission. Those factors could extend the conjugation of the biaryl system, especially in S_1 states.

Effect of Solvents on Mono(hydroxynaphthyl)benzene: The solvent effect on the emission of **9** and **12** is shown in Figure 5. Compound **9** gave an emission maximum at 386 nm in dichloromethane, and 422 nm in DMSO (λ_{em}(DMSO) – λ_{em}(CH$_2$Cl$_2$) = 36 nm). DMSO showed a bathochromic shift and

effectively stabilized the polarized S_1 state. In the case of **12**, less bathochromic shift was found in DMSO (λ_{em}; 386 nm in DMSO, 368 nm in CH_2Cl_2, λ_{em}(DMSO) – λ_{em}(CH_2Cl_2) = 18 nm), because less polarization was generated in **12** in the S_1 state. These results are consistent with the calculation results and suggest that the charged transient is a key factor for emission in this system. A similar solvent effect was observed in trisubstituted benzene **1**.[26] Compound **1** gave an emission maximum at 378 nm in dichloromethane, and 446 nm in DMSO. Polar solvent (DMSO) showed a bathochromic shift (λ_{em}(DMSO) – λ_{em}(CH_2Cl_2) = 68 nm). The *para*-OH-substituted **4** showed less bathochromic shift in DMSO (λ_{em}; 392 nm in DMSO, 374 nm in CH_2Cl_2, λ_{em}(DMSO) – λ_{em}(CH_2Cl_2) = 18 nm). This suggests that the highly polarized charge-separated state is generated in **1** as well as in **9**.
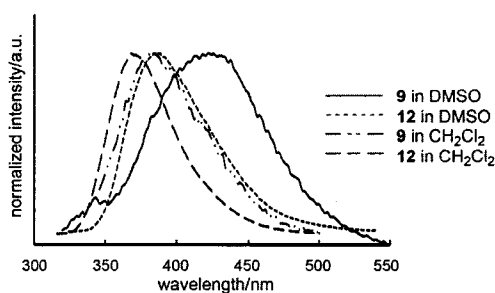
Figure 5. Solvent Effect on Emission Spectra of **9** and **12** Excited at 306 nm for **9** (CH_2Cl_2), 304 nm for **12** (CH_2Cl_2), 312 nm for **9** (DMSO), and 316 nm for **12** (DMSO).

The possibility that anion species of **1** and **9** are generated in DMSO solvent by photoirradiation is not able to be ruled out completely. More detailed discussion about this mechanism (fluorescence lifetime, transition probability, etc.) is an issue in the future. However, we thought this possibility is very low when the experiment of sodium salt of **1** and **9** in reference 14 is taken into consideration. Furthermore, the emitting spectra of **1** and **9** in CH_2Cl_2, in which anion species are not generated by photoirradiation, also showed the importance of the substituted position of OH group. Therefore, we thought that the interaction between hydroxy group and phenyl group at *peri*-position in 1-arylnaphthalene systems is important to their photophysical properties.

Various Tuning Factors in Through-Space Interaction: As the structure of naphthalene is easily modified by using coupling reactions, the through-space interaction between substituents at the *peri*-position provides the novel method to create emitting materials with various tuning factors. We investigated the two tuning factors (Figure 6); (a) the substituents R on phenyl group are able to control the electronic character of phenyl ring. (b) the hetero atoms X cause large change in the through-space interaction due to their different steric and electronic characters.
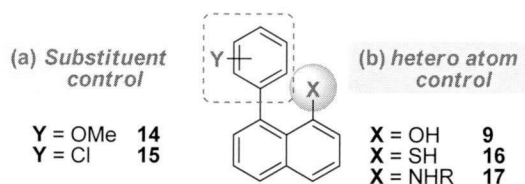
Figure 6. Various Tuning Factors in Through-Space Interaction.

The substituent effect of *peri*-OH-naphthylbenzene was investigated. We prepared methoxy- and chloro-substituted compounds **14** and **15**, respectively, as shown in Chart 2. While compound **9** was a liquid, the substituted derivatives **14** and **15** were solidified to give a crystal suitable for X-ray analyses. Their ORTEP drawings are shown in Figures 7 and 8. The torsion angles between the phenyl ring and the naphthyl plane were 84.36° for **14**, and 76.72° and 76.28° for **15**.[27] The OH groups on the naphthyl moiety were directed toward the phenyl ring, as predicted by theoretical calculation (Table 3). This can presumably be ascribed to an electronic interaction between the phenyl and the OH groups. The distances between the H and the *ipso*-carbon were 2.000 Å for **14** and 2.192 Å for **15**.

Chart 2

14
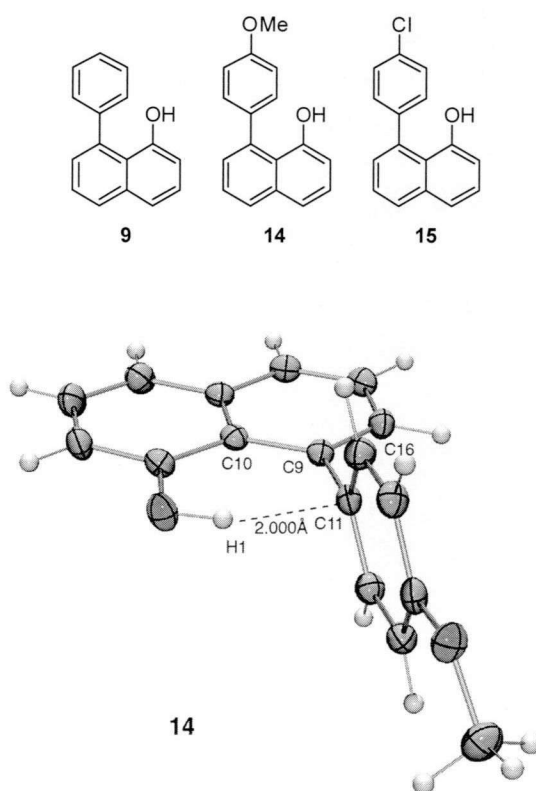
Figure 7. ORTEP Drawing of **14**. Selected Torsion Angle and Distance: C(10)-C(9)-C(11)-C(16) 84.36°, H(1)−C(11) 2.000 Å.
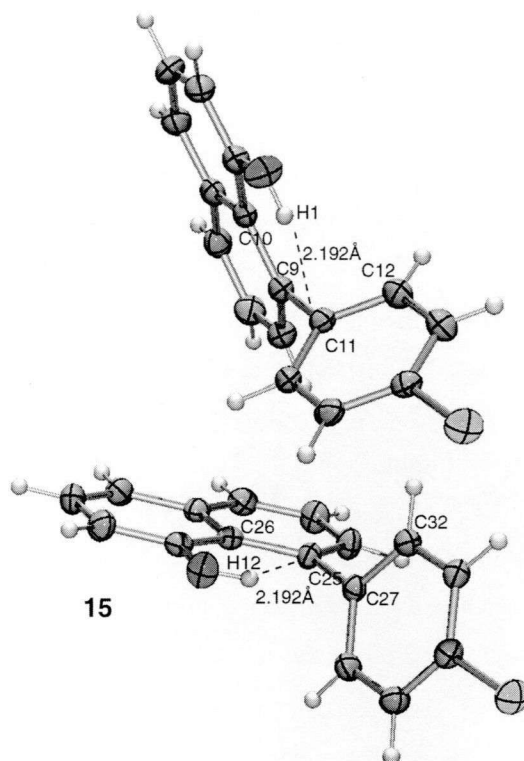
Figure 8. ORTEP Drawings of **15**. Selected Torsion Angles and Distances: C(10)-C(9)-C(11)-C(12) 76.72°, C(26)-C(25)-C(27)-C(32) 76.28°, H(1)−C(11) 2.192 Å, H(12)−C(27) 2.192 Å.

The OMe- and Cl-substituents on the phenyl ring of **9** affected the emission spectra in an interesting manner (Figure 9). The methoxy-substituted compound **14** showed emission (398 nm) at a shorter wavelength than the unsubstituted compound **9** (422 nm), although the methoxy group generally causes an emission at a longer wavelength. This result also supports the polarization mechanism in the *peri*-substituted 1-arylnaphthalene system. The methoxy group suppresses polarization with its electron-donating effect. The chloro-substituted compound **15** showed its emission maxima at a slightly longer wavelength (426 nm) than **9**, probably because of its electron-withdrawing characteristics.
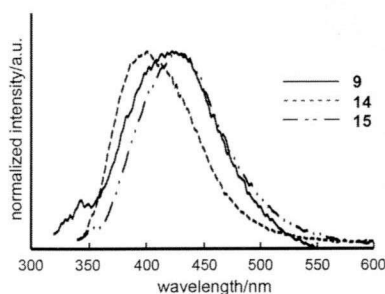
Figure 9. Emission Spectra of **9**, **14**, and **15** in DMSO Excited at 312 nm for **9**, 320 nm for **14**, and 320 nm for **15**.

The effect of the hetero atom (X) was examined. As a hetero atom, we chose sulfur atom, which has more acidic character and larger atom size, and nitrogen atom, which has more basic character, as

107

compared with oxygen atom. Furthermore, *N*-substituted derivatives have additional tuning factor (R) on their nitrogen atom as a substituent, which is useful for precise control of emitting wavelength.

To investigate the effect of a sulfur atom and a nitrogen atom, we synthesized a series of derivatives of **1** (Scheme 3). The SH- and NHR- substituted phenylnaphthalenes **16** and **17** were prepared in three steps. The compound **9** was converted to the corresponding trifluoromethanesulfonate **C** (Scheme 3a). The palladium catalyzed reaction of triflates **C** with triisopropylsilanethiol provided the SH-substituted pheylnaphthalene **16** (Scheme 3b).[32] Next, we carried out a palladium-catalyzed amination of aryl triflate **C** under the condition (Pd(OAc)$_2$/BINAP (2 mol% Pd) and NaOtBu (1.4 eq) in toluene at 80 °C) reported by Buchwald.[29] However, this method gave no desired product **17a-d** and only phenol compound **9** resulting from attack at the electrophilic sulfur center by sodium *tert*-butoxide. To prevent the cleavage of the triflate moiety, we investigated the base-free condition by using metal amide and found that the reaction of triflate **C** with lithium amide employing a solution of Pd(dba)$_2$/BINAP (2 mol% Pd) in dioxane at 100 °C gave the desired compounds **17a-d** (Scheme 3c).

Scheme 3. Synthetic Route 1-Phenylnaphthalene Compounds Bearing Hetero Atoms at *peri*-Position.
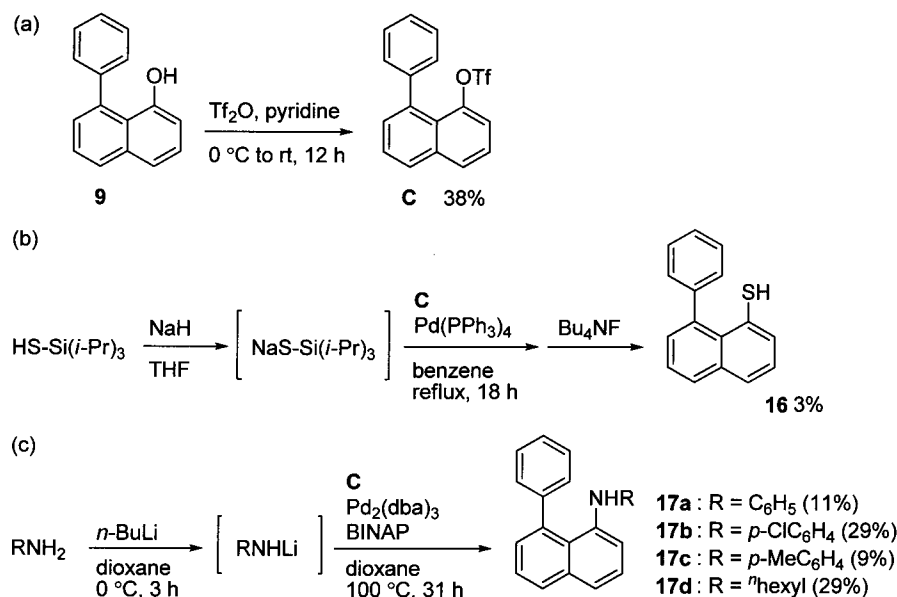
The *peri*-heteroatom-substituted phenylnaphthalene **9**, **16**, and **17a** were investigated by UV/vis absorption and emission spectroscopies. The emission spectra of **9**, **16**, and **17a** were shown in Figure 10. As compared to emission maximum of **9** (422 nm), the *peri*-SH-substituted compound **16** showed an emission at a shorter wavelength (354 nm), while the *peri*-NHPh-substituted compound **17a** led to an emission at a longer wavelength (468 nm). These data suggest that the hetero atoms played an important role in controlling the emitting properties in the through-space system.
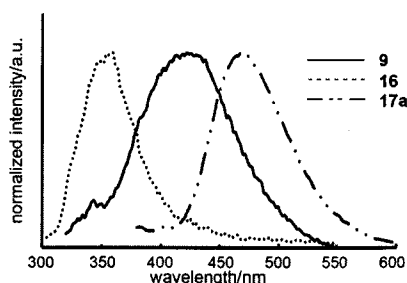
Figure 10. Emission Spectra of **9**, **16**, and **17a** in DMSO Excited at 312 nm for **9**, 292 nm for **16**, and 360 nm for **17**.

The photophysical properties of **16**, **17a-d** are summarized in Table 5. The emission maximum of the *peri*-SH-substituted phenylnaphthalene **16** (354 nm) was almost same with that of the parent unsubstituted compound **11** (352 nm), while the absorption maximum of **16** (314 nm) was bathochromically shifted from that of **11** (291 nm). The large size of sulfur atom probably prevented the biaryl framework from approaching a planar shape in the excited state (Figure 11a). According to these results, the size of hetero atom is critical for the through-space interaction and a plannar shape of the biaryl framework in excited state play an important role in efficient interaction between phenyl group and *peri*-hetero atom in naphthalene. The *peri*-NHPh-substituted phenylnaphthalene **17a** had characteristic feature for emission, which was observed at 468 nm, bathochromically shifted by 116 nm from that of **11**, while the absorption wevelength was bathochromically shifted only by 55 nm. Amino group of **17a** causes more bathochromic shift of emission wavelength than that of absorption wavelength. These results suggest that the polarized charge-separated state was generated in excited state by the through-space interaction between the *peri*-substituted NHPh group and the phenyl group in the similar manner with **9** as shown in Figure 11b.

Table 5. Photophysical Data of 1-Phenylnaphthalene Compounds Bearing Hetero Atoms at *peri*-Position.

Compound	Absorption		Emission	
	λ_{max} [nm]	$\varepsilon/10^4$ [M^{-1}cm^{-1}]	$\lambda_{max}(\lambda_{ex})$ [nm]	Φ
16	314	0.79	354(292)	0.02
17a	346	0.09	468(360)	0.06
17b	362	0.04	464(362)	0.15
17c	355	0.08	490(364)	0.04
17d	349	0.89	488(352)	0.15

17a R = Ph
17b R = *p*-ClPh
17c R = *p*-MePh
17d R = ^{n}hex
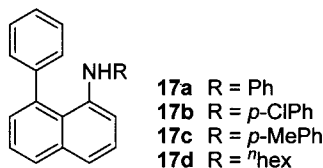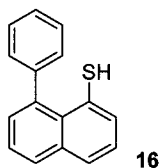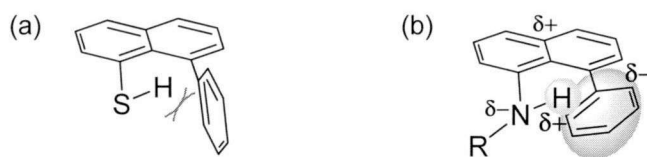
Figure 11. The Plausible Structure of **16** and **17** in Excited State.

Next, we investigated the effect of the substituents on N atom by using **17a-d**. The compound **17b**, which has electron-withdrawing substituent on nitrogen atom, showed a shorter emission maximum than that of **17a** (Δ(**17a** → **17b**) = –4 nm). On the other hand, the electron-donating substituent in **17c** and **17d** led to longer emission maximum (Δ(**17a** → **17c**) = 26 nm, Δ(**17a** → **17d**) = 24 nm, respectively). The substituents on a nitrogen atom are able to give a new tuning factor to the through-space interaction.

3-3. Conclusion

A *peri*-OH-substituted 1-arylnaphthalene system showed characteristic photophysical properties, particularly on emission. The conjugation of biaryl systems was effectively enhanced by the hydroxy group at the *peri*-position in the excited state. The hydrogen on the *peri*-OH group interacted with the phenyl ring on naphthalene and induced polarity in the molecule, while the methoxy substituent was not directed to the phenyl ring due to its steric hindrance. Compared with the lower SOMO energy, the higher SOMO energy was relatively lowered by a polarized transient structure, and thus a bathochromic shift was observed. The *peri*-position of the OH-substituent was critical for the emission wavelength, while the *para*-substituted compound did not show this property. 1,3,5-Tris(*peri*-hydroxynaphthyl)benzene (**1**) gave an interesting blue emission and significant bathochromic shifts were observed in the emission spectra. In the compounds **1** and **9**, the substituted position of OH was quite critical because the hydroxy group mediated the different π-systems by through-space interaction to stabilize the excited state.

3-4. Experimental Section

General Procedures. IR spectra were recorded as thin films or as solids in KBr pellets. ^{1}H and ^{13}C NMR spectra were obtained with a 400 and 100 MHz spectrometer, respectively, with TMS as an internal standard. UV-vis spectra and emission spectra were obtained at room temperature using 0.01 mM in DMSO unless otherwise specified. Absorption spectra of naphthalene derivatives **6-8** were obtained using 0.2 mM in DMSO.

Materials. 1-Hydroxynaphthalene **6**, 1-methoxynaphthalene **7**, naphthalene **8**, 1-phenylnaphthalene **11**, 1,3,5-tribromobenzene, bromobenzene, aniline, *p*-chloroaniline, *p*-methylaniline, hexylamine, BINAP, *n*-BuLi (1.6 M in hexane), Pd(dba)$_2$, Pd(PPh$_3$)$_4$, B(OMe)$_3$, and BBr$_3$ were commercially available. 8-Methoxy-1-naphthylboronic acid **A**,[6] 1-bromo-4-methoxynaphthalene,[30] and 5-methoxy-1-naphthol[31] were prepared by known methods. 1,3,5-Tri-1-naphthylbenzene **3**,[32] 8-phenyl-1-naphthol **9**,[15] and 4-phenyl-1-naphthol

110

12[33] were prepared by Suzuki-Miyaura coupling reaction[5] and their spectra were exactly matched to the reported data. Other compounds were prepared as shown below.

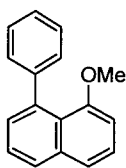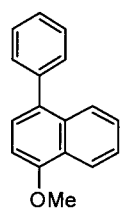## 1,3,5-Tris(8-methoxy-1-naphthyl)benzene (2)
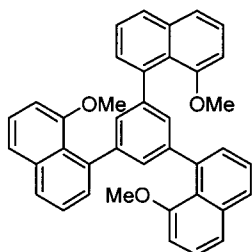
To a suspension of 8-methoxy-1-naphthylboronic acid (16.5 mmol) in toluene (15 mL), EtOH (25 mL), water (15 mL) and Na_2CO_3 (25 mmol) were added and the mixture was stirred for 1 h at room temperature. Then, the mixture was added to a solution of 1,3,5-tribromobenzene (5.0 mmol) and $Pd(PPh_3)_4$ (0.5 mmol) in toluene (10 mL) and stirred for 24 h at 90 °C.[5] The mixture was cooled to 0 °C and water (30 mL) was added. The mixture was extracted with ethyl acetate (3 x 30 mL). The combined organic layer was dried over $MgSO_4$ and evaporated. The residue was purified by column chromatography (hexane/EtOAc, 50:50) and recrystallization (hexane) to give the product as a white solid (2.34 g, 86%). mp: 155-158 °C; IR: (neat) 1577, 1269 cm^{-1}; ^{1}H NMR: (600 MHz, $CDCl_3$, 60 °C) (2-A-2-B fast equilibrium) 7.75 (m, 3H), 7.50-7.40 (m, 6H), 7.45 (t, J = 8.4 Hz, 3H), 7.35 (t, J = 7.8 Hz, 3H), 7.30 (s, 3H), 6.79 (d, J = 7.8 Hz, 3H), 3.65 (s, 9H); ^{13}C NMR: (150 MHz, $CDCl_3$, 60 °C) 157.3, 142.2, 140.1, 136.2, 129.7, 127.5, 127.3, 125.8, 125.5, 124.1, 121.4, 106.5, 55.2. ^{1}H NMR: (400 MHz, $CDCl_3$, 20 °C) (mixture of 2-A and 2-B) 7.78 (d, J = 9.0 Hz), 7.60-7.28 (m), 6.87-6.70 (m), 3.70 (s), 3.67 (s), 3.58 (s); ^{13}C NMR: (100 MHz, $CDCl_3$, 20 °C) 157.0, 156.8, 142.1, 141.8, 141.5, 139.8, 135.9, 129.7, 128.9, 127.7, 127.4, 127.2, 126.6, 125.8, 125.6, 125.4, 125.2, 123.7, 123.5, 121.1, 106.0, 105.9, 105.8, 55.3, 55.0, 54.4. ^{1}H NMR: (600 MHz, $CDCl_3$, -60 °C) (2-A: 2-B = ca. 1:1) 7.84 (m), 7.58-7.34 (m), 6.85 (d, J = 7.8 Hz), 6.83 (d, J = 7.8 Hz), 3.76 (s), 3.71 (s), 3.67 (s); ^{13}C NMR: (150 MHz, $CDCl_3$, -60 °C) 156.5, 156.2, 156.1, 141.6, 141.4, 141.2, 139.2, 135.42, 135.38, 135.32, 129.6, 129.4, 129.2, 127.6, 127.25, 127.21, 127.17, 127.11, 126.7, 125.80, 125.77, 125.74, 125.6, 125.4, 125.3, 122.78, 122.75, 122.67, 120.8, 120.7, 105.2, 105.0, 55.1, 54.7, 54.2; MS: (EI, 70 eV) m/z 546 (M$^+$, 100); HRMS: (EI, 70 eV) calcd for $C_{39}H_{30}O_3$ 546.2195 found m/z 546.2189 (M$^+$). Anal. Calcd for $C_{39}H_{30}O_3$: C, 85.69; H, 5.53. Found: C, 85.43; H, 5.59.

2-A   **2-B**
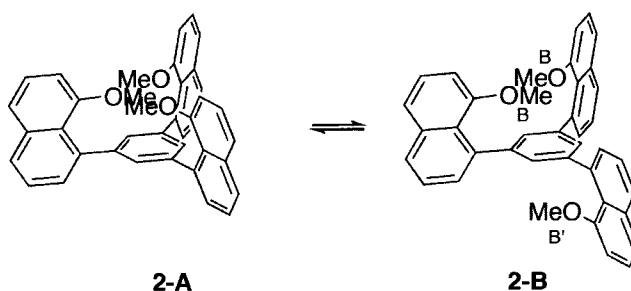
1,3,5-Tris(8-hydroxy-1-naphthyl)benzene (1)
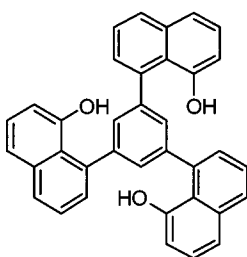
To a solution of 1,3,5-tris(8-methoxy-1-naphthyl)benzene (2.0 mmol) in CH_2Cl_2 (12 mL) was slowly added BBr_3 (1.0 M in CH_2Cl_2, 6.6 mL) at -78 °C. The mixture was stirred at -78 °C to rt for 8 h. The mixture was cooled to 0 °C and quenched by water. The mixture was extracted with ethyl acetate (3 x 10 mL). The combined organic layer was dried over $MgSO_4$ and evaporated. The residue was purified by flash column chromatography (hexane/EtOAc, 70:30) to give the product as a white solid (0.81 g, 81%).

Further, recrystallization from CH$_2$Cl$_2$/hexane afforded crystals suitable for X-ray structure analysis.[34] mp: 256-264 °C; IR: (KBr) 3510, 3432 (OH) cm^{-1}; ^{1}H NMR: (600 MHz, DMSO-d$_6$, 70 °C) 8.97 (brs, 3H), 7.81 (d, 3H, J = 7.8 Hz), 7.48 (t, 3H, J = 7.8 Hz), 7.41 (d, 3H, J = 7.8 Hz), 7.39 (d, 3H, J = 7.8 Hz), 7.32 (s, 3H) 7.31 (t, 3H, J = 7.8 Hz), 6.87 (d, 3H, J = 7.8 Hz); ^{13}C NMR: (150 MHz, DMSO-d$_6$, 70 °C) 153.9, 140.7, 138.3, 135.6, 128.3, 127.7, 127.2, 126.0, 124.6, 121.6, 119.1, 110.1. ^{1}H NMR: (600 MHz, DMSO-d$_6$, 22 °C) 9.66 (brs, 1H), 9.36 (brs, 2H), 7.81 (m, 3H), 7.48 (m, 3H), 7.44-7.35 (m, 6H), 7.31 (t, 3H, J = 7.8 Hz), 7.29 (s, 3H), 6.85 (brs, 3H); ^{13}C NMR: (150 MHz, DMSO-d$_6$, 22 °C) 154.3, 140.6, 139.0, 135.9, 128.9, 128.6, 127.5, 126.4, 125.1, 121.7, 119.3, 110.1.; MS: (EI, 70 eV) m/z 504 (M$^+$, 100.0); HRMS: (EI, 70 eV) calcd for C$_{36}$H$_{24}$O$_3$ 504.1725 found m/z 504.1723 (M$^+$). Anal. Calcd for C$_{36}$H$_{24}$O$_3$: C, 85.69; H, 4.79. Found: C, 85.50; H, 4.84
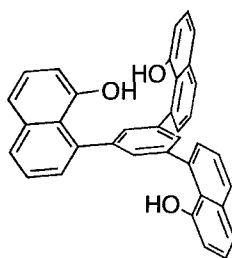
This compound has conformation shown above at room temperature.

4-Methoxy-1-naphthylboroxin (B)
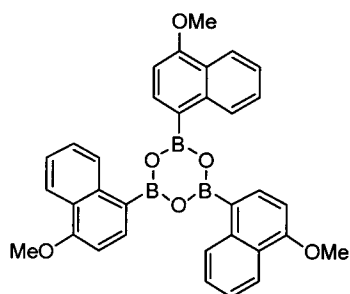
To a solution of 1-bromo-4-methoxynaphthalene[27] (40 mmol) in toluene (60 mL) and THF (15 mL) at -78 °C was slowly added n-BuLi (1.6 M in hexane, 30 mL, 48 mmol) for the period of 1.5 h. After the reaction mixture was stirred for another 1 h at -78 °C, B(OPr^i)$_3$ (48 mmol) was slowly added for the period of 30 min at the same temperature. The mixture was allowed to warm to 0 °C. HClaq solution (2M, 50 mL) and EtOAc (50 mL) was added to the mixture and it was stirred (for ca. 1 h) until the organic layer became clear. The mixture was extracted with EtOAc (3 x 30 mL). The combined organic layer was washed with sat. NaHCO$_3$aq and brine, dried over MgSO$_4$ and evaporated. The residue was washed with hexane and filtrated to give a white solid (6.4 g, 87%). mp: 250-252 °C; IR: (KBr) 1574 (aryl), 1512 (aryl), 1238 (C-O-C) cm^{-1}; ^{1}H NMR: (400 MHz, CDCl$_3$) 9.30 (d, 1H, J = 8.4 Hz), 8.64 (d, 1H, J = 7.9 Hz), 8.40 (dd, 1H, J = 8.5, 1.0 Hz), 7.68 (ddd, 1H, J = 8.5, 6.8, 1.6 Hz), 7.56 (ddd, 1H, J = 8.4, 6.8, 1.0 Hz), 7.02 (d, 1H, J = 7.9 Hz), 4.12 (s, 3H) ^{13}C NMR: (100 MHz, CDCl$_3$) 159.3, 139.0, 138.6, 128.0, 127.2, 125.7, 125.0, 122.3, 103.4, 55.6. MS: (EI, 70 eV) m/z 552 (M$^+$, 100), 158 (86), 143 (30), 115 (65); HRMS: (EI, 70 eV) calcd for C$_{33}$H$_{27}$B$_3$O$_6$ 552.2087 found m/z 552.2091 (M$^+$). Anal. Calcd for C$_{33}$H$_{27}$B$_3$O$_6$: C, 71.80; H, 4.93. Found: C, 71.52; H, 4.93

## 1,3,5-Tris(4-methoxy-1-naphthyl)benzene (5)
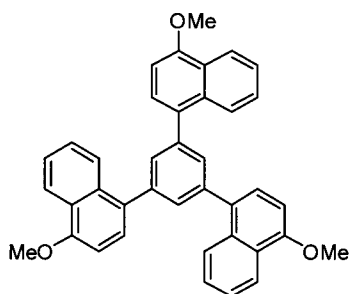
To a suspension of 4-methoxy-1-naphthylboroxin (5.2 mmol) in toluene (10 mL), EtOH (20 mL), water (12 mL), and Na_2CO_3 (20 mmol) were added and the mixture was stirred for 1 h at room temperature. Then, the mixture was added to a solution of 1,3,5-tribromobenzene (4.0 mmol) and $Pd(PPh_3)_4$ (0.4 mmol) in toluene (10 mL) and stirred for 17 h at 90 °C.[5] The mixture was cooled to 0 °C and water (30 mL) was added. The mixture was extracted with ethyl acetate (3 x 30 mL). The combined organic layer was dried over $MgSO_4$ and evaporated. The residue was purified by flash column chromatography (hexane/EtOAc, 95:5) to give the product as a white solid (1.56 g, 71%). mp: 218-221 °C; IR: (KBr) 1585 (aryl) cm^{-1}; ^1H NMR: (400 MHz, $CDCl_3$) 8.35 (m, 3H), 8.18 (m, 3H), 7.67 (s, 3H), 7.50 (m, 9H), 6.90 (d, 3H, $J = 8.0$ Hz), 4.04 (s, 9H); ^{13}C NMR: (100 MHz, $CDCl_3$) 155.0, 140.7, 132.43, 132.4, 130.6, 127.2, 126.6, 125.8, 125.7, 125.1, 122.2, 103.5, 55.6; MS: (EI, 70 eV) m/z 546 (M^+, 100); HRMS: (EI, 70 eV) calcd for $C_{39}H_{30}O_3$ 546.2195 found m/z 546.2191 (M^+). Anal. Calcd for $C_{39}H_{30}O_3$: C, 85.69; H, 5.53. Found: C, 85.44; H, 5.50.

1,3,5-Tris(4-hydroxy-1-naphthyl)benzene (4)
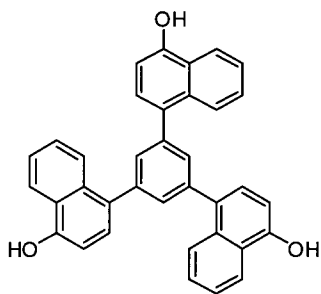
To a solution of 1,3,5-tris(4-methoxy-1-naphthyl)benzene (0.56 mmol) in CH_2Cl_2 (3 mL) was slowly added BBr_3 (1.0 M in CH_2Cl_2, 1.8 mL) at -78 °C. The mixture was stirred at -78 °C to rt for 8 h. The mixture was cooled to 0 °C and quenched by water. The mixture was extracted with ethyl acetate (3 x 10 mL). The combined organic layer was dried over $MgSO_4$ and evaporated. The residue was purified by flash column chromatography (hexane/EtOAc, 60:40) to give the product as a white solid (0.254 g, 90%). mp: decomposition 295 °C; IR: (KBr) 3533 (OH), 1585 cm^{-1}; ^1H NMR: (400 MHz, DMSO-d_6) 10.35 (brs, 3H), 8.23 (dd, $J = 8.3$, 1.1 Hz, 3H), 8.08 (d, $J = 8.5$ Hz, 3H), 7.55 (ddd, $J = 8.5$, 6.8, 1.1 Hz, 3H), 7.51 (s, 3H), 7.49 (m, 3H), 7.47 (d, $J = 7.8$ Hz, 3H), 6.97 (d, $J = 7.8$ Hz, 3H); ^{13}C NMR: (100 MHz, DMSO-d_6) 153.1, 140.6, 131.9, 129.9, 129.9, 127.9, 126.8, 125.0, 124.8, 124.7, 122.6, 107.9; MS: (EI, 70 eV) m/z 504 (M^+, 100.0); HRMS: (EI, 70 eV) calcd for $C_{36}H_{24}O_3$ 504.1725 found m/z 504.1732 (M^+).

1-Methoxy-8-phenylnaphthalene (10)

To a suspension of 8-methoxy-1-naphthylboronic acid (5.5 mmol) in toluene (15 mL), EtOH (25 mL), water (15 mL) and Na_2CO_3 (7.5 mmol) were added and the mixture was stirred for 1 h at room temperature. Then, the mixture was added to a solution of bromobenzene (5 mmol) and $Pd(PPh_3)_4$ (0.25 mmol) in toluene (10 mL) and stirred for 3 h at 90 °C.[5] The mixture was cooled to 0 °C and water (30 mL) was added. The mixture was extracted with ethyl acetate (3 x 10 mL). The combined organic layer was dried over $MgSO_4$ and evaporated. The residue was purified by column chromatography (hexane). Further purification was performed by distillation under reduced pressure to give the product as a colorless liquid (0.90 g, 78%). bp: 150 °C / 0.2 mmHg; IR: (neat) 1577 (aryl), 1253 (C-O-C) cm^{-1}; ^1H NMR: (400 MHz, $CDCl_3$) 7.81 (d, $J =$

8.0 Hz, 1H), 7.50 (d, J = 8.0 Hz, 1H), 7.46 (t, J = 8.0 Hz, 1H), 7.40 (t, J = 8.0 Hz, 1H), 7.37-7.28 (m, 5H), 7.27 (d, J = 8.0 Hz, 1H), 6.78 (d, J = 8.0 Hz, 1H), 3.48 (s, 3H); ^{13}C NMR: (100 MHz, CDCl$_3$) 156.7, 145.4, 139.0, 135.7, 129.0, 128.7, 127.6, 126.6, 126.0, 125.7, 125.4, 123.5, 121.2, 106.2, 55.2; MS: (EI, 70 eV) m/z 234 (M$^+$, 100), 218 (52); HRMS: (EI, 70 eV) calcd for C$_{17}$H$_{14}$O 234.1045 found m/z 234.1041 (M$^+$). Anal. Calcd for C$_{17}$H$_{14}$O: C, 87.15; H, 6.02. Found: C, 87.10; H, 6.01.

1-Methoxy-4-phenylnaphthalene (13)

To a suspension of 4-methoxy-1-naphthylboroxin (1.2 mmol) in toluene (5 mL), EtOH (15 mL) and water (9 mL) and Na$_2$CO$_3$ (5.0 mmol) were added and the mixture was stirred for 1 h at room temperature. Then, the mixture was added to a solution of bromobenzene (3.0 mmol) and Pd(PPh$_3$)$_4$ (0.15 mmol) in toluene (10 mL) and stirred for 5 h at 90 °C.[5] The mixture was cooled to 0 °C and water (30 mL) was added. The mixture was extracted with ethyl acetate (3 x 30 mL). The combined organic layer was dried over MgSO$_4$ and evaporated. The residue was purified by flash column chromatography (hexane/EtOAc, 95:5) to give the product as a colorless liquid (0.51 g, 71%). bp: 170 °C / 0.6 mmHg; IR: (neat) 1238 (C-O-C) cm^{-1}; ^{1}H NMR: (600 MHz, CDCl$_3$) 8.34 (m, 1H), 7.86 (m, 1H), 7.49 (ddd, J = 7.8, 6.6, 1.2 Hz, 1H), 7.48-7.46 (m, 4H), 7.44 (ddd, J = 7.8, 6.6, 1.2 Hz, 1H), 7.40 (m, 1H), 7.33 (d, J = 7.8 Hz, 1H), 6.87 (d, J = 7.8 Hz, 1H), 4.04 (s, 3H); ^{13}C NMR: (100 MHz, CDCl$_3$) 155.0, 140.9, 132.7, 132.5, 130.3, 128.2, 126.9, 126.8, 126.5, 125.8, 125.7, 125.1, 122.2, 103.4, 55.6; MS: (EI, 70 eV) m/z 234 (M$^+$, 100), 219 (M$^+$ - CH$_3$, 38), 191 (38); HRMS: (EI, 70 eV) calcd for C$_{17}$H$_{14}$O 234.1045 found m/z 234.1043 (M$^+$). Anal. Calcd for C$_{17}$H$_{14}$O: C, 87.15; H, 6.02. Found: C, 86.96; H, 6.01.

8-(4-Methoxyphenyl)-1-naphthol (14)
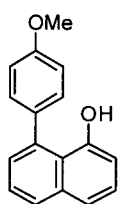
To a suspension of CsCO$_3$ (10 mmol), which was pre-dried under reduced pressure for 2 h at room temperature, in DMF (25 mL) were added PdCl$_2$ (0.13 mmol), 1-naphthol (5.0 mmol) and p-iodoanisole (6.0 mmol).[5] The mixture was stirred for 21 h at 110 °C. The mixture was cooled to 0 °C, and then water was added. The mixture was extracted with ethyl acetate (3 x 20 mL). The combined organic layer was washed with water (3 x 20 mL) and dried over MgSO$_4$. After filtration, the solvent was evaporated and purified by column chromatography (hexane/EtOAc, 80:20). Further purification was performed by distillation under reduced pressure to give the product as a pale yellow solid (0.29 g, 23%). Further, recrystallization from CH$_2$Cl$_2$/hexane afforded crystals suitable for X-ray structure analysis.[34] mp: 100-101 °C; IR: (KBr) 3464 (OH), 1516 cm^{-1}; ^{1}H NMR: (400 MHz, CDCl$_3$) 7.83 (d, J = 8.0 Hz, 1H), 7.49 (d, J = 8.0 Hz, 1H), 7.44 (d, J = 8.8 Hz, 2H), 7.42 (t, J = 8.0 Hz, 1H), 7.39 (t, J = 8.0 Hz, 1H), 7.18 (d, J = 8.0 Hz, 1H), 7.04 (d, J = 8.8 Hz, 2H), 6.90 (d, J = 8.8 Hz, 1H), 5.66 (s, 1H), 3.89 (s, 3H); ^{13}C NMR: (100 MHz, CDCl$_3$) 159.8, 153.2, 135.7, 135.7, 132.9, 130.7, 128.7, 128.5, 126.8, 124.8, 121.5, 120.9, 114.4, 111.6, 55.4; MS: (EI, 70 eV) m/z 250 (M$^+$, 100); HRMS: (EI, 70 eV) calcd for C$_{17}$H$_{14}$O$_2$ 250.0994 found m/z 250.0996 (M$^+$). Anal. Calcd for C$_{17}$H$_{14}$O$_2$: C, 81.58; H, 5.64. Found: C, 81.35; H, 5.66.

8-(4-Chlorophenyl)-1-naphthol (15)
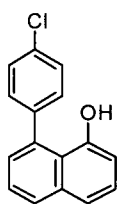
To a suspension of $CsCO_3$ (10 mmol), which was pre-dried under reduced pressure for 2 h at room temperature, in DMF (25 mL) were added $PdCl_2$ (0.13 mmol), 1-naphthol (5 mmol) and 1-chloro-4-iodobenzene (6 mmol).[5] The mixture was stirred for 21 h at 110 °C. The mixture was cooled to 0 °C, and then water was added. The mixture was extracted with ethyl acetate (3 x 20 mL). The combined organic layer was washed with water (3 x 20 mL) and dried over $MgSO_4$. After filtration, the solvent was evaporated and purified by column chromatography (hexane/EtOAc, 80:20). Further purification was performed by distillation under reduced pressure to give the product as a pale yellow solid (0.37 g, 29%). Further, recrystallization from CH_2Cl_2/hexane afforded crystals suitable for X-ray structure analysis.[34] mp: 55-57 °C; IR: (KBr) 3367 (OH) cm^{-1}; ^{1}H NMR: (400 MHz, CDCl$_3$) 7.86 (d, J = 8.0 Hz, 1H), 7.51 (d, J = 8.0 Hz, 1H), 7.48-7.41 (m, 5H), 7.40 (t, J = 8.0 Hz, 1H), 7.17 (d, J = 8.0 Hz, 1H), 6.90 (d, J = 8.0 Hz, 1H), 5.20 (s, 1H); ^{13}C NMR: (100 MHz, CDCl$_3$) 152.6, 140.0, 135.7, 135.0, 134.5, 130.8, 128.9, 128.9, 128.7, 124.9, 121.2, 121.2, 111.9; MS: (EI, 70 eV) m/z 256 (M$^+$ + 2, 34), 254 (M$^+$, 100), 218 (M$^+$ - Cl, 51), 189 (25); HRMS: (EI, 70 eV) calcd for C$_{16}$H$_{11}$ClO 254.0498 found m/z 254.0504 (M$^+$). Anal. Calcd for C$_{16}$H$_{11}$ClO: C, 75.45; H, 4.35. Found: C, 75.31; H, 4.38.

1-Trifluoromethanesulfonyloxy-8-phenylnaphthalene (C)
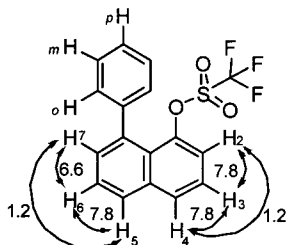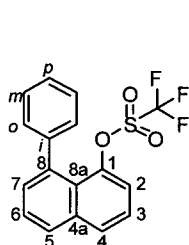
To a solution of 1-hydroxy-8-phenylnaphthalene (1.65 g, 7.50 mmol) in pyridine (12 mL) was slowly added trifluoromethanesulfonic anhydride (2.0 ml, 12.0 mmol) for 5 min at 0 °C. After the reaction mixture was stirred for 22 h at room temperature, and then quenched by water (10 mL). The mixture was extracted with ethyl acetate (10 x 3 mL). The collected organic layer was dried ($MgSO_4$). The solvent was evaporated and the residue was purified by flash column chromatography (hexane) to give the product as a white solid (0.991 g, 38%). mp: 107-109 °C; IR: (KBr) 1423 (SO_2), 1207 (SO_2) cm^{-1}; ^{1}H NMR: (600 MHz, CDCl$_3$) 7.96 (dd, J = 7.8, 1.2 Hz, 1H, 4-H), 7.91 (dd, J = 7.8, 1.2 Hz, 1H, 5-H), 7.59 (dd, J = 7.8, 6.6 Hz, 1H, 6-H), 7.50 (dd, J = 7.8, 7.8 Hz, 1H, 3-H), 7.48 (dd, J = 6.6, 1.2 Hz, 1H, 7-H), 7.46-7.39 (m, 6H, o-H, m-H, p-H and 2-H); ^{13}C NMR: (150 MHz, CDCl$_3$) 145.6 (C-1), 141.6 (C-i), 137.3 (C-8), 136.3 (C-4a), 132.1 (C-7), 129.7 (C-o), 129.6 (C-4), 128.0 (C-5), 127.8 (C-m), 127.4 (C-p), 126.5 (C-6), 125.0 (C-3), 124.4 (C-8a), 118.4 (q, $^1J_{CF}$ = 320 Hz, CF$_3$); MS: (EI, 70 eV) 352 (M$^+$, 40), 219 (M - SO$_2$CF$_3$, 100), 218 (65); HRMS: (EI, 70 eV) calcd for C$_{17}$H$_{11}$F$_3$O$_3$S 352.0381 found m/z 352.0379 (M$^+$). Anal. Calcd for C$_{17}$H$_{11}$F$_3$O$_3$S: C, 57.95; H, 3.15; F, 16.18; O, 13.62; S, 9.10. Found: C, 57.72; H, 3.02; F, 16.29; S, 9.35.

1-Thio-8-phenylnaphthalene (16)
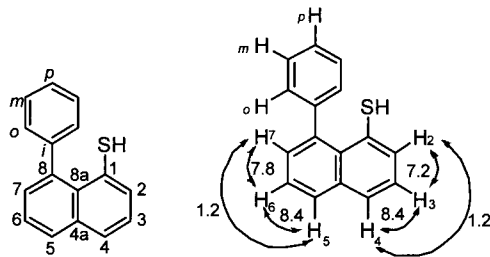
To a solution of triisopropylsilylthiol (0.962 g, 5.05 mmol) in THF (13 mL) was added NaH (in oil, 0.267 g, 5.56 mmol) at 0 °C. After the reaction mixture was stirred for 1 h at room temperature. Then, the reaction mixture was added to a solution of 1-trifluoromethanesulfonyloxy-8-phenylnaphthalene (1.12 g, 3.18 mmol) and Pd(PPh₃)₄ (0.221 g, 0.500 mmol) in benzene (13 mL)

and stirred for 18 h at 80 °C. To a solution was added TBAF at 0 °C. After the reaction mixture was stirred for 3 h at room temperature, and then quenched by HClaq (10 mL). The mixture was extracted with ethyl acetate (10 x 3 mL). The collected organic layer was dried (MgSO₄). The solvent was evaporated and the residue was purified by flash column chromatography (hexane) and GPC to give the product as a white solid (0.0236 g, 3%). mp: 74-76 °C; IR: (KBr) 3047 (C-H), 2546 (SH) cm⁻¹; ¹H NMR: (600 MHz, CDCl₃) 7.83 (dd, J = 8.4, 1.2 Hz, 1H, 5-H), 7.71 (dd, J = 8.4 1.2 Hz, 1H, 4-H), 7.47 (dd, J = 8.4, 7.8 Hz, 1H, 6-H), 7.45-7.38 (m, 5H, o-H, m-H and p-H), 7.36 (brd, J = 7.2 Hz, 1H, 2-H), 7.35 (dd, J = 8.4, 1.2 Hz 1H, 7-H), 7.27 (dd, J = 8.4, 7.2 Hz, 1H, 3-H), 3.51 (s, 1H, SH); ¹³C NMR: (150 MHz, CDCl₃) 142.3 (C-i), 139.9 (C-8), 135.3 (C-4a), 130.6 (C-o), 130.4 (C-1), 129.7 (C-7), 129.6 (C-2), 129.5 (C-8a), 128.8 (C-5), 127.7 (C-m), 127.6 (C-p), 126.8 (C-4), 125.5 (C-3), 125.1 (C-6); MS: (EI, 70 eV) 236 (M⁺, 100), 203 (M - SH, 45), 171 (19); HRMS: (EI, 70 eV) calcd for C₁₆H₁₂S 236.0660 found m/z 236.0654 (M⁺).

1-Phenylamino-8-phenylnaphthalene (17a)
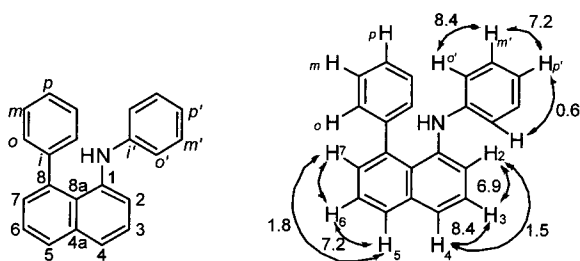
To a solution of aniline (0.6617 g, 7.12 mmol) in dioxane (4 mL) was slowly added n-BuLi (1.6 M in hexane, 4.4 mL, 7.00 mmol) for 10 min at 0 °C. After the reaction mixture was stirred for 30 min at room temperature. Then, the reaction mixture was added to a solution of 1-trifluoromethanesulfonyloxy-8-phenylnaphthalene (1.21

g, 3.45 mmol), Pd(dba)₂ (0.0456 g, 0.138 mmol) and BINAP (0.1741 g, 0.280 mmol) in dioxane (7.1 mL). The mixture was stirred for 25 h at 100 °C, cooled to room temperature, filtered through Celite, and evaporated. The residue was purified by flash column chromatography (hexane) to give the product as a pale yellow liquid (0.1163 g, 11%). IR: (neat) 3429 (NH), 1577 (Ar) cm⁻¹; ¹H NMR: (600 MHz, CDCl₃) 7.85 (dd, J = 8.4, 1.5 Hz, 1H, 4-H), 7.56 (dd, J = 7.2, 1.8 Hz, 1H, 5-H), 7.44 (dd, J = 8.4, 6.9 Hz, 1H, 3-H), 7.42-7.33 (m, 7H, 6-H, 7-H, o-H, m-H and p-H), 7.23 (dd, J = 6.9, 1.5 Hz, 1H, 2-H), 7.07 (dd, J = 8.4, 7.2 Hz, 2H, m'-H), 6.76 (tt, J = 7.2, 0.6 Hz, 1H, p'-H), 6.54 (dd, J = 8.4, 0.6 Hz, 2H, o'-H), 5.48 (brs, 1H, NH); ¹³C NMR: (150 MHz, CDCl₃) 143.7 (C-i'), 143.5 (C-1), 139.0 (C-i), 137.8 (C-8), 136.1 (C-4a), 129.0 (C-2), 128.9 (C-m'), 128.8 (C-4), 128.7 (C-o or C-m), 128.2 (C-o or C-m), 127.2 (C-p), 126.0 (C-6 or C-7), 124.7 (C-3), 124.4 (C-8a), 122.6 (C-5), 120.0 (C-p'), 116.6 (C-6 or C-7), 116.2 (C-o'); MS: (EI, 70 eV) m/z 296 (24), 295 (M⁺,100), 294 (26); HRMS: (EI, 70 eV) calcd for C₂₂H₁₇N 295.1361 found m/z 295.1362 (M⁺). Anal. Calcd for C₂₂H₁₇N: C, 89.46; H, 5.80; N, 4.74. Found: C, 89.32; H, 5.94, N, 4.62

1-(*p*-Chlorophenylamino)-8-phenylnaphthalene (17b)

To a solution of *p*-chloroaniline (0.3811 g, 3.00 mmol) in dioxane (4 mL) was slowly added *n*-BuLi (1.6 M in hexane, 1.9 mL, 3.04 mmol) for 10 min at 0 °C. After the reaction mixture was stirred for 30 min at room temperature. Then, the reaction mixture was added to a solution of 1-trifluoromethanesulfonyloxy-8-phenylnaphthalene (0.706

g, 2.00 mmol), Pd(dba)$_2$ (0.0200 g, 0.0606 mmol) and BINAP (0.0995 g, 0.160 mmol) in dioxane (4 mL). The mixture was stirred for 31 h at 100 °C, cooled to room temperature, filtered through Celite, and evaporated. The residue was purified by flash column chromatography (hexane) to give the product as a pale yellow liquid (0.1904 g, 29%). IR: (neat) 3425 (NH), 1577 (Ar) cm^{-1}; ^{1}H NMR: (600 MHz, CDCl$_3$) 7.87 (dd, J = 8.1, 1.5 Hz, 1H, 4-H), 7.61 (dd, J = 7.8, 0.6 Hz, 1H, 5-H), 7.45 (dd, J = 8.1, 7.2 Hz, 1H, 3-H), 7.42 (dd, J = 7.8, 7.8 Hz, 1H, 6-H), 7.36-7.31 (m, 6H, 7-H, *o*-H, *m*-H and *p*-H), 7.24 (dd, J = 7.2, 1.5 Hz, 1H, 2-H), 6.99 (ddd, J = 9.6, 3.0, 3.0 Hz, 2H, *m'*-H), 6.41 (ddd, J = 9.6, 3.0, 3.0 Hz, 2H, *o'*-H), 5.406 (brs, 1H, NH); ^{13}C NMR: (150 MHz, CDCl$_3$) 143.5 (C-1), 142.7 (C-*i'*), 138.3 (C-*i*), 137.8 (C-8), 136.1 (C-4a), 129.2 (C-2), 128.9 (C-4), 128.8 (C-*m'*), 128.6 (C-*o* or C-*m*), 128.2 (C-*o* or C-*m*), 127.3 (C-*p*), 125.9 (C-6), 124.9 (C-3), 124.9 (C-8a), 124.0 (C-*p'*), 123.4 (C-5), 117.9 (C-7), 116.7 (C-*o'*); MS: (EI, 70 eV) *m/z* 331 (M$^+$ + 2, 36), 330 (37), 329 (M$^+$, 100); HRMS: (EI, 70 eV) calcd for C$_{22}$H$_{16}$ClN 329.0971 found *m/z* 329.0967 (M$^+$). Anal. Calcd for C$_{22}$H$_{16}$ClN: C, 80.11; H, 4.89; Cl, 10.75; N, 4.25. Found: C, 80.08; H, 5.03; Cl, 10.90; N, 4.20.

1-(*p*-Methylphenylamino)-8-phenylnaphthalene (17c)

To a solution of *p*-methylaniline (0.647 g, 6.04 mmol) in dioxane (36 mL) was slowly added *n*-BuLi (1.6 M in hexane, 4.0 mL, 6.15 mmol) for 10 min at 0 °C. After the reaction mixture was stirred for 30 min at room temperature. Then, the reaction mixture was added to a solution of 1-trifluoromethanesulfonyloxy-8-phenylnaphthalene (0.684 g,

6.15 mmol), Pd(dba)$_2$ (0.0129 g, 0.0391 mmol) and BINAP (0.0495 g, 0.0796 mmol) in dioxane (16 mL). The mixture was stirred for 31 h at 100 °C, cooled to room temperature, filtered through Celite, and evaporated. The residue was purified by flash column chromatography (hexane) to give the product as a pale yellow liquid (0.1738 g, 9%). IR: (neat) 3425 (NH), 1577 (Ar) cm^{-1}; ^{1}H NMR: (600 MHz, CDCl$_3$) 7.84 (dd J = 8.4, 1.2 Hz, 1H, 4-H), 7.50 (dd, J = 7.8, 1.2 Hz, 1H, 5-H), 7.43 (dd, J = 8.4, 7.2 Hz, 1H, 3-H), 7.41-7.35 (m, 6H, *o*-H, *m*-H, *p*-H and 6-H), 7.30 (dd, J = 7.8, 1.2 Hz, 1H, H-7), 7.22 (dd, J = 7.2, 1.2 Hz, 1H, 2-H), 6.91 (d, J = 7.8 Hz, 2H, *m'*-H), 6.53 (d, J = 7.8 Hz, 2H, *o'*-H), 5.23 (brs, 1H, NH), 2.23 (brs, 3H, Me); ^{13}C NMR: (150 MHz, CDCl$_3$) 143.5 (C-1), 140.7 (C-*i'*), 139.9 (C-*i*), 137.8 (C-8), 136.1 (C-4a), 129.9 (C-*p'*), 129.5 (C-*m'*), 128.9 (C-2), 128.8 (C-4), 128.7 (C-*o* or C-*m*), 128.2 (C-*o* or C-*m*), 127.3 (C-*p*), 126.1 (C-6), 124.6 (C-3), 123.6 (C-8a), 121.6 (C-5), 117.4 (C-*o'*), 114.7 (C-7), 20.6 (Me); MS: (EI, 70 eV) *m/z* 310 (33), 309 (M$^+$,100), 308 (20); HRMS: (EI, 70 eV) calcd for C$_{23}$H$_{19}$N 309.1517 found *m/z* 309.1516 (M$^+$).

1-Hexylamino-8-phenylnaphthalene (17d)

To a solution of hexylamine (0.403 g, 3.99 mmol) in dioxane (1 mL) was slowly added *n*-BuLi (1.6 M in hexane, 2.5 mL, 4.00 mmol) for 10 min at 0 °C. After the reaction mixture was stirred for 3 h at room temperature. Then, the reaction mixture was added to a solution of 1-trifluoromethanesulfonyloxy-8-phenylnaphthalene (0.704 g, 2.00 mmol), Pd(dba)$_2$ (0.0260 g, 0.0788 mmol) and BINAP (0.0970 g, 0.156 mmol) in dioxane (4 mL). The mixture was stirred for 31 h at 100 °C, cooled to room temperature, filtered through Celite, and evaporated. The residue was purified by flash column chromatography (hexane) to give the product as a pale yellow liquid (0.1766 g, 29%). IR: (neat) 3448 (NH), 2927 (CH), 1581 (Ar) cm^{-1}; ^{1}H NMR: (600 MHz, CDCl$_3$) 7.76 (dd, J = 8.4, 1.2 Hz, 1H, 5-H), 7.44-7.40 (m, 5H, *o*-H, *m*-H and *p*-H), 7.37 (dd, J = 8.4, 7.2 Hz, 1H, 6-H), 7.34 (dd, J = 7.8, 7.8 Hz, 1H, 3-H), 7.22 (d, J = 7.8 Hz, 1H, 4-H), 7.11 (dd, J = 7.2, 1.2 Hz, 1H, 7-H), 6.44 (d, J = 7.8 Hz, 1H, 2-H), 3.83 (brs, 1H, NH), 2.86 (td, J = 6.6, 6.6 Hz, 2H, 1'-H$_2$), 1.23 (m, 2H, 5'-H$_2$), 1.11 (m, 4H, 2'-H$_2$ and 4'-H$_2$), 1.00 (m, 2H, 3'-H$_2$), 0.87 (t, J = 7.2 Hz, 3H, 6'-H$_3$); ^{13}C NMR: (150 MHz, CDCl$_3$) 145.3 (C-1), 143.7 (C-*i*), 137.9 (C-8), 135.8 (C-4a), 129.2 (C-*o* or C-*m*), 128.7 (C-5), 128.0 (C-*o* or C-*m*), 128.0 (C-7), 127.4 (C-*p*), 126.9 (C-3), 124.3 (C-6), 120.4 (C-8a), 116.7 (C-4), 104.5 (C-2), 44.0 (C-1'), 31.6 (C-2' or C-4'), 28.8 (C-2' or C-4'), 26.9 (C-3'), 22.6 (C-5'), 14.1 (C-6'); MS: (EI, 70 eV) *m/z* 303 (M$^+$, 100), 232 (M - C$_5$H$_{11}$, 65), 217 (21), 216 (32), 202 (M - C$_6$H$_{14}$N, 15); HRMS: (EI, 70 eV) calcd for C$_{22}$H$_{25}$N 303.1987 found *m/z* 303.1988 (M$^+$). Anal. Calcd for C$_{22}$H$_{25}$N: C, 87.08; H, 8.30; N, 4.62. Found: C, 87.03; H, 8.43; N, 4.52

Electronic Spectra.
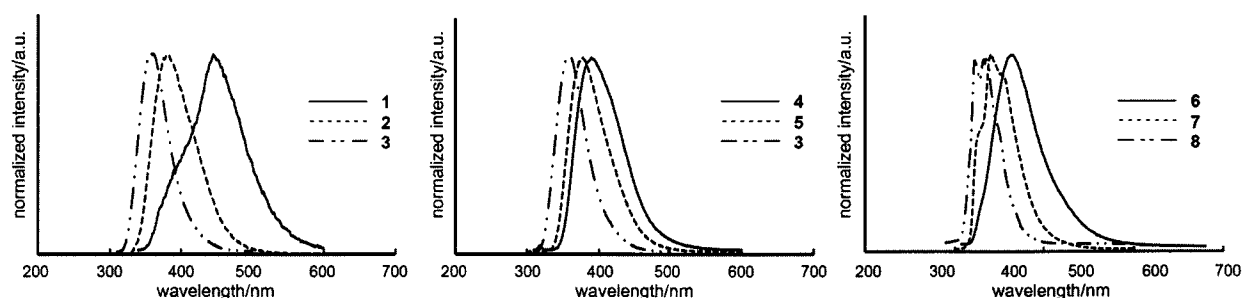
Figure S1. Emission spectra of **1-8** in DMSO excited at 334 nm for **1**, 306 nm for **2**, 298 nm for **3**, 320 nm for **4**, 316 nm for **5**, 300 nm for **6**, 296 nm for **7**, and 278 nm for **8**.
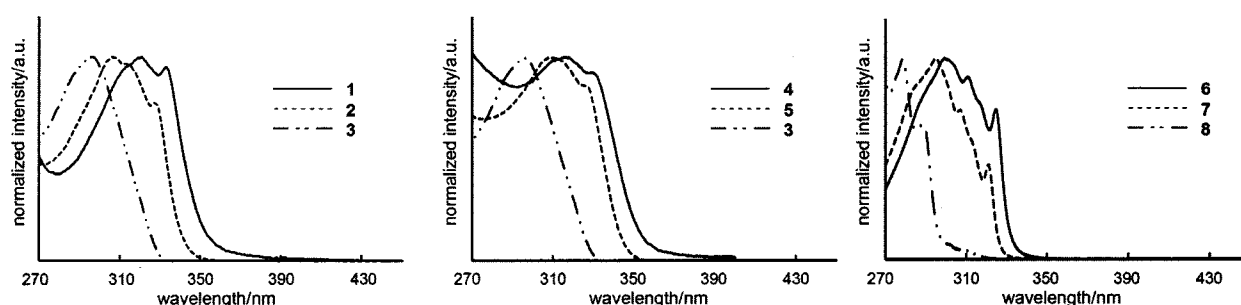
Figure S2. Absorption spectra of **1-8** in DMSO.
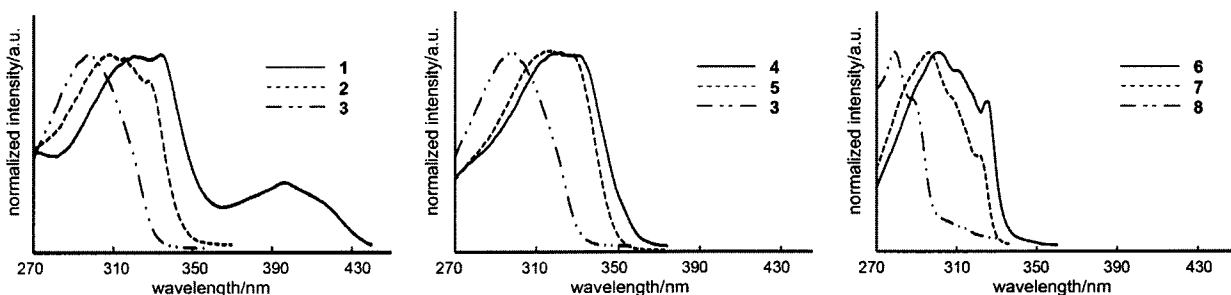
Figure S3. Excitation spectra of **1-8** in DMSO monitored at 446 nm for **1**, 382 nm for **2**, 360 nm for **3**, 392 nm for **4**, 378 nm for **5**, 366 nm for **6**, 340 nm for **7**, and 336 nm for **8**.
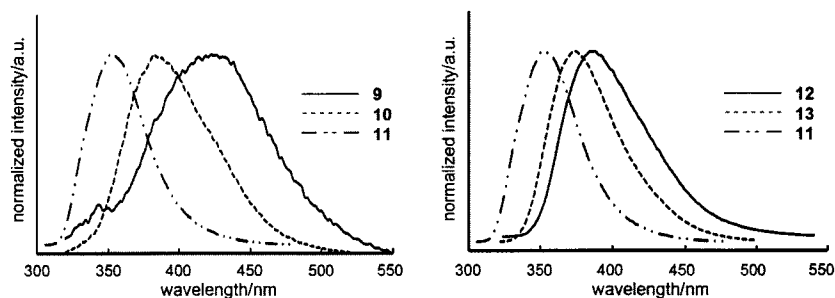
Figure S4. Emission spectra of **9-13** in DMSO excited at 312 nm for **9**, 304 nm for **10**, 294 nm for **11**, 316 nm for **12**, and 308 nm for **13**.
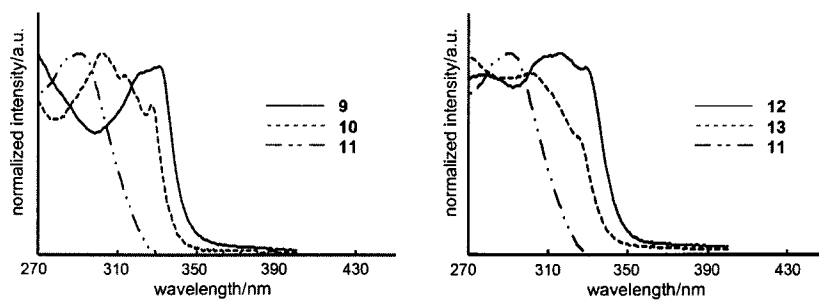
Figure S5. Absorption spectra of **9-13** in DMSO.
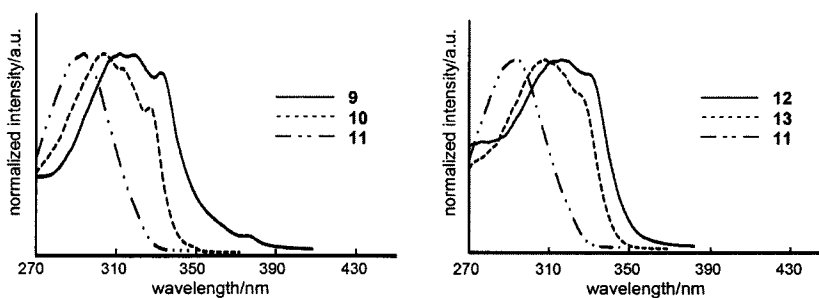
Figure S6. Excitation spectra of **9-13** in DMSO monitored at 422 nm for **9**, 382 nm for **10**, 352 nm for **11**, 386 nm for **12**, and 374 nm for **13**.
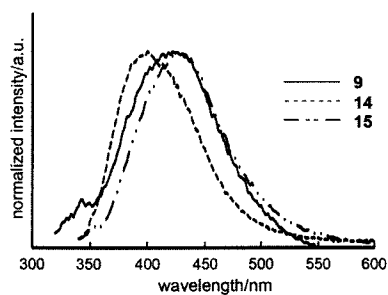
Figure S7. Emission spectra of **9**, **14**, and **15** in DMSO excited at 312 nm for **9**, 320 nm for **14**, and 320 nm for **15**.
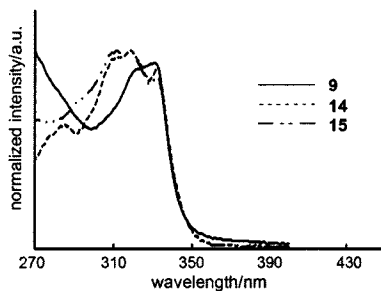
Figure S8. Absorption spectra of **9**, **14**, and **15** in DMSO.

120
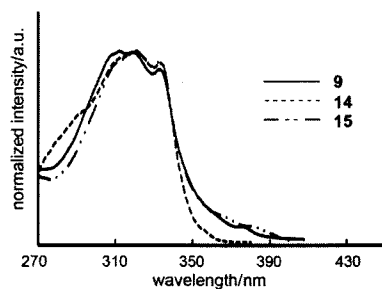
Figure S9. Excitation spectra of **9**, **14**, and **15** in DMSO monitored at 422 nm for **9**, 398 nm for **14**, and 428 nm for **15**.
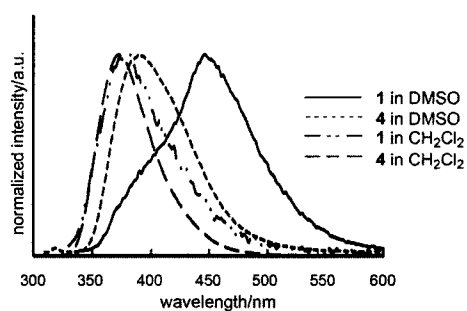
Figure S10. Solvent effect on emission spectra of **1** and **4** excited at 316 nm for **1** (CH_2Cl_2), 310 nm for **4** (CH_2Cl_2), 334 nm for **1** (DMSO), and 320 nm for **4** (DMSO).
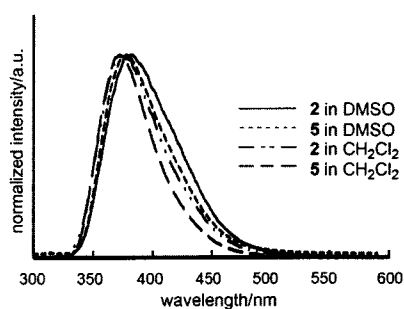
Figure S11. Solvent effect on emission spectra of **2** and **5** excited at 306 nm for **2** (CH_2Cl_2), 312 nm for **5** (CH_2Cl_2), 306 nm for **2** (DMSO), and 316 nm for **5** (DMSO).
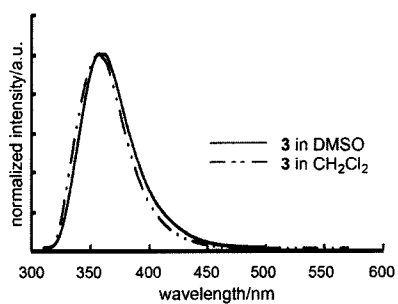
Figure S12. Solvent effect on emission spectra of **3** excited at 296 nm (CH_2Cl_2) and 298 nm (DMSO).
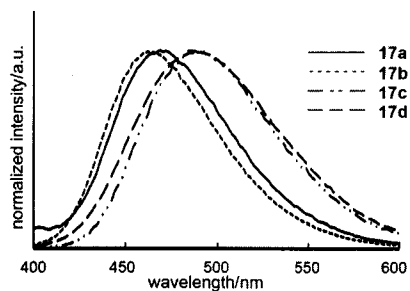
Figure S13. Emission spectra of **17a**, **17b**, **17c**, and **17d** in DMSO excited at 360 nm for **17a**, 362 nm for **17b**, 364 nm for **17c**, and 352 nm for **17d**.
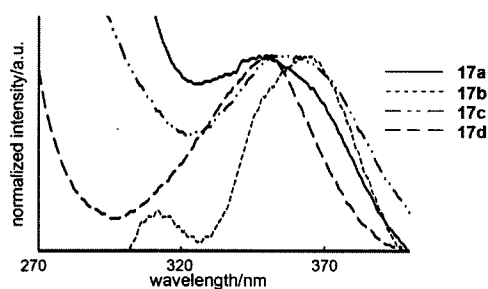
Figure S14. Absorption spectra of **17a**, **17b**, **17c**, and **17d** in DMSO.
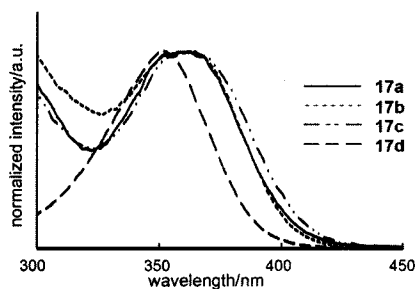
Figure S15. Excitation spectra of **17a**, **17b**, **17c**, and **17d** in DMSO monitored at 468 nm for **17a**, 464 nm for **17b**, 490 nm for **17c**, and 488 nm for **17d**.
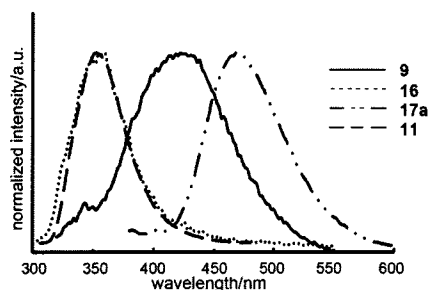
Figure S16. Emission spectra of **9**, **16**, **17a**, and **11** in DMSO excited at 312 nm for **9**, 292 nm for **16**, 360 nm for **17a**, and 294 nm for **11**.
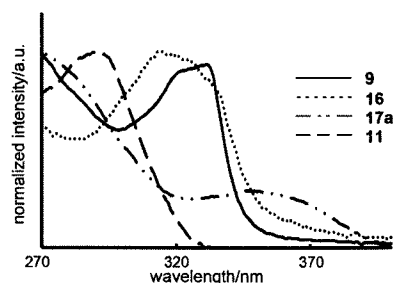
Figure S17. Absorption spectra of **9, 16, 17a** and **11** in DMSO.
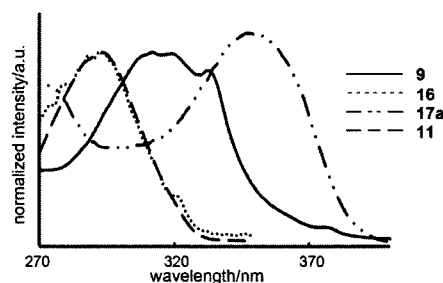
Figure S18. Excitation spectra of **9, 16, 17a,** and **11** in DMSO monitored at 422 nm for **9**, 354 nm for **16**, 468 nm for **17a**, and 352 nm for **11**.

Effect of Electronic Substituent on Mono(hydroxynaphthyl)benzene

Photophysical data of **14** and **15** are summarized in Table S1.

Table S1.

compound	absorption		emission	
	λ_{max}/nm	$\varepsilon/10^4 M^{-1}cm^{-1}$	λ_{max} ($\lambda_{excited}$)/nm	Φ
14	319	0.92	398 (320)	0.02
15	312	1.00	426 (320)	0.03

Quantum yields

All measurement were performed at rt. Quantum yields were calculated using the equation below.

$$\Phi_x = \Phi_{ref} \left(\frac{A_{ref}}{K_{ref}} \right) \left(\frac{K_x}{A_x} \right) \left(\frac{n_x}{n_{ref}} \right) \left(\frac{I_{ref}}{I_x} \right)$$

Φ is the quantum yield of sample x and reference ref, n is the refractive index (1.4783 in DMSO, 1.361 in EtOH), A the absorbance at the excitation wavelength, I the intensity of the corrected excitation spectrum at the excitation wavelength, and K the maximum intensity of emission spectrum. In this case, I_x and I_{ref} are enough close that we approximately estimate I_x is equal to I_{ref}. We used EtOH solution of naphthalene ($\Phi = 0.21^{35}$) as a reference.
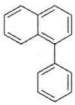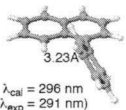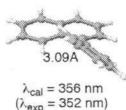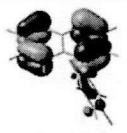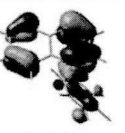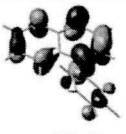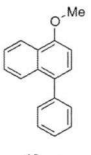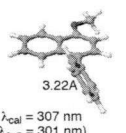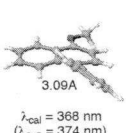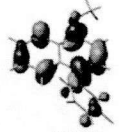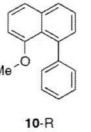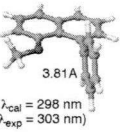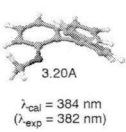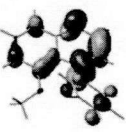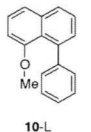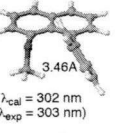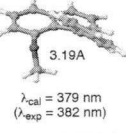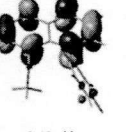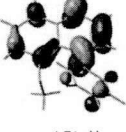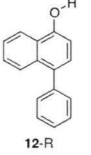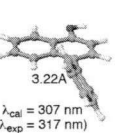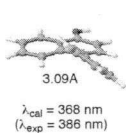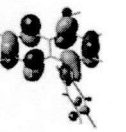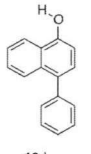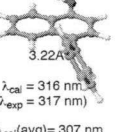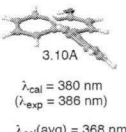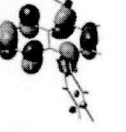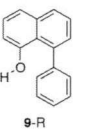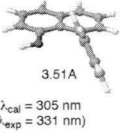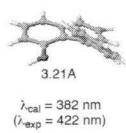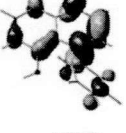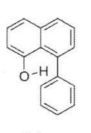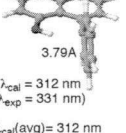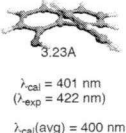
Computational Method

The ground (S_0) state minimum (S_0min) structures were obtained at the hybrid density functional theory (DFT) (with the B3LYP exchange-correlation functional) levels, while the first excited singlet (S_1) state minimum (S_1min) structures were done at the configuration interaction singles (CIS) level. The S_1 absorption maximum wavelengths were calculated from vertical excitation energies using the time-dependent density functional theory (TDDFT) with the B3LYP functional at the B3LYP S_0min, while the emission (fluorescence) wavelengths were done from TDDFT(B3LYP) excitation energies at the CIS S_1min. HOMO and LUMO at the B3LYP S_0min and the CIS S_1min were obtained using the Hartree-Fock (HF) method. In this paper, we call HOMO and LUMO at the CIS S_1min lower SOMO and higher SOMO, respectively. Atomic charges were calculated from the natural atomic orbital (NAO) analysis. The NAO atomic charges of the S_0 state at the B3LYP S_0min were obtained at the HF level and those of the S_1 state at the CIS S_1min were done at the CIS level. We employed 6-31G* basis set in all the calculations. All computations were performed with Gaussian03.[19]

S_0 energies at the B3LYP S_0min and the S_1 energies at the CIS S_1min (in hartree). The S_0 energies were calculated at the B3LYP level and each S_1 energy was obtained by a sum of the B3LYP S_0 energy and the TDB3LYP S_1 excitation energy.

Compound	@B3LYP S_0min	@CIS S_1min
6-L	-461.1064	-460.9445
6-R	-461.1091	-460.9424
9-L	-692.1591	-692.0279
9-R	-692.1544	-692.0157
10-L	-731.4570	-731.3165
10-R	-731.4605	-731.3209
11	-616.9462	-616.8038
12-L	-692.1598	-692.0247
12-R	-692.1626	-692.0235
13	-731.4692	-731.3301

Table S2. Theoretical Calculated Data of **9-13**.

compound	S₀		S₁		MO diagram and energy at S₀		MO diagram and energy at S₁	
	optimized structure $C_{Naph-peri}$–$C_{Ph-ortho}$ absorption λ	dihedral angle of biaryl	optimized structure $C_{Naph-peri}$–$C_{Ph-ortho}$ emission λ	dihedral angle of biaryl	HOMO	LUMO	lower SOMO	higher SOMO
11	3.23A $λ_{cal}$ = 296 nm ($λ_{exp}$ = 291 nm)	57.24°	3.09A $λ_{cal}$ = 356 nm ($λ_{exp}$ = 352 nm)	32.53°	−7.46 eV	2.48 eV	−6.83 eV	1.84 eV
13	3.22A $λ_{cal}$ = 307 nm ($λ_{exp}$ = 301 nm)	56.36°	3.09A $λ_{cal}$ = 368 nm ($λ_{exp}$ = 374 nm)	32.79°	−7.17 eV	2.72 eV	−6.50 eV	2.13 eV
10-R	3.81A $λ_{cal}$ = 298 nm ($λ_{exp}$ = 303 nm) ΔE(L-R) = 2.20 kcal/mol	92.35°	3.20A $λ_{cal}$ = 384 nm ($λ_{exp}$ = 382 nm) ΔE(L-R) = 2.97 kcal/mol	25.65°	−7.32 eV	2.82 eV	−6.59 eV	1.85 eV
10-L	3.46A $λ_{cal}$ = 302 nm ($λ_{exp}$ = 303 nm) $λ_{cal}$(avg)= 298 nm ($λ_{exp}$ = 303 nm)	61.89°	3.19A $λ_{cal}$ = 379 nm ($λ_{exp}$ = 382 nm) $λ_{cal}$(avg)= 384 nm ($λ_{exp}$ = 382 nm)	25.84°	−7.41 eV	2.48 eV	−6.70 eV	1.71 eV
12-R	3.22A $λ_{cal}$ = 307 nm ($λ_{exp}$ = 317 nm) ΔE(L-R) = 1.75 kcal/mol	56.62°	3.09A $λ_{cal}$ = 368 nm ($λ_{exp}$ = 386 nm) ΔE(L-R) = 1.19 kcal/mol	33.41°	−7.22 eV	2.66 eV	−6.56 eV	2.07 eV
12-L	3.22A $λ_{cal}$ = 316 nm ($λ_{exp}$ = 317 nm) $λ_{cal}$(avg)= 307 nm ($λ_{exp}$ = 317 nm)	57.07°	3.10A $λ_{cal}$ = 380 nm ($λ_{exp}$ = 386 nm) $λ_{cal}$(avg)= 368 nm ($λ_{exp}$ = 386 nm)	35.93°	−7.27 eV	2.48 eV	−6.63 eV	1.91 eV
9-R	3.51A $λ_{cal}$ = 305 nm ($λ_{exp}$ = 331 nm) ΔE(L-R) = -2.94 kcal/mol	66.69°	3.21A $λ_{cal}$ = 382 nm ($λ_{exp}$ = 422 nm) ΔE(L-R) = -8.28 kcal/mol	27.77°	−7.30 eV	2.65 eV	−6.63 eV	1.82 eV
9-L	3.79A $λ_{cal}$ = 312 nm ($λ_{exp}$ = 331 nm) $λ_{cal}$(avg)= 312 nm ($λ_{exp}$ = 331 nm)	91.72°	3.23A $λ_{cal}$ = 401 nm ($λ_{exp}$ = 422 nm) $λ_{cal}$(avg)= 400 nm ($λ_{exp}$ = 422 nm)	31.87°	−7.26 eV	2.70 eV	−6.70 eV	1.67 eV

Calculated wavelength in absorption and emission spectra are well-consistent with measured ones as shown in Figure S13.
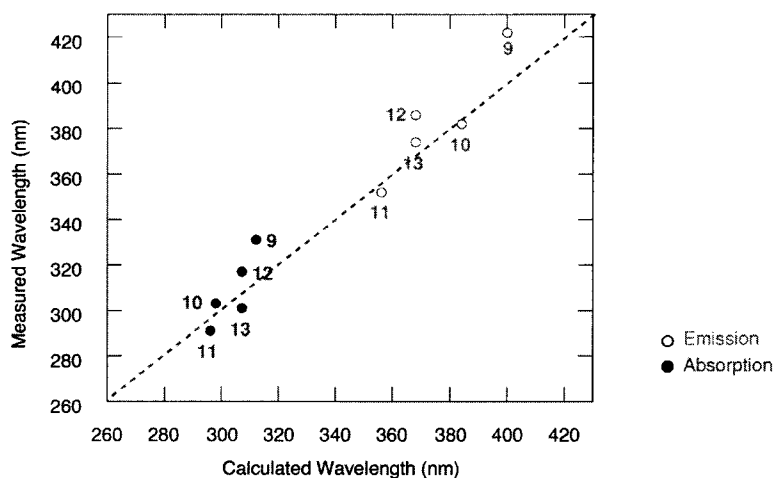
Figure S13. Plot of Calculated Wavelength versus Measured Wavelength.

NAO atomic charges of 6-L, 6-R, 9-L, 9-R, 11, 12-L and 12-R

The calculation results are summarized in Table S3.

Table S3. NAO Atomic Charges at S_0 or S_1 States[a]

Compound	State	R/L	OH	O of OH	H of OH	Ph	Naph
9	S_0	R	-0.246	-0.725	0.499	0.008	0.238
		L	-0.242	-0.764	0.523	-0.005	0.246
9	S_1	R	-0.241	-0.737	0.496	0.011	0.230
		L	-0.223	-0.742	0.520	-0.060	0.283
6	S_0	R	-0.256	-0.757	0.501	-	0.008
		L	-0.253	-0.752	0.499	-	0.043
6	S_1	R	-0.235	-0.734	0.498	-	-0.003
		L	-0.230	-0.733	0.504	-	0.022
11	S_0		-	-	-	0.001	-0.242
11	S_1		-	-	-	-0.005	-0.231
12	S_0	R	-0.255	-0.756	0.501	-0.003	0.259
		L	-0.253	-0.753	0.500	-0.003	0.256
12	S_1	R	-0.237	-0.736	0.498	-0.018	0.256
		L	-0.236	-0.738	0.501	0.002	0.234

[a] The charge of Ph was defined as a sum of atomic charges on atoms of phenyl (C_6H_5) and that of Naph was done as a sum of atomic charges on atoms of $C_{10}H_6$ in naphthyl moiety.

9-R   9-L   6-R   6-L   11   12-R   12-L

126
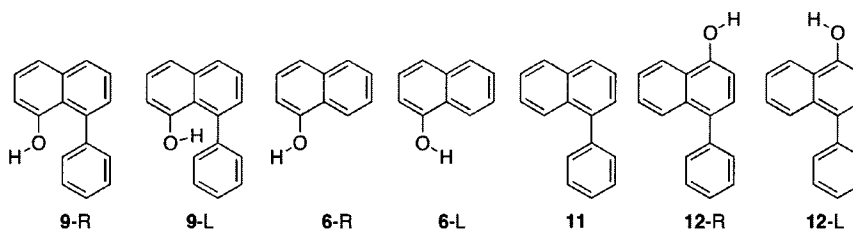
Calculation with Considering the Solvent Effect in Compound 9

To investigate the relative stability of 9-L and 9-R in DMSO, we included the solvent effect by the polarized continuum model (PCM) and used hybrid functional CAM(Coulomb-attenuating method)-B3LYP[19,36] as well as B3LYP, because B3LYP underestimates charge transfer state energies due to the long-range interaction problem and overestimates the polarization induced by a polar solvent, whereas CAM-B3LYP improves that problem. The results are summarized in the following Table. While in vacuum both B3LYP and CAM-B3LYP results show that 9-L is more stable than 9-R by 3 kcal/mol, in DMSO B3LYP and CAM-B3LYP results show that 9-L is less and more stable, respectively. It is considered from the above reason that the CAM-B3LYP relative energy in the polar solvent of DMSO is much more reliable and that 9-L is more stable than 9-R even in DMSO from the viewpoints of theoretical calculations. Therefore in this case we consider that it is no problem to discuss the absorption/emission maxima in DMSO using calculated results in vacuum, which is supported by the fact that the TDDFT(B3LYP) vertical excitation energies calculated in vacuum show good agreement with the experimental absorption/emission maxima in DMSO.

Method	Solvent	ΔE (9-L - 9-R) (kcal/mol)
B3LYP	vacuum	-2.9
	DMSO	+1.0
CAM-B3LYP	vacuum	-3.0
	DMSO	-1.6

The solvent effects were included by PCM.

S_0 energies at the B3LYP S_0min (DMSO), CAM-B3LYP S_0min (vacuum), and CAM-B3LYP S_0min (DMSO) (in hartree).

Compound	@B3LYP S0min (DMSO)	@CAM-B3LYP S0min (vacuum)	@CAM-B3LYP S0min (DMSO)
9-L	-692.1710	-691.7717	-691.7782
9-R	-692.1727	-691.7669	-691.7756

127

3-5. References

(1) (a) Tour, J. M. *Chem. Rev.* **1996**, *96*, 537–553. (b) Kertesz, M.; Choi, C. H.; Yang, S. *Chem. Rev.* **2005**, *105*, 3448–3481. (c) Roncali, J. *Chem. Rev.* **1997**, *97*, 173–205. (d) Kaur, I.; Stein, N. N.; Kopreski, R. P.; Miller, G. P. *J. Am. Chem. Soc.* **2009**, *131*, 3424–3425. (e) Chan, J. M. W.; Tischer, J. R.; Kooi, S. E.; Bulović, V.; Swager, T. M. *J. Am. Chem. Soc.* **2009**, *131*, 5659–5666. (f) Mukherjee, A.; Pati, K.; Liu, R. –S. *J. Org. Chem.* **2009**, *74*, 6311–6314. (g) Itami, K.; Ohashi, Y.; Yoshida, J.-i. *J. Org. Chem.* **2005**, *70*, 2778–2792 and references cited in. (h) Liu, W. –J.; Zhou, Y.; Zhou, Q. –F.; Ma, Y.; Pei, J. *Org. Lett.* **2008**, *10*, 2123–2126.

(2) (a) Brookins, R. N.; Schanze, K. S.; Reynolds, J. R. *Macromolecules* **2007**, *40*, 3524–3526. (b) Burnell, T.; Cella, J. A.; Donahue, P.; Duggal, A.; Early, T.; Heller, C. M.; Liu, J.; Shiang, J.; Simon, D.; Slowinska, K.; Sze, M.; Williams, E. *Macromolecules* **2005**, *38*, 10667–10677.

(3) (a) Trotter, J. *Acta Cryst.* **1961**, *14*, 1135–1140. (b) Charbonneau, G. -P.; Delugeard, Y. *Acta Cryst.* **1976**, *B32*, 1420–1423. (c) Karpfen, A.; Choi, C. H.; Kertesz, M. *J. Phys. Chem. A* **1997**, *101*, 7426–7433. (d) Benniston, A. C.; Harriman, A.; Li, P.; Patel, P. V.; Sams, C. A. *J. Org. Chem.* **2006**, *71*, 3481–3493.

(4) Miyaura, N.; Suzuki, A. *Chem. Rev.* **1995**, *95*, 2457–2483.

(5) Yoshikawa, S.; Odaira, J.; Kitamura, Y.; Bedekar, A. V.; Furuta, T.; Tanaka, K. *Tetrahedron* **2004**, *60*, 2225–2234.

(6) Ford, A.; Sinn, E.; Woodward, S. *J. Chem. Soc., Perkin Trans. 1* **1997**, 927–934.

(7) Although the tris(hydroxynaphthyl)benzenes **1** and **4** have low solubility to typical organic solvent such as hexane, ether, chloroform, and dichloromethane, they dissolve in DMSO.

(8) The reason why compound **1** exists mainly as one conformer with up-up-up form is not clear and now under investigation.

(9) The ratio of the two conformers of **2** is approximately 2:1 (= up-up-down:up-up-up) at room temperature and 1.2:1 (= up-up-down:up-up-up) at –60 °C.

(10) The distance between H and O of two different hydroxy groups which are located in the same side is 2.57 Å. This distance is much longer than that between H of OH group and *ipso*-carbon (2.205 Å). Therefore, the compound **1** does not have intramolecular hydrogen bonding between two hydroxyl groups.

(11) (a) Marciniak, B. *Acta Cryst.* **2007**, *C63*, o419–o422. (b) Parthasarathi, R.; Subramanian, V.; Sathyamurthy, N.; Leszczynski, J. *J. Phys. Chem. A,* **2007**, *111*, 2–5. (c) Stoyanov, E. S.; Hoffmann, S. P.; Kim, K. -C.; Tham, F. S.; Reed, C. A. *J. Am. Chem. Soc.* **2005**, *127*, 7664–7665. (d) Grabowski, S. J. *J. Phys. Chem. A,* **2007**, *111*, 13537–13543. (e) Maity, S.; Patwari, G. N. *J. Phys. Chem. A,* **2009**, *113*, 1760–1769. (f) Meng, S.; Ma, J.; Jiang, Y. *J. Phys. Chem. B,* **2007**, *111*, 4128–4136.

(12) The fluorescence spectrum of compound **1** given in Figure 3 shows a shoulder. Probably, this shoulder derived from conformers of **1** (OH direction; up-up-up or up-up-down).

(13) Solntsev, K. M.; McGrier, P. L.; Fahrni, C. J.; Tolbert, L. M.; Bunz, U. H. F. *Org. Lett.* **2008**, *10*, 2429–2432.

(14) Phenols are activated as acids by photoirradiation. (a) Lewis, F. D.; Cromptom, E. M. *J. Am. Chem. Soc.* **2003**, *125*, 4044–4045. (b) Cromptom, E. M.; Lewis, F. D. *Photochem. Photobiol. Sci.* **2004**, *3*, 660–668. However, our system does not include an anion of phenols, because sodium salt of **1** and **9** did not show the same fluorescence with neutral **1** and **9**, respectively.

(15) Satoh, T.; Inoh, J.; Kawamura, Y.; Kawamura, Y.; Miura, M.; Nomura, M. *Bull. Chem. Soc. Jpn.* **1998**, *71*, 2239–2246.

(16) The electronic absorption spectra of **9-13** are given in Experimental Section.

(17) The methoxy-substituted compound **13** does not give the conformationally different stable isomers probably because of steric hindrance of methoxy group with *ana*-hydrogen. It solely exists with methyl group far from *ana*-hydrogen as shown in Table 3.

(18) To investigate the S_0 relative stability of **9-L** and **9-R** in DMSO, hybrid DFT calculations including the solvent effect of DMSO by the polarized continuum model (PCM) were performed at the CAM(Coulomb-attenuating method)-B3LYP/6-31G* level with the Gaussian 09 program.[19] These results show that **9-L** is more stable than **9-R** in DMSO as well as in vacuum. Therefore, in this case it is no problem to discuss the absorption/emission maxima in DMSO using the calculated ones in vacuum, which is supported by the fact that the TDDFT(B3LYP) vertical excitation energies calculated in vacuum show good agreement with the experimental absorption/emission maxima in DMSO. The calculated results are given in the Experimental Section.

(19) Frisch, M. J.; Trucks, G. W.; Schlegel, H. B.; Scuseria, G. E.; Robb, M. A.; Cheeseman, J. R.; Scalmani, G.; Barone, V.; Mennucci, B.; Petersson, G. A.; Nakatsuji, H.; Caricato, M.; Li, X.; Hratchian, H. P.; Izmaylov, A. F.; Bloino, J.; Zheng, G.; Sonnenberg, J. L.; Hada, M.; Ehara, M.; Toyota, K.; Fukuda, R.; Hasegawa, J.; Ishida, M.; Nakajima, T.; Honda, Y.; Kitao, O.; Nakai, H.; Vreven, T.; Montgomery, J. A., Jr.; Peralta, J. E.; Ogliaro, F.; Bearpark, M.; Heyd, J. J.; Brothers, E.; Kudin, K. N.; Staroverov, V. N.; Kobayashi, R.; Normand, J.; Raghavachari, K.; Rendell, A.; Burant, J. C.; Iyengar, S. S.; Tomasi, J.; Cossi, M.; Rega, N.; Millam, J. M.; Klene, M.; Knox, J. E.; Cross, J. B.; Bakken, V.; Adamo, C.; Jaramillo, J.; Gomperts, R.; Stratmann, R. E.; Yazyev, O.; Austin, A. J.; Cammi, R.; Pomelli, C.; Ochterski, J. W.; Martin, R. L.; Morokuma, K.; Zakrzewski, V. G.; Voth, G. A.; Salvador, P.; Dannenberg, J. J.; Dapprich, S.; Daniels, A. D.; Farkas, Ö.; Foresman, J. B.; Ortiz, J. V.; Cioslowski, J.; Fox, D. J.; Gaussian 09 (Revision B.01), Gaussian, Inc., Wallingford CT, USA, 2009.

(20) Examples wherein the protic hydrogen of an amino group controlled intramolecular charge transfer were reported. In our system, however, charge transfer was not the main reason for the bathochromic shifts in **1** and **9**, judging from NAO atomic charge. (a) Stalin, T.; Rajendiran, N. *Chem. Phys.* **2006**, *322*, 311–322. (b) Dahiya, P.; Kumbhakar, M.; Maity, D. K.; Mukherjee, T.; Tripathi, A. B. R.; Chattopadhyay, N.; Palb, H. *J. Photochem. Photobiol. A: Chem.* **2006**, *181*, 338–347. (c) Pereira, R. V.; Gehlen, M. H. *Chem. Phys. Lett.* **2006**, *426*, 311–317.

(21) (a) Niezborala, C.; Hache, F. *J. Am. Chem. Soc.* **2008**, *130*, 12783–12786. (b) Millar, D. P.; Eisenthal, K. B. *J. Chem. Phys.* **1985**, *83*, 5076–5083. (c) Bowman, R. M.; Eisenthal, K. B.; Millar, D. P. *J. Chem. Phys.* **1988**, *89*, 762–769. (d) Takei, Y.; Yamaguchi, T.; Osamura, Y.; Fuke, K.; Kaya, K. *J. Phys. Chem.*

1988, *92*, 577–581. (e) Mank, D.; Raytchev, M.; Amthor, S.; Lambert, C.; Fiebig, T. *Chem. Phys. Lett.* **2003**, *376*, 201–206.

(22) The distances are shown in the Experimental Section.

(23) The calculated values of absorption and emission wavelengths are shown in the Experimental Section. HOMO and LUMO at the B3LYP S_0min and the CIS S_1min were obtained using the Hartree-Fock (HF) method. We employed the HF orbitals rather than the Kohn-Sham (KS) orbitals for more quantitative orbital analysis, because the HF theory satisfies Koopmans' theorem while the KS theory does not as long as an approximate exchange-correlation functional is used.

(24) The average of wavelengths was estimated based on the Boltzmann distribution of both isomers.

(25) The NAO atomic charges of **6-L** and **12-L** are also given in the Experimental Section. We excluded these species in the discussion in Table 4 because they are an unstable conformer compared to the corresponding **6-R** and **12-R**. The compound **6-R** was more stable than **6-L** (E(L)–E(R) = 1.69 kcal/mol).

(26) The solvent effect of trisubstituted benzene **1-5** was investigated. The unsubstituted compound **3** and the methoxy-substituted compounds **2** and **5** showed less solvent effect than **1**, indicating that their excited states are less polarized than that of **1**. The electronic emission spectra are given in the Experimental Section.

(27) In the asymmetric unit of **15**, two crystallographically independent molecular structures of **15** were observed.

(28) Rane. A. M.; Miranda, E. I.; Soderquist, J. A. *Tetrahedron Letters,* **1994**, *35*, 3225-3226.

(29) Wolfe, J. P.; Buchwald, S. L. *J. Org. Chem.* **1997**, *62*, 1264–1267.

(30) O'Meara, J. A.; Yoakim, C.; Bonneau, P. R.; Bös, M.; Cordingley, M. G.; Déziel, R.; Doyon, L.; Duan, J.; Garneau, M.; Guse, I.; Landry, S.; Malenfant, E.; Naud, J.; Ogilvie, W. W.; Thavonekham, B.; Simoneau, B. *J. Med. Chem.* **2005**, *48*, 5580–5588. NMR spectrum; Yadav, J. S.; Reddy, B. V. S.; Reddy, P. S. R.; Basak, A. K.; Narsaiah, A. V. *Adv. Synth. Catal.* **2004**, *346*, 77–82.

(31) Kamila, S.; Mukherjee, C.; De, A. *Tetrahedron Lett.* **2001**, *42*, 5955–5957. NMR spectrum; Macklin, T. K.; Snieckus, V. *Org. Lett.* **2005**, *7*, 2519–2522.

(32) Plater, M. J. *J. Chem. Soc., Perkin Trans. 1* **1997**, 2897–2901.

(33) Nishii, Y.; Tanabe, Y. *J. Chem. Soc., Perkin Trans. 1* **1997**, 477–486.

(34) CCDC-803341 (**1**), CCDC-803339 (**14**), and CCDC-803340 (**15**) contain the supplementary crystallographic data for this paper. These data can be obtained free of charge from The Cambridge Crystallographic Data Centre via www.ccdc.cam.ac.uk/data_request/cif

(35) Parker C. A.; Joyce, T. A. *Trans. Faraday Soc.* **1966**, *62*, 2785.

(36) Yanai, T.; Tew, D.; Handy, N. *Chem. Phys. Lett.* **2004**, *393*, 51–57.

Conclusion

This research investigates cage-shaped metal complexes with phenoxy moieties based on novel structural design. This cage-shaped ligand system provides the systematic template for fine-tunable main group metal complexes. The results obtained from present work are summarized as follows.

Chapter 1

Various types of cage-shaped borate complexes were created by using the ligands in which three phenoxy moieties are linked by uni atom. A cage-shaped geometry led to high Lewis acidity and catalytic activity on boron. In addition, the Lewis acidity of the borate complexes was precisely tuned by changing the cage-shaped geometry and introducing various electronic substituents. The rigid structure of the cage enabled the creation of the specific reaction field which selectively activates aromatic aldehyde over aliphatic ones.
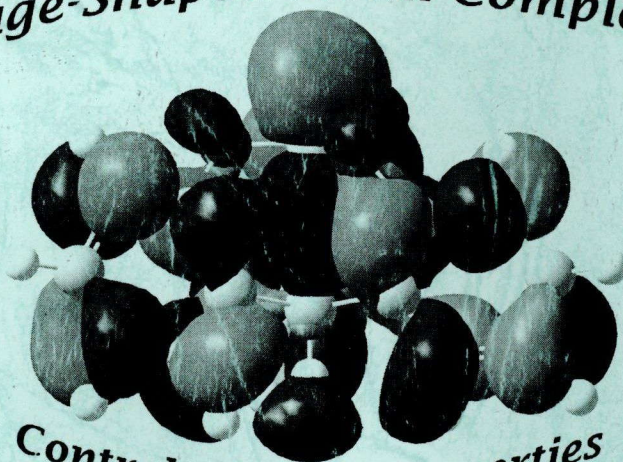
Chapter 2

Two types of cage-shaped metal complexes were synthesized by using the ligands in which three phenoxy moieties are linked by a benzene ring. One is a cage-shaped gallium complex, in which the back-shielding framework of the cage keeps their Lewis acidity high by inhibiting the coordination of the external ligand to the gallium center. The substituents on the bottom benzene ring tuned their characteristic Lewis acidity, which was supported by theoretical calculation as well as catalytic application in a hetero Diels-Alder reaction. The other is a lithium complex. A stable lithium phenolate $(ArOLi)_6 \cdot L_6$ was isolated by a cage-shaped triphenolic ligand, which had a hexagonal-prismatic Li_6O_6 core at room temperature, because of the rigid structure of the tridentate ligand and its reduction of the problematic steric repulsion. The structures of the lithium phenolates and their properties were analyzed by X-ray crystallography and NMR spectroscopy.

Chapter 3

The OH-substituents at the *peri*-position in 1-arylnaphthalene systems, which are biaryl compounds, showed interesting and unexpected photophysical properties of a large bathochromic shift of emission that was induced by polarization based on intramolecular OH-aryl interaction. Quantum chemical calculations (TDDFT) accurately reproduced the large bathochromic shifts of *peri*-OH-substituted arylnaphthalenes. The through-space interaction between the *peri*-substituted OH and aryl groups generated an unexpected extended conjugation system. The substituting position of OH in 1-arylnaphthalenes is quite critical, because the hydroxy group mediates the independent π-systems to expand conjugation. This through-space protocol will provide the new strategy to design the emitting material with biaryl-framework.

This research has developed the novel method to finely control the properties of the main group metal complexes by using the cage-shaped ligand system. This methodology based on new type of the ligand-design will contribute to development of chemistry of main group metal complexes.

Cage-Shaped Metal Complexes

Control of Metal Properties